HEALTH MONITORING OF STRUCTURES UNDER AMBIENT VIBRATIONS USING SEMIACTIVE DEVICES

by

Mohamed Ihab Sherif Elmasry

A Dissertation Presented to the
FACULTY OF THE GRADUATE SCHOOL
UNIVERSITY OF SOUTHERN CALIFORNIA
In Partial Fulfillment of the
Requirements for the Degree
DOCTOR OF PHILOSOPHY
(CIVIL AND ENVIRONMENTAL ENGINEERING)

May 2005

DEDICATION

In the Name of GOD the Most Gracious the Most Merciful, I dedicate this thesis to my beloved father, Sherif Mohamed Elmasry (September 26, 1935–October 11, 2004) and to my beloved mother, Magda Osman Ramzy. May GOD bless them and help me and my family overcome the sorrow of my father's sudden absence.

ACKNOWLEDGEMENTS

My full thanks to GOD the most gracious the most merciful for his help all along the course of this research work and my life in general. I would like to give my heartful thanks and appreciation to my parents Mr. and Mrs. Sherif Elmasry; their love and good hands have always been there in every step of my life, even when I am far away. To my wife, Rania, and baby, Nadeen, I thank them for their support and for being there beside me when I needed them the most. Their love and smiles have always filled me with joy and hope. To my sister Riham, my brother Tamer, and all my family, I wish you all success and happiness. Finally, I devote all the efforts that I spent in this work to the soul of my beloved father who passed away in October 2004. Our life together will always be remembered. May GOD have his mercy on him and make heaven be his destination.

I would like to gratefully thank my advisor, Prof. Erik A. Johnson for his friendship, encouragement, and support. His advice, guidance and remarks during the course of this research are invaluable. I am very grateful to all faculty members that I took classes with and especially my committee members, Prof. L. Carter Wellford, Prof. Sami F. Masri, Prof. James C. Anderson, and Prof. Bingen Yang. Their advice has always been of great value and help.

The author gratefully acknowledge, the partial support of this research work by Caltrans and the USDoT through the National Center for Metropolitan

Transportation Research (METRANS) under projects 01-10 and 03-17, and by the National Science Foundation (NSF) under CAREER grant 00-94030.

TABLE OF CONTENTS

LIST OF TABLES

LIST OF FIGURES

ABBREVIATIONS

SHM: Structural Health Monitoring

SI: System Identification

VSDD: Variable Stiffness and Damping Device

FHWA: Federal Highway Administration

ASCE: American Society of Civil Engineering

2DOF: 2 Degree Of Freedom

6DOF: 6 Degree Of Freedom

nDOF: *n* Degree of Freedom

TF: Transfer Function

LSN: Least Squares Numerator method

ILSN: Iterative-Least Squares Numerator method

INVFLS: INVfreqs-Least Squares method

RMS: Root Mean Square

RMSE: Root Mean Square Error

MSE: Mean Square Error

ERA: Eigensystem Realization Algorithm

ARMA: AutoRegressive Moving Average

ARMAX: AutoRegressive Moving Average with eXternal input

SISO: Single Input Single Output

SIMO: Single Input Multi Output

MIMO: Multi Input Multi Output

BLWN: Band Limited White Noise

FBLWN: Filtered Band Limited White Noise

ABSTRACT

Structural health monitoring (SHM) is the process of monitoring structural health and identifying damage existence, severity and location. Clear needs for SHM exist for various types of civil structures. Yet, the dominant method for monitoring the health of civil structures is manual visual inspection. Global vibration-based SHM techniques have been studied, but no approach has been well established and accepted due to the limitations of ambient excitation for most civil structures and the small sensitivity of global vibration characteristics to damage. One approach that may alleviate some of the SHM difficulties for civil structures is using variable stiffness and damping devices (VSDDs) to improve damage estimates. In addition to providing near optimal structural control strategies for vibration mitigation, these low-power and fail-safe devices can provide parametric changes to increase global vibration measurement sensitivity to damage.

This dissertation proposes using VSDDs in structures to improve SHM, and demonstrates the benefits analytically and experimentally in contrast with conventional passive structures. A two degree-of-freedom (2DOF) bridge structure model and two shear building models, are used as test beds to study the VSDD approach with several identification algorithms. Using multiple channels of data from multiple VSDD configurations, a least-squares error formulation is used to estimate unknown structural parameters. The improvements in identification are even more effective when adding higher effective levels of stiffness or damping to a

structural system; the resulting VSDD forces are small due to low ambient excitation. A 2DOF shear building laboratory structure is excited at the base using a small shaking table and its parameters are identified; using VSDDs gives parameter estimates that have better means and smaller variations than the conventional structure approach. Finally, a controlled approach is introduced for SHM. A state feedback gain matrix is chosen to minimize a cost function of parameter identification error and control effort. This controlled approach is applied to the 2DOF bridge model where an ARMAX (Auto Regressive Moving Average eXogenous disturbance) model is assumed to represent the controlled system.

1 INTRODUCTION

Detecting damage in structures at an early stage, before they deteriorate, is a vital action to protect these structures. Generally, damage may be caused by acute events, such as earthquakes and other natural disasters, or sometimes long-term degradation from environmental effects and human use (and abuse). Whatever the cause, structural damage can threaten both danger to human life and huge economic losses. Consequently, a process that can detect damage as early as possible would be extremely useful. The process of monitoring structural health and identifying damage existence, severity and location is generally termed *structural health monitoring* (SHM). Chang (1999) defined structural health monitoring to be an "autonomous [system] for the continuous monitoring, inspection, and damage detection of [a structure] with minimum labor involvement."

The SHM process includes system identification as a major step. Thus, high fidelity modeling and accurate response estimation are required. This would help to monitor the changes of structural characteristics and response, and subsequently predict the onset of failure or the expected remaining life. With identification at different points in time — periodic or shortly after natural disasters — changes in these characteristics may be monitored. With damage models, changes in structural characteristics are used to predict damage severity and location. This study proposes using smart, controllable passive devices such as Variable Stiffness and Damping

devices (VSDDs) in structures to improve SHM, and demonstrates the benefits over conventional passive structures.

1.1 SHM Benefits

Clear needs for SHM exist for both building and bridge structures. This is reflected in the significant expenditures after the 1994 Northridge and the 1995 Kobe earthquakes that went to inspecting joints of steel buildings for damage (Mita, 1999). The problem lies in the fact that these joints are often hidden within a structure, such as behind walls or encased in concrete (*e.g.* see Fig. 1-1 to Fig. 1-3).

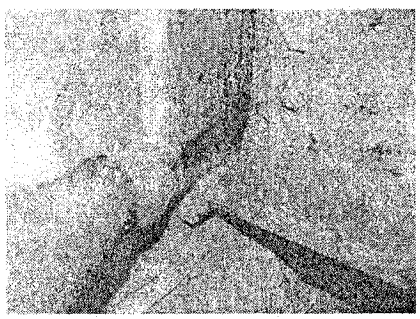

Fig. 1-1. Beam-column connection damage (Kiremedjian, 1999)

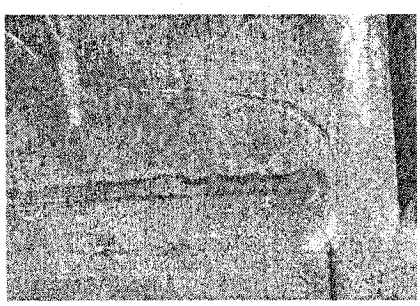

Fig. 1-2. Cracks through column flange and extending into web (Hall, 1995)

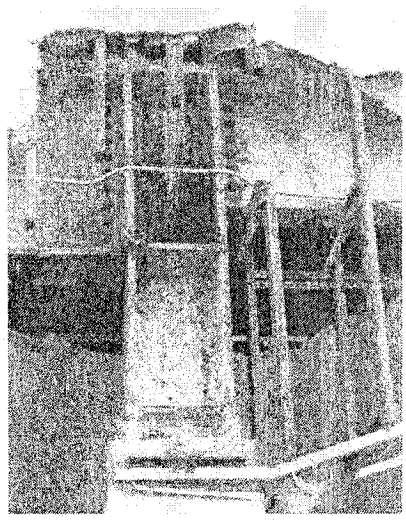

Fig. 1-3. Plastic hinging at top of column (Hall, 1995)

Moreover, a recent report to the U.S. Congress by the Federal Highway Administration (FHWA, 2002) indicates that approximately 25% of the bridges in

the U.S. are rated as deficient. It is estimated that it will require 7 billion dollars per year for the next two decades to rebuild or replace the bridge infrastructure in the U.S. (Patten *et al.*, 1999). All of these facts indicate the essential need for effective SHM systems.

1.2 Difficulties of Conventional SHM Approaches

One approach to SHM is based on global vibration methods. In applying these methods, many global vibration SHM studies assume a class of mathematical models that may represent the actual structure. When considering damage detection, studies have focused on identifying changes in modal parameters (natural frequencies, mode shapes, and modal damping ratios) obtained from measured vibration response. Recent state-of-the-art surveys of global vibration SHM techniques applied to civil engineering are given by Doebling *et al.* (1996, 1998).

Unfortunately, no global technique has been well established and accepted as an overall successful approach (Sanayei *et al.*, 1998). Some explanatory reasons are that (*i*) models cannot exactly predict the full behavior of real structures, (*ii*) periodic environmental effects such as thermally-induced variations may mask the effects of damage on global vibration characteristics, (*iii*) measurement noise can cause significant variation from one test to the next, (*iv*) excitation is limited to ambient sources for most civil structures, and (*v*) sensitivity of global vibration characteristics to damage may be small. These can all lead to variations in the identified model

parameters characteristics that are not due to true changes in the structure, raising uncertainty in damage estimates (Vanik *et al.*, 2000).

Using forced structural response strategies can overcome some of the aforementioned problems. For example, forced response interrogation can be timed to minimize periodic environmental effects from one test to the next, and may provide greater excitation energy to decrease signal-to-noise ratios in comparison with ambient excitation. For structures with embedded active vibration control systems, the actuators can be used to enhance damage detection by tuning the actuation signals to directly increase closed-loop damage sensitivity of global vibration characteristics (Ray and Tian, 1999). However, large actuation devices are not being used in a continuous manner for civil structures (except a few isolated cases in Asia) due to large power requirements, concerns about stability and so forth, rendering them impractical for damage mitigation or SHM of civil structures. Further, building and bridge owners typically prefer their structures not be deliberately shaken, both for comfort of occupants and to lessen the chance of risking further damage.

Given these limitations, one is restricted to analyzing response to ambient excitation in order to perform SHM. Ambient excitation of structures takes a number of forms (*e.g.*, wind, traffic, waves and microtremors). The ambient excitation approach has several advantages over approaches using forced vibration response. For example, for low amplitude excitations typically experienced during ambient vibration, most structural systems are well characterized with linear models. In

addition, continuous ambient vibration tests can be performed at a very low cost. However, the sensitivity of the measured signals to noise is a pressing question. Due to small structural response under such ambient excitations, measurement signal-to-noise ratios are small enough to make SHM difficult and results uncertain.

1.3 Use of VSDDs to Improve SHM

One approach that may help alleviate some of the SHM difficulties for civil structures would be to use "smart" variable stiffness and damping devices (VSDDs) — controllable, low-power and fail-safe passive devices that have received significant study for vibration mitigation (Spencer and Sain, 1997; Symans and Constantinou, 1999) — in a synergistic manner to provide internal parametric changes to affect sensitivity to damage. Further, the integration of smart damping and SHM can exploit, in a synergistic manner, the common aspects of both technologies as seen in the flowcharts in Fig. 1-4.

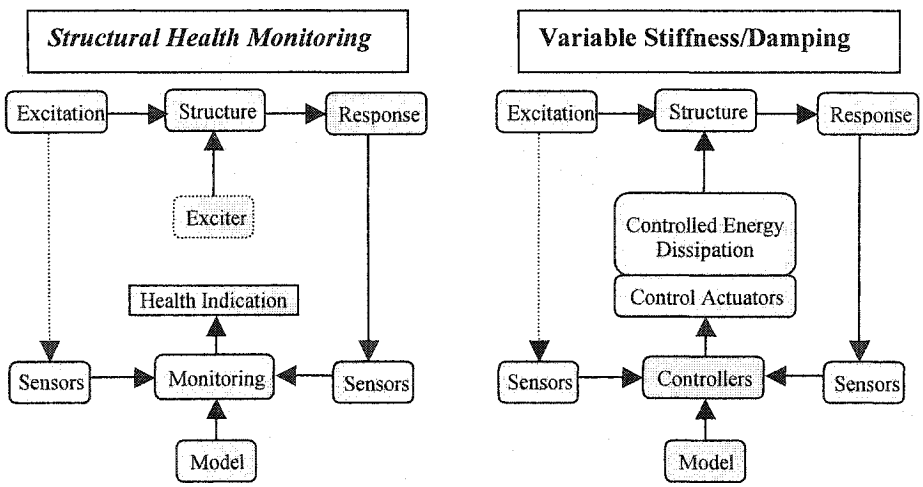

Fig. 1-4. SHM and variable stiffness/damping flow charts

VSDDs can adjust the behavior of a structure by real-time modification of stiffness and damping at discrete points within the structure. By commanding different behavior for each VSDD in a structure, multiple structural configurations can be tested, each of which can be designed to increase the sensitivity to damage in different portions of the structure (see Fig. 1-5). For example, consider a structure with four stiffness devices with "on" and "off" settings; there are 2^4, or 16, distinct configurations, each of which can provide some information about the structural characteristics. The SHM is provided, then, with multiple signatures of the structure, each of which can provide additional and, if done efficiently, mostly complementary information.

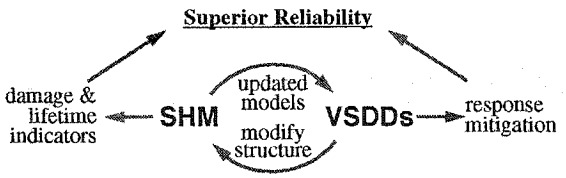

Fig. 1-5. Mutual benefits of SHM and VSDDs

1.4 Overview of the VSDD/SHM Research Studied Herein

This study proposes using VSDDs in structures to improve SHM, and demonstrates the benefits in contrast with conventional passive structures. The focus herein is introducing a better approach for estimating the structural dynamic parameters through the use of variable stiffness and damping devices. The study in general can be divided into three parts. The first part is an analytical study of the benefits of applying VSDDs in SHM. The second part studies the VSDD approach benefits in SHM from an experimental perspective. The third part introduces a

controlled monitoring approach for SHM. Since controllable stiffness/damping devices are used to give the parametric changes necessary for improved monitoring, the structural models must be *control-oriented* dynamic models — *i.e.*, low-order models that still capture most of the salient dynamic characteristics of a real structure, particularly in locations of the controllable devices and in the frequency ranges driven by the excitation.

Using different identification techniques in investigating the use of VSDDs for SHM gives a broad view of how VSDDs are useful for SHM. In this study, the VSDDs are investigated primarily in the context of parametric frequency domain identification to determine structural parameters. Conventional parametric identification in the frequency domain is described. The direct transfer function polynomial identification is rather complex in the unknown parameters. Consequently, one simplification discussed in the literature is explained. However, it is shown that this simplification can often lead to significant bias in parameter estimates due to unwanted magnification of sensor noise effects. The numerical examples herein use a fairly noisy signal to challenge the methods. Thus, an iterative method is proposed that approximates the more direct method. In addition, one subspace method, the Eigensystem Realization Algorithm (ERA) technique, is also used in investigating the effectiveness of adding VSDD in improving the identification of structural parameters. Moreover, time domain techniques, such as the ARMAX model, are also used in the application of online controlled monitoring

of the structures. These methods are applied to conventional structural identification, assuming no VSDD within the structure, and then with VSDDs.

In the analytical part (Chapter 3), several structures are studied, with one or more VSDDs installed. First, two degree-of-freedom (2DOF) and then six-degree-of-freedom (6DOF) shear building structural models are studied, each in several configurations: the 2DOF structure with a VSDD in (*i*) the first story, (*ii*) the second story, and (*iii*) both stories, and the 6DOF building with VSDDs in the first three stories. Then, a 2DOF bridge structure model (Erkus *et al.*, 2002) is studied with a VSDD attached in the bearing layer between the pier and the deck. In each case, the VSDD is chosen to act as an ideal variable stiffness/damping device, with one of several discrete stiffness/damping values. These devices are located in the structures in the form of lateral bracing or, in the bridge example, in the isolation layer between the bridge deck and the pier supports. Two sets of VSDD stiffness/damping levels are studied: a lower level where the additional VSDD stiffness/damping is a fraction of the corresponding story stiffness/damping; and a higher level where the additional stiffness/damping is several times the order of the corresponding story stiffness/damping.

As a result, it is shown that using the least squares approach on the modified version of the error in transfer functions with known starting guesses, both using VSDD and conventional identification techniques give parameter estimates. The VSDD approach gives better means and rather smaller variation when the additional stiffness/damping by a VSDD is only up to 40% of the corresponding story

stiffness/damping. However, using higher levels of additional stiffness/damping, the VSDD approach is found to significantly improve the mean estimates and reduce the variations compared to the conventional structure approach. Using the ERA technique, it is found that the root mean square error (RMSE) of the estimated structure stiffnesses is considerably reduced, indicating more accurate results.

In the experimental part (Chapter 4), a 2DOF shear building structure, composed of vertical aluminum plates and horizontal plexi-glass plates, with weak springs elements in the diagonal bracing, is the test bed of the study. A small shake-table excites the structure to replicate ambient ground motion. The ground acceleration takes two forms: a band limited white noise and a filtered band limited white noise. The effect of VSDDs in the structure is replicated by a set of stiff springs that are added, in the diagonal bracing, in pairs. The number of pairs added varies as per the assumed additional stiffness by a VSDD in the same story. The outcome of the experimental study is found to validate the improvements exhibited in the analytical study. The VSDD approach gives better means and smaller variations, whereas the conventional structure approach indicated less confidence in its results.

In the controlled SHM study (Chapter 5), the 2DOF bridge model is the test bed. A quadratic cost function, that includes the error in the estimated system parameters and the force exerted by the actuator, is defined. This cost function is minimized by an optimal choice of control gains. The structure is assumed subjected to traffic loads on its deck and to ambient ground excitation at the base of the pier,

both represented by Gaussian noise. The actuator is assumed located in the isolator layer between the deck and the pier. The identified parameters, in this case, are the ARMAX model coefficients. Using the controlled SHM approach, the estimates of the structural parameters are expected to rapidly converge to their correct values faster than with the conventional structure approach.

Finally, the conclusions (Chapter 6) summarize the results and provide some thoughts on future directions of this work.

2 LITERATURE REVIEW

2.1 Introduction

The field of structural health monitoring has been quite rich with research in the last few decades. The potential impact and benefits, both economic and societal, of SHM have drawn the interest of many researchers. The results of relevant work in the literature can be loosely broken down into several related categories; some representative examples in each category are briefly highlighted in this chapter. First, an overview of SHM approaches is given, followed by a discussion of modeling issues. Then several classes of system identification methods are described. Finally, variable stiffness and damping devices are reviewed, highlighting the various types and some applications in which they have been studied.

2.2 Research on Structural Health Monitoring

Conventional research in SHM and damage detection for civil structures can be roughly classified into local and global methods. Local SHM methods detect changes in a structure in localized regions using, for example, ultrasound, x-ray, piezoelectric devices and so forth. Unfortunately, local SHM methods have limited range; *e.g.*, piezoelectric devices have an effective range on the order of 30 cm (Wang and Chang, 1999). For large civil structures, this would require a staggering number of devices to monitor the entire structure. Furthermore, other local methods usually require significant human involvement or are limited to areas where damage

might be expected to occur. Consequently, service costs and errors in expected damage locations limit the usefulness of such methods.

Conventional global vibration SHM methods (Doebling *et al.*, 1996, 1998) typically focus on identifying changes in modal parameters (*e.g.*, natural frequencies, mode shapes, and modal damping ratios) computed from measured vibration response. With identification at different points in time — periodic or shortly after natural disasters — changes in these characteristics may be monitored. However, these approaches also have their difficulties. Global methods based on ambient excitation are easy to implement as they require no additional excitation source, but simply may not reveal certain defects since some damage mechanisms are only strongly observable with narrowband excitation that ambient sources alone cannot provide. Using known excitation with force actuators can overcome this difficulty but, with a few exceptions in Asia, such active devices are not used in civil structures for other purposes, so widespread permanent installation and use is unlikely. As a result, no global technique has been well established and accepted as an overall successful approach (Sanayei *et al.*, 1998).

A benchmark study in structural health monitoring based on simulated structural response data was developed by the joint IASC-ASCE task group on structural health monitoring. This benchmark was created to facilitate a comparison of various methods employed for the health monitoring of structures. The focus of the problem is simulating acceleration response data from an analytical model of an existing physical structure. This problem was addressed and studied by various

researchers including Yuen *et al.* (2004), Hera and Hou (2004), Yang *et al.* (2004), Bernal and Gunes (2004), Caicedo *et al.* (2004), Johnson *et al.* (2004), Lam *et al.* (2004) and Luş *et al.* (2004). This SHM benchmark problem, both the definition and the application of a number of SHM methods to solve the problem, was published in a special issue of the *Journal of Engineering Mechanics* in January 2004.

SHM approaches, particularly ones based on global vibration, often involve some level of structural modeling and some type of system identification. The modeling, which is described in more detail in the following section, whether discrete or continuous in nature, has the difficulty that no model has the exact same dynamic properties as the structure it is intended to represent. Fortunately, the small motion levels typical of ambient vibration response can alleviate some of these issues. In addition to various modeling approaches, there are numerous system identification techniques, some of which are described in the third section of this chapter.

2.3 Modeling of Structures for SHM

Picking the right model to represent a particular structure has been a critical issue in the application of SHM. Capecchi and Vestroni (1999) state that, from a theoretical point of view, it is convenient to distinguish between continuous and discrete structures. Although all structures are in fact continuous, structures in which concentrated masses are dominant are considered discrete in dynamic analysis. In the context of damage identification, structures are considered as discrete if the damage

cannot affect a portion smaller than the element. Thus frames, for example, are seen as discrete structures whereas bridge decks and pipelines are usually considered continuous. For continuous structures, it is conceptually correct to pose the problem of localizing of a crack, because its position affects the entire dynamics. For a discrete structure the problem is different; for example, it is not possible to precisely determine where, in an element, a crack exists because the structure is modeled discretely, with all characteristics of the element taken as a whole.

Despite extensive research in modeling, structural models cannot be expected to perfectly predict the full behavior of the structure. For example, the model may not account for effects such as thermally-induced daily variations and amplitude dependence of modal parameters. Further, the available measured information is restricted by limits on the amount of instrumentation. Nonlinearities are also a major obstacle where the model becomes very difficult to implement and each nonlinear system is a special case of its own. Moreover, while finite element modeling is convenient, it often produces a dynamic model that neither is of modest order nor accurately captures the dynamics of the built structure. Some reasons for the latter are mismodeling of structural elements, differences between actual and modeled material properties and dimensions, approximation in finite element derivations, and poor convergence of the numerical model (Juang, 1994). For SHM, models of extremely high order are of limited utility as often only a small number of the lower modes of a structure can be identified with confidence (Beck *et al.*, 2001). Additionally, a real structure often has nonlinearities and higher frequency modes (or

local vibration modes) that may be missed in the analytical modeling, leading to what is generally termed "model error." All of these difficulties make clear the complexity of the modeling problem.

Using ambient excitation sources may simplify the modeling problem necessary for SHM. Basically, the structural model can be considered linear (see, *e.g.*, Beck *et al.*, 2001) since ambient excitations are small, and civil structures are highly rigid, making them behave linearly under small external excitations. Linear behavior and safety considerations have encouraged numerous researchers to adopt ambient excitation approaches in SHM.

2.4 System Identification for SHM

As there is no unique and general mathematical definition for damage, researchers tend to relate damage to changes in structural model parameters (such as stiffness, damping, and masses) or, sometimes, modal parameters (such as natural frequencies and mode shapes). This may be done by assigning damage indices that are functions of the structural parameters or by evaluating the damage as the reduction in one or more of these parameters. Accordingly, identifying these parameters, whether modal or model parameters, is crucial for SHM application. Unfortunately, these parameters cannot be easily or directly mathematically derived from structural response but rather require extensive measurements and signal processing that are generally termed *system identification* techniques. System identification is the process of developing or improving a mathematical

representation of a physical system using experimental data (Juang, 1994). Thereafter, this model is used to estimate the properties of the dynamic system, such as stiffness, damping, frequencies, etc., through computational techniques that use the known input/output data.

System identification (SI) techniques to study the actual states of civil engineering structures have received considerable attention in recent years, as extensive full-scale experimental studies are expensive and often difficult to perform. Identification techniques are divided into frequency domain and time domain methods. Some of the key approaches among these techniques are discussed in the next two sections, followed by brief summaries of ERA/subspace approaches and some research in the literature that focuses specifically on structural model parameter identification.

2.4.1 Frequency Domain Techniques

Frequency-domain identification (parametric/non-parametric) techniques in control engineering and system identification gained relevance with stability and design methods based on frequency response measurements (Juang, 1994). This approach began with the technique known as transfer function (TF) analysis. Many frequency dependent methods, such as the empirical transfer-function estimate (ETFE), bootstrap methods, separable least squares methods, etc., are detailed by Ljung (1999).

One of the first methods that used the frequency domain data in the identification of the transfer function of the system was attributed to the efforts by Levy (1959). Levy's method, for a single-input-single-output (SISO) system was based upon expressing the TF in the form of frequency-dependent numerator $A(j\omega)$ and denominator $B(j\omega)$ polynomials as $H(j\omega) = B(j\omega)/A(j\omega)$ where ω is any frequency within the frequency range of interest in the specific problem. The experimental TF $\hat{H}(j\omega)$ is obtained from input/output measured data. Thereafter, Levy (1959) considered the difference between the experimental and theoretical TFs as the error $e(j\omega) = [B(j\omega)/A(j\omega)] - \hat{H}(j\omega)$; as minimizing the numerator of the error is computationally simpler, Levy uses the simpler form $\hat{e}(j\omega) = B(j\omega) - A(j\omega)\hat{H}(j\omega)$. Finally, by differentiating, with respect to the unknown coefficients of the polynomials $B(j\omega)$ and $A(j\omega)$, the norm of the sum of the squares of the simplified error evaluated at known frequencies, a number of equations (equivalent to the number of the unknown coefficients) are obtained. By solving these equations, the coefficients of $B(j\omega)$ and $A(j\omega)$ are obtained.

2.4.2 Time Domain Techniques

Time domain methods became quite popular as well later in the last century especially with the great advance of computational resources (Juang, 1994). Many time domain identification techniques are explained thoroughly in Ljung (1999). Some examples of time domain identification techniques are ARX, ARMA, ARMAX, recursive least squares, etc. Also, Beck *et al.* (1994a) presented a

methodology for determining the modal characteristics of a structure from its measured ambient vibration response at several instrumented locations, an extension of the MODE-ID algorithm that uses a Bayesian probability framework to build a linear model based on a classical normal modes approach (Beck, 1978; Beck, 1990).

2.4.3 ERA and Subspace Identification Techniques

One example of non-parametric time-domain methods is given by Juang and Pappa (1985), which proposed a method called the Eigensystem Realization Algorithm (ERA) for state-space identification from measured responses. This method uses a singular-value decomposition to derive the basic formulation for a minimum-order realization, which is an extended version of the Ho-Kalman algorithm (Ho and Kalman, 1965). First, a block Hankel matrix is obtained by arranging the pulse response data into the blocks of the Hankel matrix. By examining the singular values of the Hankel matrix, the order of the system is determined. A minimum-order realization (**A**, **B**, and **C** state-space matrices) is constructed using a shifted block Hankel matrix. By finding the eigensolution of the realized state matrix, modal damping ratios and frequencies may be obtained. The method then evaluates coherence and co-linearity accuracy parameters to separate system modes from noise modes. Based on these accuracy parameters, the system model is determined and the Hankel matrix based on identified state space matrices is reconstructed and compared with the measurement data.

Some modifications were later considered to improve the ERA method. Juang *et al.* (1988) introduced a modification to the ERA algorithm, using response

data correlations (ERA/DC) rather than the pulse response values in the formulation of the Hankel matrix. The ERA/DC modified method was found to reduce measurement noise bias without model over-specification. However, when over-specification is permitted and singular value decomposition is used to obtain a minimum order realization, both old and modified methods give equally good results for the data used.

Other subspace techniques have also been introduced and studied. Quek *et al.* (1999) introduced the Eigen-space Structural Identification technique for tall buildings subjected to stationary ambient excitations and based on the forward innovation model of the Kalman filter sequence. The method used QR decomposition and Quotient Singular Value Decomposition (QSVD) techniques, which are substituted into a least-square formulation to obtain a non-unique solution. Luş *et al.* (1999) presented an algorithm, based on the ERA and Observer/Kalman filter Identification (OKID) approaches, that uses earthquake-induced ground accelerations and structural vibrations as input/output data sets for identification purposes.

2.4.4 Structural Model Parameter Identification

Having accurate and updated information about the condition of structures, that may suffer hazardous shaking or loading, is crucial. This would save many lives as well as a lot of money. Accordingly, identifying the structural model parameters such as stiffness and damping is done to predict the behavior of structures under expected future loadings. Significant research effort, therefore, has been directed to

find methods to identify these parameters. Some methods, such as that by Takewaki *et al.* (2000), have studied the simultaneous stiffness-damping identification of building structures using limited earthquake records with higher intensity level. Other research has been based on probabilistic methods related to Bayesian theory, such as Vanik *et al.* (2000) and Katafygiotis and Yuen (2001).

The focus of model parameter identification to achieve SHM is usually on local loss of stiffness as a proxy for local damage (Capecchi and Vestroni, 1999; Caicedo *et al.*, 2001; Elmasry and Johnson, 2002; Beck *et al.*, 1994b, 2001). Some research has sought to identify relationships between change in the modal characteristics and changes in structural properties such as mass, stiffness, and damping. For example, Bayesian methodologies have been used for identifying the loss of structural stiffness, such as in Beck *et al.* (1994b, 2001). Bayes' theorem is invoked to develop a probability density function (PDF) for the model stiffness parameters conditioned on modal data and the chosen class of models. This method estimates the natural frequencies, damping ratios, and mode shape components of a linear model with classical normal modes that best fits the measured data in a least squares sense. Then, the parameters of the structural model are determined from the computed modal data. The critical assumption is that the change in the structural model implies changes in the parts of the real structure. As a first step, changes in the values of the modal parameters are identified and, then as a second step, the corresponding loss of stiffness within the structure is identified.

In other previous research work focusing on identifying model parameters, ambient vibration, such as ambient wind response measurements, is used for excitation. Béliveau and Chater (1984) outlined a procedure to estimate modal parameters (natural frequencies, and corresponding mode shapes) based on relatively simple ambient wind response measurements of story accelerations. Also, several other research studies have considered ambient vibration for identification of stiffness parameters and, in turn, stiffness loss, such as Beck *et al.* (1994, 2001), and Caicedo *et al.* (2001). Ray and Tian (1999) introduced a method, intended for smart structures embodying self-actuation and self-sensing capabilities, that enhances modal frequency sensitivity to damage using feedback control.

2.5 Variable Stiffness/Damping Devices

"Smart" variable stiffness/damping devices (VSDDs), such as semiactive dampers and controllable stiffness devices, are controllable passive devices that potentially offer the reliability of passive devices, yet maintain the versatility and adaptability of fully active systems (Dyke *et al.*, 1996). These devices have received significant study for mitigating various types of natural hazards for many types of civil structures (Spencer and Sain, 1997; Symans and Constantinou, 1999) and are useful for improving SHM.

2.5.1 Passive, Active and Semiactive Devices

Control devices for civil structures can be divided into four classes: passive, active, semiactive and hybrid. Passive devices, generally, are those that have fixed

properties and require no energy to function. In contrast, the controllable forces generated by active devices are induced directly by energy (electrical or otherwise) put into the device. Between passive and active are semiactive devices that are passive devices with properties that are controllable by application of a small amount of energy. Hybrid devices are combinations of the other three classes. Each of these is discussed briefly in the following paragraphs, with greater detail on semiactive devices.

Passive devices, such as visco-elastic dampers, viscous fluid dampers, friction dampers, metallic yielding dampers, tuned mass dampers, and tuned liquid dampers can partially absorb structural vibration energy and reduce response of the structure (Soong and Dargush, 1997). These passive devices are relatively simple and easily replaced. However, the effectiveness of passive devices is always limited due to the narrow frequency ranges in which they tend to be effective, the dependence of their force only on local information, and their inability to be modified if goals (or design codes) change.

Active control devices, including active mass dampers and active tendon systems, can reduce structural response more effectively than passive devices because feedback and/or feed-forward control systems are used (Housner *et al.*, 1997). However, large power requirements during strong earthquakes and other hazards hamper their implementation in practice. Further, active devices have the ability to inject dynamic energy into the structural system; if done improperly, this energy has the potential to cause further damage to the structure. In particular, this

can occur when the assumptions used to design the control algorithm are incorrect (*e.g.*, linear control design models for a nonlinear structure) or do not have a proper characterization of the structural dynamics.

In contrast, "smart" devices are controllable passive devices that require small amounts of power to control certain passive behavior. Moreover, these devices cannot add energy to the structural/mechanical system; rather, they may only (temporarily) store and dissipate energy. Furthermore, they offer highly reliable operation at a modest cost and can be viewed as fail-safe in that they default to passive devices should the control hardware malfunction (Dyke *et al.*, 1996).

2.5.2 Types of Semiactive Devices

Different types of semiactive devices have been developed recently. One type is the semiactive damper, such as a variable-orifice damper, a controllable fluid damper, or a controllable friction device. Variable-orifice dampers use an electromechanical variable orifice to alter the resistance to flow in a conventional hydraulic fluid. Controllable fluid dampers are passive hydraulic dampers containing a fluid, such as magnetorheological (MR) or electrorheological (ER) fluid, with controllable yield stress (Spencer *et al.*, 1997). Another type of semiactive device is a semiactive stiffness device such those developed by Kobori and Takahashi (1993), Patten *et al.* (1999) and Yang *et al.* (1996). They are on-off hydraulic devices capable of providing mainly variable damping and limited variable stiffness capability. Nagrarajaiah and Ma (1996) introduced a variable stiffness device that consists of four sets of spring elements and telescoping tube elements; varying the

position of the springs with a servomotor produces the continuously variable stiffness.

Controllable fluid dampers use fluids with properties that can be modified by some outside influence. MR or ER fluids change their properties in the presence of a magnetic or electric field, respectively. These fluids were originally developed in the 1940s (Rabinow, 1948; Winslow, 1949), but few applications were foreseen at that time. While ER fluids showed early promise for civil applications (see, *e.g.*, Ehrgott and Masri, 1992), most of the attention of the civil structural control community has shifted to using MR fluids due to their insensitivity to impurities, relatively constant behavior over a wide range of operating temperatures, and the low voltage required to activate them (Spencer *et al.*, 1997). MR dampers typically consist of a hydraulic cylinder containing micron-sized magnetically polarizable particles suspended within a fluid. In the presence of a magnetic field, the particles polarize and form particle chains that resist fluid flow. By varying the magnetic field, the mechanical behavior of an MR damper can be modulated. Since MR fluids can be changed from a viscous fluid to a yielding semisolid within milliseconds and the resulting damping force can be considerably large with a low-power requirement, MR dampers are applicable to large civil engineering structures.

2.5.3 Applications of Semiactive Control to Civil Structures

The idea of incorporating variable stiffness/damping devices in civil structures is not new. These devices have been extensively researched for base isolation of structures and other structural control applications, particularly in the last

decade. Some researchers have investigated MR dampers for control of seismic response such as Dyke *et al.* (1996), Spencer *et al.* (1997, 1998) and Yang *et al.* (2002). ER dampers were studied for seismic response control by Ehrgott and Masri (1992), Gavin *et al.* (1996a,b), Makris *et al.* (1996), and others. Dyke *et al.* (1996) proposed a clipped-optimal force control algorithm with acceleration feedback and obtained excellent results when this algorithm was applied to control a seismically excited three story scaled building model. Ribakov and Gluck (1999) investigated the effectiveness of ER dampers in mitigating seismic response of frame structures. They used an optimal linear passive control strategy to determine the viscous constant of the ER damper and then use active control strategy to determine control forces. Through numerical simulation they found that ER dampers could reduce the peak displacement response of a seven-story frame structure up to 65 per cent without increases in base shear forces and accelerations. In Xu *et al.* (2000), the force-displacement relationship of an MR damper or an ER damper, based on a parallel-plate model, is first extended to include the flexibility of the chevron brace supporting the smart damper. An extensive parameter study is performed in terms of the maximum yield shear stress and the Newtonian viscosity of the fluid, the brace stiffness, and the earthquake intensity. VSDDs are also studied for damping of stay cables in suspended bridges. Johnson *et al.* (2003) investigated the potential of improving the damping to these cables through the use of semiactive damping devices. The response of the cables with a semiactive damper is found to be reduced dramatically compared to the optimal passive linear viscous damper for typical

damper configurations, thus demonstrating the efficacy of a semiactive damper for absorbing cable vibratory energy. Varadarajan and Nagrarajaiah (2000) introduce the use of a semiactive variable stiffness tuned mass damper to control the response of tall buildings excited by wind. Using the semiactive variable stiffness tuned mass damper is able to reduce the response similar to using an active tuned mass damper.

2.5.4 Experimental and Full Scale Studies Using Semiactive Devices

Since theoretical VSDD research has shown significant promise, researchers have progressed to experimental work to apply semiactive control in real world applications. Symans and Constantinou (1997) describe shaking table tests of a multi-story scale-model building structure subjected to seismic excitation and controlled by a semiactive fluid damper control system. The semiactive dampers were installed in the lateral bracing of the structure and the mechanical properties of the dampers were modified according to control algorithms that utilized the measured response of the structure.

Patten *et al.* (1999) reported the first successful full scale demonstration of semiactive control technology, installing an Intelligent Stiffener for Bridges (ISB) on an in-service bridge on interstate I-35. The ISB consists of an otherwise generic stiffener, retrofitted to a bridge, that is equipped with an adjustable hydraulic link used to regulate the amount of stiffness (and damping) provided by the stiffener as vehicles pass over the bridge. The ISB acts much like a muscle, sometimes flexing, and other times remaining relaxed. A 12-volt automobile battery energizes the ISB.

The performance of the system was assessed via experimental results (see Fig. 2-1). The results indicate that the ISB system can add decades of service life to an existing bridge.

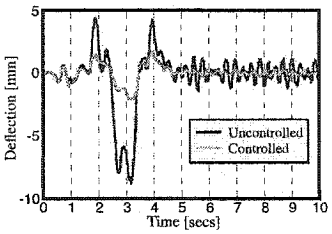

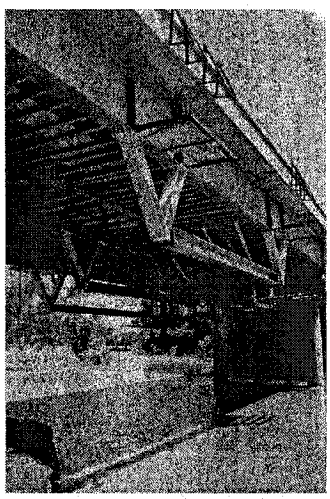

Fig. 2-1. ISB vibration absorber on I-35 bridge (Patten *et al.*, 1999)

The Kajima Corporation has developed a semiactive hydraulic damper (SHD) and installed it in an actual building (Kurata *et al.*, 2000). This was the first application of a semiactive seismic building control system that continuously changes the device damping coefficient. A forced vibration test was carried out by an exciter with a maximum force of 100 kN to investigate the building vibration characteristics and to determine the control system performance. As a result, the primary resonance frequency and the damping ratio of a building (without semiactive hydraulic dampers) decreased as the exciting force increased due to the influence of non-linear members such as plain concrete curtain walls. After the eight semiactive hydraulic dampers were installed in the building, the control system performance was identified by a response control test for steady-state vibration. The elements that composed the semiactive damper system demonstrated the specified performance and the whole system operated successfully, considerably reducing the displacements at the roof of the structure.

To prove the scalability of MR fluid technology to devices of size appropriate for civil engineering applications, Yang *et al.* (2002) study an MR fluid damper with a nominal maximum damping force of 200 kN (20 tons). For design purposes, two quasi-static models, an axisymmetric and a parallel-plate model, are derived for the force-velocity relationship of the MR damper, and both models give results that closely match the experimental data.

3 PARAMETRIC FREQUENCY DOMAIN AND SUBSPACE IDENTIFICATION WITH VSDDs

3.1 Introduction

This chapter investigates, analytically, whether variable stiffness and damping devices can be effectively used to identify local damage in structures. This study is based on simulation of structural motion due to ambient excitation. Using one or more variable stiffness and damping devices (VSDDs) to modify the response, structural parameters are estimated. Two of the identification methods used herein to identify the structure model parameters are based on a least-squares error convergence technique and conventional frequency domain structural identification. One simplification that is discussed in the literature (Levy, 1959) is used to overcome the complexity of the direct transfer function polynomial identification. An iterative method, based on Levy (1959), is proposed that approximates the more direct exact method. Also, a modified frequency domain identification technique, the INVFREQS-Least Squares method, is introduced. The derivation of the new method is given and a numerical example is used to demonstrate the effectiveness of the VSDD approach. Later in this chapter, it is shown that increasing the stiffness and damping levels that are induced by the VSDDs in the structures gives even better results compared to the conventional structure approach. In addition, the Eigensystem Realization Algorithm (ERA), a subspace technique, is described and

applied with the VSDD approach. The work in this chapter is adapted from METRANS project 01-10 and 03-17 reports (Johnson and Elmasry, 2003, 2005a), and from Elmasry and Johnson (2002, 2004a), and Johnson and Elmasry (2005b).

3.2 Least Squares Numerator Method (LSN)

One method of identifying parameters of a dynamical system is by representing transfer functions (TFs) in the frequency domain as ratios of polynomials. For simplicity, in the method developed herein, the input force is assumed to be a single scalar force. The transfer functions generally are defined by the ratio between the Fourier transforms of the output and input signals. For example, consider a linear structural model of the form:

$$\mathbf{M}\ddot{\mathbf{x}} + \mathbf{C}_d\dot{\mathbf{x}} + \mathbf{K}\mathbf{x} = \mathbf{b}f\,, \quad \mathbf{y} = \mathbf{C}_1\mathbf{x} + \mathbf{C}_2\dot{\mathbf{x}} + \mathbf{d}f + \mathbf{v} \tag{3-1}$$

where $\mathbf{M}$, $\mathbf{K}$, and $\mathbf{C}_d$ are the mass, stiffness and damping matrices of the system, and $\mathbf{C}_1$, $\mathbf{C}_2$, and $\mathbf{d}$ are the output influence matrices for the displacement, velocity and the external force f. Similarly, one can write the model in state-space form

$$\dot{\mathbf{q}} = \tilde{\mathbf{A}}\mathbf{q} + \tilde{\mathbf{B}}f\,, \qquad \mathbf{y} = \mathbf{C}\mathbf{q} + \mathbf{D}f + \mathbf{v} \tag{3-2}$$

where $\mathbf{q} = \begin{bmatrix}\mathbf{x}^T & \dot{\mathbf{x}}^T\end{bmatrix}^T$ is the state vector, $\tilde{\mathbf{A}}$ is the system state matrix that is dependent on the mass, damping, and stiffness matrices, $\tilde{\mathbf{B}}$ is the input influence matrix, $\mathbf{C}$ is the output influence matrix for the state vector $\mathbf{q}$, and $\mathbf{D}$ is the direct transmission matrix. In both equations, f is an excitation force, and $\mathbf{y}$ is a $m \times 1$ vector of measured responses corrupted by $m \times 1$ sensor noise vector $\mathbf{v}$.

Thus, the system can be represented by the $m \times 1$ transfer function matrix $\mathbf{H}(j\omega)$. Each element of $\mathbf{H}(j\omega)$ can be expressed as the ratio of numerator and denominator polynomials at a certain frequency with coefficients depending on matrices in Eqs. (3-1) or (3-2). It is important to state that, for many structural systems, the denominator polynomial is the same for all transfer functions from the same input. Therefore, identifying the denominator polynomial is crucial in defining the system dynamics. The transfer function vector from a single input to the outputs can, consequently, be written in polynomial ratio form as:

$$\mathbf{H}(j\omega) = \mathbf{B}(j\omega) / A(j\omega) \tag{3-3}$$

where $\mathbf{B}(j\omega)$ and $A(j\omega)$ are the numerator and denominator polynomials, which may be expanded as:

$$\begin{aligned} B_r(j\omega) &= b^r_{n_B-1}(j\omega)^{n_B-1} + b^r_{n_B-2}(j\omega)^{n_B-2} + \ldots + b^r_0 \\ A(j\omega) &= (j\omega)^{n_A} + a_{n_A-1}(j\omega)^{n_A-1} + \ldots + a_0 \end{aligned} \tag{3-4}$$

where the b's and a's are real coefficients.

Assuming that the transfer function has been determined experimentally through standard procedures from measured input and output data (Bendat and Piersol, 2000), the experimental transfer function matrix, expressed as

$$\hat{\mathbf{H}}(j\omega_i), \; i=1, 2, \ldots, n_\omega \tag{3-5}$$

is known at various discrete frequency points. Therefore, the difference between the estimated theoretical transfer function $\mathbf{H}(j\omega)$ and the actual experimental one $\hat{\mathbf{H}}(j\omega)$

represents the error equation, which is then used in the parameter identification process.

Parametric frequency-domain methods to match such theoretical and measured transfer functions date back to the work of Levy (1959) who parameterized a continuous-time TF by the coefficients of numerator and denominator polynomials. One approach to this problem is to follow Levy's procedure in determining the polynomial coefficients and then, as a subsequent step, estimate structural parameters such as mass, stiffness and damping coefficients. The latter could be through an intermediate step of first identifying modal characteristics such as modal frequency, damping ratio and mode shapes. In this study, however, the parameterization method is chosen to be through the structural parameters directly without calculating the coefficients of the polynomials as an intermediate step.

For a structure with one or more variable stiffness and/or damping devices, the properties of which are determined through a local control system, some of the coefficients in the transfer function polynomials may be adjusted through changing the VSDD control algorithms. Thus, it is convenient to introduce notation to explicitly state that the transfer function polynomials are functions of unknown structural parameters, denoted by the $n \times 1$ vector $\boldsymbol{\theta}$, which is to be estimated, and of known controllable structural parameters, denoted by the vector $\boldsymbol{\kappa}$. The transfer function expression is thus modified to be:

$$\mathbf{H}(j\omega) = \mathbb{B}(j\omega, \boldsymbol{\theta}, \boldsymbol{\kappa}) / A(j\omega, \boldsymbol{\theta}, \boldsymbol{\kappa}) \tag{3-6}$$

For a given structural model, the A and $\mathbf{B}$ polynomials are specific known functions of their parameters. Substituting the measured TF in place of the exact TF leaves a residual error $\mathbf{e}$ that may be defined by

$$\mathbf{e}(j\omega_i, \boldsymbol{\theta}, \boldsymbol{\kappa}) = \frac{\mathbf{B}(j\omega_i, \boldsymbol{\theta}, \boldsymbol{\kappa}) - A(j\omega_i, \boldsymbol{\theta}, \boldsymbol{\kappa})\hat{\mathbf{H}}(j\omega_i, \boldsymbol{\kappa})}{A(j\omega_i, \boldsymbol{\theta}, \boldsymbol{\kappa})} \tag{3-7}$$

A conventional least-squares approach may be adopted to solve this problem, forming a global square error

$$\Delta^2(\boldsymbol{\theta}) = \sum_i \mathbf{e}^*(j\omega_i, \boldsymbol{\theta}, \boldsymbol{\kappa}) \cdot \mathbf{e}(j\omega_i, \boldsymbol{\theta}, \boldsymbol{\kappa}) \tag{3-8}$$

where $(\cdot)^*$ denotes complex conjugate transpose. The optimal choice of the unknown parameters is found by minimizing the square error — *i.e.*, take the derivatives of the square error Eq. (3-8) with respect to the elements of unknown vector $\boldsymbol{\theta}$, set them equal to zero, and solve the resulting (generally nonlinear) equations. However, if there are known controllable structural parameters in a structure with multiple configurations — which is the case when using VSDDs, for example — the square error equation can be augmented by using several combinations of known controllable structural parameters

$$\Delta^2(\boldsymbol{\theta}) = \sum_k \sum_i \mathbf{e}^*(j\omega_i, \boldsymbol{\theta}, \boldsymbol{\kappa}_k) \cdot \mathbf{e}(j\omega_i, \boldsymbol{\theta}, \boldsymbol{\kappa}_k) \tag{3-9}$$

where the symbol $\boldsymbol{\kappa}_k$ denotes one of multiple distinct sets of parametric changes to the structure. The error is, then, minimized simultaneously for all configurations.

Because the residual error $\mathbf{e}$ in Eq. (3-7) is a ratio of polynomials, the square error in Eq. (3-9) is an extremely complex function of the unknown parameters $\boldsymbol{\theta}$. One simplification, which has been suggested and used in various studies in the literature, is to recognize that the denominator of Eq. (3-7) is nonzero for systems with damping, so minimizing the error in the numerator may prove sufficient (*e.g.*, Levy, 1959). In other words, minimize the sum of the squares of:

$$\tilde{\mathbf{e}}(j\omega_i,\boldsymbol{\theta},\boldsymbol{\kappa}_k) = \mathbf{B}(j\omega_i,\boldsymbol{\theta},\boldsymbol{\kappa}_k) - A(j\omega_i,\boldsymbol{\theta},\boldsymbol{\kappa})\hat{\mathbf{H}}(j\omega_i,\boldsymbol{\kappa}_k) \tag{3-10}$$

which is, herein, denoted the *least-squares numerator* (LSN) method.

3.3 Iterative-Least Squares Numerator Method (ILSN)

It may be shown that the alternate error measure Eq. (3-10) in the LSN method, while simpler to solve, can be susceptible to strong bias from sensor noise in frequency ranges where $A(j\omega_i,\boldsymbol{\theta},\boldsymbol{\kappa})$ is large (*i.e.*, often the case where $\mathbf{H}(j\omega)$ is small). To avoid this bias, and to avoid the difficulty in solving the least-squares problem for the standard error measure $\mathbf{e}$, an *iterative* method, described as follows, is adopted here using an approximation to the denominator in Eq. (3-7).

Assume that iteration l begins with a starting approximation $\hat{\boldsymbol{\theta}}_{l-1}$ to the unknown parameter vector $\boldsymbol{\theta}$; then, the denominator of Eq. (3-7) is estimated based on the vector $\hat{\boldsymbol{\theta}}_{l-1}$ of estimated parameters and is no longer a function of these unknowns, but only in the frequency and the multiple distinct sets of parametric changes to the structure

$$\hat{A}_l(j\omega_i, \boldsymbol{\kappa}_\kappa) \equiv A(j\omega_i, \hat{\boldsymbol{\theta}}_{l-1}, \boldsymbol{\kappa}_\kappa) \tag{3-11}$$

The error is, thus, formed as:

$$\hat{\mathbf{e}}_l(j\omega_i, \boldsymbol{\theta}, \boldsymbol{\kappa}_\kappa) = \frac{\mathbf{B}(j\omega_i, \boldsymbol{\theta}, \boldsymbol{\kappa}_\kappa) - A(j\omega_i, \boldsymbol{\theta}, \boldsymbol{\kappa}_\kappa)\hat{\mathbf{H}}(j\omega_i, \boldsymbol{\kappa}_\kappa)}{\hat{A}_l(j\omega_i, \boldsymbol{\kappa}_\kappa)} \tag{3-12}$$

And the squared error takes the form:

$$\Delta_l^{\,2}(\boldsymbol{\theta}) = \sum_k \sum_i \hat{\mathbf{e}}_l^{\,*}(j\omega_i, \boldsymbol{\theta}, \boldsymbol{\kappa}_\kappa) \cdot \hat{\mathbf{e}}_l(j\omega_i, \boldsymbol{\theta}, \boldsymbol{\kappa}_\kappa) \tag{3-13}$$

Minimizing the sum of the square error in Eq. (3-13) will result in an updated estimate $\hat{\boldsymbol{\theta}}_l$ to the unknown parameter vector $\boldsymbol{\theta}$. The iterations continue until the relative differences between $\hat{\boldsymbol{\theta}}_{l-1}$ elements and the corresponding elements of $\hat{\boldsymbol{\theta}}_l$ are all below some threshold. (Absolute or relative norms of the difference could also be used.) A maximum number of iterations may also be set to stop the algorithm in the case that the iterative method does not converge (though this termination criterion was not required in this study as convergence always occurred within a limited number of iterations).

Whichever method is used to estimate the unknown parameter vector $\boldsymbol{\theta}$, the use of multiple structural configurations, denoted by the different values of known parameters $\boldsymbol{\kappa}_k$, provided by VSDDs in a structure, can generate more accurate estimates of $\boldsymbol{\theta}$ than with a comparable amount of data in a conventional structure with a fixed $\boldsymbol{\kappa}$. This is demonstrated for some examples in the following section.

3.4 Illustrative Examples

The least-squares identification with VSDDs may be applied to various types of structures. In this study, both building and bridge models are considered.

3.4.1 Two Degree-of-Freedom Shear Building Model

Consider the two degree-of-freedom (2DOF) shear building structure model shown in Fig. 3-1. The structure is subject to ambient excitation from the ground. Absolute acceleration measurements of the ground, $\ddot{x}_g$, and of the two floors, $(\ddot{x}_1 + \ddot{x}_g)$ and $(\ddot{x}_2 + \ddot{x}_g)$, are used to generate a 2×1 experimental transfer function at n_ω distinct frequency values. (Note that x_i herein denotes the displacement of the i^{th} floor relative to the ground.)

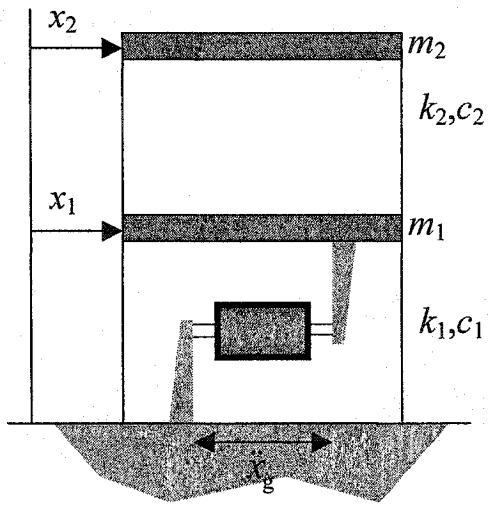

Fig. 3-1. 2DOF shear building model

Let the unknown parameter vector be given by:

$$\theta = \left[\frac{k_1}{m_1} \quad \frac{k_2}{m_2} \quad \frac{c_1}{m_1} \quad \frac{c_2}{m_2} \quad \frac{m_2}{m_1} \right]^T \tag{3-14}$$

A VSDD that can provide a number of distinct stiffness levels is located in the first story of the structure. The VSDD is installed in the lateral bracing of the

structure and the mechanical properties of the dampers are modified according to control algorithms, which utilize the measured response of the structure. The device is considered ideal and semiactive; *i.e.*, it can generate the desired forces with no delay and with no actuator dynamics (Ramallo *et al.*, 2000).

Therefore, the known controllable vector is related to the stiffness of a variable stiffness device such that

$$\boldsymbol{\kappa} = \kappa = k_{VSDD} / m_1 \tag{3-15}$$

or to the damping coefficient of a variable damping device

$$\boldsymbol{\kappa} = \kappa = c_{VSDD} / m_1 \tag{3-16}$$

Then, the theoretical transfer function can be written in the polynomial form as:

$$\mathbf{H}(j\omega,\kappa) = \left[\frac{\mathbf{B}_1(j\omega,\boldsymbol{\theta},\kappa)}{A(j\omega,\boldsymbol{\theta},\kappa)} \quad \frac{\mathbf{B}_2(j\omega,\boldsymbol{\theta},\kappa)}{A(j\omega,\boldsymbol{\theta},\kappa)} \right]^{\mathrm{T}} \tag{3-17}$$

Note that the denominator polynomial $A(j\omega,\boldsymbol{\theta},\kappa)$ is the same for all transfer functions from the same input. The numerator and denominator polynomials can be expressed as:

$$\begin{aligned} A(s,\boldsymbol{\theta},\kappa) &= s^4 + (\theta_3 + \theta_4 + \theta_4\theta_5)s^3 + (\theta_1 + \theta_2 + \theta_2\theta_5 + \theta_3\theta_4 + \kappa)s^2 \\ &\quad + (\theta_1\theta_4 + \theta_2\theta_3 + \kappa\theta_4)s + (\theta_1\theta_2 + \kappa\theta_2) \\ \mathbf{B}_1(s,\boldsymbol{\theta},\kappa) &= (\theta_3)s^3 + (\theta_1 + \theta_3\theta_4 + \kappa)s^2 + (\theta_1\theta_4 + \theta_2\theta_3 + \kappa\theta_4)s + (\theta_1\theta_2 + \kappa\theta_2) \\ \mathbf{B}_2(s,\boldsymbol{\theta},\kappa) &= (\theta_3\theta_4)s^2 + (\theta_1\theta_4 + \theta_2\theta_3 + \kappa\theta_4)s + (\theta_1\theta_2 + \kappa\theta_2) \end{aligned} \tag{3-18}$$

The parameter identification methods discussed in the previous section can then be applied. The explicit reference to m_1 has dropped out of the transfer function polynomials; it will be assumed here that of all the parameters, only m_1 is known.

Different VSDD locations in the structure are studied in order to investigate the best way of using these VSDDs to improve SHM through better identification of the structural model parameters. Accordingly, this example is also solved considering a VSDD that can provide a number of distinct stiffness levels located in the second story of the structure and in both stories as well, as shown in Fig. 3-2 and Fig. 3-3. This will generally give an idea of how VSDDs should be distributed in a structure for good SHM. In all cases, the VSDD is chosen to act as an ideal variable stiffness/damping device, with one of several discrete stiffness/damping values. Some examples from simulation are used to demonstrate the proposed method.

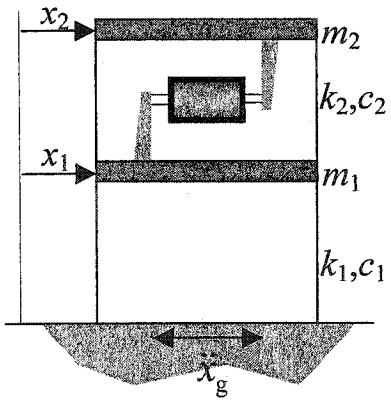

Fig. 3-2. VSDD in 2nd story of 2DOF model

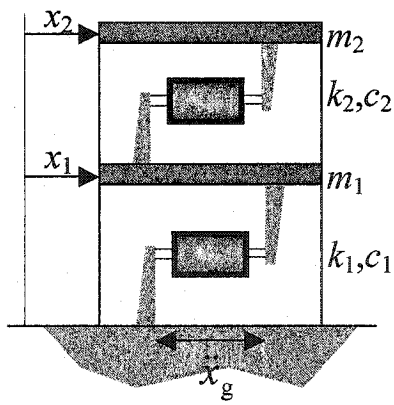

Fig. 3-3. VSDDs in both stories of 2DOF model

This 2DOF model system identification was solved for the variable stiffness VSDD and for a conventional structure (no VSDD). In the simulations, each installed VSDD is assumed to provide additional stiffness at five discrete levels: 0%, 10%, 20%, 30% and 40% of the stiffness of the story at which it is located.

3.4.2 Two Degree-of-Freedom Pier-Deck Bridge Model

Consider a bridge structure such as the one shown in Fig. 3-4, which is a typical elevated highway bridge that consists of decks, bearings, and piers. The behavior of the bridge deck and piers, with a bearing between them, while complex, can be well approximated with the simple 2DOF model shown in Fig. 3-5*c*. This 2DOF model may be used to represent a passive system with rubber bearings if the girder is continuous with one pier and one bearing, or for several piers and bearings with identical properties. Also, this model can be used for VSDD systems if the devices are attached as shown in Fig. 3-6 and commanded to provide identical force levels. It is assumed in this problem that the pier mass m_1 is known.

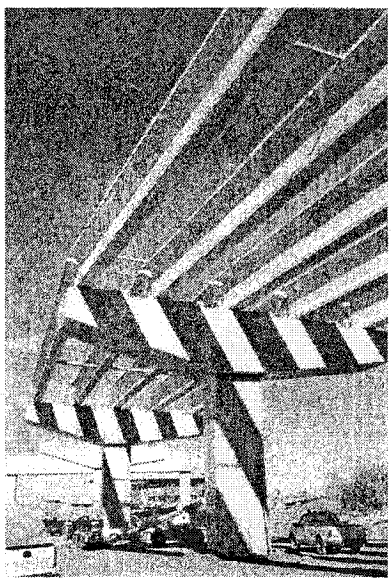

Fig. 3-4. General view during construction of high occupancy vehicle (HOV) lanes (ADOT, 2001)

The theoretical polynomial transfer function matrix $\mathbf{H}(j\omega,\kappa)$ is defined similarly to Eq. (3-17) where, here, $\mathbf{B}_1(j\omega,\theta,\kappa)/A(j\omega,\theta,\kappa)$ is the transfer function

between the ground acceleration and the absolute acceleration of the pier and $\mathbf{B}_2(j\omega,\boldsymbol{\theta},\kappa)/A(j\omega,\boldsymbol{\theta},\kappa)$ is the transfer function between the ground acceleration and that of the bridge deck. The unknown parameter vector $\boldsymbol{\theta}$ is defined similarly to Eq. (3-14). The vector of known parameters $\boldsymbol{\kappa}$ denotes the additional stiffness added through the VSDD connected between the pier and the deck. In the simulations, the installed VSDD is assumed to provide additional stiffness at five discrete levels: 0%, 10%, 20%, 30% and 40% of the stiffness of the deck. A second related example will use five similar discrete levels of VSDD damping instead of stiffness.

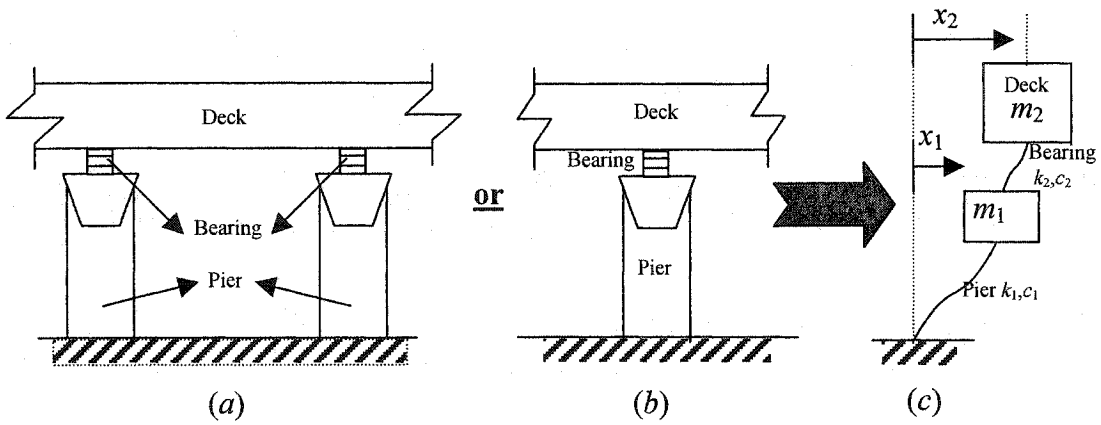

Fig. 3-5. 2DOF bridge model

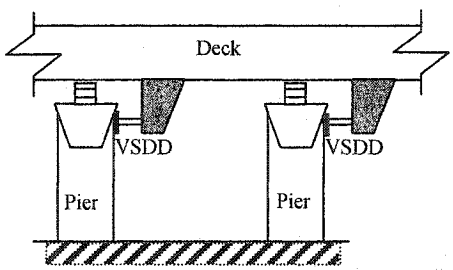

Fig. 3-6. Placement of VSDDs in bridge

3.4.3 Six Degree-of-Freedom Shear Building Model

To demonstrate that these methods can be extended to more complex problems, a six degree-of-freedom shear building model is also studied. The shear building model is found to be a good representation for general problems that may exist in multi-story (or multi-degree-of-freedom (MDOF)) structures. This 6DOF model system identification was solved for the variable stiffness VSDD and the conventional structure (no VSDDs). In simulation, each installed VSDD is assumed to provide additional stiffness at four discrete levels: 0%, 10%, 20%, and 30% of the stiffness in the story at which it is located. The VSDD devices included in the structure are also considered ideal; *i.e.*, they can generate the desired forces with no delay and with no actuator dynamics. In this problem, the VSDDs are considered to be located in the first three stories only, as shown in Fig. 3-7.

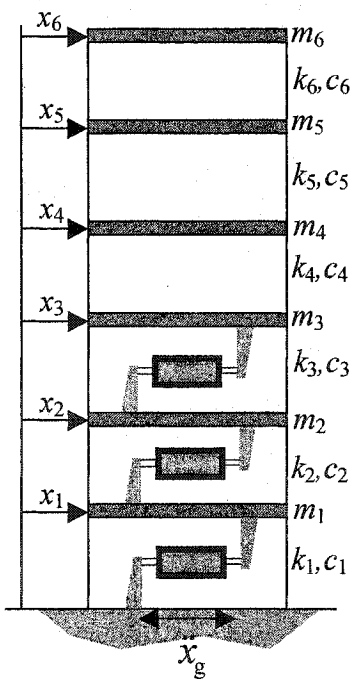

Fig. 3-7. 6DOF model with VSDDs in first three stories

In this example, the masses are assumed known *a priori* whereas the previous 2DOF model assumed knowledge only of the first mass. The unknown parameter vector $\boldsymbol{\theta}$ for the six degree-of-freedom model is, then, a set of unknown stiffness k_i and damping c_i coefficients as follows:

$$\boldsymbol{\theta}=[k_1 \;\; k_2 \;\; k_3 \;\; k_4 \;\; k_5 \;\; k_6 \;\; c_1 \;\; c_2 \;\; c_3 \;\; c_4 \;\; c_5 \;\; c_6]^T \tag{3-19}$$

Finally, the solution for the parameters was done using the MATLAB® software and using the function `fsolve()` for the solution of the non-linear equations in the unknown parameters $\boldsymbol{\theta}$. It is important to note that applying the ILSN method for estimation of parameters in case of higher degrees of freedom (such as the 6DOF model) was very challenging in terms computational speed and memory.

3.5 NUMERICAL EXAMPLES AND ANALYSIS OF RESULTS

To demonstrate the benefits and the advantages of testing a structure with VSDDs configured in multiple settings, some numerical examples are considered.

3.5.1 Two Degree-of-Freedom Shear Building Model

First, a numerical example of the 2DOF structure is studied. For simplicity, the floor masses and story stiffnesses are taken to be unity in the numerical model. The story damping coefficients are set to 0.05, which results in 1.5% and 4.0% modal damping in the two modes, respectively. The single VSDD is assumed to provide additional stiffness in the story at which it is located with five discrete stiffness levels, corresponding to an additional 0%, 10%, 20%, 30% and 40%

stiffness; *i.e.*, $\kappa_1 = 0.0$, $\kappa_2 = 0.1$, ..., $\kappa_5 = 0.4$. The primary comparison reported here is the difference between:

- The *VSDD* approach, using five experimental transfer function matrices, one per VSDD stiffness level, and
- The conventional structure approach with $\kappa = 0.0$ — to make for a fair comparison using the same amount of data, the conventional approach uses a square error based on five separate experimental transfer functions.

The experimental transfer functions are generated in MATLAB® by using the exact transfer functions plus the Fourier transform of a Gaussian pulse process that would be typical of band-limited Gaussian white sensor noise vector processes. The sensor noise used in generating the five experimental *VSDD* transfer functions is the same as those used for the conventional structure approach. The number of evenly spaced frequency points, n_ω, is taken equivalent to 51.

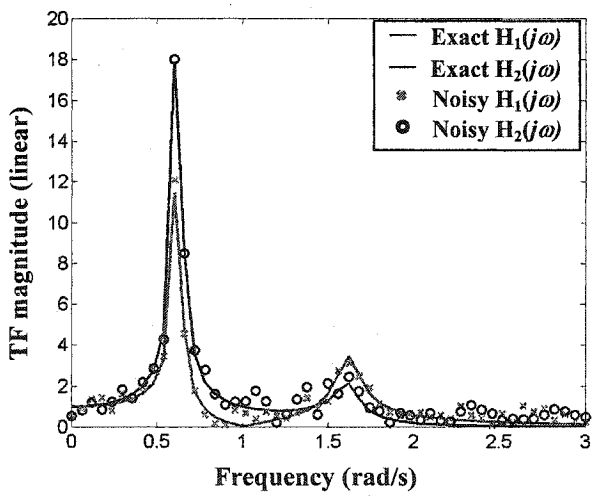

Fig. 3-8. Exact and noisy TF magnitudes (linear scale)

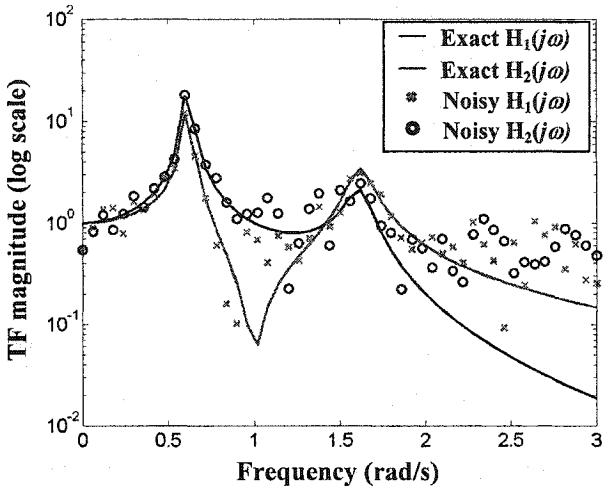

Fig. 3-9. Exact and noisy TF magnitudes (log scale)

Fig. 3-8 and Fig. 3-9 show a comparison, in both linear and log scales, of the exact transfer function magnitudes that represents the true model with those of the experimental transfer function corrupted by a quite challenging noise, when VSDD stiffness is zero.

Once the experimental transfer functions are generated, MATLAB® code employing the Symbolic Math Toolbox™ is used to determine the total square error symbolically. The result is then differentiated with respect to the unknown parameter vector $\boldsymbol{\theta}$, giving a number of equations that should equal zero. These equations, which are cubic polynomials in $\boldsymbol{\theta}$ for the parameterization in Eq. (3-14), are solved numerically using the `fsolve()` function in the Optimization Toolbox™ of MATLAB® with function tolerances and $\boldsymbol{\theta}$ solution tolerances both set to 10^{-5}. The iterative approach uses a relative tolerance of 10^{-4} (which must be met for all elements of the unknown parameter vector $\boldsymbol{\theta}$) as a termination criterion.

3.5.1.1 Least-Squares Numerator Method Results

First, the expected bias in the LSN method is verified by minimizing the sum of the squares of the numerator error in Eq. (3-10). The VSDD and conventional structure approaches are used to determine the unknown parameters. Each approach is performed 26 times, with different seed sets for generating the random noise, to see the distribution of estimation error that may be expected with the least-squares numerator method. The initial guess provided to the numerical equation solver is the exact value.

Fig. 3-10, which shows the error in the stiffness estimates for the 26 trials, demonstrates that both approaches give significant error in the estimates as well as a wide systematic bias. This bias is expected, as the denominator magnitude is quite large for higher frequency points as shown in Fig. 3-11, causing the noise to significantly skew the parameter estimates.

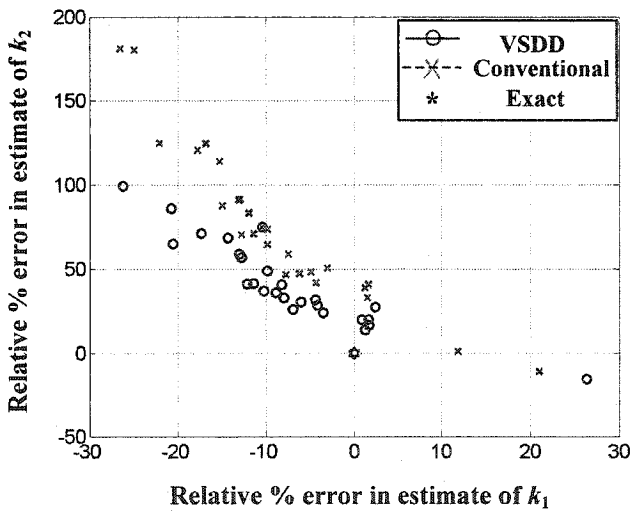

Fig. 3-10. Stiffness estimate error levels with least-squares numerator method

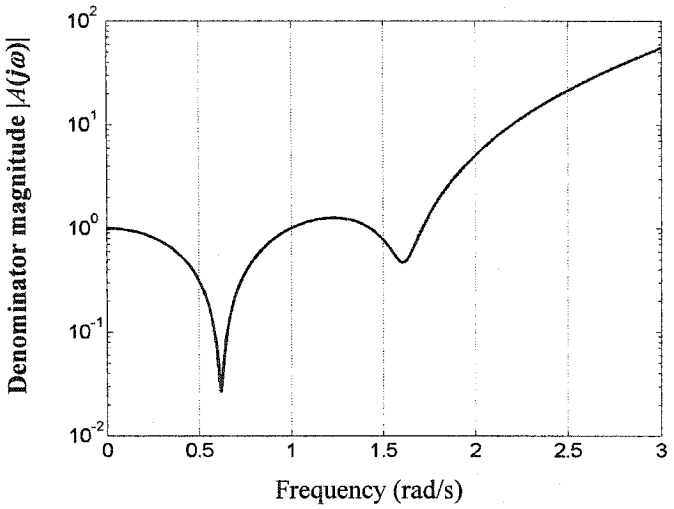

Fig. 3-11. Denominator magnifies error at higher frequency with LSN method

Therefore, one can conclude that, as expected, this simplified technique cannot be adopted for fair comparison between the VSDD and conventional structure approaches because the results are not accurate with either approach.

3.5.1.2 Results with the Iterative Method

The iterative approach gives significantly better results in contrast with the LSN method. Using the true parameter vector as an initial starting guess for the iterative procedure, the algorithm converges, generally in 3–5 iterations, to estimates that are fairly accurate — much better than the least-squares numerator method.

3.5.1.2.1 VSDD in First Story

Fig. 3-12 shows the relative error in the estimates of the stories stiffness for the conventional structure and VSDD approaches. Here, 100 separate estimates were computed (each with a different noise seed) to examine the variation due to sensor

noise. The graph also shows approximate one-, two- and three-sigma (standard deviation) curves for the two approaches. The curves are generated, assuming a Gaussian distribution, using the means and covariance matrix of the 100 estimates. The variation in stiffness estimates of first- and second-story using VSDD approach are about half and two-thirds of those using the conventional structure approach.

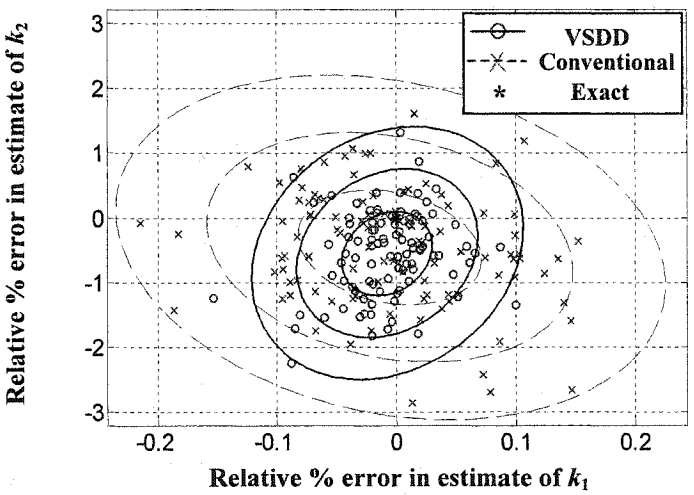

Fig. 3-12. Stiffness estimate error levels for iterative method with exact start for 2DOF model with VSDD in 1st story only

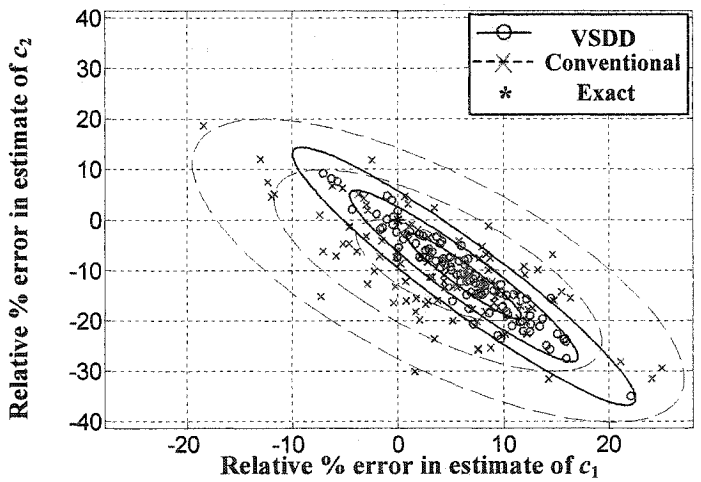

Fig. 3-13. Damping estimate error levels for the iterative method with exact start for 2DOF model with VSDD in 1st story only

Damping estimates are, as expected, much less accurate for both approaches. Fig. 3-13 shows the error variation in damping coefficient estimates using the ILSN method, and demonstrates that the VSDD approach has again generated a smaller variation as sensor noise changes. The maximum (absolute) three-sigma limits in this case are somewhat larger than that of the stiffness estimates: equals 22% using VSDDs and 27% for the conventional structure approach estimating the damping coefficient in the first floor c_1; 36% and 40% for estimating the damping coefficient in the second floor c_2. This larger relative damping estimate error, for both VSDD and conventional structure approaches, compared to stiffness, is typical of most identification methods. Yet, it is clear that the VSDD approach, while not making vast improvements, shows some decrease in error compared to the conventional approach.

An initial guess that is biased, offset from the correct parameter vector by some amount, would be expected to give poorer estimates. This is indeed the case. Using an initial parameter vector that is 20% higher (in all components) than the exact values, 20 separate estimates were computed. Fig. 3-14 shows that both approaches, as anticipated, are much less accurate in estimating the story stiffnesses than with the exact initial guess. Here, the VSDD approach gives estimate means that are less biased than the conventional structure approach, though with slightly larger variation in the estimate of k_1. Again, this indicates that using VSDDs improved the stiffness estimates.

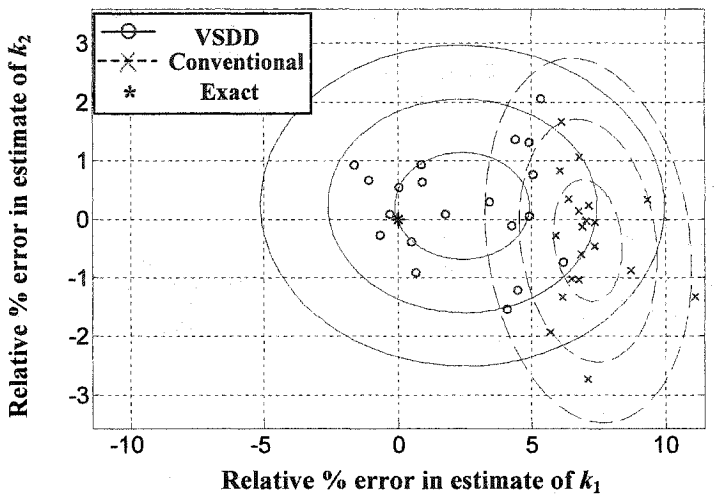

Fig. 3-14. Stiffness estimate error levels for the iterative method with offset start for 2DOF model with VSDD in 1st story only

The computational effort to solve these problems symbolically was much higher than anticipated. To compute one estimate with the correct initial starting guess took approximately 15 minutes on a 600 MHz Pentium III computer. With an offset starting guess, more iterations were required, both in the iterative approach outlined above as well as within the numerical solver `fsolve( )`, requiring slightly longer time to converge. The estimate means and coefficients of variation are shown for the two approaches in Table 3-1. The average number of iterations required for the MATLAB® solver to converge are always less in case of VSDD approach than the conventional structure approach as shown in Table 3-1.

Table 3-1. Estimate Means and Coefficients-of-Variation for 2DOF Shear Building Model

Var.	Exact	Mean				Coeff. of Variation [%]			
		Exact Init. Guess		*Offset Init. Guess*		*Exact Init. Guess*		*Offset Init. Guess*	
		Conv. St.	VSDD	Conv. St.	VSDD	Conv. Struct.	VSDD	Conv. Struct.	VSDD
θ_1	1	0.9999	0.9999	1.0711	1.0241	0.0770	0.0390	1.1990	2.4560
θ_2	1	0.9972	0.9970	0.9337	0.9845	0.5310	0.3660	1.2620	1.8750
θ_3	0.05	0.0519	0.0531	0.0523	0.0521	7.4810	5.0920	6.2690	7.1560
θ_4	0.05	0.0450	0.0445	0.0477	0.0460	11.224	9.5930	9.2310	13.491
θ_5	1	0.9982	0.9975	1.0672	1.0183	0.3780	0.2950	1.1220	1.8370
k_1	1	0.9999	0.9999	1.0711	1.0241	0.0770	0.0390	1.1990	2.4560
k_2	1	0.9955	0.9945	0.9964	1.0023	0.8930	0.6570	1.0410	0.9100
c_1	0.05	0.0519	0.0531	0.0523	0.0521	7.4810	5.0920	6.2960	7.1560
c_2	0.05	0.0449	0.0444	0.0509	0.0469	11.163	9.6220	9.1460	14.165
m_2	1	0.9982	0.9975	1.0672	1.0183	0.3780	0.2950	1.1220	1.8370
Average No. of Iterations		4.98	4.06	5.05	4.85				

3.5.1.2.2 VSDD in Second or Both Stories

To understand the effect of VSDD location(s) on the estimation, this 2DOF numerical example is modified to consider a VSDD in the second story and in both stories. The parametric frequency domain identification is applied and the results with a VSDD in the second story or one in each of the two stories are compared with those in conventional structure case.

From Fig. 3-15, it can be observed that the variation of the stiffness in the second story was clearly reduced, giving better identification of the second-story stiffness compared to a VSDD in the first story only. However, the variation in estimation of the first-story stiffness k_1 is larger with the second-story VSDD than with the conventional approach. Fig. 3-16 shows that the damping estimation is still

poor, as seen in the previous section. Yet, the VSDD approach still improves over the conventional structure approach.

Finally, two VSDDs are considered, one located in each story. Several simultaneous values of both VSDDs are considered. Each VSDD is controlled to exert an extra stiffness of 0%, 20%, 30%, and 40% each in its location. Five different profiles of simultaneous values of the exerted extra stiffness by both VSDDs are considered in the identification problem such that the values of additional stiffness are (0%,0%), (0%,40%), (20%,30%), (30%,20%) and (40%,0%) of the stiffness of each story, respectively. The results of the stiffness parameter identification problem are compared to those from similar amounts of data for the conventional structure case.

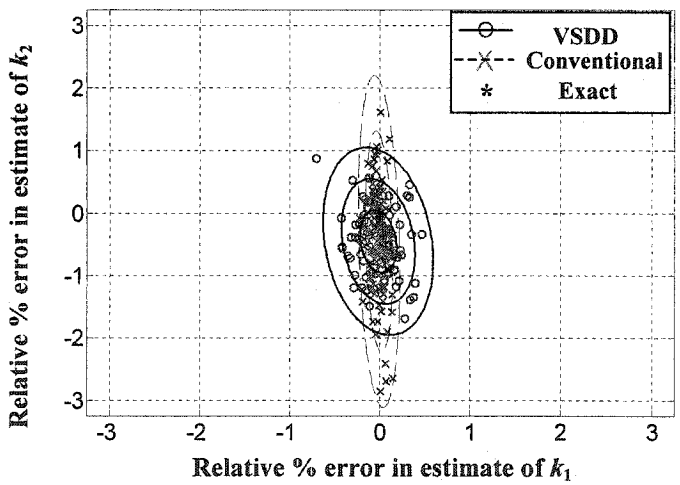

Fig. 3-15. Stiffness error levels for the iterative method with exact start for 2DOF model with VSDD in 2nd story only

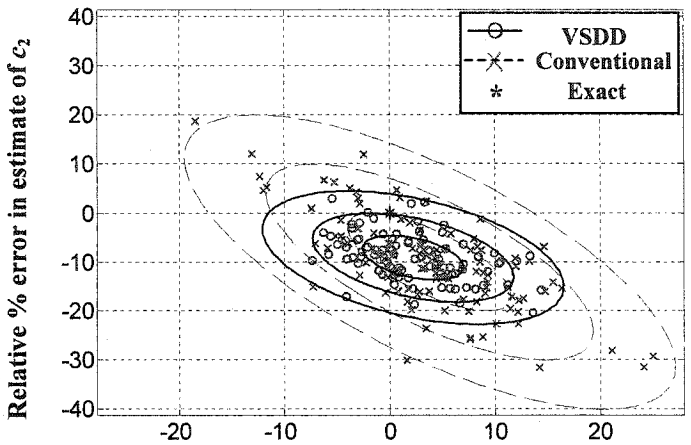

Fig. 3-16. Damping error levels for the iterative method with exact start for 2DOF model with VSDD in 2nd story only

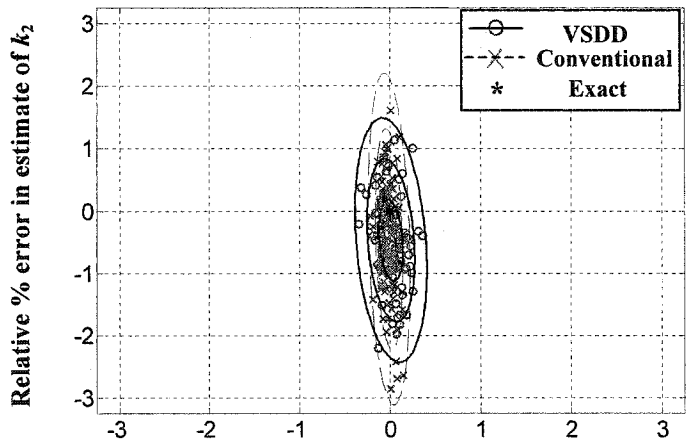

Fig. 3-17. Stiffness error levels for the iterative method with exact start for 2DOF model with VSDD in both 1st and 2nd stories

The stiffness estimate results in Fig. 3-17 show that though the variation of the stiffness identification of the second story is clearly decreased and improved, the variation of the stiffness identification of the first story is still more than the conventional approach case. However, some improvement in the variation of the stiffness of the first story compared to the case of a VSDD in the second story can be

observed. As a result, it can be inferred that VSDDs may be most effective in identifying the stiffness of the stories or levels where they are located. However, multiple VSDDs simultaneously may provide decreasing returns in a 2DOF structure. This may not be the fact for more complex structures. Comparing Fig. 3-13, Fig. 3-16 and Fig. 3-18, it is obvious that using a VSDD in each story simultaneously results in better identification of the damping coefficients of the 1st and 2nd stories where the variation is reduced significantly and the means are more accurate.

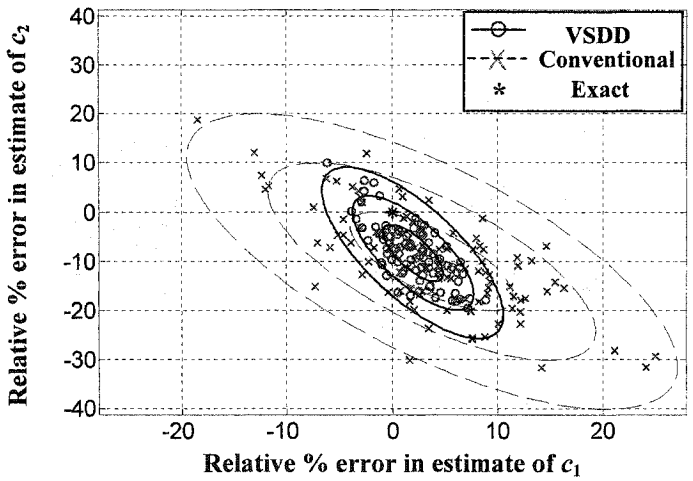

Fig. 3-18. Damping error levels for the iterative method with exact start for 2DOF model with VSDD in both 1st and 2nd stories

Table 3-2 shows the ranges for three standard deviations of stiffness and damping estimate error for the different cases of the 2DOF shear building model. Note that in all VSDD configurations in the 2DOF structure model, the number of estimations was 100 times with exact starting guesses and 20 times for the case with biased starting guesses.

Table 3-2. Range of 3σ Stiffness and Damping Estimate Relative Errors for 2DOF Shear Model

Init. Guess	Case	k_1	k_2	c_1	c_2
Exact	Conv. structure	[−0.24%, 0.23%]	[−3.1%, 2.2%]	[−20%, 27%]	[−40%, 20%]
	VSDD in 1st story	[−0.13%, 0.11%]	[−2.4%, 1.4%]	[−10%, 23%]	[−22%, 5.0%]
	VSDD in 2nd story	[−0.70%, 0.70%]	[−2.0%, 1.1%]	[−12%, 16%]	[−20%, 20%]
	VSDDs in both stories	[−0.50%, 0.40%]	[−2.3%, 1.5%]	[−5.0%, 10%]	[−25%, 10%]
Biased	Conv. structure	[3.50%, 12.00%]	[−3.5%, 2.8%]	[−16%, 25%]	[−26%, 30%]
	VSDD in 1st story	[−5.00%, 10.0%]	[−2.5%, 3.0%]	[−18%, 27%]	[−46%, 34%]

3.5.2 Two Degree-of-Freedom Pier-Deck Bridge Model

The 2DOF bridge model shown in Fig. 3-5 provides an example that has full-scale structural parameters. A VSDD, attached between the deck and the pier as shown in Fig. 3-6, is assumed to provide an additional 0%, 10%, 20%, 30% or 40% stiffness; *i.e.*, $\kappa_1 = 0.0$, $\kappa_2 = 0.1$, ..., $\kappa_5 = 0.4$. Numerical quantities for this model, drawn from Erkus *et al.* (2002), are considered as an illustrative example $k_1 = 15.791$ MN/m, $k_2 = 7.685$MN/m, $m_1 = 100$ Mg (tons), $m_2 = 500$ Mg, $c_1 = 125.6$ kN s/m, and $c_2 = 196$ kN s/m. The experimental transfer functions are simulated in MATLAB® by using the exact transfer functions plus the Fourier transform of a Gaussian pulse process typical of band-limited Gaussian white sensor noise vector processes. The noise induced in the experimental transfer function of the 2DOF bridge model is shown in Fig. 3-19, in linear and log scales.

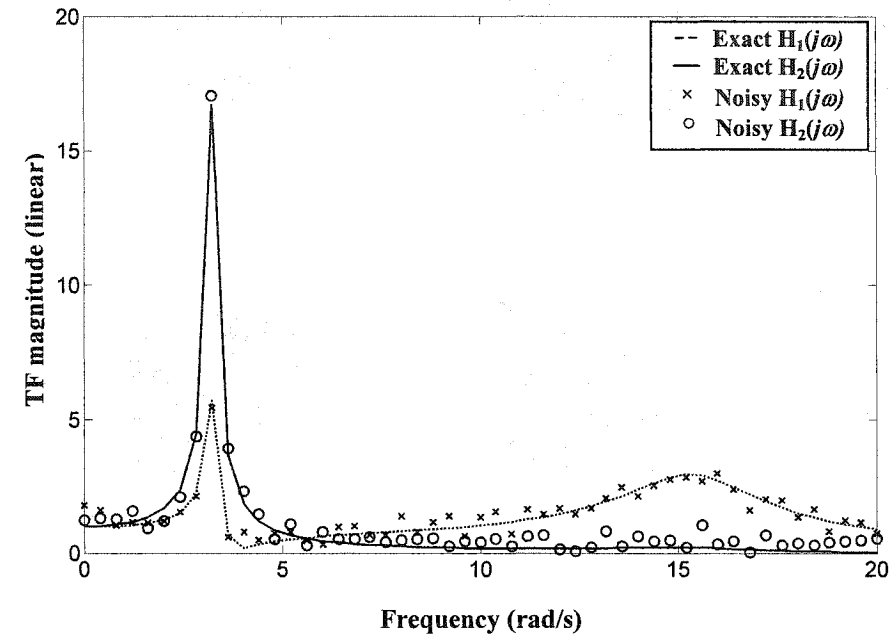

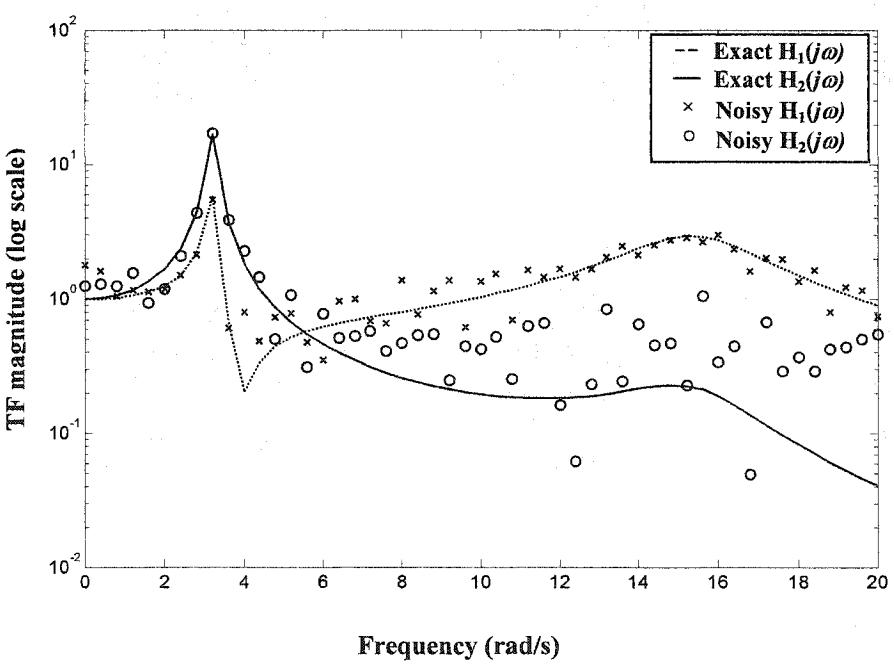

Fig. 3-19. Exact and noisy TF magnitudes for 2DOF bridge model

The iterative least-squares parametric frequency domain identification is performed on this 2DOF bridge model, both with a VSDD in the isolation layer between the deck and pier and without. The results show error reductions in both stiffness and damping estimates (though with the latter more modest than the former). The relative error in the stiffness estimates, shown in Fig. 3-20, have some small bias — about 0.5% in the estimate of the pier stiffness and about 2% in that of the isolator — that exists both with and without the VSDD (though the bias is to higher pier stiffness estimates with the VSDD, and lower without). While the bias is similar, the VSDD approach shows reductions in stiffness estimate variation, demonstrating that the VSDDs improve the identification. Similar observations may be made regarding damping estimates, as shown in Fig. 3-21. The VSDD approach slightly decreases the bias in the pier damping coefficient estimate, and modestly decreases the variation in both pier and isolator damping estimates.

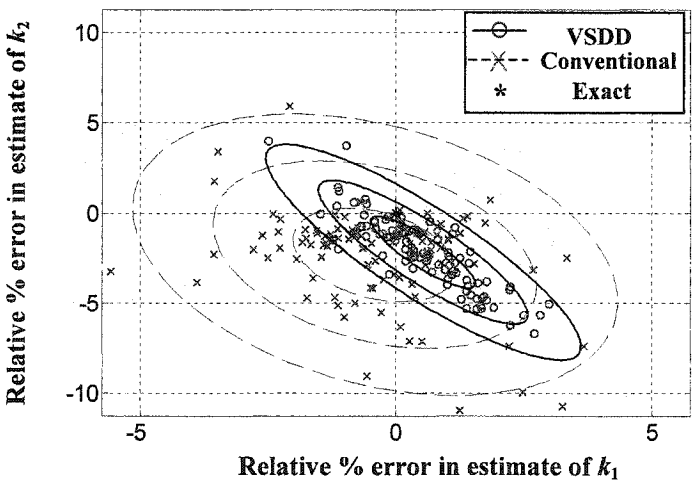

Fig. 3-20. Stiffness estimate error levels for the iterative method with exact start in 2DOF bridge model

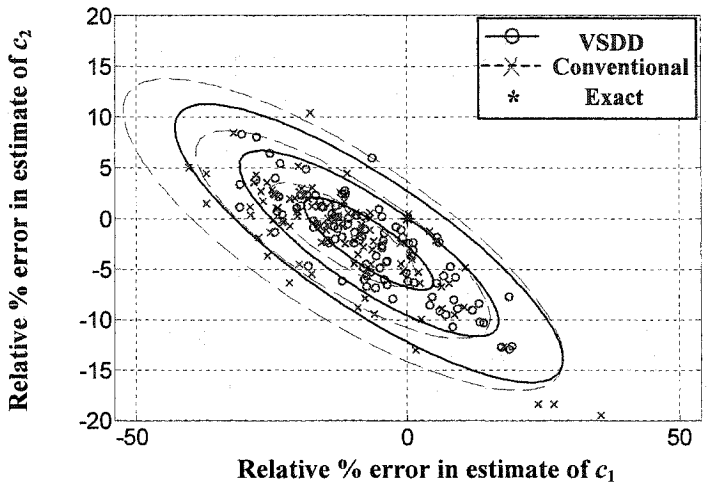

Fig. 3-21. Damping estimates error levels for the iterative method with accurate start in 2DOF bridge model

3.5.3 Six Degree-of-Freedom Shear Building Model

The six degree-of-freedom structure has story and VSDD characteristics similar to the 2DOF building structure discussed previously. The story stiffnesses and floor masses are chosen, for simplicity, to be unity. The damping coefficient in each story is 0.05. There are three VSDDs in this structure, one in each of the first three stories, that can each provide five discrete stiffness levels that are 0, 10, 20, 30 and 40 percent of the story stiffness. The transfer functions are generated using the exact transfer function plus noise (shown in Fig. 3-22 for one noise realization), and the estimation is performed 20 times (each with a different random seed). In each estimation, the VSDD approach uses four sets of VSDD stiffness combinations: (0%,0%,0%), (10%,20%,30%), (20%,30%,10%), and (30%,10%,20%) in the first, second and third floors, respectively. For fair comparison, the conventional structure approach uses four realizations of the TFs, similar to the VSDD approach case.

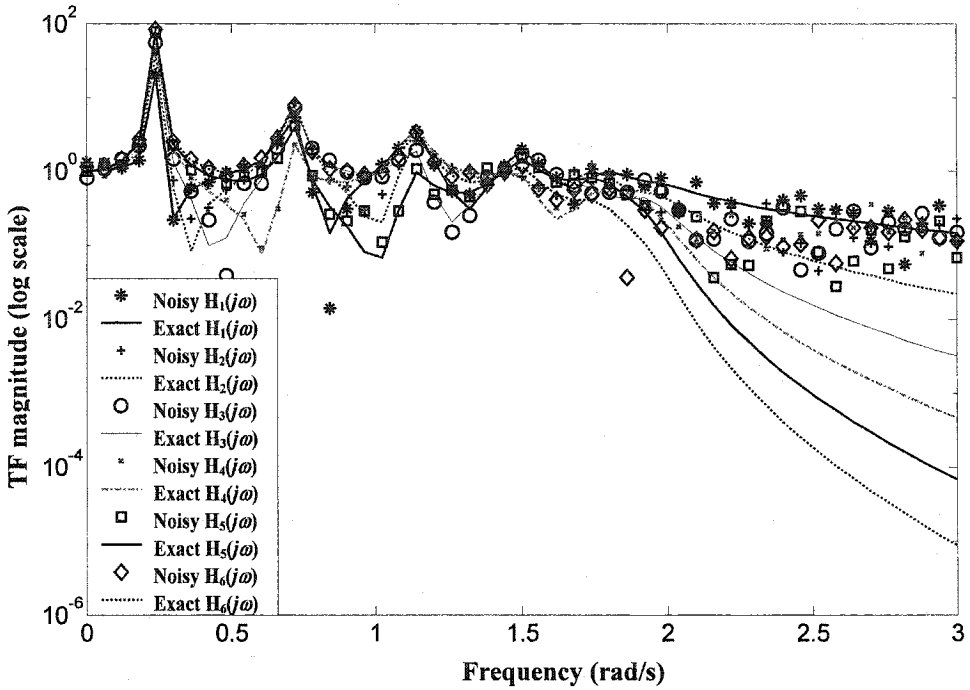

Fig. 3-22. Exact and noisy TF magnitudes for 6DOF shear building model

Fig. 3-23 shows the improvement in the estimates of the stiffness and damping coefficients when using VSDDs in the structural model. It is quite evident that the variations are dramatically reduced — up to 3 times for stiffness estimates and up to 4 times in the damping estimates. These results are similar to the improvements observed in lower-order 2DOF shear building model and the 2DOF bridge model. However, it may be inferred that the expected improvements may be more contrasted for higher degree of freedom models (*i.e.*, more complex models). Table 3-3 shows the resulting estimates of the mean and the coefficient of variations for the stiffness and damping coefficients.

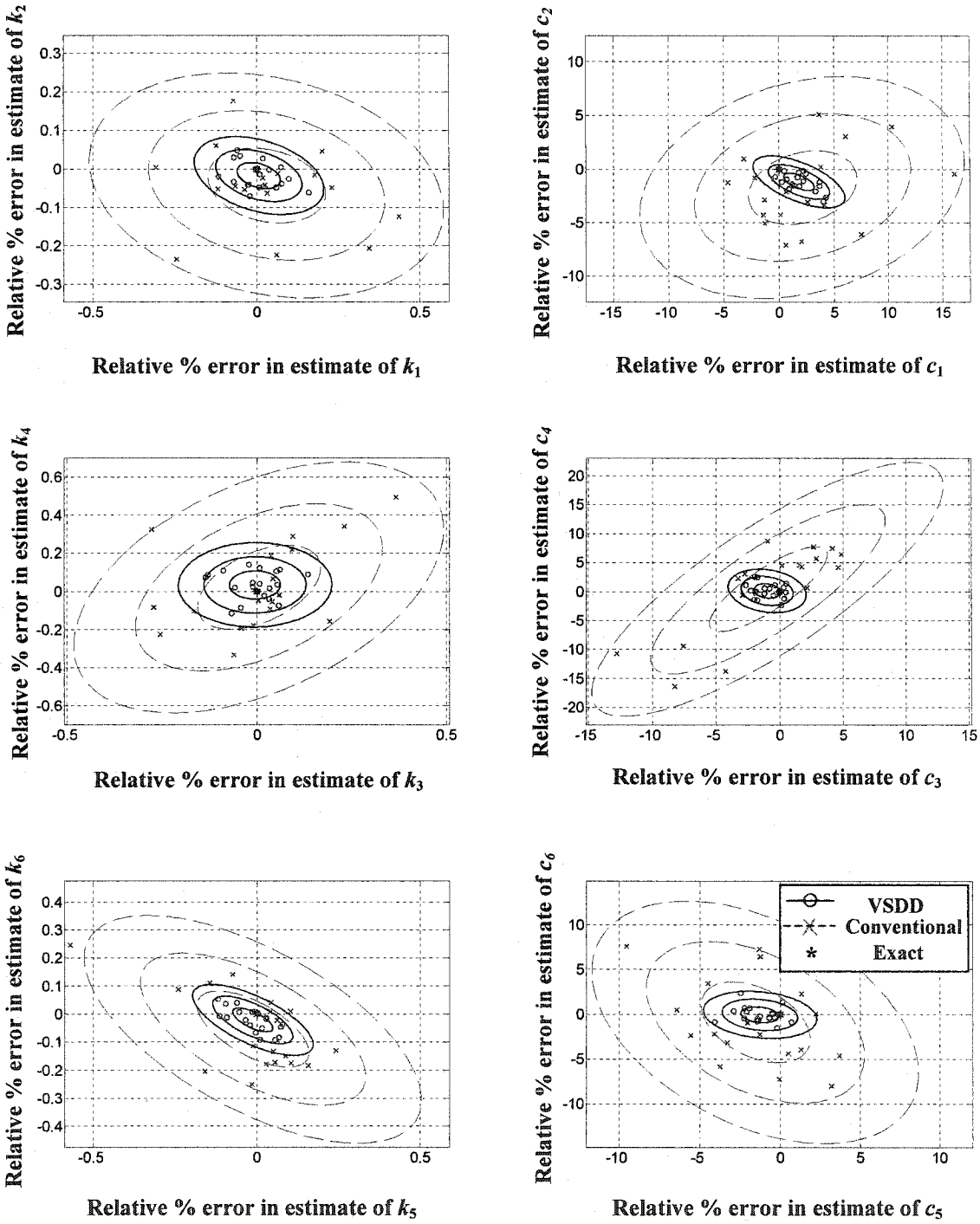

Fig. 3-23. Stiffness and damping estimates error levels for the iterative method with exact starting guess in 6DOF model

Table 3-3. Estimate Means and Coefficients-of-Variation for 6DOF Shear Building Model

Variables	Exact	*Exact Init. Guess*			
		Mean		*Coeff. of Variation* [%]	
		Conv. Struct.	VSDD	Conv. Struct.	VSDD
k_1	1.0	1.0003	1.0001	0.18	0.066
k_2	1.0	0.9996	0.9998	0.097	0.034
k_3	1.0	1.0001	0.9999	0.163	0.068
k_4	1.0	1.0002	1.0003	0.219	0.074
k_5	1.0	0.9999	0.9999	0.172	0.062
k_6	1.0	0.9995	0.9998	0.135	0.042
c_1	0.05	0.051095	0.050920	4.824	1.364
c_2	0.05	0.049145	0.049415	3.497	0.816
c_3	0.05	0.049555	0.049515	4.667	1.032
c_4	0.05	0.050210	0.050065	7.281	1.248
c_5	0.05	0.049230	0.049365	3.444	1.188
c_6	0.05	0.049560	0.049965	4.553	0.877

3.6 Using VSDDs with Variable Damping Only

Whereas the previous sections investigated the effects of VSDDs operating in a variable stiffness mode, it is possible that inducing added damping would have an effect on the SHM as well. Using variable damping would be of great interest since "smart" semiactive damping devices have received extensive study for vibration mitigation purposes (Soong and Spencer, 2002) and capitalizing on the synergies between control and SHM would be a cost-effective solution. In this example, the 2DOF bridge model is studied with a variable damping device in the isolation layer between the pier and deck. The damping levels of the device are 0%, 10%, 20%, 30%, and 40% of the isolator damping coefficient. As in the other numerical examples, the device is considered ideal (no internal device dynamics), the transfer

functions are measured through standard means, and the iterative least-squares parametric frequency-domain identification technique is applied.

The results, shown in Fig. 3-24 and Fig. 3-25, indicate that the VSDD approach, with the damping levels described above, did not differ significantly from the conventional structure approach. The relative error in stiffness estimates in Fig. 3-24, have similar bias in both approaches and a slightly larger variation with the VSDD damping device. Similar observations may be made about the damping estimates (Fig. 3-25).

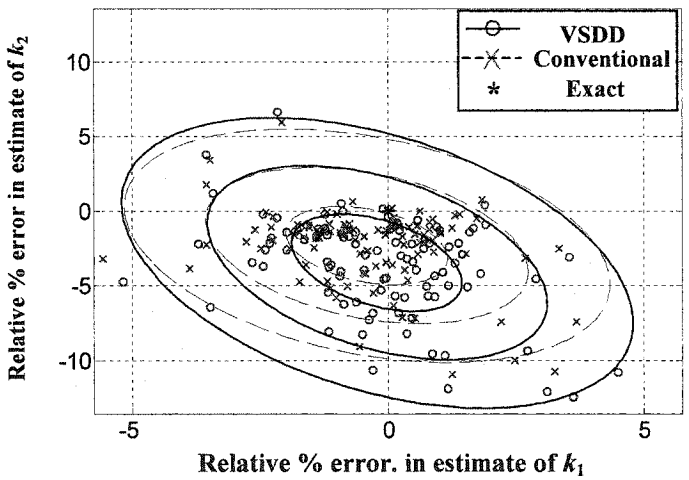

Fig. 3-24. Stiffness estimates error levels for the iterative method with exact starting guess in bridge model with multiple variations of damping coefficients

One reason that the variable damping here did not provide any notable improvement is the very small force levels generated by the damping device. The damping forces in the isolation layer of this bridge model are about two orders of magnitude smaller than the stiffness forces. As a result, changing the damping by a fraction of this small amount has relatively little effect. Using larger force levels in the variable damper may overcome this difficulty and are studied in Section 3.7.

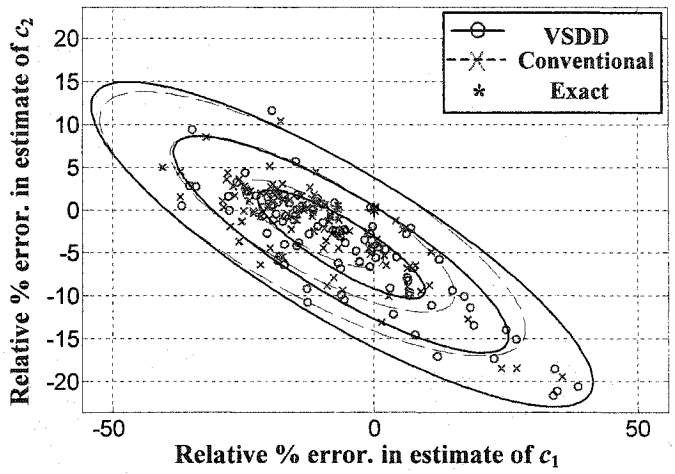

Fig. 3-25. Damping estimates error levels for the iterative method with exact starting guess in bridge model with multiple variations of damping coefficients

3.7 Effect of Using Larger VSDD Stiffness/Damping Forces

To improve the advantages of the VSDD approach, larger VSDD stiffness/damping levels may be used. This section studies and verifies the effect of adding higher levels of stiffness or damping to a structural system for improving the system identification process. The ILSN method is used for identification of parameters in the examples within this section. The initial guess provided to the numerical equation solver is the exact value. The primary test bed here is the 2DOF bridge model, however, some results for the 2DOF and 6DOF shear building models are also given. The transfer functions are measured through standard means. As in the other previous numerical examples, the VSDD device is considered ideal (*i.e.*, no internal device dynamics are considered).

3.7.1 Case of 2DOF Bridge Model

Sections 3.5.2 and 3.6 investigated the effects of VSDDs operating in a variable stiffness or damping modes on the 2DOF bridge model, however, the levels of stiffness or damping of the VSDD device were limited to 0%, 10%, 20%, 30%, and 40% of that of the isolator — between the bridge deck and the pier — stiffness or damping coefficients, respectively. In contrast, the VSDDs in this section are assumed to: (*i*) add {0,1,2,3,4} times the bearing stiffness, (*ii*) add {0,5,10,15,20} times the bearing stiffness, (*iii*) add {0,25,50,75,100} times the bearing damping, and (*iv*) add {0,100,200,300,400} times the bearing damping.

It is found that by increasing the level of stiffness that the VSDD induces at the isolator level, the variation of the relative error of stiffness coefficients estimation decreases dramatically as shown in Fig. 3-26*a,b*. In addition, the variation of the relative error of the damping coefficients estimation, as seen in Fig. 3-26*c,d*, improves considerably compared to cases of lower levels of induced VSDD stiffness (Fig. 3-21), though the improvement is limited and the damping coefficient estimation error is up to 5-10%. For the case of varying VSDD damping, it is shown in Fig. 3-26*e,f* that the estimation of the stiffness coefficients are improved by increasing the damping levels. Moreover, the variation of the relative error decreases dramatically at highest level of damping (Fig. 3-26*f*). The damping estimates are also improved considerably, though the variation of the relative error tends to have a linear trend with a maximum error of 5% of the damping coefficients of the system as shown in Fig. 3-26*g,h*.

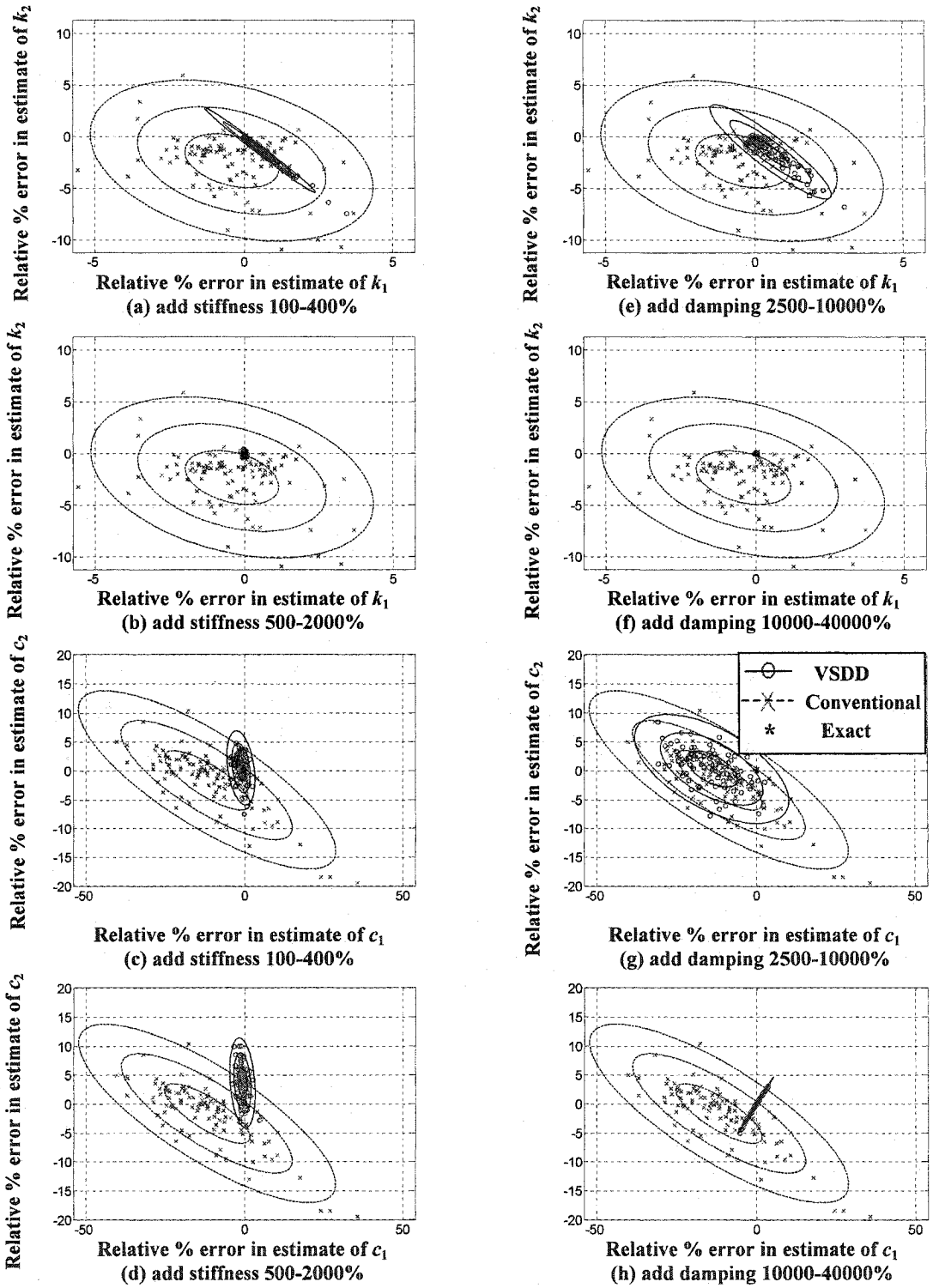

Fig. 3-26. Comparison of stiffness and damping estimate error levels for higher VSDD induced stiffness/damping for 2DOF bridge model

Furthermore, Table 3-4 shows the improvements in the mean estimates and the mean-square error percentage of the identified structural parameters with higher levels of variable stiffness or damping. The improvements are demonstrated in terms of better mean estimates and much smaller variation (root mean square error (RMSE) percentage).

Table 3-4. Estimate Means and Root Mean-Square Error Percentage for 2DOF Pier-Deck Bridge Model Using Higher Levels of Induced Stiffness or Damping

VSDD Loc.	Struct. Param.	Exact Values	Mean			RMSE(%)		
			No VSDD	Add k_{VSDD}	Add c_{VSDD}	No VSDD	Add k_{VSDD}	Add c_{VSDD}
One VSDD in the bearing between deck and pier	k_1[MN/m]	15.791	15.726	15.791	15.791	1.634	0.034	0.013
	k_2[MN/m]	7.685	7.507	7.683	7.685	3.484	0.160	0.027
	c_1[kN s/m]	125.6	110.8	124.8	125.4	17.931	1.499	1.846
	c_2[kN s/m]	196	192.8	203.2	195.7	5.390	4.492	1.625
	M_2 [tons]	100	98.29	100	100	2.398	0.030	0.035

One initial reaction to this approach is that the stiffness/damping levels sound unreasonable. However, it must be understood that these are effective levels of stiffness and damping forces exerted during low-level ambient excitation. Thus, the actual forces are well within the capabilities of current VSDDs.

To verify that the force levels are reasonable, the response of the structure to a low-level earthquake excitation (Kanai-Tajimi filtered white noise with a 0.002g root mean square (RMS) ground acceleration) is computed. With the VSDD producing 20 times the bearing stiffness, the RMS pier and deck drifts are 1.5 mm and 0.125 mm, respectively, RMS absolute pier and deck accelerations are 0.0037g and 0.0041g, respectively, and RMS VSDD force is 19.2 kN. This force level is quite

small relative to the masses (500 ton deck, 100 ton pier). Meanwhile, with the VSDD producing 400 times the bearing damping, the RMS pier and deck drifts are 1.44 mm and 0.074 mm, respectively, RMS absolute accelerations are 0.003g at both deck and pier, and the RMS VSDD force is about 15 kN, which is also small compared to the masses. In contrast, when no VSDDs are used, the RMS pier and deck drifts are 0.85 mm and 1.61 mm, respectively, RMS absolute pier and deck accelerations are 0.0032g and 0.0025g, respectively.

3.7.2 2DOF Shear Building Model with Larger VSDD Forces

The identification results for the 2DOF shear building also showed considerable improvement by increasing the additional stiffness level induced by the VSDDs. The identification results introduced here add VSDD stiffness that is {0,5,10,15,20} times the stiffness of the corresponding story or VSDDs damping that is {0,100,200,300,400} times the damping of the corresponding story. The improvements are well demonstrated in Table 3-5.

By using higher levels of induced VSDD stiffness/damping, faster convergence in the identification code is observed. Using the true parameter vector as an initial starting guess for the iterative procedure, the algorithm converges, generally in 3–5 iterations, to estimates that are fairly accurate.

The results in Table 3-5 for a single VSDD in the first story show that the identification of the stiffness in the first story is quite accurate using both conventional and VSDD approaches. On the other hand, the means of all other

identified structural parameters are better when using the VSDD approach. The results in Table 3-5 indicate that the root mean square errors are reduced by more than two times for the second story stiffness, and by nearly ten times for the second story damping coefficient by varying VSDD stiffness with these higher levels.

Table 3-5. Estimate Means and Root Mean-Square Error Percentage for 2DOF Shear Building Model

VSDD Loc.	Struct. Param.	Exact Values	Mean			RMSE (%)		
			No VSDD	Add k_{VSDD}	Add c_{VSDD}	No VSDD	Add k_{VSDD}	Add c_{VSDD}
One VSDD in 1st story (exact guesses)	k_1	1.0000	0.9999	0.9993	0.9980	0.078	0.288	0.428
	k_2	1.0000	0.9955	0.9985	0.9966	0.994	0.443	0.710
	c_1	0.0500	0.0519	0.0495	0.0495	8.646	4.160	5.553
	c_2	0.0500	0.0449	0.0497	0.0496	14.303	1.422	2.799
	m_2	1.0000	0.9982	0.9987	0.9967	0.417	0.413	0.716
One VSDD in 1st story (offset guesses)	k_1	1.0000	1.0368	0.9993	_	4.174	0.289	_
	k_2	1.0000	0.9953	0.9985	_	1.021	0.445	_
	c_1	0.0500	0.0520	0.0495	_	9.759	4.167	_
	c_2	0.0500	0.0482	0.0497	_	12.403	1.424	_
	m_2	1.0000	1.0343	0.9987	_	3.958	0.416	_
One VSDD in 2nd story (Exact guesses)	k_1	1.0000	0.9999	1.0022	1.0004	0.078	0.272	0.099
	k_2	1.0000	0.9955	0.9835	0.9989	0.994	1.877	0.581
	c_1	0.0500	0.0519	0.0501	0.0500	8.646	2.758	2.429
	c_2	0.0500	0.0449	0.0465	0.0467	14.303	9.952	9.946
	m_2	1.0000	0.9982	0.9949	0.9990	0.417	0.587	0.195
Two VSDDs in 1st and 2nd stories (Exact guesses)	k_1	1.0000	0.9999	1.0001	1.0002	0.078	0.125	0.093
	k_2	1.0000	0.9955	0.9996	0.9989	0.994	0.092	0.234
	c_1	0.0500	0.0519	0.0500	0.0499	8.646	1.934	2.296
	c_2	0.0500	0.0449	0.0498	0.0495	14.303	2.303	2.889
	m_2	1.0000	0.9982	0.9999	0.9993	0.417	0.027	0.173

For the case of an initial parameter vector that is 20% higher (in all components) than the exact values, 100 separate estimates were computed. Fig. 3-27,

showing the variation of the identified stiffnesses using higher levels of induced VSDD stiffness, indicates that the VSDD approach did very well compared to the conventional structure approach that shows large bias and variation. Similar results are observed in the identified damping coefficients of the first and second stories, as shown in Fig. 3-28. Both Fig. 3-27 and Fig. 3-28 show approximate one-, two- and three-sigma (standard deviation) curves for the two approaches.

For a VSDD in the second story, one can observe that the results resemble those with a VSDD in the first story only, yet the improvement is more reflected in the case of varying VSDD damping only. Moreover, the variation of the stiffness estimate of the 1st story is reduced compared to the case of having the VSDD in the first story only (Table 3-5).

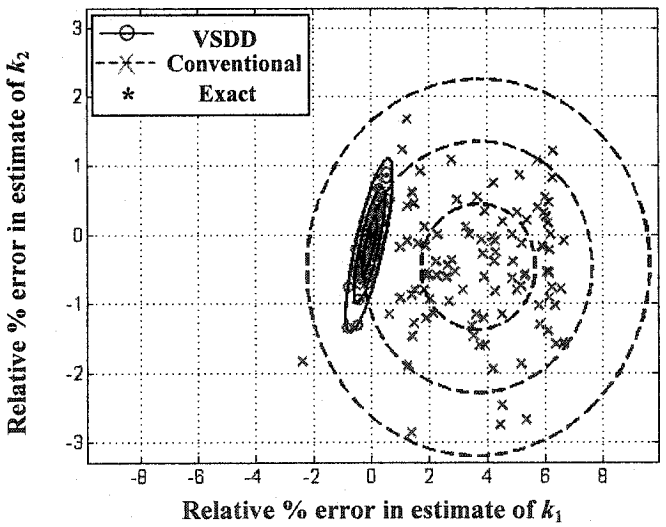

Fig. 3-27. Stiffness estimate error levels for the iterative method with offset start for 2DOF model with VSDD in 1st story only (varying stiffness case)

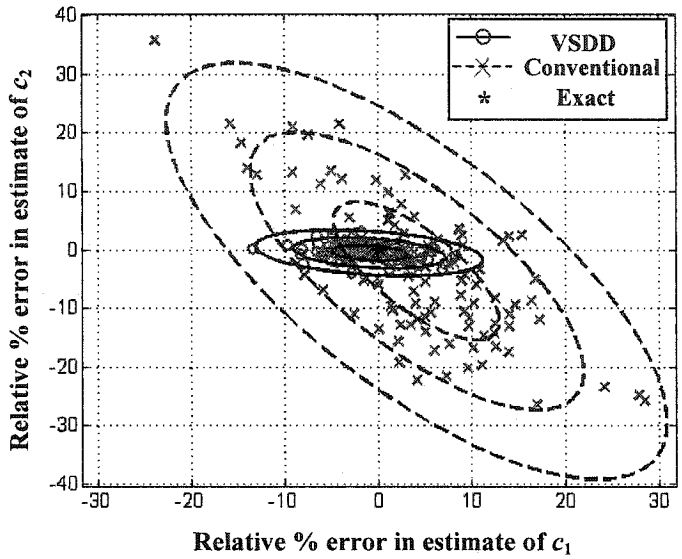

Fig. 3-28. Damping estimate error levels for the iterative method with offset start for 2DOF model with VSDD in 1st story only (varying stiffness case)

For the case of having VSDDs in both stories of the structure, Fig. 3-29 and Fig. 3-30 show that the variation of the stiffness identification of the second story is clearly decreased and improved. The mean of the first story stiffness estimate is now almost similar to that of the conventional approach case, as shown in Table 3-5. However, some improvement in the variation of the stiffness of the first story, compared to the case of a VSDD in the first and second stories only, can be observed. Generally, the variations are vastly improved compared to any of the previous cases of a single VSDD in the structure such that it is now one tenth that of the conventional approach case for the second story stiffness and nearly one fifth for the damping coefficients in both stories. However, the variance of the identified stiffness coefficient in the first story is still a little more than the conventional structure approach case.

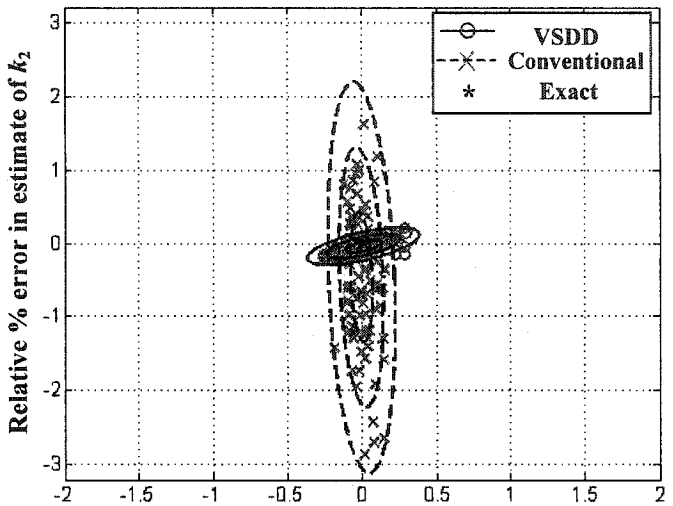

Fig. 3-29. Stiffness error levels for the iterative method with exact start for 2DOF model with VSDD in both 1st and 2nd stories (varying stiffness case)

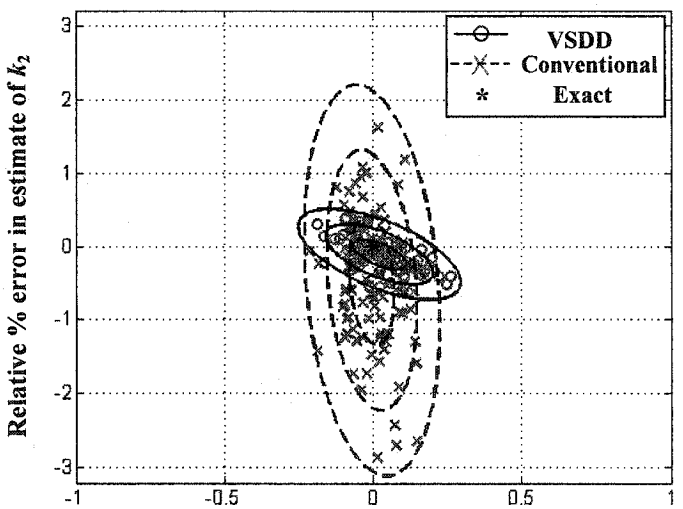

Fig. 3-30. Stiffness error levels for the iterative method with exact start for 2DOF model with VSDD in both 1st and 2nd stories (varying damping case)

3.7.3 Case of 6DOF Shear Building Model

The 6DOF model system identification in this section is solved for the variable stiffness VSDD and the conventional structure (no VSDDs) approaches,

using the ILSN method with exact starting guesses of the unknown parameters. The VSDDs are located in the first three stories only. The masses are assumed known *a priori*. In simulation, each installed VSDD is assumed to provide additional stiffness at four discrete levels: 0%, 500%, 1000%, and 1500% of the corresponding story stiffness.

Table 3-6 shows the improvement in the estimates of the stiffness and damping coefficients when using VSDDs in the structural model. Also, it is quite evident that the variations are dramatically reduced — up to 12 times for stiffness estimate in the 6th story and up to nearly 23 times in the damping estimates. The results here confirm the improvements observed before for the lower-order 2DOF shear building model and the 2DOF bridge model.

Table 3-6. Estimate Means and Mean-Square Error Percentage for 6DOF Shear Building Model (Varying Stiffness)

VSDD Loc.	Structural Parameters	Exact Values	Mean		RMSE(%)	
			No VSDD	Varying k	No VSDD	Varying k
Three VSDDs in 1st, 2nd, and 3rd stories	k_1	1.0000	1.0003	1.0000	0.183	0.036
	k_2	1.0000	0.9996	1.0000	0.105	0.071
	k_3	1.0000	1.0001	0.9999	0.163	0.083
	k_4	1.0000	1.0002	1.0000	0.220	0.020
	k_5	1.0000	0.9999	1.0000	0.172	0.026
	k_6	1.0000	0.9995	1.0000	0.144	0.011
	c_1	0.0500	0.0511	0.0500	5.399	0.783
	c_2	0.0500	0.0491	0.0501	3.877	1.444
	c_3	0.0500	0.0496	0.0496	4.698	2.028
	c_4	0.0500	0.0502	0.0500	7.321	0.296
	c_5	0.0500	0.0492	0.0500	3.748	0.267
	c_6	0.0500	0.0496	0.0500	4.587	0.202

3.8 INVFREQS-Least Squares Method

The INVFREQS-Least Squares (INVFLS) method is a frequency domain identification method, based on the general definition of the transfer function and the least squares error approach. The method is composed of two stages. The first stage, called the INVFREQS stage, concerns estimating the coefficients of polynomials of the transfer functions of structural systems. The second, also by least squares, estimates the structural parameters, such as stiffness and damping coefficients, from direct relations with the coefficients of the transfer function polynomials. The INVFREQS stage for Single-Input-Single-Output (SISO) systems already exists as a MATLAB® function. In this study, the first stage is extended to Single-Input-Multi-Output (SIMO) and Multi-Input-Multi-Output (MIMO) systems as well. To explain the method, the first stage application to the SISO systems is explained thoroughly, and then the extension to SIMO and MIMO systems is introduced. The second stage, using a least squares technique to find the structure parameters, is then discussed.

3.8.1 INVFREQS Method for SISO System

To explain the general derivation of this method, a SISO system is a good start (Ljung, 2000). Generally, the transfer function $H(j\omega)$ for a SISO system can be represented in the form of a numerator polynomial $B(j\omega)$ and a denominator polynomial $A(j\omega)$ as:

$$H(j\omega) = B(j\omega) / A(j\omega) \tag{3-20}$$

The numerator and denominator polynomials $B(j\omega)$ and $A(j\omega)$ can be expressed in a polynomial form as in Eq. (3-4), and are considered of orders n_B and n_A, respectively.

By measuring the output response for known input excitation, an experimental transfer function $\hat{H}(j\omega)$ may be obtained. The residual error between the theoretical and experimental transfer functions can, consequently, be defined as:

$$e(j\omega) = \frac{B(j\omega) - A(j\omega)\hat{H}(j\omega)}{A(j\omega)} \tag{3-21}$$

However, to simplify the conventional transfer function problem, the error in the numerator of Eq. (3-21), $\tilde{e}$, at any frequency ω is used instead of the residual error such that:

$$\tilde{e}(j\omega, \tilde{\mathbf{x}}) = [b_{n_B}(j\omega)^{n_B} + \ldots + b_0] - \hat{H}(j\omega)[(j\omega)^{n_A} + a_{n_A-1}(j\omega)^{n_A-1} + \ldots + a_0] \tag{3-22}$$

where $\tilde{\mathbf{x}}$ is the vector of unknown coefficients,

$$\tilde{\mathbf{x}} = \left[a_{n_A-1} \quad a_{n_A-2} \quad \ldots \quad a_0 \;\vdots\; b_{n_B} \quad b_{n_B-1} \quad \ldots \quad b_0\right]^{\mathrm{T}} \tag{3-23}$$

Then, rearranging the components of Eq. (3-22) as

$$\hat{H}(j\omega)[a_{n_A-1}(j\omega)^{n_A-1} + \ldots + a_0] - [b_{n_B}(j\omega)^{n_B} + \ldots + b_0] = -\hat{H}(j\omega)(j\omega)^{n_A} - \tilde{e}(j\omega, \tilde{\mathbf{x}}) \tag{3-24}$$

which can be expressed in a matrix form

$$\mathbf{D}_{n_\omega \times (n_B+n_A+1)} \tilde{\mathbf{x}}_{(n_B+n_A+1)\times 1} = \mathbf{V}_{n_\omega \times 1} - \tilde{\mathbf{e}}_{n_\omega \times 1} \tag{3-25}$$

where n_ω is the number of frequencies in the frequency domain of interest. The **D** matrix is, thus, expressed for n_ω frequencies as:

$$\mathbf{D}=\left[\begin{array}{ccc|ccc} (j\omega_1)^{n_A-1}\hat{H}(j\omega_1) & \cdots & \hat{H}(j\omega_1) & -(j\omega_1)^{n_B} & -(j\omega_1)^{n_B-1} & \cdots & -1 \\ \vdots & & \vdots & \vdots & \vdots & & \vdots \\ (j\omega_i)^{n_A-1}\hat{H}(j\omega_i) & \cdots & \hat{H}(j\omega_i) & -(j\omega_i)^{n_B} & -(j\omega_i)^{n_B-1} & \cdots & -1 \\ \vdots & & \vdots & \vdots & \vdots & & \vdots \\ (j\omega_{n_\omega})^{n_A-1}\hat{H}(j\omega_{n_\omega}) & \cdots & \hat{H}(j\omega_{n_\omega}) & -(j\omega_{n_\omega})^{n_B} & -(j\omega_{n_\omega})^{n_B-1} & \cdots & -1 \end{array}\right] \quad (3\text{-}26)$$

and the vector **V** is defined as:

$$\mathbf{V}_{n_\omega\times 1}=\left[-(j\omega_1)^{n_A}\hat{H}(j\omega_1) \quad \cdots \quad -(j\omega_i)^{n_A}\hat{H}(j\omega_i) \quad \cdots \quad -(j\omega_{n_\omega})^{n_A}\hat{H}(j\omega_{n_\omega})\right]^{\mathrm{T}} \quad (3\text{-}27)$$

Minimizing the squared error vector $\tilde{\mathbf{e}}^*\tilde{\mathbf{e}}$, with respect to the vector of unknown coefficients $\tilde{\mathbf{x}}$, gives

$$\begin{aligned}\frac{\partial\tilde{\mathbf{e}}^*\tilde{\mathbf{e}}}{\partial\tilde{\mathbf{x}}} &= \frac{\partial}{\partial\tilde{\mathbf{x}}}((\mathbf{D}\tilde{\mathbf{x}}-\mathbf{V})^*(\mathbf{D}\tilde{\mathbf{x}}-\mathbf{V})) = \frac{\partial}{\partial\tilde{\mathbf{x}}}(\tilde{\mathbf{x}}^{\mathrm{T}}\mathbf{D}^*\mathbf{D}\tilde{\mathbf{x}}-\tilde{\mathbf{x}}^{\mathrm{T}}\mathbf{D}^*\mathbf{V}-\mathbf{V}^*\mathbf{D}\tilde{\mathbf{x}}+\mathbf{V}^*\mathbf{V}) \\ &= 2(\mathbf{D}^*\mathbf{D}\tilde{\mathbf{x}}-\mathbf{D}^*\mathbf{V})^{\mathrm{T}}=\mathbf{0}^{\mathrm{T}}\end{aligned} \quad (3\text{-}28)$$

where $(\cdot)^*$ denotes complex conjugate transpose. For the system to be causal, all coefficients should be real. Thus, the vector of unknown coefficients $\tilde{\mathbf{x}}$ can be obtained from the equation,

$$\tilde{\mathbf{x}}=(\mathbf{D}^*\mathbf{D})^{-1}\mathrm{Re}(\mathbf{D}^*\mathbf{V}) \quad (3\text{-}29)$$

The Re(·) is not theoretically necessary but, in numerical computation, this eliminates small imaginary components resulting from round-off.

The results from Eq. (3-29) are initial estimates of the transfer function coefficients. The stability of the estimated system is checked by calculating the roots of the estimated denominator polynomial, $\hat{A}(j\omega)$, and verifying the roots have negative real parts.

An iterative technique refines the estimates by reducing the residual transfer function error, in terms of the estimated polynomials $\hat{B}(j\omega)$ and $\hat{A}(j\omega)$,

$$\hat{e}(j\omega) = \hat{B}(j\omega)/\hat{A}(j\omega) - \hat{H}(j\omega) \tag{3-30}$$

The estimated coefficients of the numerator and denominator polynomials are not yet the best estimates. Therefore, each of the coefficients of $\hat{B}(j\omega)$ and $\hat{A}(j\omega)$ has error Δb and Δa, respectively. In other words, the estimated polynomials equal the exact polynomials plus some error such that:

$$\hat{B}(j\omega) = (b_{n_B} + \Delta b_{n_B})(j\omega)^{n_B} + (b_{n_B-1} + \Delta b_{n_B-1})(j\omega)^{n_B-1} + \ldots + (b_0 + \Delta b_0) \tag{3-31}$$

$$\hat{A}(j\omega) = (j\omega)^{n_A} + (a_{n_A-1} + \Delta a_{n_A-1})(j\omega)^{n_A-1} + \ldots + (a_0 + \Delta a_0) \tag{3-32}$$

Substituting Eqs. (3-31) and (3-32) into Eq. (3-30) and simplifying, results in

$$\begin{aligned}\hat{e}(j\omega)\hat{A}(j\omega) = &\left[(b_{n_B} + \Delta b_{n_B})(j\omega)^{n_B} + \ldots + (b_0 + \Delta b_0)\right] \\ &- \hat{H}(j\omega)\left[(a_{n_A-1} + \Delta a_{n_A-1})(j\omega)^{n_A-1} + \ldots + (a_0 + \Delta a_0)\right]\end{aligned} \tag{3-33}$$

The right hand side of Eq. (3-33) can be divided into two parts: one includes the coefficients of the actual polynomials and the other formed of the error coefficients

$$\hat{e}(j\omega)\hat{A}(j\omega) = B(j\omega) - \hat{H}(j\omega)A(j\omega) + [\Delta b_{n_B}(j\omega)^{n_B} + \ldots + \Delta b_0] - \hat{H}(j\omega)[\Delta a_{n_A-1}(j\omega)^{n_A-1} + \ldots + \Delta a_0] \tag{3-34}$$

For the exact actual $B(j\omega)$ and $A(j\omega)$, the first two terms in the right hand side of Eq. (3-34) cancel and, thus, the resulting equation of the error is

$$\hat{e}(j\omega) = \frac{1}{\hat{A}(j\omega)}\left\{\left[\Delta b_{n_B}(j\omega)^{n_B} + \ldots + \Delta b_0\right] - \hat{H}(j\omega)\left[\Delta a_{n_A-1}(j\omega)^{n_A-1} + \ldots + \Delta a_0\right]\right\} \tag{3-35}$$

The new residual error Eq. (3-35) is used for the evaluation of the error coefficients. This is done by rewriting Eq. (3-35) in a matrix form such that

$$\mathbf{\Delta D}_{n_\omega \times (n_B+n_A+1)} \mathbf{\Delta \tilde{x}}_{(n_B+n_A+1)\times 1} = \hat{\mathbf{e}}_{n_\omega \times 1} \tag{3-36}$$

where the error coefficients vector $\mathbf{\Delta \tilde{x}}$ is

$$\Delta \tilde{\mathbf{x}} = \left[\Delta a_{n_A-1} \quad \Delta a_{n_A-2} \quad \ldots \quad \Delta a_0 \;\vdots\; \Delta b_{n_B} \quad \Delta b_{n_B-1} \quad \ldots \quad \Delta b_0\right]^{\mathrm{T}} \tag{3-37}$$

and the matrix $\mathbf{\Delta D}$ is defined as

$$\mathbf{\Delta D} = \left[\begin{array}{ccc:ccc} -\dfrac{(j\omega_1)^{n_A-1}\hat{H}(j\omega_1)}{\hat{A}(j\omega_1)} & \cdots & -\dfrac{\hat{H}(j\omega_1)}{\hat{A}(j\omega_1)} & \dfrac{(j\omega_1)^{n_B}}{\hat{A}(j\omega_1)} & \dfrac{(j\omega_1)^{n_B-1}}{\hat{A}(j\omega_1)} & \cdots \; \dfrac{1}{\hat{A}(j\omega_1)} \\ \vdots & & \vdots & \vdots & \vdots & \vdots \\ -\dfrac{(j\omega_i)^{n_A-1}\hat{H}(j\omega_i)}{\hat{A}(j\omega_i)} & \cdots & -\dfrac{\hat{H}(j\omega_i)}{\hat{A}(j\omega_i)} & \dfrac{(j\omega_i)^{n_B}}{\hat{A}(j\omega_i)} & \dfrac{(j\omega_i)^{n_B-1}}{\hat{A}(j\omega_i)} & \cdots \; \dfrac{1}{\hat{A}(j\omega_i)} \\ \vdots & & \vdots & \vdots & \vdots & \vdots \\ -\dfrac{(j\omega_{n_\omega})^{n_A-1}\hat{H}(j\omega_{n_\omega})}{\hat{A}(j\omega_{n_\omega})} & \cdots & -\dfrac{\hat{H}(j\omega_{n_\omega})}{\hat{A}(j\omega_{n_\omega})} & \dfrac{(j\omega_{n_\omega})^{n_B}}{\hat{A}(j\omega_{n_\omega})} & \dfrac{(j\omega_{n_\omega})^{n_B-1}}{\hat{A}(j\omega_{n_\omega})} & \cdots \; \dfrac{1}{\hat{A}(j\omega_{n_\omega})} \end{array}\right] \tag{3-38}$$

Multiplying both sides of Eq. (3-36) by the complex conjugate transpose $\Delta\mathbf{D}^*$, taking the real parts and solving for the error coefficients vector $\Delta\tilde{\mathbf{x}}$,

$$\Delta\tilde{\mathbf{x}} = (\Delta\mathbf{D}\Delta\mathbf{D}^*)^{-1}\mathrm{Re}(\Delta\mathbf{D}^*\hat{\mathbf{e}}) \tag{3-39}$$

The calculation of error coefficients helps in finding a general direction to better estimate the transfer function coefficients. The new resulting coefficients vector $\tilde{\mathbf{x}}_{\mathrm{mod}}$ is equal to the sum of the initial estimates vector $\tilde{\mathbf{x}}$ and the error coefficients vector $\Delta\tilde{\mathbf{x}}$. For enhancement however, a check is performed on the evaluated error coefficients $\Delta\tilde{\mathbf{x}}$ before adding them to the initial estimates $\tilde{\mathbf{x}}$. In the check, the new modified coefficients will be represented as,

$$\tilde{\mathbf{x}}_{\mathrm{mod}} = \tilde{\mathbf{x}} + k(\Delta\tilde{\mathbf{x}}) \tag{3-40}$$

The convergence check starts with calculating the squared residual error $\hat{\mathbf{e}}^*\hat{\mathbf{e}}$ where

$$\hat{\mathbf{e}}^*\hat{\mathbf{e}} = \left[\frac{\hat{B}(j\omega)}{\hat{A}(j\omega)} - \hat{H}(j\omega)\right]^*\left[\frac{\hat{B}(j\omega)}{\hat{A}(j\omega)} - \hat{H}(j\omega)\right] \tag{3-41}$$

The result is then compared to the modified squared residual error $\hat{\mathbf{e}}^*_{\mathrm{mod}}\hat{\mathbf{e}}_{\mathrm{mod}}$, considering k=1, where

$$\hat{\mathbf{e}}^*\hat{\mathbf{e}} = \left[\frac{\hat{B}_{\mathrm{mod}}(j\omega)}{\hat{A}_{\mathrm{mod}}(j\omega)} - \hat{H}(j\omega)\right]^*\left[\frac{\hat{B}_{\mathrm{mod}}(j\omega)}{\hat{A}_{\mathrm{mod}}(j\omega)} - \hat{H}(j\omega)\right] \tag{3-42}$$

If $\hat{\mathbf{e}}^*\hat{\mathbf{e}}$ is smaller than $\hat{\mathbf{e}}^*_{\mathrm{mod}}\hat{\mathbf{e}}_{\mathrm{mod}}$, then $\tilde{\mathbf{x}}_{\mathrm{mod}}$ is recalculated from Eq. (3-40) by taking k equivalent to half of its previous value. The comparison is repeated between $\hat{\mathbf{e}}^*\hat{\mathbf{e}}$ and $\hat{\mathbf{e}}^*_{\mathrm{mod}}\hat{\mathbf{e}}_{\mathrm{mod}}$ till the latter is smaller. After the check is fulfilled, another loop of

recalculating the error coefficients vector $\Delta\tilde{\mathbf{x}}$ is applied. In the new loop, the vector $\tilde{\mathbf{x}}_{\text{mod}}$ is considered as the initial estimate. These loops of evaluation of $\Delta\tilde{\mathbf{x}}$ and modification of the estimated coefficients are repeated until the norm of the error coefficients vector becomes smaller than a tolerance factor

$$\left\|\Delta\tilde{\mathbf{x}}\right\| \leq tol \tag{3-43}$$

This tolerance factor is dependent on the sensitivity that the user requires.

3.8.2 INVFREQS Method for SIMO and MIMO Systems

For the case of SIMO and MIMO systems, a series of transfer functions is identified rather than the single one in the SISO case. Each transfer function represents the ratio between one of the inputs and one of the outputs. The global transfer function matrix is represented such that each column corresponds to one of the inputs, and each row to one of the outputs.

To start solving the problem, consider a system that is subjected to M excitation inputs and has L measured outputs. Then, the transfer function to the l^{th} output of the system from the m^{th} input is expressed as

$$H_{lm}(j\omega) = B_{lm}(j\omega) / A_m(j\omega) \tag{3-44}$$

where the denominator polynomial $A_m(j\omega)$ of the transfer functions of all measured outputs is considered unique for a single input, and the numerator polynomial $B_{lm}(j\omega)$ is considered unique for each input/output combination. Accordingly, the

residual error between the polynomial transfer function and the corresponding experimental transfer function $\hat{H}_{lm}(j\omega)$ is defined as

$$e_{lm}(j\omega) = \frac{B_{lm}(j\omega) - A_m(j\omega)\hat{H}_{lm}(j\omega)}{A_m(j\omega)} \tag{3-45}$$

where

$$B_{lm}(j\omega) = b^{(l,m)}_{n_B(l,m)}(j\omega)^{n_B(l,m)} + b^{(l,m)}_{n_B(l,m)-1}(j\omega)^{n_B(l,m)-1} + \ldots + b^{(l,m)}_0 \tag{3-46}$$

$$A_m(j\omega) = (j\omega)^{n_A(m)} + a^{(m)}_{n_A(m)-1}(j\omega)^{n_A(m)-1} + \ldots + a^{(m)}_0 \tag{3-47}$$

By simplification of residual error Eq. (3-45) one would get an equation for each input/output transfer function similar to Eq. (3-22) in SISO systems case. However, in contrast to SISO systems, the residual error in SIMO/MIMO case is defined as a vector error for transfer functions from a single input to all related outputs such that

$$\boldsymbol{err}^{(m)}(j\omega) = \begin{bmatrix} [b^{(1,m)}_{n_B(1,m)}(j\omega)^{n_B(1,m)} + \ldots + b^{(1,m)}_0] - \hat{H}_{1,m}(j\omega)[(j\omega)^{n_A(m)} + \ldots + a^{(m)}_0] \\ \vdots \\ [b^{(L,m)}_{n_B(L,m)}(j\omega)^{n_B(L,m)} + \ldots + b^{(L,m)}_0] - \hat{H}_{L,m}(j\omega)[(j\omega)^{n_A(m)} + \ldots + a^{(m)}_0] \end{bmatrix} \tag{3-48}$$

Eq. (3-48) can be set in a matrix form as

$$\mathbf{D}^{(m)}_{Ln_\omega \times (\sum_l n_B(m,l)+n_A(m)+L)} \tilde{\mathbf{x}}^{(m)}_{(\sum_l n_B(m,l)+n_A(m)+L)\times 1} = \mathbf{V}^{(m)}_{Ln_\omega \times 1} - \mathbf{err}^{(m)}_{Ln_\omega \times 1} \tag{3-49}$$

where the vector $\mathbf{V}$ for the m^{th} input is defined as

$$\mathbf{V}_{Ln_\omega \times 1}^{(m)} = \begin{bmatrix} \hat{H}_{1,m}(j\omega_1)(j\omega_1)^{n_A(m)} \\ \vdots \\ \hat{H}_{1,m}(j\omega_{n_\omega})(j\omega_{n_\omega})^{n_A(m)} \\ \hline \vdots \\ \hline \hat{H}_{L,m}(j\omega_1)(j\omega_1)^{n_A(m)} \\ \vdots \\ \hat{H}_{L,m}(j\omega_{n_\omega})(j\omega_{n_\omega})^{n_A(m)} \end{bmatrix}^{\mathrm{T}} \tag{3-50}$$

and $\mathbf{D}$ is a matrix that is defined for m^{th} input as

$$\mathbf{D}^{(m)} = \begin{bmatrix} \overline{\mathbf{D}}_1^{(m)} & \widetilde{\mathbf{D}}_1^{(m)} & \mathbf{0} & \cdots & \mathbf{0} \\ \overline{\mathbf{D}}_2^{(m)} & \mathbf{0} & \widetilde{\mathbf{D}}_2^{(m)} & & \vdots \\ \vdots & \vdots & \ddots & \ddots & \mathbf{0} \\ \overline{\mathbf{D}}_L^{(m)} & \mathbf{0} & \cdots & \mathbf{0} & \widetilde{\mathbf{D}}_L^{(m)} \end{bmatrix} \tag{3-51}$$

where submatrices $\overline{\mathbf{D}}_l^{(m)}$ are given by

$$\overline{\mathbf{D}}_l^{(m)} = \begin{bmatrix} (j\omega_1)^{n_A(m)-1}\hat{H}_{l,m}(j\omega_1) & (j\omega_1)^{n_A(m)-2}\hat{H}_{l,m}(j\omega_1) & \cdots & \hat{H}_{l,m}(j\omega_1) \\ (j\omega_2)^{n_A(m)-1}\hat{H}_{l,m}(j\omega_2) & (j\omega_2)^{n_A(m)-2}\hat{H}_{l,m}(j\omega_2) & & \hat{H}_{l,m}(j\omega_2) \\ \vdots & \vdots & & \vdots \\ (j\omega_{n_\omega})^{n_A(m)-1}\hat{H}_{l,m}(j\omega_{n_\omega}) & (j\omega_{n_\omega})^{n_A(m)-2}\hat{H}_{l,m}(j\omega_{n_\omega}) & \cdots & \hat{H}_{l,m}(j\omega_{n_\omega}) \end{bmatrix} \tag{3-52}$$

and block matrices $\widetilde{\mathbf{D}}_l^{(m)}$ that sit along a diagonal in $\mathbf{D}^{(m)}$ are

$$\widetilde{\mathbf{D}}_l^{(m)} = \begin{bmatrix} -(j\omega_1)^{n_B(l,m)} & -(j\omega_1)^{n_B(l,m)} & \cdots & -1 \\ -(j\omega_2)^{n_B(l,m)} & -(j\omega_2)^{n_B(l,m)} & \cdots & -1 \\ \vdots & \vdots & \ddots & \vdots \\ -(j\omega_{n_\omega})^{n_B(l,m)} & -(j\omega_{n_\omega})^{n_B(l,m)} & \cdots & -1 \end{bmatrix} \tag{3-53}$$

and $\tilde{\mathbf{x}}$, the vector of the coefficients of the numerator and denominator polynomials of all transfer functions from the m^{th} input to all L outputs is

$$\tilde{\mathbf{x}}^{(m)} = \left[a_{n_A-1}^{(m)} \;\cdots\; a_0^{(m)} \;\vdots\; b_{n_B(1,m)}^{(1,m)} \;\cdots\; b_0^{(1,m)} \;\vdots\; \cdots \;\vdots\; b_{n_B(L,m)}^{(L,m)} \;\cdots\; b_0^{(L,m)} \right]^{\mathrm{T}} \quad (3\text{-}54)$$

Similarly to SISO systems, the vector of unknown coefficients $\tilde{\mathbf{x}}$ is evaluated from

$$\tilde{\mathbf{x}} = (\mathbf{D}^{*}\mathbf{D})^{-1}\mathrm{Re}(\mathbf{D}^{*}\mathbf{V}) \quad (3\text{-}55)$$

The procedure described by Eq. (3-48) to Eq. (3-55) computes the initial approximate estimation part of the INVFREQS method for SIMO systems case. However, for MIMO systems, the same procedure is executed M times in order to obtain the transfer functions with respect to each input. The stability of the estimated system is checked by calculating the roots of the estimated denominator polynomial for each input m, $A_m(j\omega)$, and verifying that the real parts of the roots are negative.

The iterative part of INVFREQS method for SIMO and MIMO systems considers the estimated vector $\tilde{\mathbf{x}}$ as an initial estimate. Similarly to SISO case, the estimated coefficients of the transfer function polynomials are assumed biased by an error Δ where,

$$\hat{B}_{lm}(j\omega) = (b_{n_B(l,m)}^{(l,m)} + \Delta b_{n_B(l,m)}^{(l,m)})(j\omega)^{n_B(l,m)} + \ldots + (b_0^{(l,m)} + \Delta b_0^{(l,m)}) \quad (3\text{-}56)$$

$$\hat{A}_m(j\omega) = (j\omega)^{n_A(m)} + (a_{n_A(m)-1}^{(m)} + \Delta a_{n_A(m)-1}^{(m)})(j\omega)^{n_A(m)-1} + \ldots + (a_0^{(m)} + \Delta a_0^{(m)}) \quad (3\text{-}57)$$

where

$$\hat{a}_i^{(m)} = a_i^{(m)} + \Delta a_i^{(m)} \quad \text{and} \quad \hat{b}_i^{(l,m)} = b_i^{(l,m)} + \Delta b_i^{(l,m)} \quad (3\text{-}58)$$

By substituting the estimated polynomial coefficients, the vector error as defined in Eq. (3-48) is evaluated,

$$\hat{\boldsymbol{err}}^{(m)}(j\omega)=\begin{bmatrix}(\hat{b}^{(1,m)}_{n_B(1,m)}(j\omega)^{n_B(1,m)}+\ldots+\hat{b}^{(1,m)}_0)-\hat{H}_{1,m}(j\omega)((j\omega)^{n_A(m)}+\ldots+\hat{a}^{(m)}_0)\\ \vdots\\ (\hat{b}^{(L,m)}_{n_B(L,m)}(j\omega)^{n_B(L,m)}+\ldots+\hat{b}^{(L,m)}_0)-\hat{H}_{L,m}(j\omega)((j\omega)^{n_A(m)}+\ldots+\hat{a}^{(m)}_0)\end{bmatrix} \tag{3-59}$$

whereas by substituting Eqs. (3-56) and (3-57) into Eq. (3-48) gives a matrix form of the resulting equation similar to that in the SISO case

$$\Delta\mathbf{D}^{(m)}_{Ln_\omega\times(\sum_l n_B(m,l)+n_A(m)+L)}\Delta\tilde{\mathbf{x}}^{(m)}_{(\sum_l n_B(m,l)+n_A(m)+L)\times 1}=\hat{\mathbf{err}}^{(l,m)}_{Ln_\omega\times 1)} \tag{3-60}$$

The $\Delta\mathbf{D}$ matrix for m^{th} input is

$$\Delta\mathbf{D}^{(m)}=\begin{bmatrix}\Delta\overline{\mathbf{D}}^{(m)}_1 & \Delta\tilde{\mathbf{D}}^{(m)}_1 & \mathbf{0} & \cdots & \mathbf{0}\\ \Delta\overline{\mathbf{D}}^{(m)}_2 & \mathbf{0} & \Delta\tilde{\mathbf{D}}^{(m)}_2 & & \vdots\\ \vdots & \vdots & \ddots & \ddots & \mathbf{0}\\ \Delta\overline{\mathbf{D}}^{(m)}_L & \mathbf{0} & \cdots & \mathbf{0} & \Delta\tilde{\mathbf{D}}^{(m)}_L\end{bmatrix} \tag{3-61}$$

where submatrices $\Delta\overline{\mathbf{D}}^{(m)}_l$ are given by

$$\Delta\overline{\mathbf{D}}^{(m)}_l=\begin{bmatrix}\dfrac{(j\omega_1)^{n_A(m)-1}\hat{H}_{l,m}(j\omega_1)}{\hat{A}(j\omega_1)} & \dfrac{(j\omega_1)^{n_A(m)-2}\hat{H}_{l,m}(j\omega_1)}{\hat{A}(j\omega_1)} & \cdots & \dfrac{\hat{H}_{l,m}(j\omega_1)}{\hat{A}(j\omega_1)}\\ \dfrac{(j\omega_2)^{n_A(m)-1}\hat{H}_{l,m}(j\omega_2)}{\hat{A}(j\omega_2)} & \dfrac{(j\omega_2)^{n_A(m)-2}\hat{H}_{l,m}(j\omega_2)}{\hat{A}(j\omega_2)} & & \dfrac{\hat{H}_{l,m}(j\omega_2)}{\hat{A}(j\omega_2)}\\ \vdots & \vdots & & \vdots\\ \dfrac{(j\omega_{n_\omega})^{n_A(m)-1}\hat{H}_{l,m}(j\omega_{n_\omega})}{\hat{A}(j\omega_{n_\omega})} & \dfrac{(j\omega_{n_\omega})^{n_A(m)-2}\hat{H}_{l,m}(j\omega_{n_\omega})}{\hat{A}(j\omega_{n_\omega})} & \cdots & \dfrac{\hat{H}_{l,m}(j\omega_{n_\omega})}{\hat{A}(j\omega_{n_\omega})}\end{bmatrix} \tag{3-62}$$

and block matrices $\Delta\widetilde{\mathbf{D}}_l^{(m)}$ that sit along a diagonal in $\Delta\mathbf{D}^{(m)}$ are

$$\Delta\widetilde{\mathbf{D}}_l^{(m)} = \begin{bmatrix} \dfrac{-(j\omega_1)^{n_B(l,m)}}{\hat{A}(j\omega_1)} & \dfrac{-(j\omega_1)^{n_B(l,m)}}{\hat{A}(j\omega_1)} & \cdots & \dfrac{-1}{\hat{A}(j\omega_1)} \\ \dfrac{-(j\omega_2)^{n_B(l,m)}}{\hat{A}(j\omega_2)} & \dfrac{-(j\omega_2)^{n_B(l,m)}}{\hat{A}(j\omega_2)} & \cdots & \dfrac{-1}{\hat{A}(j\omega_2)} \\ \vdots & \vdots & \ddots & \vdots \\ \dfrac{-(j\omega_{n_\omega})^{n_B(l,m)}}{\hat{A}(j\omega_{n_\omega})} & \dfrac{-(j\omega_{n_\omega})^{n_B(l,m)}}{\hat{A}(j\omega_{n_\omega})} & \cdots & \dfrac{-1}{\hat{A}(j\omega_{n_\omega})} \end{bmatrix} \tag{3-63}$$

In case of SIMO systems, the vector of the error coefficients is defined as,

$$\Delta\widetilde{\mathbf{x}}^{(m)} = \left[\Delta a_{n_A(m)-1}^{(m)} \ \cdots \ \Delta a_0^{(m)} \,\middle|\, \Delta b_{n_B(1,m)}^{(1,m)} \ \cdots \ \Delta b_0^{(1,m)} \,\middle|\, \cdots \,\middle|\, \Delta b_{n_B(L,m)}^{(L,m)} \ \cdots \ \Delta b_0^{(L,m)}\right]^{\mathrm{T}} \tag{3-64}$$

Then the error coefficients vector $\Delta\widetilde{\mathbf{x}}^{(m)}$ is evaluated through the following equation,

$$\Delta\widetilde{\mathbf{x}}^{(m)} = (\Delta\mathbf{D}^{(m)^*}\Delta\mathbf{D}^{(m)})^{-1}\mathrm{Re}(\Delta\mathbf{D}^{(m)^*}\hat{\mathbf{e}}\mathbf{r}\mathbf{r}^{(m)}) \tag{3-65}$$

For MIMO systems, the same procedure is repeated M times to obtain the error coefficients of transfer functions with respect to each input. A similar convergence check to that explained for SISO systems is applied. These loops of evaluation of $\Delta\widetilde{\mathbf{x}}$ and modification of the estimated coefficients are repeated untill the norm of the error coefficients vector becomes smaller than the value of a tolerance factor as in Eq. (3-43).

3.8.3 Least Squares Estimation of Structural Parameters

The next task, then, is to use estimates of the polynomial coefficients of the transfer functions to obtain estimates of structural parameters such as stiffness and damping coefficients. This, however, requires knowledge of the direct relations between the transfer function coefficients and the structural parameters. To develop such relations, a method is used that is based on the conventional definition of the transfer function in the frequency domain.

By considering a state-space representation of a structural system

$$\dot{\mathbf{q}} = \tilde{\mathbf{A}}\mathbf{q} + \tilde{\mathbf{B}}f, \qquad \mathbf{y} = \mathbf{C}\mathbf{q} + \mathbf{D}f + \mathbf{v} \tag{3-66}$$

where $\mathbf{q} = [\mathbf{x}^T \quad \dot{\mathbf{x}}^T]^T$ is the state vector, $\tilde{\mathbf{A}}$ is the system state matrix which is dependent on the mass $\mathbf{M}$, damping $\mathbf{C}_d$, and stiffness $\mathbf{K}$ matrices of the structural system such that,

$$\tilde{\mathbf{A}} = \begin{bmatrix} \mathbf{0}_{n\text{DOF}\times n\text{DOF}} & \mathbf{I}_{n\text{DOF}\times n\text{DOF}} \\ \left(-\mathbf{M}^{-1}\mathbf{K}\right)_{n\text{DOF}\times n\text{DOF}} & \left(-\mathbf{M}^{-1}\mathbf{C}_d\right)_{n\text{DOF}\times n\text{DOF}} \end{bmatrix} \tag{3-67}$$

and nDOF is the number of degrees of freedom of the system. The $\tilde{\mathbf{B}}$ matrix is the input influence matrix, $\mathbf{C}$ is the output influence matrix for the state vector $\mathbf{q}$, and $\mathbf{D}$ is the direct transmission matrix. In both equations, f is an excitation force, and $\mathbf{y}$ is a $m \times 1$ vector of measured responses corrupted by $m \times 1$ sensor noise vector $\mathbf{v}$.

Thus, the system can be represented by the $m \times 1$ transfer function (TF) matrix $\mathbf{H}(j\omega)$, expressed as the ratio of numerator and denominator polynomials as

$$\mathbf{H}(j\omega) = \mathbf{B}(j\omega) / A(j\omega) \tag{3-68}$$

However, another definition of the TF that depends on the system state matrix $\widetilde{\mathbf{A}}$ is,

$$\mathbf{H}(j\omega) = \mathbf{C}[(j\omega)\mathbf{I}_{(2\times n\text{DOF})\times(2\times n\text{DOF})} - \widetilde{\mathbf{A}}]^{-1}\widetilde{\mathbf{B}} + \mathbf{D} \tag{3-69}$$

Equating the right hand sides of Eqs. (3-66) and (3-67) gives

$$\mathbf{B}(j\omega) / A(j\omega) = \mathbf{C}[(j\omega)\mathbf{I}_{(2\times n\text{DOF})\times(2\times n\text{DOF})} - \widetilde{\mathbf{A}}]^{-1}\widetilde{\mathbf{B}} + \mathbf{D} \tag{3-70}$$

Knowing the structure of the system state matrix, the dependence of **C**, the output influence matrix, on **M**, $\mathbf{C}_d$, and **K** matrices, and the dependence of the $\widetilde{\mathbf{B}}$ and **D** on the type of the excitation force *f*, one can obtain a parametric representation of the coefficients of the numerator and denominator polynomials in terms of **M**, $\mathbf{C}_d$, and **K** matrices components which will be denoted $\widetilde{\mathbf{x}}(\mathbf{M},\mathbf{C}_d,\mathbf{K})$.

Finally, the difference between the parametric forms of the coefficients of the polynomials, $\mathbf{B}(j\omega)$ and $A(j\omega)$, from Eq. (3-68) and the estimates of these coefficients obtained from the INVFREQS stage $\widetilde{\mathbf{x}}_{\text{final}}$, is defined as an error vector

$$\mathbf{error} = \widetilde{\mathbf{x}}_{\text{final}} - \widetilde{\mathbf{x}}(\mathbf{M},\mathbf{C},\mathbf{K}) \tag{3-71}$$

Minimizing the sum of the square errors in Eq. (3-69) for all coefficients will result in an estimate to the unknown parameter vector that includes the stiffness and damping coefficients.

3.8.4 Some Applications and Results for INVFLS Method

The two degree-of-freedom (2DOF) shear building structure model shown in Fig. 3-1 is studied within the context of the INVFLS method. The structure is subjected to ambient excitation from the ground. Absolute acceleration measurements at the ground, $\ddot{x}_g$, and at the two floors, $(\ddot{x}_1 + \ddot{x}_g)$ and $(\ddot{x}_2 + \ddot{x}_g)$, are used to generate a 2×1 experimental transfer function at n_ω distinct frequency values. The theoretical transfer function matrix is the same as in Eq. (3-17) where $\boldsymbol{\theta}$ is the vector of unknown structural parameters and $\boldsymbol{\kappa}$ is the vector of known parameters based on the VSDDs actions.

The experimental transfer functions are generated in MATLAB® as discussed in Section 3.5.1. The sensor noise used in generating the five experimental VSDD transfer functions is the same as those used for the conventional structure approach for both the INVFLS and ILSN applications. The VSDD is installed in the lateral bracing of the structure. For comparison with the results from ILSN method, similar VSDD locations in the structure are studied: a VSDD in the first story of the structure, then only in the second story and, finally, in both stories. As in the previous sections, the results are compared to the conventional structure approach. It is assumed that, of all structural parameters, only the mass of the 1st story m_1 is known.

In the numerical model considered here, the floor masses and story stiffnesses are taken to be unity. The story damping coefficients are set to 0.05. The

single VSDD is assumed to provide additional stiffness in the story at which it is located with five discrete stiffness levels, corresponding to an additional 0%, 10%, 20%, 30% and 40% stiffness; *i.e.*, $\kappa_1 = 0.0$, $\kappa_2 = 0.1$, ..., $\kappa_5 = 0.4$ where, in this case, $\boldsymbol{\kappa} = \kappa = k_{VSDD} / m_1$. For this study, the number of evenly spaced frequency points, n_ω, is 251 when comparing results of VSDD approach and the conventional structure approach, and is 2001 when comparing the INVFLS and ILSN methods. (The ILSN study in the previous sections used only 51 frequency points; such a larger number of frequency points is used here since INVFREQS is non-parametric so it can handle the computation for a large number of frequencies in much shorter time than ILSN method.) In addition, picking a larger number of frequency points is done since the least squares solution in the ILSN method depends on more information than the least squares stage in case of INVFLS method. It is also assumed that the same noise level exists for the simulated experimental transfer functions.

The comparisons reported here are the differences between:

- The VSDD approach, using five experimental transfer function matrices, one per VSDD stiffness level, and
- The conventional structure approach with $\kappa = 0.0$ where the conventional approach uses a square error based on five separate experimental transfer functions.

3.8.5 Analysis of Results

The INVFLS method is found to be successful in estimating stiffness coefficients. However, the estimation of the damping coefficients exhibits large deviations from the exact values. The results are shown in Fig. 3-31 for a VSDD in the first story, in Fig. 3-32 for a VSDD in the second story, and in Fig. 3-33 for VSDDs in both stories. Based on 100 noisy patterns of the simulated transfer function, the results indicate that, for the VSDD approach, the relative error in the estimates of stiffness coefficients has a maximum standard deviation of 3% for the first story and 1% for the second story. Meanwhile, the relative error in the estimates of the damping coefficients has a maximum standard deviation of 35% for the 1^{st} story and 20% for the 2^{nd} story.

Comparing the VSDD and conventional structure approaches, it is observed from Fig. 3-31, for one VSDD in the 1^{st} story, that the stiffness coefficient estimate of the 1^{st} story is improved by using VSDDs whereas better estimation of the 2^{nd} floor stiffness coefficient is achieved using the conventional structure approach. The trend of the variation of the damping coefficients estimates, however, shows no clear difference between the two approaches.

For a VSDD in the 2^{nd} story only, the stiffness estimates for both stories have smaller variations using VSDD approach. Also, the damping coefficients estimates for both stories, though still with large variations, show some modest improvement with the VSDD approach.

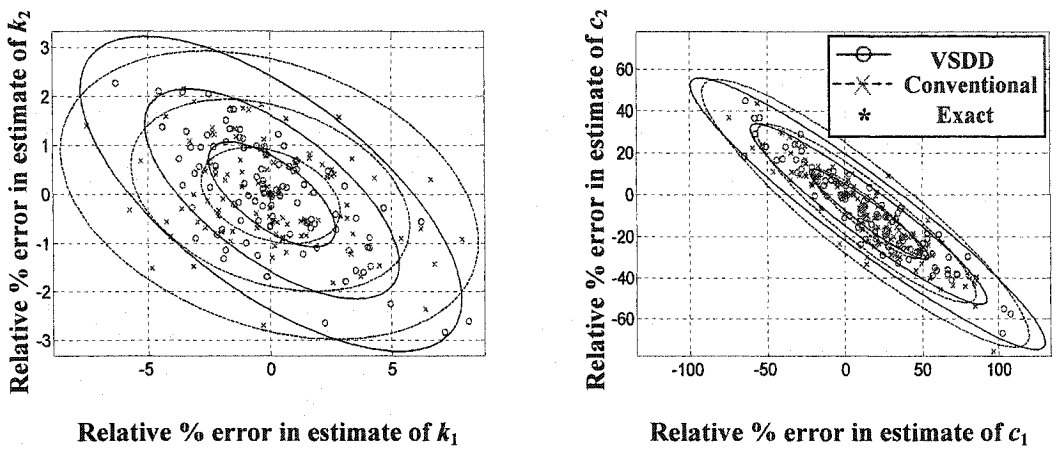

Fig. 3-31. Stiffness and damping estimate error levels for INVFLS method for 2DOF model with VSDD in 1st story only

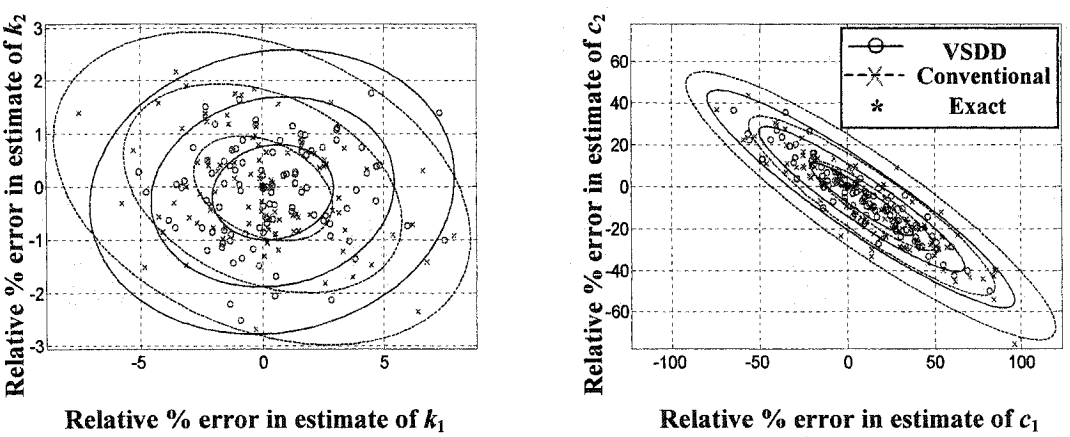

Fig. 3-32. Stiffness and damping estimate error levels for INVFLS method for 2DOF model with VSDD in 2nd story only

Using VSDDs in both stories, the variation of the stiffness coefficient estimate in the 2nd story is smaller than any other VSDD or conventional structure case. However, while the variation of the estimate of the stiffness coefficient of the 1st story is smaller than that of the conventional structure approach, locating a single VSDD in the 1st story or 2nd story only gives slightly smaller variation for the relative error of estimation as shown in Fig. 3-31 and Fig. 3-32. The variation of the relative

error of the damping estimates shows the same trend as using a VSDD in the 2nd story only.

By increasing the number of frequencies, n_ω, the results for stiffness and damping coefficients identification are improved. This is clear by comparing the results of INVFLS method in Fig. 3-31 to Fig. 3-33 to those in Fig. 3-34.

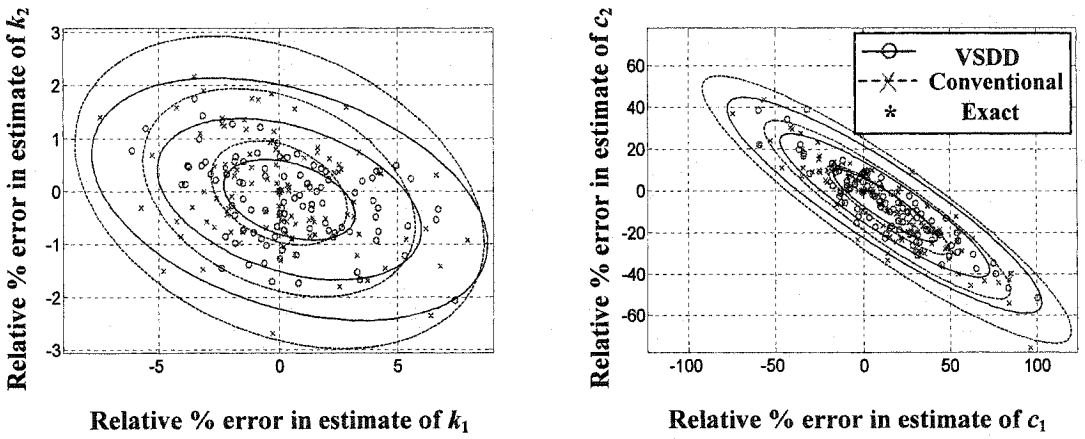

Fig. 3-33. Stiffness and damping estimate error levels for INVFLS method for 2DOF model with VSDDs in both stories

Comparing the results from the INVFLS method to those of ILSN method, shown in Fig. 3-34, one can observe that the ILSN method gives better estimates for the stiffness coefficients in the first story whereas INVFLS method gives better estimates for the stiffness coefficients of the second story. This is the case for all three VSDDs configurations in the 2DOF shear building structure.

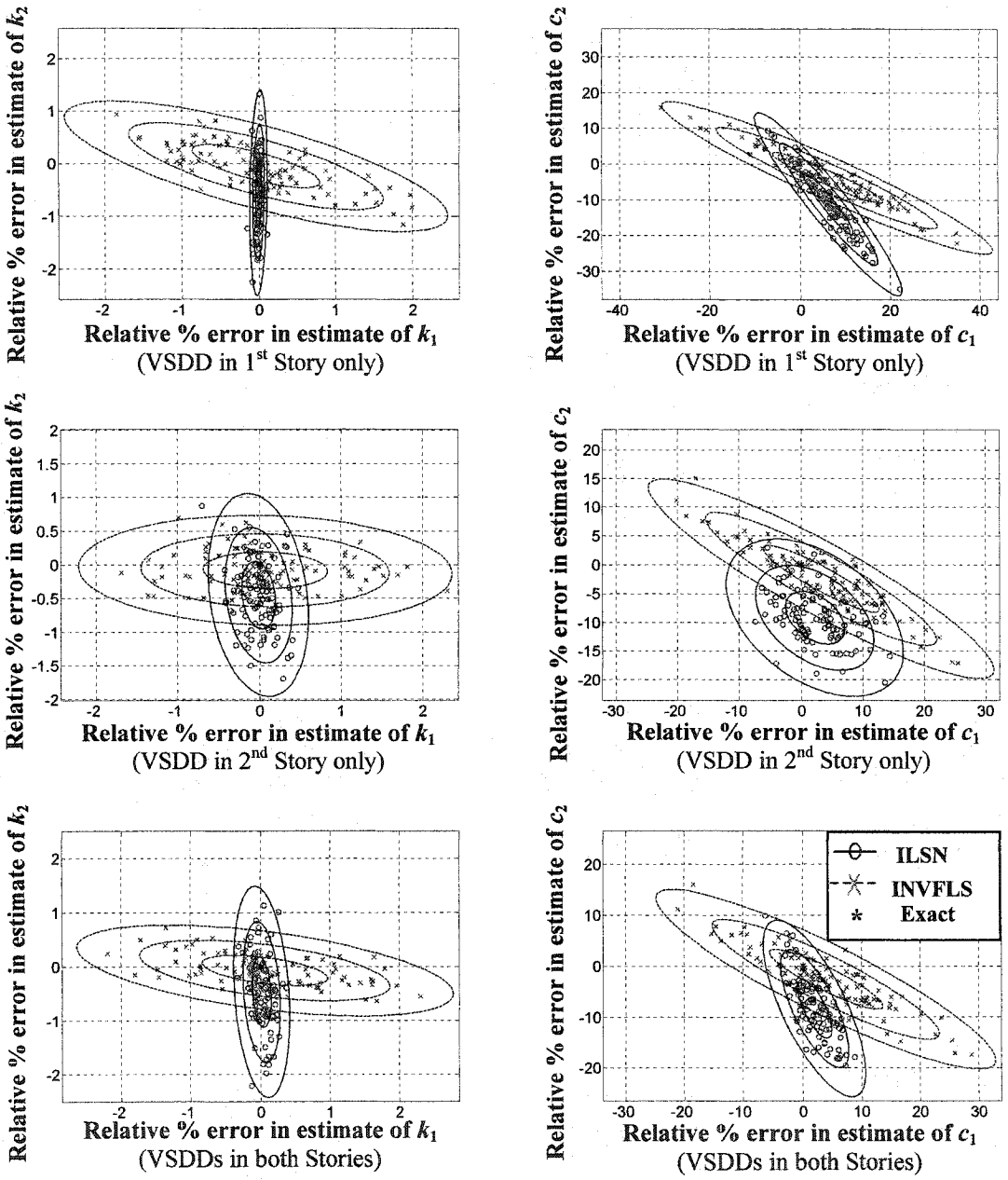

Fig. 3-34. Comparison of stiffness and damping estimate error levels between INVFLS and ILSN methods for 2DOF shear building model

However, the estimates of the damping coefficients are found to have less variation using the ILSN method for solving the identification problem. Nevertheless, Fig. 3-34 shows that the mean estimates for either stiffness or damping coefficients are always better using the INVFLS method. This may be attributed to the large number of frequency points used in the optimization problem in the INVFLS method. The INVFLS method also proved to consume much less computational time and converged faster to the results. This may be attributed to the fact that the INVFREQS stage of the INVFLS method uses a non-parametric numerical technique that is easily handled numerically, in contrast with the parametric problems in the ILSN method. Moreover, the application of the ILSN method requires some *a priori* initial guesses of the parameters to be estimated, whereas the INVFLS method has no such requirement and is able to estimate the stiffness parameters successfully with relatively small errors.

When it comes to choosing which method is applied on-site, the control designer should study the priorities whether absolute accuracy is more important than computation time or vice versa. Also, the designer should consider that using the ILSN method may require some prior guesses of the estimated parameters, which may require some experience. A good suggestion is to use the results of INVFLS method as an initial guess for the ILSN method.

3.9 VSDDs in Subspace ID

3.9.1 Introduction

The identification of modal parameters for structures from experimental data is sometimes carried out using methods that operate in the time domain. Typically, a curve is fit to free decay response data. This is based on a difference equation or state space mathematical model for the structure. In addition, the state space model has received considerable attention for system analyses and design in control and systems research during the last three decades. The basic development in state space realization is attributed to Ho and Kalman (1965) who introduced the important principle of minimum realization theory, which is the process of constructing a state space representation (Juang and Pappa, 1985). The Eigensystem Realization Algorithm (ERA), a modification and an extension to the minimum realization theory, was developed by Juang and Pappa (1985). The ERA is a state-space realization identification technique from noisy measurement data. Then, based on the identified state space model, the modal parameters can be obtained. This method is very effective in the identification of lightly damped structures (like many civil structures) and can also be applied to multi-input/multi-output systems. This Section studies the improvement in identifying structural parameters (stiffness) using the ERA method for identification when VSDDs are included and commanded to induce additional stiffness.

3.9.2 Eigen System Realization Algorithm

The Eigensystem Realization Algorithm (ERA) is a modal testing method (Juang and Pappa, 1985) developed at the NASA Langley research center. This state space method makes use of model overspecification in the initial stage in order to reduce bias. Spurious results are minimized by reducing an over-specified model order by singular value truncation. Moreover, a judicious choice of data and its proper arrangement in the block matrix can also be used to minimize the computational requirements of the method. The important features of the ERA method (Juang and Pappa, 1985) can be summarized in the following:

1. From the computational standpoint, simple numerical operations are needed.
2. The computational procedure is numerically stable.
3. The structural dynamics requirements for modal parameter identification and the control design requirements for a reduced state space model are satisfied.
4. Data from more than one test can be used simultaneously to efficiently identify closely spaced eigenvalues.
5. Computational requirements are moderate.

Generally, the ERA algorithm consists of two major parts, namely, the basic formulation of the minimum-order realization and the modal parameter computation. The technique begins by forming a block data matrix which is obtained by deleting some rows and some columns of the generalized Hankel matrix of the pulse response (Markov Parameters), but maintaining the first block matrix intact. Singular value decomposition is then applied on the system Hankel matrix to compute the singular

values and unitary matrices (all of the columns are orthonormal) of a system, which are subsequently used to know the order of the system and to obtain a realization for the state space matrices. Natural frequencies, damping ratios, and mode shapes of the simulated structure can be obtained from the realized system matrix.

The system to be identified is assumed to be discrete-time, linear, and time invariant of the form:

$$\mathbf{x}(k+1) = \mathbf{A}\mathbf{x}(k) + \mathbf{B}\mathbf{u}(k), \qquad \mathbf{y}(k) = \mathbf{C}\mathbf{x}(k) \tag{3-72}$$

with n_u inputs and n_y outputs. The Markov (pulse response) parameters are given by:

$$\mathbf{Y}(0) = \mathbf{D}, \qquad \mathbf{Y}(k) = \mathbf{C}\mathbf{A}^{k-1}\mathbf{B}, \; k>0 \tag{3-73}$$

where **A** is the discrete state matrix, **B** is the input influence matrix that characterizes the location and type of inputs, **C** is the output influence matrix for the state vector **x**, and **D** is direct transmission matrix.

For the application in this chapter, the Markov parameters are measured in the time domain by introducing impulses to system inputs. Then, a generalized Hankel matrix $\mathbf{H}(k)$ of the Markov parameters is formed where $\mathbf{H}(k)$ is in the form:

$$\mathbf{H}(k) = \begin{bmatrix} \mathbf{Y}(k) & \mathbf{Y}(k+1) & \cdots & \mathbf{Y}(k+s) \\ \mathbf{Y}(k+1) & \mathbf{Y}(k+2) & \cdots & \mathbf{Y}(k+s+1) \\ \cdots & \cdots & \ddots & \cdots \\ \mathbf{Y}(k+r) & \mathbf{Y}(k+r+1) & \cdots & \mathbf{Y}(k+r+s) \end{bmatrix} \tag{3-74}$$

where r and s are arbitrary integers. The variables r and s are taken as 20-30 and 10 times, respectively, the assumed order of the system for best results (Caicedo *et al.*, 2004).

The generalized Hankel matrix is then evaluated for k=0. This is followed by performing a singular value decomposition on the Hankel matrix $\mathbf{H}(0)$ such that:

$$\mathbf{H}(0) = \mathbf{P}\Sigma\mathbf{Q}^{\mathrm{T}} \tag{3-75}$$

where the $\mathbf{P}$ and $\mathbf{Q}$ matrices are unitary matrices (all of the columns are orthonormal), and the matrix Σ is the diagonal matrix of singular values. The order of the system will be apparent in the absence of noise because the first n singular values are non-zero while the rest are zeros or approximately zero. When noise exists, the order may not be so clear and one must choose what order n to use. The smaller singular values in the diagonal of Σ correspond to computational or noise (non-physical) modes. Once the estimated order of the system is chosen, the rows and columns associated with the computational modes are eliminated to form a condensed version of the singular values and unitary matrices, Σ_n, $\mathbf{P}_n$, and $\mathbf{Q}_n$, respectively.

Using these truncated matrices, estimates of the state space matrices for the discrete-time structural model are found by using the formulas (Juang, 1994):

$$\hat{\mathbf{A}} = \Sigma_n^{-1/2}\mathbf{P}_n^{\mathrm{T}}\mathbf{H}(1)\mathbf{Q}_n\Sigma_n^{-1/2} \tag{3-76}$$

$$\hat{\mathbf{B}} = \Sigma_n^{1/2}\mathbf{Q}_n^{\mathrm{T}}\mathbf{E}_m \tag{3-77}$$

$$\hat{\mathbf{C}} = \mathbf{E}_n^{\mathrm{T}} \mathbf{P}_n \boldsymbol{\Sigma}_n^{1/2} \tag{3-78}$$

where

$$\mathbf{E}_n^{\mathrm{T}} = [\mathbf{I} \quad \mathbf{0}], \qquad \mathbf{E}_m = [\mathbf{I} \quad \mathbf{0}] \tag{3-79}$$

The eigenvalues and eigenvectors of the system can then be computed from the identified system matrix $\hat{\mathbf{A}}$ using a standard eigenvalue problem. The output matrix $\hat{\mathbf{C}}_n$ is used to transform the computed eigenvectors (corresponding to non-physical states in the identified model) to displacement at the floors of the structure using the equation

$$\boldsymbol{\gamma} = \hat{\mathbf{C}} \hat{\boldsymbol{\Phi}} \tag{3-80}$$

where $\boldsymbol{\gamma}$ is the matrix of the output shapes and $\hat{\boldsymbol{\Phi}}$ is the matrix of the eigenvectors of the state space matrix $\hat{\mathbf{A}}$. The ERA method was implemented using MATLAB®.

3.9.3 Least Squares Stiffness Estimation of the Eigenvalue Problem Solution

The structural parameters, especially the stiffness parameters, are the main interest herein. Thus, a technique that would evaluate such parameters from the modal parameters is required. The method used herein follows that of Caicedo *et al.* (2004), which is summarized as follows.

By considering a lumped mass system (such as a shear building model and the 2DOF bridge model) with n_d degrees of freedom, the mass matrix, **M**, and the stiffness matrix, **K**, are assumed to be of the form

$$\mathbf{M} = \begin{bmatrix} m_1 & 0 & \cdots & 0 & 0 \\ 0 & m_2 & \cdots & 0 & 0 \\ \vdots & \vdots & \ddots & \vdots & \vdots \\ 0 & 0 & \cdots & m_{n_d-1} & 0 \\ 0 & 0 & \cdots & 0 & m_{n_d} \end{bmatrix} \tag{3-81}$$

$$\mathbf{K} = \begin{bmatrix} k_1 + k_2 & -k_2 & \cdots & 0 & 0 \\ -k_2 & k_2 + k_3 & \ddots & \vdots & \vdots \\ 0 & \ddots & \ddots & -k_{n_d-1} & 0 \\ \vdots & \cdots & -k_{n_d-1} & k_{n_d-1} + k_{n_d} & -k_{n_d} \\ 0 & \cdots & 0 & -k_{n_d} & k_{n_d} \end{bmatrix} \tag{3-82}$$

The eigenvalue problem of such a structure is (Chopra, 1995)

$$(\mathbf{K} - \lambda_j \mathbf{M})\boldsymbol{\varphi}_j = 0 \quad \text{or} \quad \mathbf{K}\boldsymbol{\varphi}_j = \lambda_j \mathbf{M}\boldsymbol{\varphi}_j \tag{3-83}$$

where λ_j and $\boldsymbol{\varphi}_j$ are the j^{th} eigenvalue and eigenvector of the structure, respectively.

Substituting the mass and stiffness matrices into the eigenvalue problem and reorganizing so that the stiffness coefficients can be assembled in a vector

$$\Delta_j \mathbf{k} = \Lambda_j \tag{3-84}$$

where

$$\Delta_j = \begin{bmatrix} \phi_{1,j} & \phi_{1,j}-\phi_{2,j} & 0 & \cdots & 0 \\ 0 & \phi_{2,j}-\phi_{1,j} & \phi_{2,j}-\phi_{3,j} & \cdots & 0 \\ \vdots & \vdots & \ddots & \ddots & \vdots \\ 0 & 0 & \cdots & \phi_{n_d-1,j}-\phi_{n_d-2,j} & \phi_{n_d-1,j}-\phi_{n_d,j} \\ 0 & 0 & \cdots & 0 & \phi_{n_d,j}-\phi_{n_d-1,j} \end{bmatrix} \tag{3-85}$$

and the stiffness vector $\mathbf{k}$ is

$$\mathbf{k} = [k_1 \quad k_2 \quad \ldots \quad k_n]^T \tag{3-86}$$

and the vector Λ is

$$\Lambda = [\phi_{1,j}\lambda_j m_1 \quad \phi_{2,j}\lambda_j m_2 \quad \ldots \quad \phi_{n_d,j}\lambda_j m_{n_d}]^T \tag{3-87}$$

where $\phi_{i,j}$ is the i^{th} element of the eigen vector $\boldsymbol{\varphi}_j$.

Eq. (3-82) can be applied for each of the n_d eigenvalues and eigenvector pairs identified. Thus, by gathering all of the equations corresponding to Eq. (3-82) into one big matrix equation gives

$$\begin{bmatrix} \Delta_1 \\ \Delta_2 \\ \vdots \\ \Delta_n \end{bmatrix} \begin{bmatrix} k_1 \\ k_2 \\ \vdots \\ k_n \end{bmatrix} = \Delta\mathbf{k} = \Lambda = \begin{bmatrix} \Lambda_1 \\ \Lambda_2 \\ \vdots \\ \Lambda_n \end{bmatrix} \tag{3-88}$$

representing n_d^2 equations which are used to solve for the vector of stiffnesses $\mathbf{k}$ by the relation

$$\mathbf{k} = \Delta^{-1}\Lambda \tag{3-89}$$

It is important to note that the matrix Δ is not square and, consequently, a pseudo-inverse of this matrix is computed to obtain a least squares estimate of the stiffnesses. Using multiple eigenvectors improves the resulting estimations.

3.9.4 Applying VSDD approach to the ERA method

In order to apply the VSDD approach to the ERA method, some assumptions are considered. The stiffnesses of VSDDs are assumed known for any desired configuration of VSDD stiffnesses. Once the identification process (of the structure including VSDDs) is complete, the added VSDD stiffness in each corresponding story is subtracted from the estimated stiffness parameter. Thus, the results are considered estimates of the structure's stiffnesses at this configuration of the VSDDs stiffnesses.

This can be expressed through the equation

$$k_{\text{actual}} = k_{\text{estimated}} - k_{\text{VSDD}} \tag{3-90}$$

Then, by applying the same operation for each case of the VSDD stiffness and obtaining the resulting corresponding stiffness estimates, a mean estimate of the stiffnesses for all different VSDD cases can be obtained. This can be expressed in the form of the equations

$$k_i = \frac{1}{n_\kappa} \sum_{k=1}^{n_\kappa} k_{i,\text{VSDD}_k} \tag{3-91}$$

where n_κ is the number of the VSDD stiffness configuration cases.

3.9.5 Application to the 2DOF Bridge Model

The ERA approach with VSDDs is applied to the 2DOF bridge model shown in Fig. 3-5. The bridge stiffness and damping parameters are the same as in Section 3.5.2. The suggested technique is applied such that every realization of the stiffness parameters is averaged over 100 different patterns of noisy data. This is done for 20 times. The RMS noise level was taken as 10% of that of the original signal. The impulse response was generated in MATLAB® based on the exact parameters of the structure bridge structure. The additional stiffnesses induced by the VSDD are 0%, 125%, 250%, 375%, and 500% of the isolator stiffness. The system is assumed of the 4^{th} order in the identification process, so the ERA algorithm chooses the first four singular values to represent the system. The arbitrary integers r and s are taken equivalent to 50 and 20, respectively. In addition, the state space system matrices **A**, **B**, **C**, and **D** are

$$\mathbf{A}=\begin{bmatrix} 0 & 0 & 1 & 0 \\ 0 & 0 & 0 & 1 \\ -\dfrac{(k_1+k_2)+k_{VSDD}}{m_1} & \dfrac{k_2+k_{VSDD}}{m_1} & -\dfrac{(c_1+c_2)}{m_1} & \dfrac{c_2}{m_1} \\ \dfrac{k_2+k_{VSDD}}{m_2} & -\dfrac{k_2+k_{VSDD}}{m_2} & \dfrac{c_2}{m_2} & -\dfrac{c_2}{m_2} \end{bmatrix} \tag{3-92}$$

$$\mathbf{B}=[0 \quad 0 \quad 1/m_1 \quad 1/m_2]^T \tag{3-93}$$

$$\mathbf{C} = \begin{bmatrix} -\dfrac{(k_1 + k_2) + k_{VSDD}}{m_1} & \dfrac{k_2 + k_{VSDD}}{m_1} & -\dfrac{(c_1 + c_2)}{m_1} & \dfrac{c_2}{m_1} \\ \dfrac{k_2 + k_{VSDD}}{m_2} & -\dfrac{k_2 + k_{VSDD}}{m_2} & \dfrac{c_2}{m_2} & -\dfrac{c_2}{m_2} \end{bmatrix} \tag{3-94}$$

$$\mathbf{D} = [1/m_1 \quad 1/m_2]^T \tag{3-95}$$

3.9.6 Results of Identification Process

Fig. 3-35 shows the relative error in the stiffness estimates. It demonstrates that using a VSDD was beneficial in giving more accurate means of the estimated stiffnesses. In addition, the root mean square error (RMSE) of the identified stiffnesses in the first and second stories, with the VSDD approach, are about two-thirds and half, respectively, of those obtained through the conventional structure approach. Thus, it can be concluded that using VSDDs also has potential for improving the accuracy of sub-space techniques such as ERA method in identification.

Table 3-7. Estimate means and mean-square error percentage for 2DOF bridge model using ERA method (Varying stiffness)

	Exact	With VSDD		No VSDD	
		Mean (kN/m)	RMSE (%)	Mean (kN/m)	RMSE (%)
k_1	15791	15734.9	0.67	15651.65	0.99
k_2	7685	7692.5	0.73	7781.995	1.42

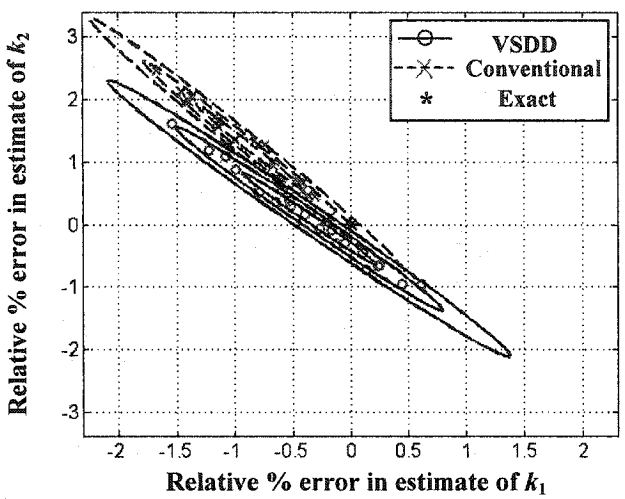

Fig. 3-35. Variation in the stiffness parameters of the pier and deck of the 2DOF Bridge system model

4 EXPERIMENTAL VERIFICATION OF THE BENEFITS OF VSDDs IN SHM

4.1 Introduction

Experimental investigations are essential to obtain a fundamental understanding of many phenomena. To verify the advantages gained by using VSDDs in structures for SHM, it is vital to identify these advantages in an experimental basis. This chapter introduces a laboratory experiment that replicates the effect of VSDDs on structures when used for SHM. A two degree-of-freedom (2DOF) experimental shear building structure is subjected to a band-limited white noise (BLWN) ground acceleration and a filtered band-limited white noise (FBLWN) through a small-scale shaking table. The acceleration of the table and the absolute accelerations of the first and second stories are recorded. The measurements are processed to obtain an identification of the stiffness of the first and second stories of the 2DOF structure before and after damage. The results verify the observations from the theoretical results in the previous chapters that the identification is improved by using VSDDs.

4.2 Experiment Description

In the area of control and SHM of civil structures, it is well recognized that experimental verification is necessary to focus research efforts in the most promising

directions (Housner *et al.*, 1994a,b). Consequently, a small-scale shaking table experiment is performed to validate the analytical results that show the improvements to SHM when using VSDDs. A schematic of the experiment, where a two degree-of-freedom (2DOF) shear building structure is mounted on and fixed to a small shaking table, is shown in Fig. 4-1. Fig. 4-1 also shows the blue power module that passes the analog command voltage signals from the MultiQ (D/A, A/D converter) board to the table and passes back the accelerometer analog measurement signals. The experiment was built and run in the SHM and Control Lab at the University of Southern California (USC).

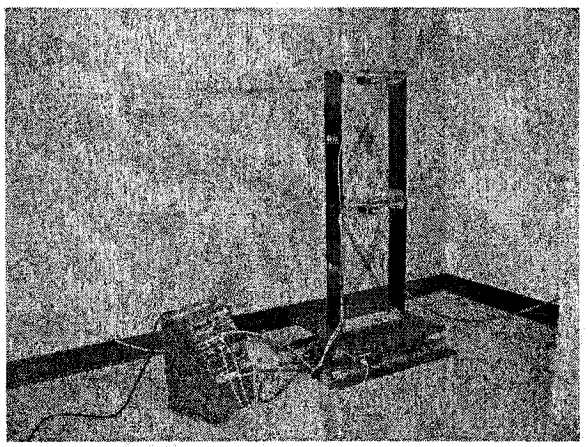

Fig. 4-1. The shaking table with the 2DOF shear building structure mounted on it

The components of the experiment, in general, include the shaking table, 2DOF shear building model, digital controller (MultiQ I/O) board, the power module for the table, PC computer, three accelerometers and two sets of steel springs necessary to replicate the various stiffness levels that would be achieved with VSDDs in a real-world application. The computer used in the experiment is a Windows 98 466MHz Pentium 3.

4.2.1 Experiment Steps

The experiment goal can be summarized in identifying damage in an experimental 2DOF structure composed of the shear building structure and two pairs of weak springs per floor, acting as bracing to the structure, as shown in Fig. 4-1. The damage in the structure will be effected by changing the stiffness of one of the two stories by removing a pair of the weak diagonal bracing springs.

The damage identification problem is solved once with no VSDDs included in the system (conventional structure) and then again when VSDDs exist in the system. In the course of the experiment, the additional forces induced by the VSDDs in the system are replicated by adding strong springs in the diagonal bracing with different configurations giving different stiffness levels. The identification process, in each damage case, is performed using four sets of measured ground and floor absolute accelerations data, obtained using four different configurations of the strong springs. For fairness in comparison, the conventional structure approach uses the same amount of measured data.

The 2DOF structure, during the experiment, is subjected to ambient ground excitation induced by the shake table. The ambient ground excitation is generated in two ways: by a band-limited white noise (BLWN) ground excitation with a cutoff frequency of approximately 20Hz, and by a filtered BLWN using the Kanai-Tajimi filter to simulate ground effects (Soong and Grigoriou, 1993; Ramallo *et al.*, 2002).

Once the data is obtained, the Iterative Least Squares Numerator (ILSN) identification method is then applied to estimate the stiffness coefficients for both

floors of the 2DOF structure. This is done in a manner similar to the simulation study in Chapter 3. (The ILSN identification technique is not detailed here; the reader is referred to Chapter 3 for more information.) Finally, the identification results of the stiffnesses in both stories are compared, before and after damage occurs, both with VSDDs in the system and without VSDDs. The experimental results confirm the simulation observations showing more accurate damage assessment when using VSDDs.

4.2.2 Components of the Experiment

Before introducing the results, the properties and nature of each component of the experiment are detailed in the following subsections.

4.2.2.1 Shaking Table Properties

The key component of the experiment is a bench-scale shake table, shown in Fig. 4-2. The shaking table is a small-scale uniaxial earthquake simulator manufactured by Quanser Consulting Inc. The table is located in the SHM and Control Lab at the University of Southern California (USC). The specifications of the table have been developed to produce a unit that is effective for a wide variety of experiments for civil engineering structures. The table is computer-controlled with a user-friendly interface. The design specifications of the shaking table, as supplied by the manufacturer, are shown in Table 4-1.

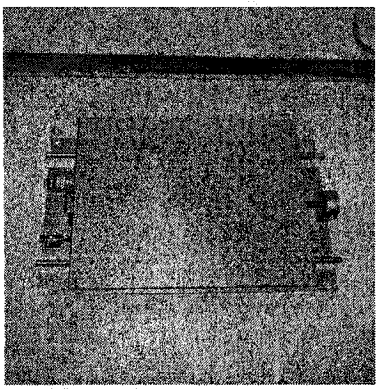

Fig. 4-2. Plan view of the shaking table

Table 4-1. Design Specifications of the Shaking Table

Specification	Value	Unit
Shake table system overall dimensions (L×W×H)	61×46×13	cm
Shake table system mass	27.2	kg
Table dimensions (payload area), (L×W)	46×46	cm
Maximum payload at 2.5g	15	kg
Peak Displacement	±7.5	cm
Operational bandwidth	20	Hz
Peak velocity	83.8	cm/s
Peak acceleration	24.5	m/s^2
Accelerometer range	±49	m/s^2
Accelerometer sensitivity	1/9.81	Vs^2/m
Lead screw spread pitch	12.7	mm/rev
Brushless servo motor power	745.7	W
Maximum continuous current	12.5	A
Motor maximum torque	1.65	N m
Linear bearing load carrying capability	131.5	kg
Linear bearing life expectancy (total travel)	6350	km
Leadscrew encoder resolution	4096	counts/rev
	3.1	μm/count

The nominal operational frequency range of the simulator is 0-20 Hz. Because the shake table motor is inherently open loop unstable, position feedback, measured from the shake table motor, is employed to stabilize the table (Christenson *et al.*, 2003).

4.2.2.2 Digital Controller

The digital controller, used in the experiment, is the MultiQ I/O board (http://www.quanser.com/English/html/solutions/fs_soln_hardware.html) with the WinCon (http://www.quanser.com/English/html/solutions/fs_soln_software_wincon.html) real time controller installed in a Windows computer. The MultiQ interface board is connected to the MultiQ I/O board by a ribbon cable, and to the power module that is, in turn, connected to the shake table. The extended terminal of the MultiQ interface board, as shown in Fig. 4-3, has 13-bit analog/digital (A/D) and 12 bit digital/analog (D/A) connections with eight input and eight output analog channels. Eight digital encoders are also available. The table control algorithm is developed using SIMULINK (1999) under MATLAB® 5.3 and executed in real time using the WinCon software. The SIMULINK code is converted to C++ code using the Real Time workshop in MATLAB® and interfaced through the WinCon software to run the control algorithms on the CPU of the PC (Quanser Consulting, 1995; Christenson *et al.*, 2003).

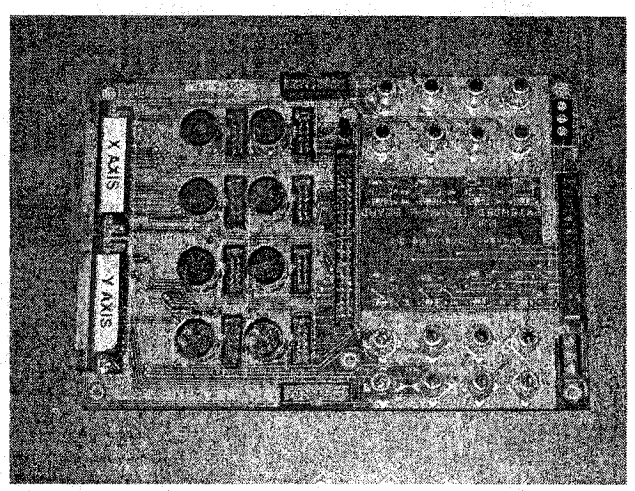

Fig. 4-3. Plan view of the extended terminal of the MultiQ interface board

4.2.2.3 2DOF Structure

A 2DOF shear building structure, shown in Fig. 4-1, is the test bed of this experiment. The structure is composed of two vertical aluminum plates in each story, with thick plexi-glass plates at the bottom, first and second stories of the structure to connect the vertical plates. The horizontal plexi-glass plates and the vertical aluminum plates are fixed to each other by three 8-32 UNC bolts in each side at each level. The interstory height is 490 mm.

The experimental structure also includes two pairs of weak steel springs located in each story as shown in Fig. 4-4. Including these weak springs as part of the experimental structure allows inducing damage in the structure, by removing one or two of these pairs, without damaging the original structure. Each pair of the weak springs represents about 7.38 % of the estimated stiffness of each story of the original structure.

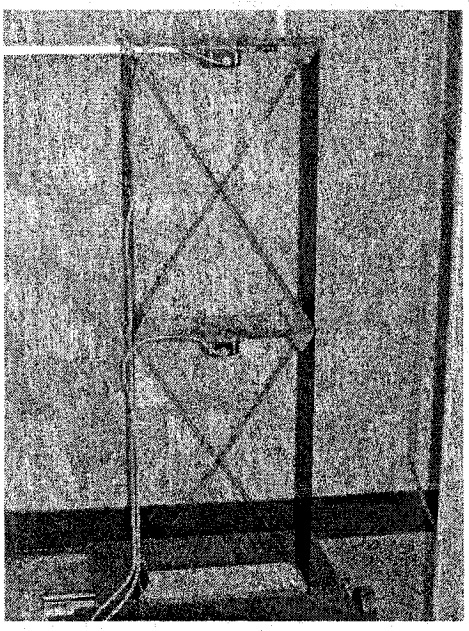

Fig. 4-4. Front view of the experimental 2DOF structure including the added weak steel springs

Prior to experimentation, the 2DOF structure was disassembled so that its dimensions and measurements could be recorded. A caliper was used to measure the thickness of the structure's components. The lengths, widths, and heights were measured using a measuring tape with accuracy of 1/32 of an inch. An electronic scale, with measurement sensitivity 1 gm, was used to weigh each component of the structure. Table 4-2 lists the measured dimensions in centimeters and masses in kilograms. It is important to note that the mass tabulated for the plexi-glass plate, also includes the mass of the screws, washers, fastener plates, and accelerometers located at the corresponding level. The weak springs are manufactured by Century Spring Corp. (Los Angeles) and have vendor stock #80039. The physical properties of the weak steel springs, as per the manufacturer's catalogue, are shown in Table 4-3.

Table 4-2. Measured Dimensions and Masses of the 2DOF Structure

	Mass (kg)	Length (cm)	Width (cm)	Thickness (cm)
Plexi-glass plate at shake table level	0.654	30.48	10.80	1.24
Plexi-glass plate at 1st story level	0.654	30.48	10.80	1.24
Plexi-glass plate at 2nd story level	0.654	30.48	10.80	1.24
Vertical Aluminum Plates (1st story)	0.236	50.17	10.80	0.18
Vertical Aluminum Plates (2nd story)	0.236	50.17	10.80	0.18

Table 4-3. Physical Properties of Weak Spring #80039 as per Manufacturer Catalogue

Stock No.	Outer Diameter (mm)	Length without Hooks (mm)	Stiffness (N/m)	Initial Tension (N)	Suggested Max. Deflection (mm)	Suggested Max. Load (N)
80039	2.39	25.40	90.00	0.30	37.00	3.60

For the sake of accuracy in the processing of results, the stiffnesses of the weak springs are verified by applying an additional test using a spring tester at the manufacturer main office (see Appendix B for manufacturer test reports). The tests are applied on two pairs of the weak springs. One of the two pairs is the one removed from the first story to replicate damage there, and the other pair is the one removed from the second story to replicate damage there. The results of the tests are shown in Table 4-4. It is found that, based on the verification tests results, that the mean stiffness of the weak springs (#80039) is 83.11 N/m, which is less than that documented in the catalogue. Thus, a pair of the weak springs represents 7.38% of the estimated overall stiffness of each floor of the experimental 2DOF structure. The

configurations of the weak springs pairs in the structure, in order to replicate damage in the structure, are shown in Table 4-5.

Table 4-4. Weak Spring (#80039) Stiffness Test Results Supplied by Manufacturer

Spring #80039	Location	Stiffness (N/m)
Sample 1	1st story	83.46
Sample 2	1st story	82.41
Sample 3	2nd story	82.06
Sample 4	2nd story	84.51

Table 4-5. Different Configurations of Spring Pairs in the 2DOF Structure to Replicate Damage in the Structure

	Case	Location	No. of Pairs
Induced Damage	No damage	1st story	2 pairs
		2nd story	2 pairs
	7.38% damage in 1st story	1st story	1 pair
		2nd story	2 pairs
	7.38% damage in 2nd story	1st story	2 pairs
		2nd story	1 pair

4.2.2.4 Accelerometers

The resulting response of the structure during the experiment is measured by accelerometers as shown in Fig. 4-5. One accelerometer is fixed to the table base level. Another two are fixed to each of the two stories in the middle bottom of the plexi-glass plates at each story. The range of the accelerometers is ± 5*g* with an output of ± 5 volts. Each accelerometer is connected via cable to the power module which is, in turn, connected to the MultiQ® unit.

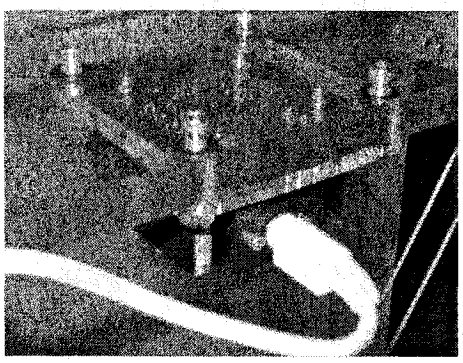

Fig. 4-5. Isometric view of the mounted accelerometer

4.2.2.5 Springs Representing VSDDs

The theoretical simulations in Chapter 3 (*e.g.*, the 2DOF bridge model problem) show that using higher VSDD stiffness to story stiffness ratio improves the results considerably. For the case of the experimental structure, the small cross-section of the aluminum plates limits the feasible added stiffness per floor because too much added vertical load could cause the vertical plates to buckle. Consequently, the springs used to represent the additional forces exerted by VSDD are chosen to have stiffness of the same order as that of the columns per story. Therefore, Century Spring Corp. spring stock number #80222 is chosen. The physical properties of this stiff spring, from the manufacturer catalogue, are shown in Table 4-6.

Table 4-6. Physical Properties, as per Manufacturer Catalogue, of Stiff Springs Used to Replicate the Effect of VSDD Forces

Stock No.	Outer Diameter (mm)	Length without Hooks (mm)	Stiffness (N/m)	Initial Tension (N)	Suggested Max. Deflection (mm)	Suggested Max. Load (N)
80222	4.57	69.90	840.00	3.00	37.00	34.00

Fig. 4-6 shows the experimental structure with the stiff springs attached. Due to the short lengths of the springs, steel links are used to connect the springs to

aluminum connections as shown in Detail A, Fig. 4-7, at each joint of the 2DOF structure. The springs are staggered across the depth of the structure, as shown in Detail B, Fig. 4-8, so that the springs do not rub against each other.

To replicate the effect of varying forces by VSDDs, the stiff spring pairs are added in four configurations. Table 4-7 shows the different configurations of the stiff spring pairs in the 2DOF structure.

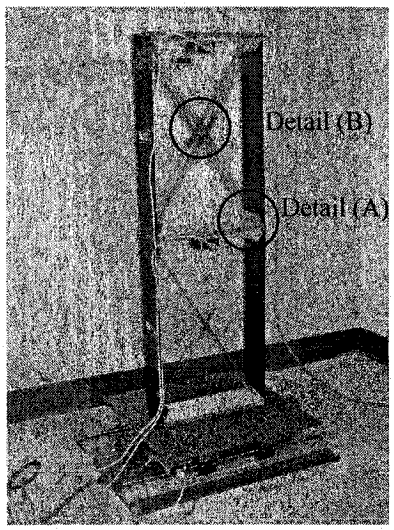

Fig. 4-6. Experimental structure with springs representing VSDDs

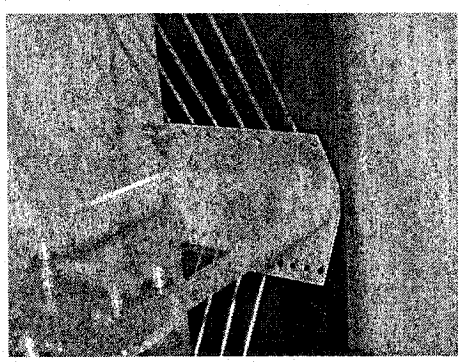

Fig. 4-7. Detail (A) showing aluminum connections and steel link

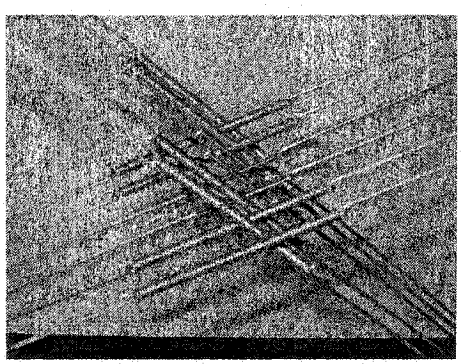

Fig. 4-8. Detail (B) showing staggered springs connected by steel link

Table 4-7. Different Configurations of Stiff Springs Pairs in the Two Stories of the 2DOF Structure

Configuration No.	No. of Pairs in 1st Story	No. of Pairs in 2nd Story
1	0	0
2	4	0
3	4	2
4	2	4

The reason for even numbered spring pairs per configuration, in each story, is to minimize any coupling of the transverse modes with those of torsion. The results obtained in system identification with the stiff springs included in the structure are compared to the case without any stiff springs in either of the two stories (conventional structure).

Since an accurate estimate of the VSDD stiffness is required in the identification, spring stiffness tests are performed by the manufacturer on the stiff springs (#80222). (See Appendix B for the test report by the manufacturer.) During the experiment, a maximum of six pairs are required (Table 4-7). Thus, the twelve springs forming these six pairs are tested to obtain the stiffnesses as shown in Table 4-8. The results show differences from those documented in the manufacturer catalogue. The measured stiffnesses are the ones used in the identification process.

Where Table 4-7 shows four pairs of stiff springs in a story, they are samples 1,3,4,5,6,7,8, and 12 Table 4-8. Where Table 4-7 shows two pairs, they are samples 2, 9, 10 and 11.

Table 4-8. Stiff Spring (#80222) Stiffness Test Results Supplied by Manufacturer

Spring #80222	Stiffness (N/m)
Sample 1	989.291
Sample 2	974.563
Sample 3	962.464
Sample 4	978.069
Sample 5	991.396
Sample 6	969.653
Sample 7	993.499
Sample 8	980.875
Sample 9	980.875
Sample 10	966.146
Sample 11	963.165
Sample 12	967.549

4.2.3 Modeling and Stiffness Calculations for the Experimental Structure

A critical precursor to SHM is the development of an accurate dynamic model of the structural system. For this study, the approach used for system identification is to construct a mathematical model to replicate the input/output behavior of the system (Dyke *et al.* 1996). The model assumed here is a shear-building model. Thus, in the calculation of the stiffness for the first and second floors, the total stiffness is considered the sum of the columns' stiffnesses and the additional equivalent stiffness due to spring pairs. Accordingly, the stiffness of each story is calculated from

$$k_{\text{story}} = \left(\sum^{n_c} k_{\text{col}} \right) + n_{\text{p}} \times 2 \times k_{\text{s}} \times \cos^2 \theta \qquad (4\text{-}1)$$

where n_c=2 is the number of columns, k_{col} is the stiffness of each vertical aluminum plate. The stiffness of each spring is k_s and n_p is the number of spring connections pairs. θ is the angle of inclination of the spring, calculated from

$$\theta = \tan^{-1}(B/h) \tag{4-2}$$

where B is the horizontal width of the 2DOF structure and h is the interstory height of each story of the 2DOF structure.

E_{AL}, the modulus of elasticity of aluminum (material of the plates), is taken as 75GPa. All cross sections of the aluminum and plexi-glass plates are rectangular. Thus, the moment of inertia of each plate can be calculated from

$$I = \frac{bt^3}{12} \tag{4-3}$$

where t is the thickness of the plate and b is the plate width. Consequently, the stiffness matrix for the undamaged structure is

$$\mathbf{K} = \left[\frac{24E_{AL}I_{AL}}{h^3} + 4 \times k_{80039} \times \cos^2\theta\right]\begin{bmatrix} 2 & -1 \\ -1 & 1 \end{bmatrix} \tag{4-4}$$

where I_{AL} is the moment of inertia of each of the aluminum plates and k_{80039} is the stiffness of the stiff spring #80039. Note that this stiffness matrix is based on the measured dimensions and assumed material properties and may not be exact due to the difference between actual and assumed material properties and modeling idealization.

4.2.4 Generation of Simulated Ground Acceleration

During the shake table experiment, the laboratory structure is assumed subjected to ambient ground excitation induced by the shake table. The ambient ground excitation is generated in two ways: by a band-limited white noise (BLWN) ground excitation with a cutoff frequency of 20Hz and by a filtered band-limited white noise (FBLWN) using the Kanai-Tajimi filter (Soong and Grigoriou, 1993; Ramallo *et al.*, 2002). The procedure for obtaining each excitation type is explained in the following paragraphs.

4.2.4.1 Band-Limited White Noise (BLWN) Generation

The SIMULINK toolbox under MATLAB® 5.3 is used for designing the excitation model that commands the shake table to generate white noise ground acceleration. The software WinCon 3.1, supplied by the manufacturer of the shake table (Quanser), uses the SIMULINK toolbox to generate models and compile them using C++. Fig. 4-9 shows the BLWN acceleration generator model used in the experiment.

The generator model of white noise ground acceleration is designed such that a BLWN displacement is commanded to the shake table. Theoretically, the commanded white noise displacement should produce BLWN acceleration. However, due to noise resulting from imperfections, frequency dependence of table dynamics and nonlinearities in the table system, this is not the case. Thus, the commanded BLWN displacement to the table should be filtered through some

frequency domain filters in order to obtain the desired white noise ground acceleration, and to enforce table safety and limitations. Consequently, two filters (Filter_1 and Filter_2 in Fig. 4-9) are added to the designed generator SIMULINK model. The first filter (Filter_1) ensures that the power spectral density (PSD) of the resulting table acceleration has a constant magnitude in the frequency domain. The second filter (Filter_2) is a low pass filter that limits the effective frequency range of the table motion with a cutoff frequency at 20 Hz. For the safety of the table, the magnitude of the commanded displacement is scaled so as not to exceed one inch, and its magnitude is only allowed to ramp up at the start of the table motion.

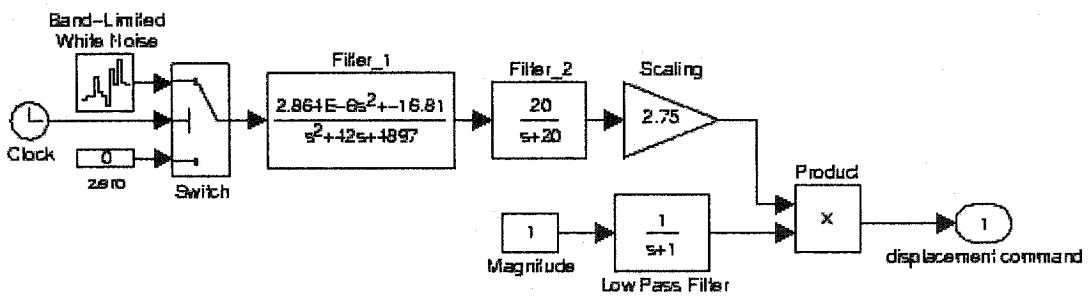

Fig. 4-9. SIMULINK model for generation of band-limited white noise ground acceleration using the shaking table

Fig. 4-10 shows a sample time history of the generated ground acceleration as measured by the accelerometer located on the table. The power spectral density (PSD) of this sample ground acceleration is shown in Fig. 4-11. (The sampling frequency is 1000 Hz.)

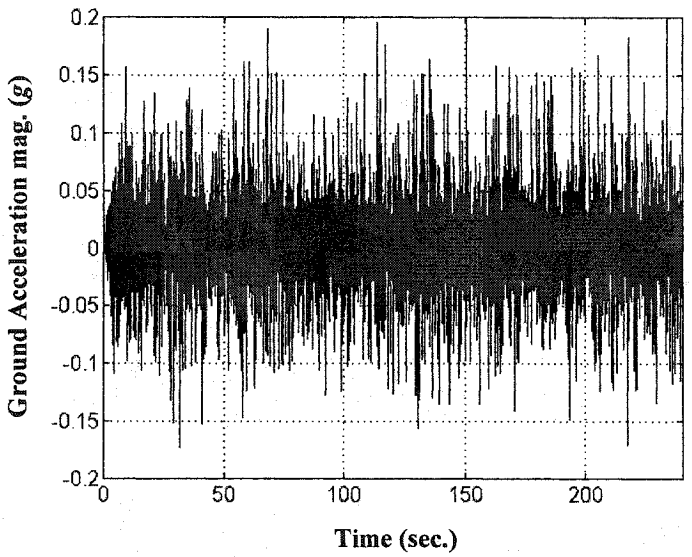

Fig. 4-10. Sample four minute realization of the band-limited white noise acceleration at the table level

The Hanning window with an overlap of 75% between the consecutive data samples is used for the evaluation of the PSD. To obtain a correct PSD, the time history was detrended to remove any DC gains that may exist due to any static charges or manufacturing defects in the accelerometers.

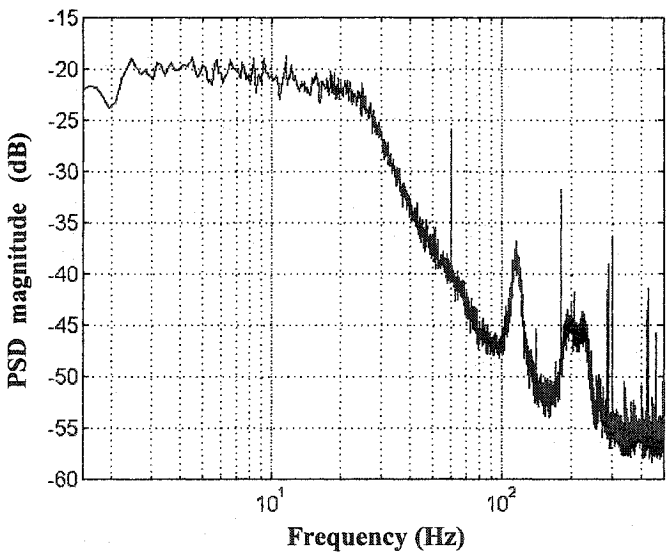

Fig. 4-11. PSD magnitude of the generated BLWN ground acceleration

4.2.4.2 Filtered Band-Limited White Noise (FBLWN) Generation

For a more realistic loading model to replicate ground motion, it is better to consider the effect of the soil on the propagation of ground vibrations. A good assumption for the experiment applied here is to consider the soil as a filter through which the vibrations pass before reaching the location of interest. This assumption, however, is complicated by the fact that the soil conditions and layers are different in different site locations. Thus, the approximation here considers a simple stationary representation of the soil that was originally proposed by Kanai (1957) and Tajimi (1960), who suggested that surface ground acceleration can be approximated by the motion of a simple oscillator with a concentrated mass supported by a linear spring and a dashpot and subjected to a white noise excitation (bedrock acceleration) of spectral density S_0. Thus, the power spectral density of the absolute surface ground acceleration becomes

$$S_g(\omega) = \frac{\omega_g^4 + 4\zeta_g^2\omega_g^2\omega^2}{(\omega_g^2 - \omega^2)^2 + 4\zeta_g^2\omega_g^2\omega^2} S_0 \qquad (4\text{-}5)$$

where ω_g and ζ_g are the natural frequency and the damping ratio of the assumed oscillator determined by the characteristics of the local ground conditions. The intensity S_0 of the excitation is determined by the strength of the excitation waves (Soong and Grigoriou, 1993). The Kanai-Tajimi model is widely used as an earthquake excitation for engineering structures because of its ability to simulate earthquake-induced ground motions in a very simple way.

To use the Kanai-Tajimi model, the three parameters, namely ω_g, ζ_g, and S_0, are estimated from representative earthquake records by means of statistical estimation procedures. Thus, an approximation based on the study of frequency content of a number of two strong ground-motion records each in the USA and Japan is considered. In the experiment here, the natural frequency of the oscillator, ω_g, is taken equivalent to 17 rad/s; the oscillator damping ratio ζ_g is taken equivalent to 0.3 (Ramallo *et al.*, 2002). Fig. 4-12 shows the frequency response of this Kanai-Tajimi filter used in the experiment.

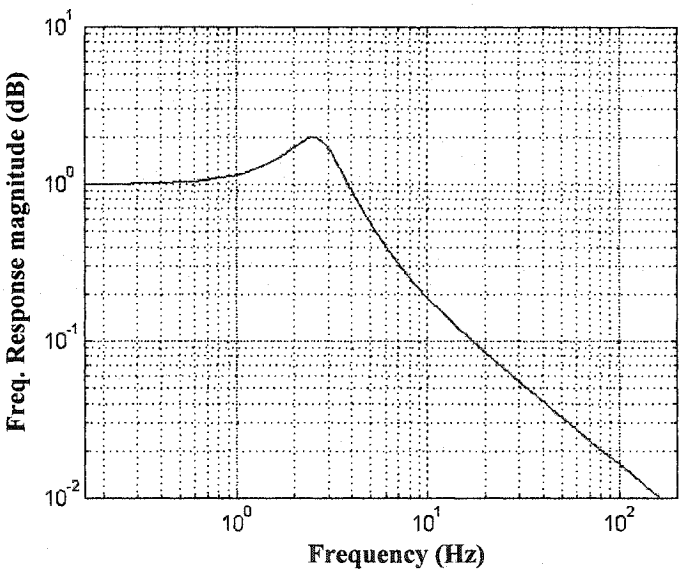

Fig. 4-12. Frequency response of the Kanai-Tajimi filter used in the experiment

4.2.5 Determination of the Transfer Function from Measurement Data and Identifying the Structure

The ILSN identification method (previously explained in Chapter 3) used here attempts to match a parametric model of a transfer function to measured transfer

function data. To apply the ILSN identification technique, the experimental transfer function needs to be obtained. Thus, based on the measurement acceleration I/O data (Bendat and Piersol, 2000), the transfer function between the ground acceleration excitation input and the absolute acceleration outputs at the first and the second stories can be evaluated. In the application here, the input $u(t)$ to the structure is the measured table (ground) accelerations data, and the measured first and second story accelerations are the outputs $y_1(t)$ and $y_2(t)$, respectively. The PSD matrix of the acceleration input $u(t)$ is

$$S_{uu}(\omega) = U^*(\omega)U(\omega) \tag{4-6}$$

The cross-spectral density (CSD) function between the table acceleration and the measured story accelerations are

$$S_{y_1u}(\omega) = U^*(\omega)Y_1(\omega) \qquad \text{and} \qquad S_{y_2u}(\omega) = U^*(\omega)Y_2(\omega) \tag{4-7}$$

Finally, the transfer functions $H_1(\omega)$ and $H_2(\omega)$ from the ground acceleration input to the absolute accelerations of the two floors are evaluated from the ratio between the CSDs and PSD

$$H_1(\omega) = \frac{S_{y_1u}(\omega)}{S_{uu}(\omega)} \qquad \text{and} \qquad H_2(\omega) = \frac{S_{y_2u}(\omega)}{S_{uu}(\omega)} \tag{4-8}$$

Thus, having the experimental transfer functions, the ILSN technique can be used to obtain the values of the structural parameters by minimizing the residual error between the experimental and the theoretical parametric transfer functions.

4.3 Data Analysis

The main task of the experiment is to detect a small amount of damage (about 7.38% of the estimated story stiffness) located in one of the two stories of the structure. The accuracy of the identified damage is then compared between the cases when VSDDs are used in a structure and when they are not. The damage is defined as a loss in stiffness. There are two damage cases, one where a pair of weak springs are removed from the first story (to simulate damage there), and one removing a pair of weak springs from just the second story.

4.3.1 Experimental Challenges and Solutions

The main task of the experiment is complicated by different factors. These difficulties include accuracy of modeling, nonlinearities in the experiment, the sensitivity of the accelerometers (sensor noise), and unmeasured vibrations coming from the ground under the table or from connecting cables. Moreover, the memory of the computer, used in the storage of the data, is limited. Consequently, the amount of data that can be stored is also limited. These problems add to the complexity of the identification problem.

In order to overcome some of these challenges, some actions are considered. For example, the experiment was performed in the basement of a building in order to minimize the ground vibrations under the table and to avoid building vibrations encountered in higher levels. Moreover, the level of excitation is kept small enough that the 2DOF structure response is linear and the weak and stiff springs in the

bracings exhibit only elastic behavior. Further, the weak and stiff springs are pretensioned to nearly half their maximum elastic deflection so they are always in tension during the experiment and, thus, the bracing forces exerted by the springs never vanish. In addition, all flexible cables connected to the structure (such as those connected to the accelerometers) in the first and the second stories are banded and fixed to the structure, as shown in Fig. 4-4.

To ensure good structure modeling, the 2DOF structure is designed as a shear building where the moment of inertia of the plexi-glass plate is 327 times that of the aluminum vertical plate. Moreover, all weights and dimensions are accurately measured.

4.3.2 Data Processing

The excitation generator models of the table are designed to excite the structure for 3800 seconds continuously (the limits of memory in the laboratory computer). The stored data is divided into non-overlapping two-minute samples of data or six-minute samples of data; in both cases, ten seconds is omitted between each sample to eliminate coherence between successive samples. The data is split into a number of samples, each of which is used to generate one set of parameter estimates, in order to get a statistical distribution of the identified structure parameters. The sample duration is varied in order to observe the effect of the amount of data in each sample on the identification of the structure parameters. Each of the samples is processed in a separate identification problem for the unknown structure parameters, which are here assumed to be only the stiffness coefficients.

Thus, it is assumed that the masses and damping coefficients of the two stories of the structure are known *a priori*. The masses of each of the two floors are considered equivalent to 1.125 kg. Based on the measurements recorded in Table 4-2. The logarithmic decrement method is used to obtain modal damping ratios of the 2DOF structure. The results of testing the damping ratios indicate a 1% damping in the first and second modes. In addition, the natural frequencies of the structure without adding the weak springs are measured and found to be 2.197 Hz and 6.24 Hz respectively. Consequently, the uncoupled damping coefficients for the two floors are computed to be 0.2 and 0.5 N·sec/m, respectively.

The ILSN method requires initial estimates of the unknown stiffness parameters. Using the dimensions of the aluminum vertical plates (Table 4-2) and assuming the modulus of elasticity of Aluminum to be 75 GPa, the initial estimates of the stiffnesses of the first and second stories (including the springs) are computed from Eq. (4-1) to be 657.94 N/m.

4.3.3 Damage Identification Results

The damage, within the context of this research, is defined as the loss in stiffness after damage. Thus, the mean and the standard deviation (STD) of the identified values of the first and second story stiffnesses, k_1 and k_2, respectively, are evaluated for the undamaged and damaged cases. Fig. 4-17 to Fig. 4-32 show the error in the identified first and second story stiffnesses, k_1 and k_2, relative to the assumed stiffnesses which are based on the material properties. This is done for both the undamaged and damaged cases; in both cases, a one-standard deviation ellipse is

shown in the figures. The shift in the one-standard deviation ellipse, before and after damage, indicates damage quantity and location in any of the graphs. Moreover, Table 4-10 to Table 4-24 give the percentage of damage as the difference in stiffness between mean values of the identified stiffnesses, before and after damage, relative to the assumed values of the stiffnesses since it is a constant reference. In order to compare between the VSDD and conventional structure approaches, the resulting identified percentages of damage are compared to the exact ones.

4.4 Resulting Transfer Functions

To show the success of the ILSN identification technique in estimating the stiffness of the two stories of the 2DOF structure, the estimated theoretical TF of one two-minute sample and one six-minute sample data, based on the values of the identified stiffness parameters of these samples, are demonstrated here in contrast to their experimental counterparts (computed as per Section 4.2.5). This is applied for both the VSDD and conventional structure approaches, respectively. The TFs here represent a single sample case, either two-minute (Fig. 4-13 and Fig. 4-14) or six-minute (Fig. 4-15 and Fig. 4-16), for the undamaged structure when subjected to FBLWN ground excitation. The TF identification for the sample studied in this section is found to be successful for both the VSDD and the conventional structure approaches. This was not always the case for all samples when using the conventional structure approach.

4.4.1 Two-minute sample

As shown in Fig. 4-13 and Fig. 4-14, the identified theoretical TFs have done very well in tracing the experimental one for both the VSDD and the conventional structure approaches. This is the case despite the considerable noise in the experimental TFs. However, as will be shown in the coming sections, for the conventional structure approach, the identification is not always ideal.

4.4.2 Six-minute sample

Similarly, the identified theoretical TFs, for the VSDD and conventional structure approaches, are successful in defining the system in one sample of the six minutes data samples. This is expected due to better averaging of the PSD of the inputs and the CSD functions between the inputs and the outputs for longer duration data samples. This, in turn, reduces the noise in the evaluated experimental TFs. However, this is not always the case for the conventional structure approach, as will be shown later. The resulting identified TFs are shown in Fig. 4-15 and Fig. 4-16.

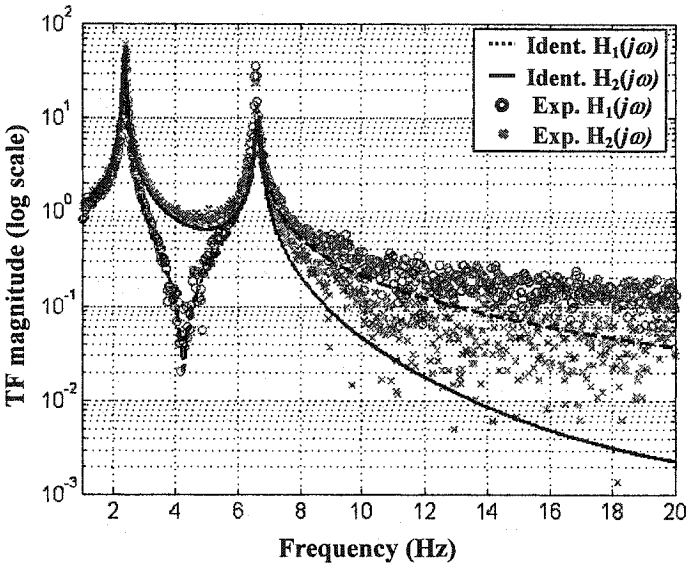

Fig. 4-13. Experimental transfer functions versus identified transfer functions of the 2DOF experimental structure without damage, using VSDDs approach, for one 2-min sample under FBLWN excitation

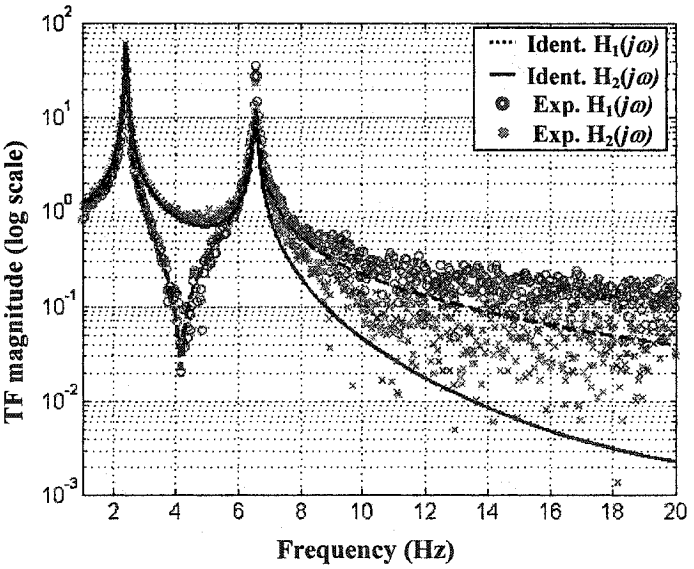

Fig. 4-14. Experimental transfer functions versus identified transfer functions of the 2DOF experimental structure without damage, using conventional structure approach, for one 2-min under FBLWN excitation

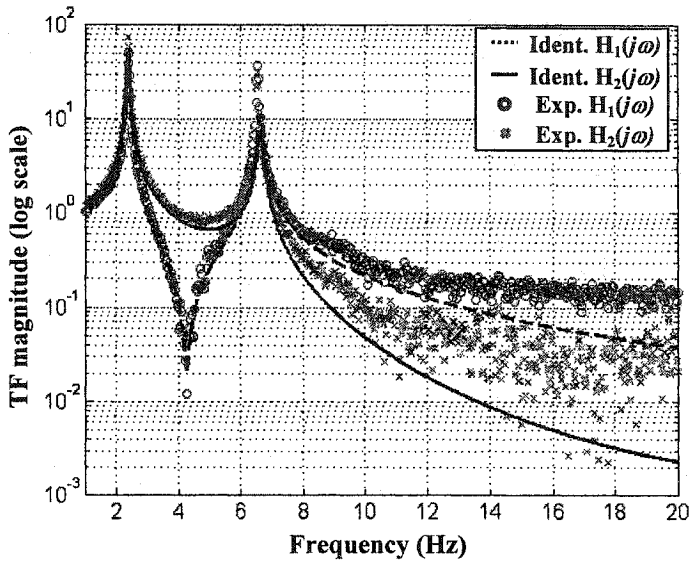

Fig. 4-15. Experimental transfer functions versus identified transfer functions of the 2DOF experimental structure without damage, using VSDDs approach, for one 6-min sample under FBLWN excitation

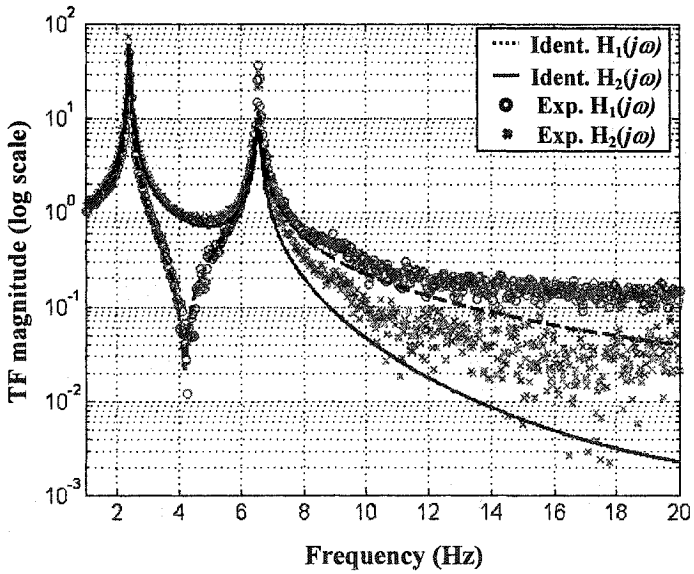

Fig. 4-16. Experimental transfer functions versus identified transfer functions of the 2DOF experimental structure without damage, using conventional structure approach, for one 6-min sample under FBLWN excitation

4.5 Damage Identification Results for BLWN Excitation

4.5.1 Two-Minute Data Samples

4.5.1.1 Damage in First Story

Fig. 4-17 and Fig. 4-18 show the results of the identification, with VSDDs and without, respectively, using two-minute samples for damage in the first story. Fig. 4-17 shows that the VSDD approach is successful in identifying the damage in the first story. In contrast, Fig. 4-18 indicates that the conventional structure approach is not successful in determining the damage; in fact, nearly half of the samples give quite inaccurate estimates for the undamaged stiffnesses. This, consequently, leads to a huge bias in the mean estimates of stiffnesses, and large variations, as shown in Table 4-9. In addition, one estimate after damage, using the conventional structure approach, gives a dramatically different result, exaggerating the variance. Table 4-10 shows that the damage is well estimated with relatively low variation using the VSDD approach whereas, in the conventional structure approach, the damage location is incorrect and the severity is exaggerated.

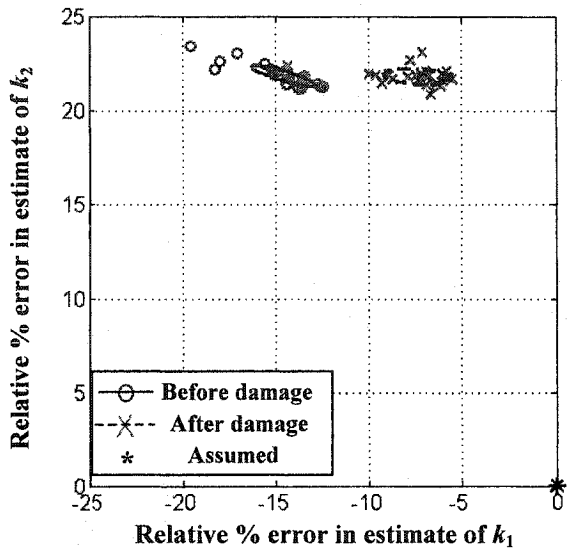

Fig. 4-17. Relative errors in identified stiffnesses of 2DOF structure to assumed ones, before and after damage in first story, (BLWN, 2-min samples, VSDDs approach)

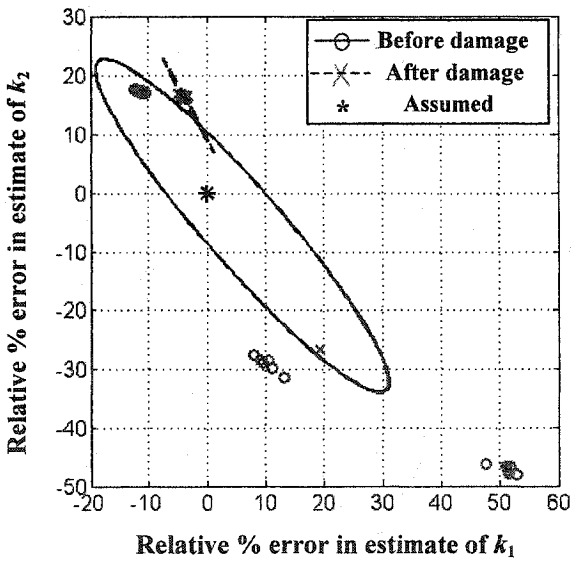

Fig. 4-18. Relative errors in identified stiffnesses of 2DOF structure to assumed ones, before and after damage in 1st story, (BLWN, 2-min samples, Conv. St. approach)

Table 4-9. Mean and COV Estimates of the Identified Stiffnesses of the 2DOF Structure for Case of Damage in 1st Story (BLWN, 2 min)

	VSDDs Approach				Conventional Structure Approach			
	Before Damage		After Damage		Before Damage		After Damage	
	Mean (N/m)	COV (%)	Mean (N/m)	COV (%)	Mean (N/m)	COV (%)	Mean (N/m)	COV (%)
k_1	609.380	1.959	562.009	1.992	636.816	4.475	697.215	23.672
k_2	801.629	0.336	801.958	0.441	756.166	6.960	621.486	30.045

Table 4-10. Mean and STD Estimates of the Identified Damage for 2DOF Structure, Relative to Assumed Stiffnesses, in Case of Damage in 1st Story Only (BLWN, 2 min)

	Damage Location	Actual % of Damage	Relative Identified Damage	
			Mean(%)	STD(%)
VSDD App.	1st	7.36	7.20	2.49
	2nd	0	0.05	0.68
Conv. St. App.	1st	7.36	-9.18	25.46
	2nd	0	20.47	29.49

4.5.1.2 Damage in Second Story

The damage in the second story is usually well identified for both the VSDD and the conventional structure approaches as demonstrated in Fig. 4-19 and Fig. 4-20. However, using the conventional structure approach, very inaccurate stiffness estimates occurred in one sample for the undamaged structure case, causing large variance as shown in Table 4-11. This, in turn, affects the credibility of the identified damage severity for the conventional structure approach. This is represented in Table 4-12 in terms of large standard deviation, bigger than the identified damage, leading to doubts about the results. In contrast, the VSDD approach supplied a good identification of damage in the second story with very small variation. Moreover, the

indication of stiffening in the first story, identified after damage in both approaches, by the negative damage mean is suspect since the magnitude of stiffening is smaller than the standard deviation.

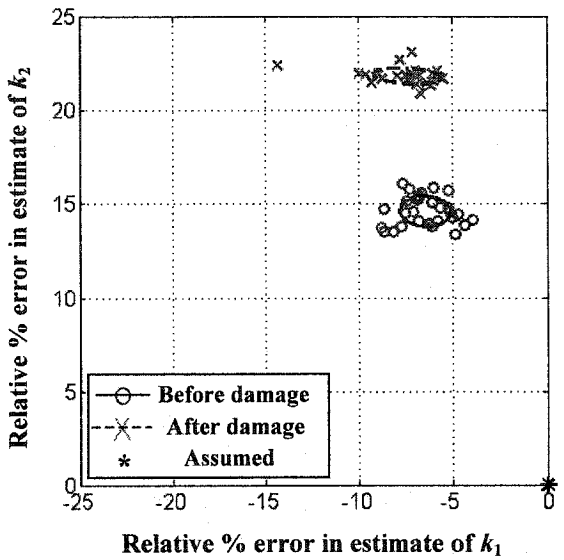

Fig. 4-19. Relative errors in identified stiffnesses of 2DOF structure to assumed ones, before and after damage in 2nd story, (BLWN, 2-min samples, VSDDs approach)

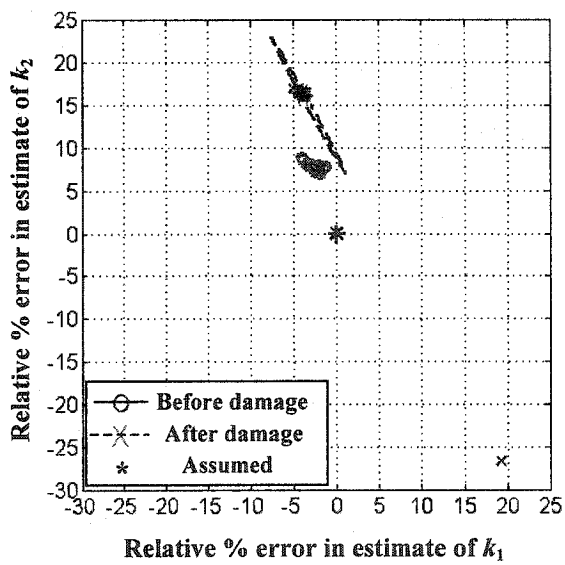

Fig. 4-20. Relative errors in identified stiffnesses of 2DOF structure to assumed ones, before and after damage in 2nd story, (BLWN, 2-min samples, Conv. St. approach)

Table 4-11. Mean and COV Estimates of the Identified Stiffnesses of the 2DOF Structure for Case of Damage in 2nd Story (BLWN, 2 min)

	VSDDs Approach				Conventional Structure Approach			
	Before Damage		After Damage		Before Damage		After Damage	
	Mean (N/m)	COV (%)	Mean (N/m)	COV (%)	Mean (N/m)	COV (%)	Mean (N/m)	COV (%)
k_1	609.380	1.959	615.433	1.414	636.816	4.475	641.553	0.704
k_2	801.629	0.336	754.192	0.690	756.166	6.960	708.729	0.418

Table 4-12. Mean and STD Estimates of the Identified Damage for 2DOF Structure, Relative to Assumed Stiffnesses, in Case of Damage in 2nd Story Only (BLWN, 2 min)

	Damage Location	Actual % of Damage	Relative Identified Damage	
			Mean(%)	STD(%)
VSDD App.	1st	0	-0.92	2.25
	2nd	7.39	7.21	0.89
Conv. St. App.	1st	0	-0.72	4.39
	2nd	7.39	7.21	8.01

4.5.2 Six-Minute Data Samples

4.5.2.1 Damage in First Story

Both approaches, VSDD (Fig. 4-21) and conventional structure (Fig. 4-22), did extremely well in identifying the damage using six-minute samples when the damage is in the first story. This shows that a longer sample duration improved the results of both approaches, particularly for the conventional structure approach. However, the VSDD approach still give better means. The VSDD approach estimates the damage at 7.38% — very close to the exact of 7.36% — whereas the conventional structure approach gives 7.43%. In Table 4-14, the extra 0.97% stiffness estimated in the second story for the conventional structure approach case

may be considered significant compared to the 0.29% standard deviation, in contrast with an insignificant 0.19% extra stiffness with a 0.36% standard deviation when using VSDDs.

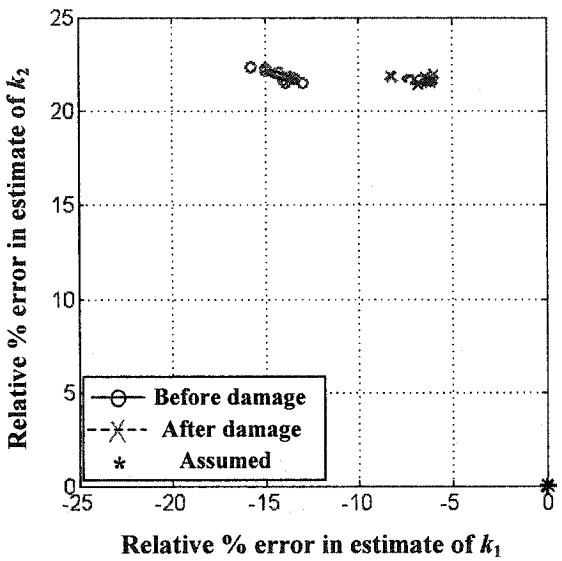

Fig. 4-21. Relative errors in identified stiffnesses of 2DOF structure to assumed ones, before and after damage in 1st story, (BLWN, 6-min samples, VSDDs approach)

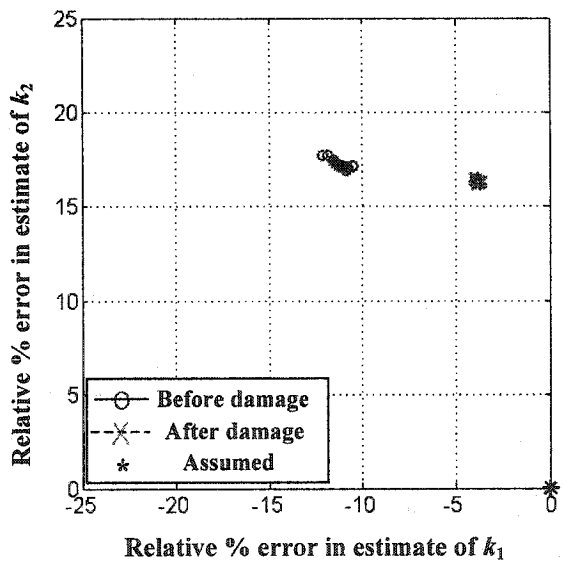

Fig. 4-22. Relative errors in identified stiffnesses of 2DOF structure to assumed ones, before and after damage in 1st story, (BLWN, 6-min samples, Conv. St. approach)

Table 4-13. Mean and COV Estimates of the Identified Stiffnesses of the 2DOF Structure for Case of Damage in 1st Story (BLWN, 6 min)

	VSDDs Approach				Conventional Structure Approach			
	Before Damage		After Damage		Before Damage		After Damage	
	Mean (N/m)	COV (%)	Mean (N/m)	COV (%)	Mean (N/m)	COV (%)	Mean (N/m)	COV (%)
k_1	613.328	0.895	564.772	1.009	632.408	0.165	583.523	0.562
k_2	800.642	0.157	801.892	0.248	765.509	0.117	771.891	0.222

Table 4-14. Mean and STD Estimates of the Identified Damage for 2DOF Structure, Relative to Assumed Stiffnesses, in Case of Damage in 1st Story Only (BLWN, 6 min)

	Damage Location	Actual % of Damage	Relative Identified Damage	
			Mean(%)	STD(%)
VSDD App.	1st	7.36	7.38	1.20
	2nd	0	-0.19	0.36
Conv. St. App.	1st	7.36	7.43	0.52
	2nd	0	-0.97	0.29

4.5.2.2 Damage in Second Story

With damage in the second story and using six-minute samples, the VSDD and the conventional structure approaches did well as shown in Fig. 4-23 and Fig. 4-24, but the VSDD approach is clearly superior. With the conventional structure approach, despite very low variations in stiffness estimates as shown in Table 4-15, the first story appears to have stiffened by 1.56% and the damage in the second story has been overestimated, as shown in Table 4-16. The very low standard deviation in the conventional structure approach suggests it may be more accurate, but that is clearly misleading.

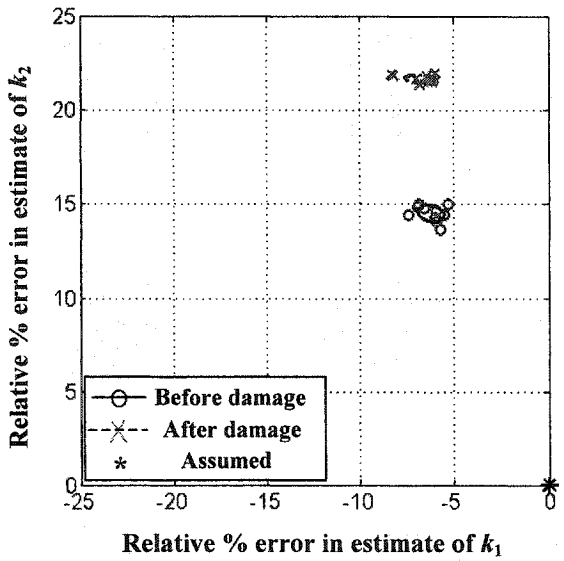

Fig. 4-23. Relative errors in identified stiffnesses of 2DOF structure to assumed ones, before and after damage in 2nd story, (BLWN, 6-min samples, VSDDs approach)

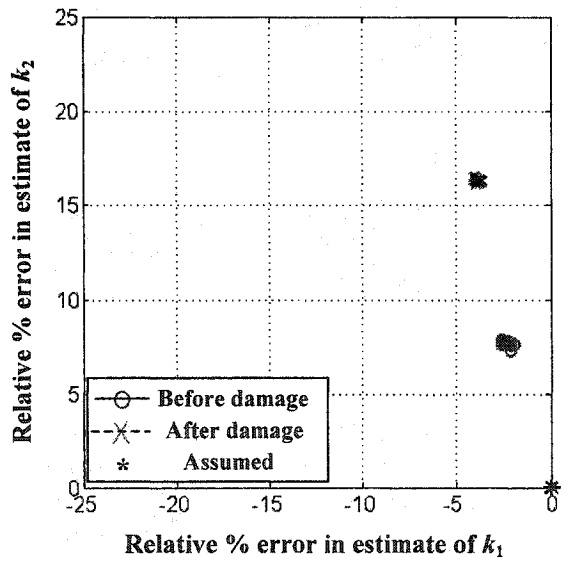

Fig. 4-24. Relative errors in identified stiffnesses of 2DOF structure to assumed ones, before and after damage in 2nd story, (BLWN, 6-min samples, Conv. St. approach)

Table 4-15. Mean and COV Estimates of the Identified Stiffnesses of the 2DOF Structure for Case of Damage in 2nd Story (BLWN, 6 Min)

	VSDDs Approach				Conventional Structure Approach			
	Before Damage		After Damage		Before Damage		After Damage	
	Mean (N/m)	COV (%)	Mean (N/m)	COV (%)	Mean (N/m)	COV (%)	Mean (N/m)	COV (%)
k_1	613.328	0.895	616.881	0.729	632.408	0.165	642.672	0.282
k_2	800.642	0.157	753.666	0.370	765.509	0.117	708.597	0.180

Table 4-16. Mean and STD Estimates of the Identified Damage for 2DOF Structure, Relative to Assumed Stiffnesses, in Case of Damage in 2nd Story Only (BLWN, 6 min)

	Damage Location	Actual % of Damage	Relative Identified Damage	
			Mean(%)	STD(%)
VSDD App.	1st	0	-0.54	1.08
	2nd	7.39	7.14	0.46
Conv. St. App.	1st	0	-1.56	0.32
	2nd	7.39	8.65	0.24

4.6 Damage Identification Results for FBLWN Excitation

4.6.1 Two-Minute Data Samples

4.6.1.1 Damage in First Story

Similar to the case of BLWN ground excitation with two-minute samples, the VSDD approach is found, with FBLWN excitation, to be able to identify the damage accurately in the first story whereas the conventional structure approach fails, as is clear from Fig. 4-25 and Fig. 4-26. Table 4-17 also shows that the damage deviations are very large for the conventional structure approach. In addition, from Table 4-18, it can be observed that the damage location is swapped and estimated to be severe in the second story when no damage has actually occurred there.

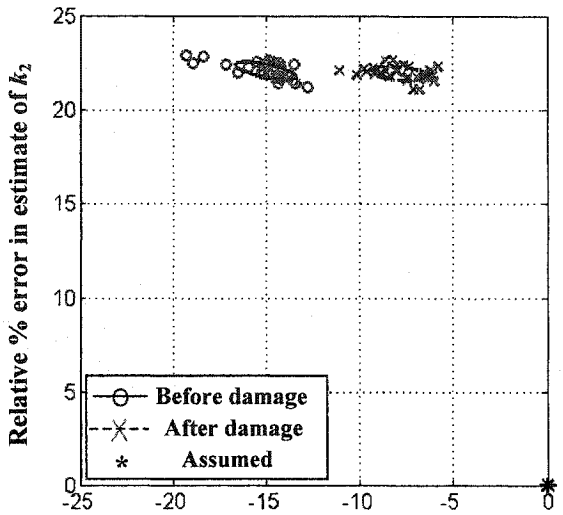

Fig. 4-25. Relative errors in identified stiffnesses of 2DOF structure to assumed ones, before and after damage in 1st story, (FBLWN, 2-min samples, VSDDs approach)

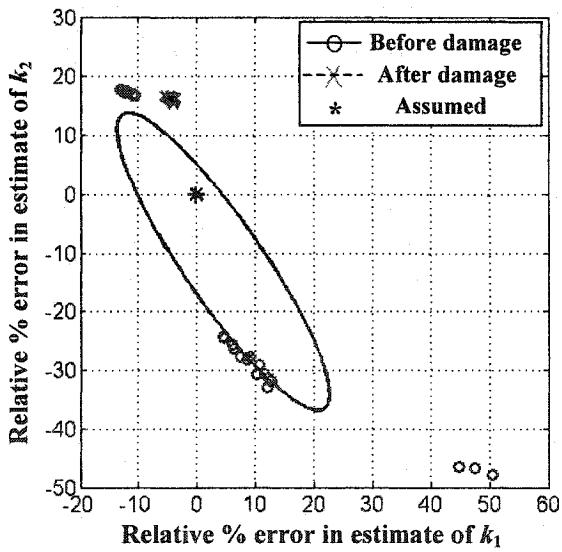

Fig. 4-26. Relative errors in identified stiffnesses of 2DOF structure to assumed ones, before and after damage in 1st story, (FBLWN, 2-min samples, Conv. St. approach)

Table 4-17. Mean and COV Estimates of the Identified Stiffnesses of the 2DOF Structure for Case of Damage in 1st Story (FBLWN, 2 Min)

	VSDDs Approach				Conventional Structure Approach			
	Before Damage		After Damage		Before Damage		After Damage	
	Mean (N/m)	COV (%)	Mean (N/m)	COV (%)	Mean (N/m)	COV (%)	Mean (N/m)	COV (%)
k_1	606.222	1.542	559.180	1.884	629.776	0.481	687.148	17.415
k_2	802.485	0.300	803.340	0.369	764.061	0.264	582.010	28.620

Table 4-18. Mean and STD Estimates of the Identified Damage for 2DOF Structure, Relative to Assumed Stiffnesses, in Case of Damage in 1st Story Only (FBLWN, 2 min)

	Damage Location	Actual % of Damage	Relative Identified Damage	
			Mean(%)	STD(%)
VSDD App.	1st	7.36	7.15	2.14
	2nd	0	-0.13	0.58
Conv. St. App.	1st	7.36	-8.72	18.19
	2nd	0	27.67	25.32

4.6.1.2 Damage in Second Story

With damage in the second story, both approaches, the VSDD and the conventional structure, did well also, as shown in Fig. 4-27 and Fig. 4-28. However, the conventional structure approach overestimated the damage in the second story and indicates significant stiffening in the first story, as shown in Table 4-20. However, these are accompanied by very small deviations, which falsely gives credibility to these results and is misleading. On the contrary, the VSDD approach gives a very good estimate of damage in the second story. While the VSDD approach estimates some extra stiffness in the first story, it is less than the deviation, which indicates that this extra stiffness is probably spurious.

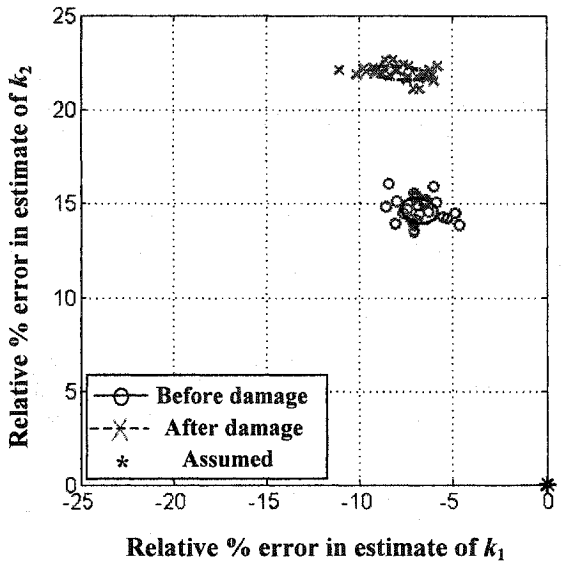

Fig. 4-27. Relative errors in identified stiffnesses of 2DOF structure to assumed ones, before and after damage in 2nd story, (FBLWN, 2-min samples, VSDDs approach)

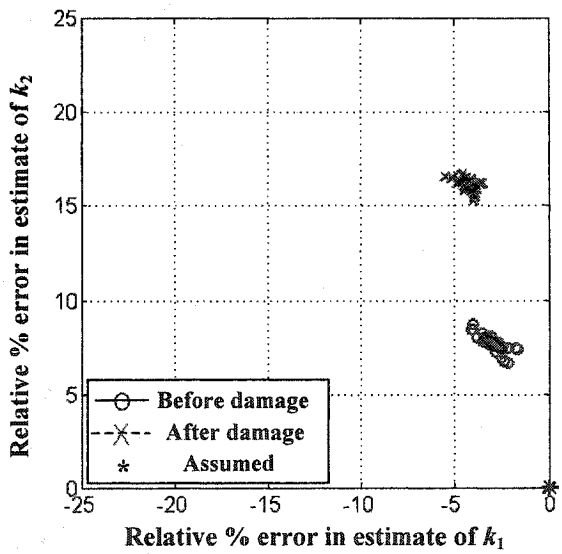

Fig. 4-28. Relative errors in identified stiffnesses of 2DOF structure to assumed ones, before and after damage in 2nd story, (FBLWN, 2-min samples, Conv. St. approach)

Table 4-19. Mean and COV Estimates of the Identified Stiffnesses of the 2DOF Structure for Case of Damage in 2nd Story (FBLWN, 2 min)

	VSDDs Approach				Conventional Structure Approach			
	Before Damage		After Damage		Before Damage		After Damage	
	Mean (N/m)	COV (%)	Mean (N/m)	COV (%)	Mean (N/m)	COV (%)	Mean (N/m)	COV (%)
k_1	606.222	1.542	613.131	1.033	629.776	0.481	638.527	0.658
k_2	802.485	0.300	754.455	0.579	764.061	0.264	708.860	0.435

Table 4-20. Mean and STD Estimates of the Identified Damage for 2DOF Structure, Relative to Assumed Stiffnesses, in Case of Damage in 2nd Story Only (FBLWN, 2 min)

	Damage Location	Actual % of Damage	Relative Identified Damage	
			Mean(%)	STD(%)
VSDD App.	1st	0	-1.05	1.72
	2nd	7.39	7.30	0.76
Conv. St. App.	1st	0	-1.33	0.79
	2nd	7.39	8.39	0.56

4.6.2 Six-Minute data samples

4.6.2.1 Damage in First Story

Despite the advantage of having the longer duration six-minute samples, the conventional structure approach performs poorly here for damage in the first story with FBLWN excitation. As seen in Fig. 4-30, many of the samples are vastly inaccurate for the undamaged case. The VSDD approach, on the other hand, is able to identify damage quite well and with very small deviations. Table 4-21 and Table 4-22 show that the conventional structure approach gives heavily biased estimates together with large deviation, in contrast with the VSDD approach which gives very good estimates with small deviations.

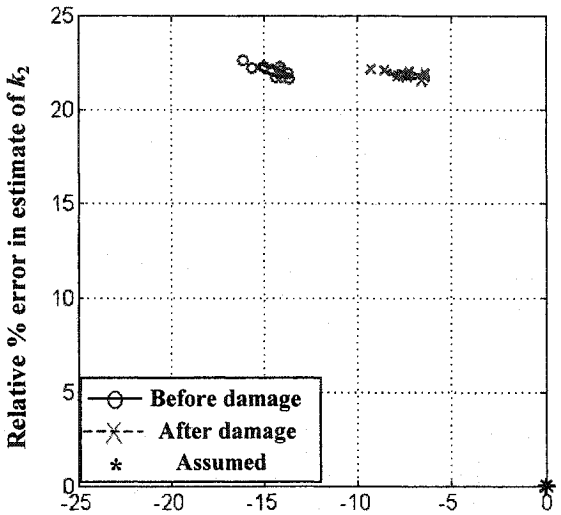

Fig. 4-29. Relative errors in identified stiffnesses of 2DOF structure to assumed ones, before and after damage in 1st story, (FBLWN, 6-min samples, VSDDs approach)

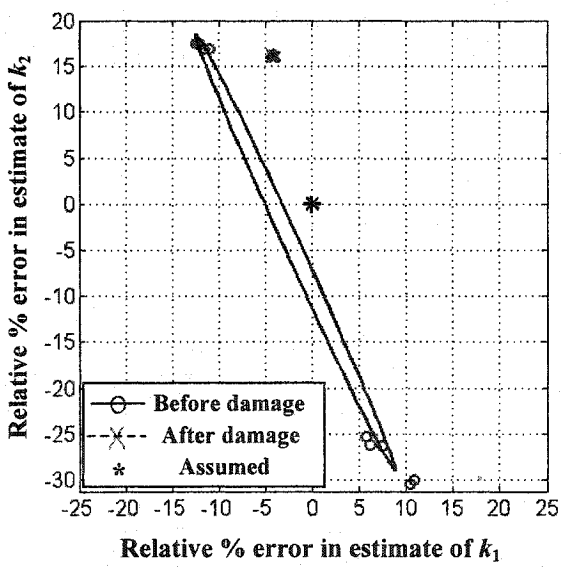

Fig. 4-30. Relative errors in identified stiffnesses of 2DOF structure to assumed ones, before and after damage in 1st story, (FBLWN, 6-min samples, Conv. St. approach)

Table 4-21. Mean and COV Estimates of the Identified Stiffnesses of the 2DOF Structure for Case of Damage in 1st Story (FBLWN, 6 min)

	VSDDs Approach				Conventional Structure Approach			
	Before Damage		After Damage		Before Damage		After Damage	
	Mean (N/m)	COV (%)	Mean (N/m)	COV (%)	Mean (N/m)	COV (%)	Mean (N/m)	COV (%)
k_1	608.854	1.013	562.272	0.940	630.632	0.193	645.830	10.809
k_2	801.958	0.156	803.143	0.249	763.864	0.132	623.723	25.013

Table 4-22. Mean and STD Estimates of the Identified Damage for 2DOF Structure, Relative to Assumed Stiffnesses, in Case of Damage in 1st Story Only (FBLWN, 6 min)

	Damage Location	Actual % of Damage	Relative Identified Damage	
			Mean(%)	STD(%)
VSDD App.	1st	7.36	7.08	1.23
	2nd	0	-0.18	0.36
Conv. St. App.	1st	7.36	-2.31	10.61
	2nd	0	21.30	23.71

4.6.2.2 Damage in Second Story

Fig. 4-31 and Fig. 4-32 indicate that both the VSDD and the conventional structure approaches did well in identifying the damage in the second story for six-minute samples with FBLWN excitation. However, the conventional structure approach overestimated the damage in the second story, and gave statistically significant stiffening in the first story, as shown in Table 4-24. This is, again, accompanied with very small variations in stiffness and damage estimates, which is misleading about the credibility of such results. In the meantime, the VSDD approach is successful in estimating the damage more accurately.

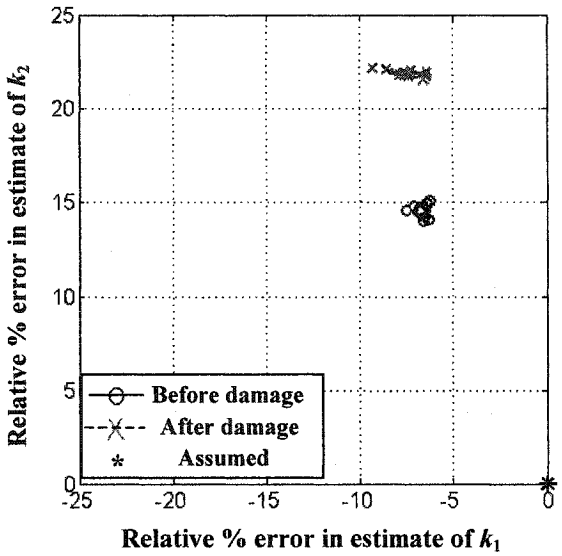

Fig. 4-31. Relative errors in identified stiffnesses of 2DOF structure to assumed ones, before and after damage in 2nd story, (FBLWN, 6-min samples, VSDDs approach)

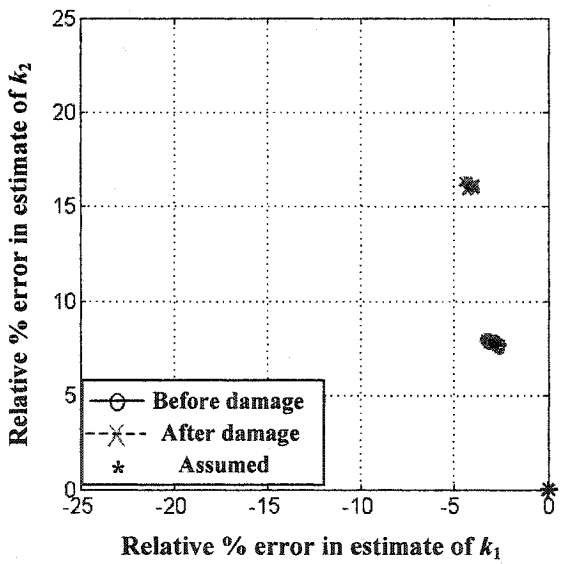

Fig. 4-32. Relative errors in identified stiffnesses of 2DOF structure to assumed ones, before and after damage in 2nd story, (FBLWN, 6-min samples, Conv. St. approach)

Table 4-23. Mean and COV Estimates of the Identified Stiffnesses of the 2DOF Structure for Case of Damage in 2nd Story (FBLWN, 6 min)

	VSDDs Approach				Conventional Structure Approach			
	Before Damage		After Damage		Before Damage		After Damage	
	Mean (N/m)	COV (%)	Mean (N/m)	COV (%)	Mean (N/m)	COV (%)	Mean (N/m)	COV (%)
k_1	608.854	1.013	614.052	0.417	630.632	0.193	638.790	0.286
k_2	801.958	0.156	753.929	0.322	763.864	0.132	709.058	0.168

Table 4-24. Mean and STD Estimates of the Identified Damage for 2DOF Structure, Relative to Assumed Stiffnesses, in Case of Damage in 2nd Story Only (FBLWN, 6 min)

	Damage Location	Actual % of Damage	Relative Identified Damage	
			Mean(%)	STD(%)
VSDD App.	1st	0	-0.79	1.02
	2nd	7.39	7.30	0.42
Conv. St. App.	1st	0	-1.24	0.33
	2nd	7.39	8.33	0.24

4.7 Overview of results and comments

Comparing the identified stiffness results obtained using the VSDD and the conventional structure approaches, it can be observed that the VSDD approach performed significantly better. This is particularly demonstrated with shorter duration data samples. With two-minute data samples, the VSDD approach is found to be successful in identifying the damage accurately, whether damage exists in either the first or the second story. The identified damage is accompanied with small deviations giving credibility to the results. Meanwhile, for the same case of two-minute data samples, the conventional structure is found to be unsuccessful in identifying damage in the first story. While damage identification is more successful

when the damage is in the second story, the conventional structure approach often overestimates the damage and assigns statistically significant extra stiffness to undamaged stories.

With longer duration data samples (six-minute), the VSDD approach gives even better damage means with much smaller variations. For the conventional structure approach, the identified results are improved in some cases compared to the two-minute samples, but often with biased mean damage estimates represented by overestimating damage.

Based on these observations, one can conclude that using the VSDD approach helps overcome the noise in the data more efficiently than the conventional structure approach. This result confirms experimentally the conclusions in the analytical part of this research comparing the two approaches.

5 CONTROLLED REALTIME HEALTH MONITORING OF STRUCTURES

5.1 Problem Definition and Introduction

Online health monitoring of structural systems with actuators in real time is not an easy process. The problem is complicated by unmodeled dynamics, unknown external forces (ambient excitation), rapidly changing control forces, and various noise sources associated with real measurements (Johnson, 1997b). Generally, the dynamics of a linear structural system with actuators driven by ambient excitation can be represented by the equation

$$\mathbf{M}\ddot{\mathbf{x}} + \mathbf{C}_d\dot{\mathbf{x}} + \mathbf{K}\mathbf{x} = \mathbf{f} = \mathbf{f}_k + \mathbf{f}_u \tag{5-1}$$

where the vector $\mathbf{x}$ denotes the n generalized degrees of freedom and vector $\mathbf{f}$ is a forcing term that can be decomposed into known and unknown parts. The known parts $\mathbf{f}_k$ may include forces that are generated by control actuators. The unknown parts $\mathbf{f}_u$ include unmodeled and unmeasurable exogeneous disturbances (*e.g.*, car motion over bridges, vibration coming from neighboring construction sites, internal vibration activity by occupants, etc.).

One of the goals of SHM is to monitor a structure's stability (through knowledge of the stiffness matrix) in order to predict and/or avoid the onset of types of failure such as sudden breakage of structural elements leading to collapse

mechanisms. Having a good form of the model of the system, composed of the structure and actuators, and sufficient output data is crucial for the success of the identification process. Once the model of a structure is fairly well established, one can begin to consider how to control the structure using actuators to better predict the onset failure. However, many of the existing damage detection and monitoring algorithms do not fully address the issues that arise in the monitoring of civil structures (Sohn and Law, 2000). In summary, the main challenges for the development of a robust damage detection and monitoring system for civil structures subjected to ambient excitation are:

- Civil structures involve significant uncertainties caused by environmental effects such as temperature, loading, humidity, etc.
- Civil structures have complicated geometry, consist of many different materials, such as steel, concrete, cable and asphalt, and involve redundancy in the design.
- Civil structures require a large number of sensors and actuators to catch detailed properties; however, this may not be economical.
- Ambient vibration tests are more suitable for civil structures; yet ambient excitation typically does not excite higher modes.

The problem is even more complicated when considering the internal dynamics of an actuator and its nonlinear behavior. In addition, available computational ability is different between laboratory and real world environments.

Thus, one can conclude that the task of identifying the structural parameters (*e.g.*, stiffness and damping) online is very complex.

In this chapter, a controlled approach for realtime health monitoring is introduced. A quadratic cost function, that includes the error in the estimated system parameters and the force exerted by the actuator, is defined. This cost function is minimized by an optimal choice of control gains. This approach is applied to the 2DOF bridge model discussed previously in Chapter 3. An ARMAX (Auto Regressive Moving Average eXogenous disturbance) model is assumed to represent the system. The RMS of the total relative error in the resulting identified parameters would be evaluated for n_k consecutive control cycles and can be compared to the corresponding values for the conventional structure approach.

5.2 Proposed Approach for Controlled Online Monitoring

The challenge in controlled SHM lies in developing a methodology for determining the best actuator force time histories to improve the structural parameter estimation. In order to develop such a methodology, some assumptions are required. As responses of civil structures are small under ambient vibration loading, the whole system is assumed linear and time-invariant. Generally, then, a structure/actuator system can be represented at time step k by the equation

$$\mathbf{y}(k) = \mathbf{G}(q)\mathbf{u}(k) + \mathbf{H}(q)\mathbf{e}(k) \tag{5-2}$$

where $\mathbf{G}(q)$ is the discrete-time transfer function from the control force input $\mathbf{u}(k)$ to the model output $\mathbf{y}(k)$, and $\mathbf{H}(q)$ is the discrete-time transfer function from the external disturbance $\mathbf{e}(k)$ to the model output $\mathbf{y}(k)$. The argument q is the forward shift operator. For example, in the case of scalar y, u and e, the transfer functions in Eq. (5-2) may be expressed as

$$G(q) = \frac{B(q)}{A(q)} \quad \text{and} \quad H(q) = \frac{C(q)}{A(q)} \tag{5-3}$$

and the corresponding polynomials $A(q)$, $B(q)$ and $C(q)$ are

$$\begin{aligned} A(q) &= 1 + a_1 q^{-1} + \ldots + a_{n_a} q^{-n_a} \\ B(q) &= b_1 q^{-1} + \ldots + b_{n_b} q^{-n_b} \\ C(q) &= c_0 + c_1 q^{-1} + \ldots + c_{n_c} q^{-n_c} \end{aligned} \tag{5-4}$$

A black-box model — an ARMAX model, for example — can be used as an identification model, where the model output at any time step, $\mathbf{y}(k)$, is expressed in terms of the old inputs and disturbances through the linear difference equation (Ljung, 2000)

$$\begin{aligned} \mathbf{y}(k) = -\mathbf{A}_1\mathbf{y}(k-1) - \ldots - \mathbf{A}_{n_a}\mathbf{y}(k-n_a) + \mathbf{B}_1\mathbf{u}(k-1) + \ldots + \mathbf{B}_{n_b}\mathbf{u}(k-n_b) \\ + \mathbf{C}_0\mathbf{e}(k) + \mathbf{C}_1\mathbf{e}(k-1) + \ldots + \mathbf{C}_{n_c}\mathbf{e}(k-n_c) \end{aligned} \tag{5-5}$$

where $\mathbf{y}(k)$ is the $m \times 1$ model output vector, and $\mathbf{u}(k)$ is an $r \times 1$ input (control force) vector. The disturbance $\mathbf{e}(k)$ is assumed a zero-mean Gaussian vector pulse process with $\mathrm{E}[\mathbf{e}(l)\mathbf{e}^{\mathrm{T}}(m)] = \mathbf{Q}\delta_{lm}$. The disturbance herein represents the effect of

the external unknown ambient excitations, assumed to be in the form of wind force or ground acceleration. The values n_a, n_b, and n_c are chosen based on the assumed order of the system model.

An optimal control algorithm that would determine the actuator forces to improve the identification process is required. The goals of the controller here are to find the best estimate of the system parameters and to ensure that the additional actuator forces are reasonable. Accordingly, an appropriate cost function to control the actuator in the discrete time interval $k_0 \le k \le k_f$ would be

$$J(k_0) = \mathrm{E}\left[\{\hat{\boldsymbol{\theta}}(k_f) - \boldsymbol{\theta}\}^T \boldsymbol{\Sigma} \{\hat{\boldsymbol{\theta}}(k_f) - \boldsymbol{\theta}\}\right] + \frac{1}{2}\sum_{k=k_0}^{k_f} \mathrm{E}\left[\mathbf{u}^T(k)\mathbf{R}\mathbf{u}(k)\right] \qquad (5\text{-}6)$$

The first term of the right hand side of Eq. (5-6) is a weighted mean square estimation error of the model parameters vector $\boldsymbol{\theta}$. The second term, however, helps limit the feedback control force within the control time interval. The matrices $\boldsymbol{\Sigma} \ge 0$ and $\mathbf{R} > 0$ are symmetric weighting matrices necessary to normalize different dimensions and units of the terms of the cost function, and to trade off the two control goals of the problem according to the priorities of the control designer.

To evaluate the cost function in Eq. (5-6), some intermediate definitions and functions need to be identified and introduced. These functions include the predicted response, the control force and the prediction error. Also, a formulation that describes how to obtain an estimate of the unknown parameters $\boldsymbol{\theta}$ is needed.

5.2.1 Predicted Response for Structural Systems

5.2.1.1 Scalar Input and Output

In order to explain the analysis of the control technique, a SISO system is taken as an example. The ambient excitation is assumed in the form of wind loads or ground acceleration. As a start, it is convenient to introduce the filtered disturbance $w(k)$ (Ljung, 2000) from Eq. (5-2) such that

$$w(k) = H(q)e(k) \tag{5-7}$$

For the case of wind ambient excitation, and since the disturbance, $e(k)$, has a zero mean, the predicted value of filtered disturbance $w(k)$, based on previous data, is

$$\begin{aligned} \hat{w}(k) &= E[w(k) \mid e(k-1), w(k-1), \ldots] = \underset{e(k)}{E}[w(k)] = \underset{e(k)}{E}\left[\sum_{l=0}^{\infty} h(l)e(k-l)\right] \\ &= \underset{e(k)}{E}[h(0)e(k)] + \underset{e(k)}{E}\left[\sum_{l=1}^{\infty} h(l)e(k-l)\right] = \sum_{l=1}^{\infty} h(l)e(k-l) = [H(q) - h(0)]e(k) \end{aligned} \tag{5-8}$$

where $h(k)$ denotes the pulse response associated with the transfer function $H(q)$. In the case of ambient ground excitation, $h(0) = 0$; thus, to accommodate that case, the following predicted value of the filtered disturbance $w(k)$ is used instead

$$\begin{aligned} \hat{w}(k) &= E[w(k) \mid e(k-2), w(k-1), \ldots] = \underset{e(k-1)}{E}[w(k)] = \underset{e(k-1)}{E}\left[\sum_{l=1}^{\infty} h(l)e(k-l)\right] \\ &= \sum_{l=2}^{\infty} h(l)e(k-l) = [H(q) - c_1 q^{-1}]e(k) \end{aligned} \tag{5-9}$$

5.2.1.1.1 Case of Ambient Wind Excitation

The following represents the solution with $h(0) \neq 0$ (*e.g.*, ambient wind excitation); the $h(0) = 0$ case (ambient ground acceleration) is similar and the modifications to the solution are explained later. The solution of the problem for the ambient wind excitation proceeds by substituting Eq. (5-8) in Eq. (5-7)

$$\hat{w}(k \mid k-1) = [H(q) - h(0)]e(k) = [1 - h(0)H^{-1}(q)]w(k) \tag{5-10}$$

In addition, the measured output $\bar{y}(k)$ is introduced as the sum of the model output $y(k)$ and the error $v(k)$ due to sensor noise, modeling error, etc.

$$\bar{y}(k) = y(k) + v(k) \tag{5-11}$$

where the stochastic properties of $v(k)$ are assumed known: $E[v(k)] = 0$ and $E[v(l)v(m)] = \gamma\delta_{lm}$. In addition, the random variables $e(k)$ and $v(k)$ are assumed independent; *i.e.*, $E[e(l)v(m)] = 0$ for all m and l.

Solving Eq. (5-2) for $w(k)$ and using Eq. (5-11)

$$w(k) = -G(q)u(k) + \bar{y}(k) - v(k) \tag{5-12}$$

Therefore, by taking the expectation of Eq. (5-2) with respect to the disturbance $e(k)$ and the noise $v(k)$, and substituting Eqs. (5-10) and (5-12) in the resulting equation, the expected output given previous outputs and measurements can be obtained from

$$\begin{aligned} \hat{y}(k \mid k-1) &= G(q)u(k) + \hat{w}(k \mid k-1) \\ &= G(q)u(k) + [1 - h(0)H^{-1}(q)][\bar{y}(k) - G(q)u(k)] \end{aligned} \tag{5-13}$$

which leads to

$$\hat{y}(k \mid k-1) = h(0)H^{-1}(q)G(q)u(k) + [1 - h(0)H^{-1}(q)]\bar{y}(k) \tag{5-14}$$

But

$$h(0) = c_0 \tag{5-15}$$

Substituting Eq. (5-15) in Eq. (5-14)

$$\hat{y}(k \mid k-1) = c_0 H^{-1}(q)G(q)u(k) + [1 - c_0 H^{-1}(q)]\bar{y}(k) \tag{5-16}$$

Simplifying Eq. (5-16) using Eq. (5-3)

$$C(q)\hat{y}(k \mid k-1) = c_0 B(q)u(k) + [C(q) - c_0 A(q)]\bar{y}(k) \tag{5-17}$$

Furthermore, by dividing both sides by c_0

$$\tilde{C}(q)\hat{y}(k \mid k-1) = B(q)u(k) + [\tilde{C}(q) - A(q)]\bar{y}(k) \tag{5-18}$$

where

$$\tilde{C}(q) = 1 + (c_1/c_0)q^{-1} + \ldots + (c_{n_c}/c_0)q^{-n_c} \tag{5-19}$$

With some rearranging, Eq. (5-18) can be rewritten as

$$\hat{y}(k \mid k-1) = B(q)u(k) + [1 - A(q)]\bar{y}(k) + [\tilde{C}(q) - 1][\bar{y}(k) - \hat{y}(k \mid k-1)] \tag{5-20}$$

Moreover, the prediction error $\varepsilon(k)$ is defined to be the difference between the output measurement $\bar{y}(k)$ and $\hat{y}(k \mid k-1)$, the predicted output given previous measurements,

$$\varepsilon(k) = \bar{y}(k) - \hat{y}(k \mid k-1) \tag{5-21}$$

Substituting Eq. (5-21) into Eq. (5-20) and expanding gives

$$\begin{aligned}\hat{y}(k \mid k-1) = -a_1\bar{y}(k-1) - \ldots - a_{n_a}\bar{y}(k-n_a) + b_1u(k-1) + \ldots + b_{n_b}u(k-n_b) \\ + (c_1/c_0)\varepsilon(k-1) + \ldots + (c_{n_c}/c_0)\varepsilon(k-n_c)\end{aligned} \tag{5-22}$$

By letting the predicted response take the form

$$\hat{y}(k \mid \boldsymbol{\theta}) = \boldsymbol{\varphi}^{\mathrm{T}}(k, \bar{\mathbf{y}}(k-1, k-n_a), \bar{\mathbf{u}}(k-1, k-n_b), \bar{\boldsymbol{\varepsilon}}(k-1, k-n_a))\boldsymbol{\theta} \tag{5-23}$$

where $\bar{\mathbf{y}}(k-1, k-n_a)$ is a shorthand for $[\bar{y}(k-1) \quad \bar{y}(k-2) \quad \ldots \quad \bar{y}(k-n_a)]$, then, the vector of unknown model parameters $\boldsymbol{\theta}$ can be defined as

$$\boldsymbol{\theta} = [a_1 \quad a_2 \quad \ldots \quad a_{n_a} \quad b_0 \quad b_1 \quad \ldots \quad b_{n_b} \quad c_1/c_0 \quad c_2/c_0 \quad \ldots \quad c_{n_c}/c_0]^{\mathrm{T}} \tag{5-24}$$

and the vector, $\boldsymbol{\varphi}$, includes previous measurements, control forces, and prediction errors.

5.2.1.1.2 Case of ambient ground excitation

As for the problem of ambient ground excitation, the main change, as shown before, is using $\bar{c} = c_1 q^{-1}$ instead of $c_0 = h(0)$ as in Eq. (5-9). A procedure similar to that described up through Eq. (5-17) would give

$$C(q)\hat{y}(k \mid k-1) = \bar{c}B(q)u(k) + [C(q) - \bar{c}A(q)]y(k) \tag{5-25}$$

Dividing both sides by $\bar{c}$

$$\bar{C}(q)\hat{y}(k \mid k-1) = B(q)u(k) + [\bar{C}(q) - A(q)]y(k) \tag{5-26}$$

where

$$\overline{C}(q) = [1 + (c_2/c_1)q^{-1} + \ldots + (c_{n_c}/c_1)q^{-n_c+1}] \tag{5-27}$$

With some rearranging, Eq. (5-26) can be rewritten as

$$\hat{y}(k \mid k-1) = B(q)u(k) + [1 - A(q)]\bar{y}(k) + [\overline{C}(q) - 1][\bar{y}(k) - \hat{y}(k \mid k-1)] \tag{5-28}$$

and, similarly as before, using Eq. (5-21),

$$\begin{aligned}\hat{y}(k \mid k-1) = -a_1\bar{y}(k-1) - \ldots - a_{n_a}\bar{y}(k-n_a) + b_1u(k-1) + \ldots + b_{n_b}u(k-n_b) \\ + (c_2/c_1)\varepsilon(k-1) + \ldots + (c_{n_c}/c_1)\varepsilon(k-n_c+1)\end{aligned} \tag{5-29}$$

By letting the predicted response take the form

$$\hat{y}(k \mid \boldsymbol{\theta}) = \boldsymbol{\varphi}^{\mathrm{T}}(k, \bar{\mathbf{y}}(k-1, k-n_a), \mathbf{u}(k-1, k-n_b), \boldsymbol{\varepsilon}(k-1, k-n_a+1))\boldsymbol{\theta} \tag{5-30}$$

then, the vector of unknown parameters $\boldsymbol{\theta}$ becomes

$$\boldsymbol{\theta} = [a_1 \quad a_2 \quad \ldots \quad a_{n_a} \quad b_0 \quad b_1 \quad \ldots \quad b_{n_b} \quad c_2/c_1 \quad c_3/c_1 \quad \ldots \quad c_{n_c}/c_1]^{\mathrm{T}} \tag{5-31}$$

and the vector, $\boldsymbol{\varphi}$, includes previous measurements, control forces, and prediction errors.

5.2.1.2 Multi-Input/Multi-Output (MIMO) System

In the general case, the input control force $\mathbf{u}(k)$ is an r-dimensional vector, the external disturbance $\mathbf{e}(k)$ is a p-dimensional vector, and the output $\mathbf{y}(k)$ is an m-dimensional vector. The linear difference equation will take the form of a vector linear difference equation as shown in Eq. (5-5), where the $\mathbf{A}_i$'s are $m \times m$ matrices, the $\mathbf{B}_i$'s are $m \times r$ matrices, and the $\mathbf{C}_i$'s are $m \times p$ matrices. Analogously to Eq.

(5-4), the polynomials of the transfer functions are now matrix polynomials such that:

$$\begin{aligned}\mathbf{A}(q) &= \mathbf{I} + \mathbf{A}_1 q^{-1} + \ldots + \mathbf{A}_{n_a} q^{-n_a} \\ \mathbf{B}(q) &= \mathbf{B}_1 q^{-1} + \ldots + \mathbf{B}_{n_b} q^{-n_b} \\ \mathbf{C}(q) &= \mathbf{C}_0 + \mathbf{C}_1 q^{-1} + \ldots + \mathbf{C}_{n_c} q^{-n_c}\end{aligned} \tag{5-32}$$

Consequently, the transfer functions for a MIMO system, similar to those in Eq. (5-2), are defined as

$$\mathbf{G}(q) = \mathbf{A}^{-1}(q)\mathbf{B}(q) \quad \text{and} \quad \mathbf{H}(q) = \mathbf{A}^{-1}(q)\mathbf{C}(q) \tag{5-33}$$

Clearly, the transfer function $\mathbf{G}(q)$ is an $m \times r$ matrix and the transfer function $\mathbf{H}(q)$ is an $m \times p$ matrix. The factorization in terms of two matrix polynomials is called the (left) *matrix fraction description* (MFD) (Ljung, 2000).

5.2.1.2.1 Case of Ambient Wind Excitation

The test bed for the analyses introduced in this chapter is a shear building structural model, used frequently for structures and sometimes for bridges as shown in Chapter 3. However, in order to apply to MIMO systems the same approach discussed previously for the scalar systems, it is required that the transfer function $\mathbf{H}(q)$ be invertible. In other words, the number of external disturbances to the system should be equivalent to the number of outputs. This is a good assumption for the ambient wind excitation case when using a shear building structure model, since each story is subjected to a load due to wind excitation. Accordingly, if $\mathbf{H}(q)$ is

invertible, then a derivation similar to the SISO system case can be applied. Thus, by introducing the filtered disturbance

$$\mathbf{w}(k) = \mathbf{H}(q)\mathbf{e}(k) \tag{5-34}$$

with $\mathbf{w}(k)$ of dimension $m \times 1$, and since the disturbance vector $\mathbf{e}(k)$ has a zero mean, the prediction of the filtered disturbance $\mathbf{w}(k)$ is

$$\begin{aligned}\hat{\mathbf{w}}(k) &= E\left[\mathbf{w}(k) \mid \mathbf{e}(k-1), \mathbf{w}(k-1), \ldots\right] = \underset{\mathbf{e}(k)}{E}\left[\mathbf{w}(k)\right] = \underset{\mathbf{e}(k)}{E}\left[\sum_{l=0}^{\infty} \mathbf{h}(l)\mathbf{e}(k-l)\right] \\ &= \underset{e(k)}{E}\left[\mathbf{h}(0)\mathbf{e}(k)\right] + \underset{e(k)}{E}\left[\sum_{l=1}^{\infty} \mathbf{h}(l)\mathbf{e}(k-l)\right] = \sum_{l=1}^{\infty} \mathbf{h}(l)\mathbf{e}(k-l) = [\mathbf{H}(q) - \mathbf{h}(0)]\mathbf{e}(k) \\ &= [\mathbf{H}(q) - \mathbf{C}_0]\mathbf{e}(k)\end{aligned} \tag{5-35}$$

where $\mathbf{h}(k)$ is the pulse response matrix associated with the transfer function matrix $\mathbf{H}(q)$, and $\mathbf{h}(0) = \mathbf{C}_0$, similar to the scalar input and output case. By substituting Eq. (5-35) into Eq. (5-34)

$$\hat{\mathbf{w}}(k \mid k-1) = [\mathbf{H}(q) - \mathbf{h}(0)]\mathbf{e}(k) = [\mathbf{I} - \mathbf{h}(0)\mathbf{H}^{-1}(q)]\mathbf{w}(k) \tag{5-36}$$

Since the measured output $m \times 1$ vector $\bar{\mathbf{y}}(k)$ is the sum of the $m \times 1$ model output vector $\mathbf{y}(k)$ and the $m \times 1$ error vector $\mathbf{v}(k)$ due to sensors noise, modeling error, etc.,

$$\bar{\mathbf{y}}(k) = \mathbf{y}(k) + \mathbf{v}(k) \tag{5-37}$$

Solving Eq. (5-2) for $\mathbf{w}(k)$ and using Eq. (5-37)

$$\mathbf{w}(k) = -\mathbf{G}(q)\mathbf{u}(k) + \bar{\mathbf{y}}(k) - \mathbf{v}(k) \tag{5-38}$$

By taking the expectation of Eq. (5-2) with respect to the disturbance $\mathbf{e}(k)$ and the noise $\mathbf{v}(k)$, and substituting in Eqs. (5-36) and (5-38), the expected outputs given previous outputs and measurements are

$$\begin{aligned}\hat{\mathbf{y}}(k \mid k-1) &= \mathbf{G}(q)\mathbf{u}(k) + \hat{\mathbf{W}}(k \mid k-1) \\ &= \mathbf{G}(q)\mathbf{u}(k) + [\mathbf{I} - \mathbf{h}(0)\mathbf{H}^{-1}(q)][\bar{\mathbf{y}}(k) - \mathbf{G}(q)\mathbf{u}(k)]\end{aligned} \tag{5-39}$$

Using $\mathbf{h}(0) = \mathbf{C}_0$ leads to

$$\hat{\mathbf{y}}(k \mid k-1) = \mathbf{C}_0\mathbf{H}^{-1}(q)\mathbf{G}(q)\mathbf{u}(k) + [\mathbf{I} - \mathbf{C}_0\mathbf{H}^{-1}(q)]\bar{\mathbf{y}}(k) \tag{5-40}$$

Simplifying Eq. (5-40) using Eq. (5-33)

$$\hat{\mathbf{y}}(k \mid k-1) - \bar{\mathbf{y}}(k) = \mathbf{C}_0\mathbf{C}^{-1}(q)\mathbf{B}(q)\mathbf{u}(k) - \mathbf{C}_0\mathbf{C}^{-1}(q)\mathbf{A}(q)\bar{\mathbf{y}}(k) \tag{5-41}$$

Considering the $m \times 1$ prediction error vector $\boldsymbol{\varepsilon}(k)$ defined as

$$\boldsymbol{\varepsilon}(k) = \bar{\mathbf{y}}(k) - \hat{\mathbf{y}}(k \mid k-1) \tag{5-42}$$

Eq. (5-41) can be rearranged as

$$\hat{\mathbf{y}}(k \mid k-1) = \mathbf{B}(q)\mathbf{u}(k) + [\mathbf{I} - \mathbf{A}(q)]\bar{\mathbf{y}}(k) + [\tilde{\mathbf{C}}(q) - \mathbf{I}]\boldsymbol{\varepsilon}(k) \tag{5-43}$$

where $\tilde{\mathbf{C}}(q)$ is defined as

$$\tilde{\mathbf{C}}(q) = \mathbf{C}(q)\mathbf{C}_0^{-1} = \mathbf{I} + \mathbf{C}_1\mathbf{C}_0^{-1}q^{-1} + \ldots + \mathbf{C}_{n_c}\mathbf{C}_0^{-1}q^{-n_c} \tag{5-44}$$

Considering the form of $\mathbf{A}(q)$, $\mathbf{B}(q)$ and $\mathbf{C}(q)$ in Eq. (5-32) and substituting Eq. (5-44) into Eq. (5-43) and expanding gives

$$\hat{\mathbf{y}}(k \mid k-1) = -\mathbf{A}_1\bar{\mathbf{y}}(k-1) - \ldots - \mathbf{A}_{n_a}\bar{\mathbf{y}}(k-n_a) + \mathbf{B}_1 u(k-1) + \ldots + \mathbf{B}_{n_b} u(k-n_b) + \mathbf{C}_1\mathbf{C}_0^{-1}\boldsymbol{\varepsilon}(k-1) + \ldots + \mathbf{C}_{n_c}\mathbf{C}_0^{-1}\boldsymbol{\varepsilon}(k-n_c) \quad (5\text{-}45)$$

By letting the predicted response be expressed as

$$\hat{\mathbf{y}}(k \mid \boldsymbol{\theta}) = \boldsymbol{\varphi}^{\mathrm{T}}(k, \bar{\mathbf{y}}(k-1, k-n_a), \mathbf{u}(k-1, k-n_b), \boldsymbol{\varepsilon}(k-1, k-n_a))\boldsymbol{\theta} \quad (5\text{-}46)$$

then, let the matrix coefficients of the $\mathbf{A}(q)$, $\mathbf{B}(q)$ and $\widetilde{\mathbf{C}}(q)$ polynomials be written in terms of their row vectors:

$$\mathbf{A}_l = [a_1^{(l)} \quad a_2^{(l)} \quad \ldots \quad a_m^{(l)}]^{\mathrm{T}}, \ \mathbf{B}_l = [b_1^{(l)} \quad b_2^{(l)} \quad \ldots \quad b_m^{(l)}]^{\mathrm{T}}$$

$$\text{and} \quad \widetilde{\mathbf{C}}_l = [\widetilde{c}_1^{(l)} \quad \widetilde{c}_2^{(l)} \quad \ldots \quad \widetilde{c}_m^{(l)}]^{\mathrm{T}} \quad (5\text{-}47)$$

Then, for each matrix coefficient, a vector of all elements in each of the polynomial coefficient matrices can be expressed

$$\begin{aligned}
\boldsymbol{\theta}_a &= [a_1^{(1)} \quad a_2^{(1)} \quad \ldots \quad a_m^{(1)} \quad a_1^{(2)} \quad a_2^{(2)} \quad \ldots \quad a_m^{(2)} \quad \ldots \quad a_1^{(n_a)} \quad a_2^{(n_a)} \quad \ldots \quad a_m^{(n_a)}]^{\mathrm{T}} \\
\boldsymbol{\theta}_b &= [b_1^{(1)} \quad b_2^{(1)} \quad \ldots \quad b_m^{(1)} \quad b_1^{(2)} \quad b_2^{(2)} \quad \ldots \quad b_m^{(2)} \quad \ldots \quad b_1^{(n_b)} \quad b_2^{(n_b)} \quad \ldots \quad b_m^{(n_b)}]^{\mathrm{T}} \\
\boldsymbol{\theta}_c &= [\widetilde{c}_1^{(1)} \quad \widetilde{c}_2^{(1)} \quad \ldots \quad \widetilde{c}_m^{(1)} \quad \widetilde{c}_1^{(2)} \quad \widetilde{c}_2^{(2)} \quad \ldots \quad \widetilde{c}_m^{(2)} \quad \ldots \quad \widetilde{c}_1^{(n_c)} \quad \widetilde{c}_2^{(n_c)} \quad \ldots \quad \widetilde{c}_m^{(n_c)}]^{\mathrm{T}}
\end{aligned} \quad (5\text{-}48)$$

then the overall vector of unknown model parameters, $\boldsymbol{\theta}$, is, then,

$$\boldsymbol{\theta} = [\boldsymbol{\theta}_a^{\mathrm{T}} \quad \boldsymbol{\theta}_b^{\mathrm{T}} \quad \boldsymbol{\theta}_c^{\mathrm{T}}]^{\mathrm{T}} \quad (5\text{-}49)$$

The matrix $\boldsymbol{\varphi}$ contains data of past control forces input $\bar{\mathbf{u}}(k-1, k-n_b)$, previous measured output $\bar{\mathbf{y}}(k-1, k-n_a)$, and the past prediction errors $\bar{\boldsymbol{\varepsilon}}(k-1, k-n_c)$ with dimension $n_\theta \times m$

$$\varphi_y = \begin{bmatrix} \varphi_y \\ \varphi_u \\ \varphi_\varepsilon \end{bmatrix} \tag{5-50}$$

where

$$\varphi_y = \begin{bmatrix} -\mathbf{y}(k-1) & \mathbf{0} \\ \mathbf{0} & -\mathbf{y}(k-1) \\ & \ddots \\ \hline -\mathbf{y}(k-2) & \mathbf{0} \\ \mathbf{0} & -\mathbf{y}(k-2) \\ & \ddots \\ \hline \vdots & \vdots \\ \hline -\mathbf{y}(k-n_a) & \mathbf{0} \\ \mathbf{0} & -\mathbf{y}(k-n_a) \\ & \ddots \end{bmatrix}, \qquad \varphi_u = \begin{bmatrix} \mathbf{u}(k-1) & \mathbf{0} \\ \mathbf{0} & \mathbf{u}(k-1) \\ & \ddots \\ \hline \mathbf{u}(k-2) & \mathbf{0} \\ \mathbf{0} & \mathbf{u}(k-2) \\ & \ddots \\ \hline \vdots & \vdots \\ \hline \mathbf{u}(k-n_b) & \mathbf{0} \\ \mathbf{0} & \mathbf{u}(k-n_b) \\ & \ddots \end{bmatrix} \tag{5-51}$$

and

$$\varphi_\varepsilon = \begin{bmatrix} \boldsymbol{\varepsilon}(k-1) & \mathbf{0} \\ \mathbf{0} & \boldsymbol{\varepsilon}(k-1) \\ & \ddots \\ \hline \boldsymbol{\varepsilon}(k-2) & \mathbf{0} \\ \mathbf{0} & \boldsymbol{\varepsilon}(k-2) \\ & \ddots \\ \hline \vdots & \vdots \\ \hline \boldsymbol{\varepsilon}(k-n_c) & \mathbf{0} \\ \mathbf{0} & \boldsymbol{\varepsilon}(k-n_c) \\ & \ddots \end{bmatrix} \tag{5-52}$$

5.2.1.2.2 Case of Ambient Ground Excitation

A similar derivation for the predicted response of a MIMO system, subjected to ambient ground excitation, can be obtained. As an example, this may be the case for the 2DOF bridge model, as described in Chapter 3, with disturbance applied to the deck due to traffic excitation and another disturbance coming from the ground due to neighboring vibrations (sometimes due to traffic as well). Thus, analogously to the case of exciting a scalar system by an ambient ground excitation, considering the prediction of the filtered disturbance $\mathbf{w}(k)$ from Eq. (5-34)

$$\begin{aligned}\hat{\mathbf{w}}(k) &= E\left[\mathbf{w}(k) \mid \mathbf{e}(k-2), \mathbf{w}(k-1), \ldots\right] = \underset{\mathbf{e}(k-1)}{E}\left[\mathbf{w}(k)\right] = \underset{\mathbf{e}(k-1)}{E}\left[\sum_{l=1}^{\infty} \mathbf{h}(l)\mathbf{e}(k-l)\right] \\ &= \sum_{l=2}^{\infty} \mathbf{h}(l)\mathbf{e}(k-l) = [\mathbf{H}(q) - \mathbf{C}_1 q^{-1}]\mathbf{e}(k)\end{aligned} \tag{5-53}$$

where $\mathbf{h}(0) = \mathbf{0}$.

By steps similar to Eq. (5-36) through Eq. (5-46), the predicted response of a MIMO system subjected to ground excitation may be expressed as

$$\begin{aligned}\hat{\mathbf{y}}(k \mid k-1) = &-\mathbf{A}_1 \bar{\mathbf{y}}(k-1) - \ldots - \mathbf{A}_{n_a} \bar{\mathbf{y}}(k-n_a) + \mathbf{B}_1 u(k-1) + \ldots + \mathbf{B}_{n_b} u(k-n_b) \\ &+ \mathbf{C}_2 \mathbf{C}_1^{-1} \boldsymbol{\varepsilon}(k-1) + \ldots + \mathbf{C}_{n_c} \mathbf{C}_1^{-1} \boldsymbol{\varepsilon}(k-n_c+1)\end{aligned} \tag{5-54}$$

Eq. (5-54) can be rearranged to a similar form to Eq. (5-43) where, now, $\tilde{\mathbf{C}}(q)$ is defined for ground excitation as

$$\tilde{\mathbf{C}}(q) = \mathbf{I} + \mathbf{C}_2 \mathbf{C}_1^{-1} q^{-1} + \ldots + \mathbf{C}_{n_c} \mathbf{C}_1^{-1} q^{-n_c-1} \tag{5-55}$$

Let the matrix coefficients of the $\mathbf{A}(q)$, $\mathbf{B}(q)$ and $\widetilde{\mathbf{C}}(q)$ polynomials be written in terms of their row vectors in a manner similarly to Eq. (5-47)

$$\begin{aligned}
\boldsymbol{\theta}_{\mathrm{a}} &= [a_1^{(1)} \quad a_2^{(1)} \quad \ldots \quad a_m^{(1)} \quad a_1^{(2)} \quad a_2^{(2)} \quad \ldots \quad a_m^{(2)} \quad \ldots \quad a_1^{(n_a)} \quad a_2^{(n_a)} \quad \ldots \quad a_m^{(n_a)}]^{\mathrm{T}} \\
\boldsymbol{\theta}_{\mathrm{b}} &= [b_1^{(1)} \quad b_2^{(1)} \quad \ldots \quad b_m^{(1)} \quad b_1^{(2)} \quad b_2^{(2)} \quad \ldots \quad b_m^{(2)} \quad \ldots \quad b_1^{(n_b)} \quad b_2^{(n_b)} \quad \ldots \quad b_m^{(n_b)}]^{\mathrm{T}} \\
\boldsymbol{\theta}_{\mathrm{c}} &= [\widetilde{c}_1^{(1)} \quad \widetilde{c}_2^{(1)} \quad \ldots \quad \widetilde{c}_m^{(1)} \quad \widetilde{c}_1^{(2)} \quad \widetilde{c}_2^{(2)} \quad \ldots \quad \widetilde{c}_m^{(2)} \quad \ldots \quad \widetilde{c}_1^{(n_c-1)} \quad \widetilde{c}_2^{(n_c-1)} \quad \ldots \quad \widetilde{c}_m^{(n_c-1)}]^{\mathrm{T}}
\end{aligned} \tag{5-56}$$

and $\boldsymbol{\varphi}$ is a matrix containing data of past control forces input $\bar{\mathbf{u}}(k-1,k-n_{\mathrm{b}})$, previous measured output $\bar{\mathbf{y}}(k-1,k-n_{\mathrm{a}})$, and the past prediction errors $\bar{\boldsymbol{\varepsilon}}(k-1,k-n_{\mathrm{c}}+1)$ with dimension $n_\theta \times m$. $\boldsymbol{\varphi}$ is the same in Eq. (5-50) and its submatrices are the same as in Eqs. (5-51) and (5-52) except $\boldsymbol{\varphi}_{\varepsilon}$ only goes back to time (k-n_{c}+1) instead of (k-n_{c}).

5.2.2 Control Force

In the applications envisioned here, the applied control forces $\mathbf{u}(k)$ are assumed to be a function of the older measurements such that

$$\mathbf{u}(k) = -\widetilde{\mathbf{K}}_1 \bar{\mathbf{y}}(k-1) - \ldots - \widetilde{\mathbf{K}}_p \bar{\mathbf{y}}(k-p) \tag{5-57}$$

$\widetilde{\mathbf{K}}_1, \widetilde{\mathbf{K}}_2, \ldots, \widetilde{\mathbf{K}}_p$ are the control gain matrices of the system such that

$$\widetilde{\mathbf{K}}_i = \begin{bmatrix} \widetilde{k}_{1,1}^{(i)} & \widetilde{k}_{1,2}^{(i)} & \cdots & \widetilde{k}_{1,m}^{(i)} \\ \widetilde{k}_{2,1}^{(i)} & \ddots & \ddots & \widetilde{k}_{2,m}^{(i)} \\ \vdots & \vdots & \ddots & \vdots \\ \widetilde{k}_{r,1}^{(i)} & \widetilde{k}_{r,2}^{(i)} & \cdots & \widetilde{k}_{r,m}^{(i)} \end{bmatrix} \tag{5-58}$$

where m is the number of measurements and r is the number of control forces inputs.

5.2.3 Estimating Model Parameters

By collecting a large number N of measured and predicted output data samples and finding the prediction error $\boldsymbol{\varepsilon}$ for each time step k, then the sample variance of the prediction error would be

$$Var_N[\boldsymbol{\varepsilon}(k) \mid \bar{\mathbf{y}}_p(k), \bar{\mathbf{u}}_p(k), \bar{\boldsymbol{\varepsilon}}_p(k)] = \frac{1}{N-1} \sum_{l=k-N+1}^{k} [\bar{\mathbf{y}}(l) - \boldsymbol{\varphi}^{\mathrm{T}}(l, \bar{\mathbf{y}}_p(l), \bar{\mathbf{u}}_p(l), \bar{\boldsymbol{\varepsilon}}_p(l))\boldsymbol{\theta}]^{\mathrm{T}} [\bar{\mathbf{y}}(l) - \boldsymbol{\varphi}^{\mathrm{T}}(l, \bar{\mathbf{y}}_p(l), \bar{\mathbf{u}}_p(l), \bar{\boldsymbol{\varepsilon}}_p(l))\boldsymbol{\theta}] \tag{5-59}$$

where $\bar{\mathbf{y}}_p(k) = \bar{\mathbf{y}}(k-1, k-n_{\mathrm{a}})$, $\bar{\mathbf{u}}_p(k) = \bar{\mathbf{u}}(k-1, k-n_{\mathrm{b}})$, and $\bar{\boldsymbol{\varepsilon}}_p(k) = \bar{\boldsymbol{\varepsilon}}(k-1, k-n_{\mathrm{c}})$.

By minimizing the variance in Eq. (5-59) with respect to the unknown parameters, $\boldsymbol{\theta}$, an estimate of the unknown model parameters at any time step, k, is obtained

$$\hat{\boldsymbol{\theta}}_N(k) = \left[\frac{1}{N-1} \sum_{l=k-N+1}^{k} \boldsymbol{\varphi}(l, \bar{\mathbf{y}}_p, \bar{\mathbf{u}}_p, \bar{\boldsymbol{\varepsilon}}_p) \boldsymbol{\varphi}^{\mathrm{T}}(l, \bar{\mathbf{y}}_p, \bar{\mathbf{u}}_p, \bar{\boldsymbol{\varepsilon}}_p) \right]^{-1} \frac{1}{N-1} \sum_{l=k-N+1}^{k} \boldsymbol{\varphi}(l, \bar{\mathbf{y}}_p, \bar{\mathbf{u}}_p, \bar{\boldsymbol{\varepsilon}}_p) \bar{\mathbf{y}}(l) \tag{5-60}$$

5.2.4 Cost Function Evaluation at the Beginning of the Control Horizon

In order to evaluate the cost function in Eq. (5-6) at time k_0, it is essential to evaluate the term $\hat{\boldsymbol{\theta}}(k_{\mathrm{f}})$ in the first term of the right hand side. This can be done using Eq. (5-60). However, from the structure of matrices $\boldsymbol{\varphi}(k_0 \rightarrow k_{\mathrm{f}})$, it can be observed that they include some unknown future output measurements $\bar{\mathbf{y}}(k_0, k_{\mathrm{f}})$,

control force inputs $\bar{\mathbf{u}}(k_0,k_f)$, and future prediction errors $\bar{\boldsymbol{\varepsilon}}(k_0,k_f)$. These future measurements are a function of the unknown deterministic parameters $\boldsymbol{\theta}$, the unknown control gains $\tilde{\mathbf{K}}_i$, the unknown stochastic disturbance $\bar{\mathbf{e}}(k_0,k_f)$ and the unknown stochastic noise error $\bar{\mathbf{v}}(k_0,k_f)$. However, due to the summation over the entire control horizon as required by the $\boldsymbol{\theta}$ evaluation Eq. (5-60), it may be very messy to directly substitute the estimated measurements of the output response, the control forces and the prediction errors and then try to obtain $\boldsymbol{\theta}$. Also, the computational resources required for such an operation are huge and a solution may not be feasible. Thus, an alternative method of finding the system parameters at the end of the control interval, $\hat{\boldsymbol{\theta}}(k_f)$, should be sought.

Consider a scalar system, where by expanding Eq. (5-60) in terms of the previous outputs, previous control inputs, and previous prediction errors, an equation for evaluating $\hat{\boldsymbol{\theta}}_N(k)$ takes the form

$$\hat{\boldsymbol{\theta}}_N(k)=\left[\frac{1}{N-1}\sum_{k=k_0}^{k_f}\boldsymbol{\varphi}(k)\boldsymbol{\varphi}^{\mathrm{T}}(k)\right]^{-1}\frac{1}{N-1}\sum_{k=k_0}^{k_f}\boldsymbol{\varphi}(k)y(k) \tag{5-61}$$

where

$$\boldsymbol{\varphi}(k)\boldsymbol{\varphi}^{\mathrm{T}}(k)=\left[\begin{array}{c|c|c|c|c} \bar{y}(k-1)\bar{y}(k-1) & \bar{y}(k-1)\bar{y}(k-2) & -\bar{y}(k-1)u(k-1) & -\bar{y}(k-1)u(k-2) & -\bar{y}(k-1)\varepsilon(k-1) \\ \bar{y}(k-2)\bar{y}(k-1) & \bar{y}(k-2)\bar{y}(k-2) & -\bar{y}(k-2)u(k-1) & -\bar{y}(k-2)u(k-2) & -\bar{y}(k-2)\varepsilon(k-1) \\ -u(k-1)\bar{y}(k-1) & -u(k-1)\bar{y}(k-2) & u(k-1)u(k-1) & u(k-1)u(k-2) & u(k-1)\varepsilon(k-1) \\ -u(k-2)\bar{y}(k-1) & -u(k-2)\bar{y}(k-2) & u(k-2)u(k-1) & u(k-2)u(k-2) & u(k-2)\varepsilon(k-1) \\ -\varepsilon(k-1)\bar{y}(k-1) & -\varepsilon(k-1)\bar{y}(k-2) & \varepsilon(k-1)u(k-1) & \varepsilon(k-1)u(k-2) & \varepsilon(k-1)\varepsilon(k-1) \end{array}\right] \tag{5-62}$$

and

$$\varphi(k)y(k)=\begin{bmatrix}\bar{y}(k-1)\bar{y}(k)\\ \bar{y}(k-2)\bar{y}(k)\\ u(k-1)\bar{y}(k)\\ u(k-2)\bar{y}(k)\\ \varepsilon(k-1)\bar{y}(k)\end{bmatrix} \tag{5-63}$$

Collecting sufficiently large amounts of data (N samples), and using the statistical laws of large numbers, averaging N samples of the product terms in each of the elements of in Eq. (5-61) converges to the autocorrelation or cross correlation functions. Thus, a new definition of the cost function may be posed in terms of the autocorrelation and the cross correlation functions of the previous measurements, control forces, and prediction errors. Moreover, considering that the input to the system is stationary, and since the system is assumed linear and time-invariant, then the response of the system is also stationary. Thus, using the properties of stationary stochastic processes, Eq. (5-61) can be modified to the following equation

$$\hat{\theta}_N(k)=\begin{bmatrix} R_{\bar{y}}(0) & R_{\bar{y}}(1) & R_{\bar{y}u}(0) & R_{\bar{y}u}(1) & R_{\bar{y}\varepsilon}(0)\\ R_{\bar{y}}(-1) & R_{\bar{y}}(0) & R_{\bar{y}u}(-1) & R_{\bar{y}u}(0) & R_{\bar{y}\varepsilon}(-1)\\ R_{u\bar{y}}(0) & R_{u\bar{y}}(1) & R_{u}(0) & R_{u}(1) & R_{u\varepsilon}(0)\\ R_{u\bar{y}}(-1) & R_{u\bar{y}}(0) & R_{u}(-1) & R_{u}(0) & R_{u\varepsilon}(-1)\\ R_{\varepsilon\bar{y}}(0) & R_{\varepsilon\bar{y}}(1) & R_{\varepsilon u}(0) & R_{\varepsilon u}(1) & R_{\varepsilon\varepsilon}(0) \end{bmatrix}^{-1}\begin{bmatrix} R_{\bar{y}}(-1)\\ R_{\bar{y}}(-2)\\ R_{u\bar{y}}(-1)\\ R_{u\bar{y}}(-2)\\ R_{\varepsilon\bar{y}}(-1)\end{bmatrix} \tag{5-64}$$

where

$$R_{\bar{y}}(n) = E[(\bar{y}(n)\bar{y}(k-n)], \quad R_{u\bar{y}}(n) = E[u(n)\bar{y}(n+k)]$$

$$R_{\varepsilon\bar{y}}(n) = E[\varepsilon(n)\bar{y}(n+k)], \quad R_{u\varepsilon}(k) = E[u(n)\varepsilon(n+k)] \tag{5-65}$$

$$R_{\varepsilon}(k) = E[\varepsilon(n)\varepsilon(n+k)], \quad R_{u}(k) = E[u(n)u(n+k)]$$

For a stationary process in a scalar system, $R(n) = R(-n)$, then

$$\hat{\boldsymbol{\theta}}_N(k) = \begin{bmatrix} R_{\bar{y}}(0) & R_{\bar{y}}(1) & R_{\bar{y}u}(0) & R_{\bar{y}u}(1) & R_{\bar{y}\varepsilon}(0) \\ R_{\bar{y}}(1) & R_{\bar{y}}(0) & R_{\bar{y}u}(1) & R_{\bar{y}u}(0) & R_{\bar{y}\varepsilon}(1) \\ R_{u\bar{y}}(0) & R_{u\bar{y}}(1) & R_{u}(0) & R_{u}(1) & R_{u\varepsilon}(0) \\ R_{u\bar{y}}(1) & R_{u\bar{y}}(0) & R_{u}(1) & R_{u}(0) & R_{u\varepsilon}(1) \\ R_{\varepsilon\bar{y}}(0) & R_{\varepsilon\bar{y}}(1) & R_{\varepsilon u}(0) & R_{\varepsilon u}(1) & R_{\varepsilon}(0) \end{bmatrix}^{-1} \begin{bmatrix} R_{\bar{y}}(1) \\ R_{\bar{y}}(2) \\ R_{u\bar{y}}(1) \\ R_{u\bar{y}}(2) \\ R_{\varepsilon\bar{y}}(1) \end{bmatrix} \tag{5-66}$$

However, for MIMO systems, $\mathbf{R}_x(n) = \mathbf{R}_x^T(-n)$ and $\mathbf{R}_{xy}(n) = \mathbf{R}_{yx}^T(-n)$; then, for the 2DOF bridge model

$$\hat{\boldsymbol{\theta}}_N(k) = \overline{\mathbf{R}}^{-1}\widetilde{\mathbf{R}} \tag{5-67}$$

where

$$\overline{\mathbf{R}} = \begin{bmatrix} \overline{\mathbf{R}}_{\bar{y}} & \overline{\mathbf{R}}_{\bar{y}u} & \overline{\mathbf{R}}_{\bar{y}\varepsilon} \\ \overline{\mathbf{R}}_{u\bar{y}} & \overline{\mathbf{R}}_{u} & \overline{\mathbf{R}}_{u\varepsilon} \\ \overline{\mathbf{R}}_{\varepsilon\bar{y}} & \overline{\mathbf{R}}_{\varepsilon u} & \overline{\mathbf{R}}_{\varepsilon} \end{bmatrix} \tag{5-68}$$

such that

$$\overline{\mathbf{R}}_{\bar{\mathbf{y}}}=\begin{bmatrix} \mathbf{R}_{\bar{\mathbf{y}}}(0) & \mathbf{0} & \mathbf{R}_{\bar{\mathbf{y}}}(1) & \mathbf{0} \\ \mathbf{0} & \mathbf{R}_{\bar{\mathbf{y}}}(0) & \mathbf{0} & \mathbf{R}_{\bar{\mathbf{y}}}(1) \\ \mathbf{R}^{\mathrm{T}}_{\bar{\mathbf{y}}}(1) & \mathbf{0} & \mathbf{R}_{\bar{\mathbf{y}}}(0) & \mathbf{0} \\ \mathbf{0} & \mathbf{R}^{\mathrm{T}}_{\bar{\mathbf{y}}}(1) & \mathbf{0} & \mathbf{R}_{\bar{\mathbf{y}}}(0) \end{bmatrix}, \quad \overline{\mathbf{R}}_{\bar{\mathbf{y}}\mathbf{u}}=\begin{bmatrix} -\mathbf{R}_{\bar{\mathbf{y}}\mathbf{u}}(0) & \mathbf{0} & -\mathbf{R}_{\bar{\mathbf{y}}\mathbf{u}}(1) & \mathbf{0} \\ \mathbf{0} & -\mathbf{R}_{\bar{\mathbf{y}}\mathbf{u}}(0) & \mathbf{0} & -\mathbf{R}_{\bar{\mathbf{y}}\mathbf{u}}(1) \\ -\mathbf{R}^{\mathrm{T}}_{\mathbf{u}\bar{\mathbf{y}}}(1) & \mathbf{0} & -\mathbf{R}_{\bar{\mathbf{y}}\mathbf{u}}(0) & \mathbf{0} \\ \mathbf{0} & -\mathbf{R}^{\mathrm{T}}_{\mathbf{u}\bar{\mathbf{y}}}(1) & \mathbf{0} & -\mathbf{R}_{\bar{\mathbf{y}}\mathbf{u}}(0) \end{bmatrix}$$

$$\overline{\mathbf{R}}_{\bar{\mathbf{y}}\varepsilon}=\begin{bmatrix} -\mathbf{R}_{\bar{\mathbf{y}}\varepsilon}(0) & \mathbf{0} \\ \mathbf{0} & -\mathbf{R}_{\bar{\mathbf{y}}\varepsilon}(0) \\ -\mathbf{R}^{\mathrm{T}}_{\varepsilon\bar{\mathbf{y}}}(1) & \mathbf{0} \\ \mathbf{0} & -\mathbf{R}^{\mathrm{T}}_{\varepsilon\bar{\mathbf{y}}}(1) \end{bmatrix}, \quad \overline{\mathbf{R}}_{\mathbf{u}\bar{\mathbf{y}}}=\begin{bmatrix} -\mathbf{R}_{\mathbf{u}\bar{\mathbf{y}}}(0) & \mathbf{0} & -\mathbf{R}_{\mathbf{u}\bar{\mathbf{y}}}(1) & \mathbf{0} \\ \mathbf{0} & -\mathbf{R}_{\mathbf{u}\bar{\mathbf{y}}}(0) & \mathbf{0} & -\mathbf{R}_{\mathbf{u}\bar{\mathbf{y}}}(1) \\ -\mathbf{R}^{\mathrm{T}}_{\bar{\mathbf{y}}\mathbf{u}}(1) & \mathbf{0} & -\mathbf{R}_{\mathbf{u}\bar{\mathbf{y}}}(0) & \mathbf{0} \\ \mathbf{0} & -\mathbf{R}^{\mathrm{T}}_{\bar{\mathbf{y}}\mathbf{u}}(1) & \mathbf{0} & -\mathbf{R}_{\mathbf{u}\bar{\mathbf{y}}}(0) \end{bmatrix},$$

$$\overline{\mathbf{R}}_{\mathbf{u}}=\begin{bmatrix} \mathbf{R}_{\mathbf{u}}(0) & \mathbf{0} & \mathbf{R}_{\mathbf{u}}(1) & \mathbf{0} \\ \mathbf{0} & \mathbf{R}_{\mathbf{u}}(0) & \mathbf{0} & \mathbf{R}_{\mathbf{u}}(1) \\ \mathbf{R}^{\mathrm{T}}_{\mathbf{u}}(1) & \mathbf{0} & \mathbf{R}_{\mathbf{u}}(0) & \mathbf{0} \\ \mathbf{0} & \mathbf{R}^{\mathrm{T}}_{\mathbf{u}}(1) & \mathbf{0} & \mathbf{R}_{\mathbf{u}}(0) \end{bmatrix}, \quad \overline{\mathbf{R}}_{\mathbf{u}\varepsilon}=\begin{bmatrix} \mathbf{R}_{\mathbf{u}\varepsilon}(0) & \mathbf{0} \\ \mathbf{0} & \mathbf{R}_{\mathbf{u}\varepsilon}(0) \\ \mathbf{R}^{\mathrm{T}}_{\varepsilon\mathbf{u}}(1) & \mathbf{0} \\ \mathbf{0} & \mathbf{R}^{\mathrm{T}}_{\varepsilon\mathbf{u}}(1) \end{bmatrix}, \quad \overline{\mathbf{R}}_{\varepsilon}=\begin{bmatrix} \mathbf{R}_{\varepsilon}(0) & \mathbf{0} \\ \mathbf{0} & \mathbf{R}_{\varepsilon}(0) \end{bmatrix}$$

$$\overline{\mathbf{R}}_{\varepsilon\bar{\mathbf{y}}}=\begin{bmatrix} -\mathbf{R}_{\varepsilon\bar{\mathbf{y}}}(0) & \mathbf{0} & -\mathbf{R}_{\varepsilon\bar{\mathbf{y}}}(1) & 0 \\ \mathbf{0} & -\mathbf{R}_{\varepsilon\bar{\mathbf{y}}}(0) & 0 & -\mathbf{R}_{\varepsilon\bar{\mathbf{y}}}(1) \end{bmatrix}, \quad \text{and} \quad \overline{\mathbf{R}}_{\varepsilon\mathbf{u}}=\begin{bmatrix} \mathbf{R}_{\varepsilon\mathbf{u}}(0) & \mathbf{0} & \mathbf{R}_{\varepsilon\mathbf{u}}(0) & 0 \\ \mathbf{0} & \mathbf{R}_{\varepsilon\mathbf{u}}(0) & 0 & \mathbf{R}_{\varepsilon\mathbf{u}}(0) \end{bmatrix}^{\mathrm{T}}$$

(5-69)

and

$$\widetilde{\mathbf{R}}=\left[\mathbf{R}^{\mathrm{T}}_{\bar{\mathbf{y}}\bar{\mathbf{y}}_1}(1)\ \mathbf{R}^{\mathrm{T}}_{\bar{\mathbf{y}}\bar{\mathbf{y}}_2}(1)\ \mathbf{R}^{\mathrm{T}}_{\bar{\mathbf{y}}\bar{\mathbf{y}}_1}(2)\ \mathbf{R}^{\mathrm{T}}_{\bar{\mathbf{y}}\bar{\mathbf{y}}_2}(2)\ \mathbf{R}^{\mathrm{T}}_{\bar{\mathbf{y}}\mathbf{u}}(1)\ \mathbf{R}^{\mathrm{T}}_{\bar{\mathbf{y}}\mathbf{u}}(2)\ \mathbf{R}^{\mathrm{T}}_{\bar{\mathbf{y}}\varepsilon_1}(1)\ \mathbf{R}^{\mathrm{T}}_{\bar{\mathbf{y}}\varepsilon_2}(1)\right]^{\mathrm{T}} \quad (5\text{-}70)$$

Thus the vector of estimated system parameters, $\hat{\boldsymbol{\theta}}(k_{\mathrm{f}})$, can be expressed in terms of the autocorrelations and cross correlations of the response measurements, the control forces and the prediction errors of the system within the control horizon

$[k_0, k_f]$ of the control problem. Therefore, Eq. (5-64) can be used in evaluating $\hat{\boldsymbol{\theta}}(k_f)$ in the first term of the right hand side of the cost function equation.

As for the second term of the right hand side of the cost function equation, Eq. (5-6), the same assumption of a large number of samples is used. In addition, the weighting matrix **R** is assumed symmetric and diagonal. Thus, the second term of Eq. (5-6) can be expressed in terms of the autocorrelation function of the control force input as

$$\frac{1}{2}\sum_{k_0}^{k_f} \mathrm{E}\left[\mathbf{u}^{\mathrm{T}}(k)\mathbf{R}\mathbf{u}(k)\right] = \frac{1}{2}\mathrm{Trace}[\mathbf{R}\mathbf{R}_{\mathrm{u}}(0)] \tag{5-71}$$

As a result, if one can obtain the autocorrelations and cross correlations of the output response, the control force, and the prediction errors, then the cost function can be evaluated in terms of the control gains $\tilde{\mathbf{K}}_i$, the system parameters $\boldsymbol{\theta}$, and the statistical properties of the disturbance **e** and the noise **v**. The following subsections derive the formulas for the auto- and cross correlations in Eqs. (5-66) to (5-71).

5.2.4.1 Evaluation of the Cross Correlation between the Stochastic Input and the Measured Response

To obtain the associated auto-/cross correlations of the measurements, it is useful to first obtain the cross correlation of the stochastic inputs (disturbance **e** and noise **v**) and the measured output response ($\bar{\mathbf{y}}$). This may, however, require modifying the originally introduced ARMAX model to an equivalent ARMA model with stochastic noise **v** and the disturbance **e** as inputs. The control force is expanded

in the ARMA model equation in terms of the control gains and the older response measurements as per Eq. (5-57).

The test bed of the application in this chapter is the 2DOF bridge model introduced in Chapter 3. Thus, the following derivations are mainly derived for this model. The system is fourth order and the response output at the deck and pier levels is measured; thus, the number of backward time steps p to express the finite linear difference equation is two. Accordingly, the ARMAX model of the 2DOF bridge model is

$$\begin{aligned}\bar{\mathbf{y}}(k) = &-\mathbf{A}_1\bar{\mathbf{y}}(k-1) - \mathbf{A}_2\bar{\mathbf{y}}(k-2) + \mathbf{B}_1\mathbf{u}(k-1) + \mathbf{B}_2\mathbf{u}(k-2) + \mathbf{C}_0\mathbf{e}(k) + \mathbf{C}_1\mathbf{e}(k-1) \\ &+ \mathbf{C}_2\mathbf{e}(k-2) + \mathbf{v}(k) + \mathbf{A}_1\mathbf{v}(k-1) + \mathbf{A}_2\mathbf{v}(k-2)\end{aligned} \tag{5-72}$$

The control force, as per Eq. (5-57) with p=2, can be expressed as

$$\mathbf{u}(k) = -\tilde{\mathbf{K}}_1\bar{\mathbf{y}}(k-1) - \tilde{\mathbf{K}}_2\mathbf{y}(k-2) \tag{5-73}$$

Therefore, Eq. (5-73) can be modified to get the closed-loop ARMA model equation

$$\begin{aligned}\bar{\mathbf{y}}(k) = &-(\mathbf{A}_1)\bar{\mathbf{y}}(k-1) - (\mathbf{A}_2 + \mathbf{B}_1\tilde{\mathbf{K}}_1)\bar{\mathbf{y}}(k-2) - (\mathbf{B}_1\tilde{\mathbf{K}}_2 + \mathbf{B}_2\tilde{\mathbf{K}}_1)\bar{\mathbf{y}}(k-3) \\ &- (\mathbf{B}_2\tilde{\mathbf{K}}_2)\bar{\mathbf{y}}(k-4) + \begin{bmatrix}\mathbf{C}_0 & \mathbf{I}\end{bmatrix}\begin{bmatrix}\mathbf{e}^{\mathrm{T}}(k) & \mathbf{v}^{\mathrm{T}}(k)\end{bmatrix}^{\mathrm{T}} + \begin{bmatrix}\mathbf{C}_1 & \mathbf{A}_1\end{bmatrix}\begin{bmatrix}\mathbf{e}^{\mathrm{T}}(k-1) & \mathbf{v}^{\mathrm{T}}(k-1)\end{bmatrix}^{\mathrm{T}} \\ &+ \begin{bmatrix}\mathbf{C}_2 & \mathbf{A}_2\end{bmatrix}\begin{bmatrix}\mathbf{e}^{\mathrm{T}}(k-2) & \mathbf{v}^{\mathrm{T}}(k-2)\end{bmatrix}^{\mathrm{T}}\end{aligned} \tag{5-74}$$

Now, let $\psi(k) = \begin{bmatrix}\mathbf{e}^{\mathrm{T}}(k) & \mathbf{v}^{\mathrm{T}}(k)\end{bmatrix}^{\mathrm{T}}$ and let the coefficients of the finite linear difference equation of the closed-loop ARMA model, Eq. (5-74), be written as

$$\alpha_1 = \mathbf{A}_1, \quad \alpha_2 = \mathbf{A}_2 + \mathbf{B}_1\tilde{\mathbf{K}}_1, \quad \alpha_3 = \mathbf{B}_1\tilde{\mathbf{K}}_2 + \mathbf{B}_2\tilde{\mathbf{K}}_1, \quad \alpha_4 = \mathbf{B}_2\tilde{\mathbf{K}}_2 \tag{5-75}$$

and

$$\varsigma_0 = [\mathbf{C}_0 \quad \mathbf{I}], \quad \varsigma_1 = [\mathbf{C}_1 \quad \mathbf{A}_1], \quad \varsigma_2 = [\mathbf{C}_2 \quad \mathbf{A}_2] \tag{5-76}$$

Thus, Eq. (5-74) can be expressed in a more compact way such that

$$\bar{\mathbf{y}}(k) = -\sum_{i=1}^{4} \alpha_i \bar{\mathbf{y}}(k-i) + \sum_{j=0}^{2} \varsigma_j \psi(k-j) \tag{5-77}$$

Since $\bar{\mathbf{y}}$ and ψ are assumed stationary and zero mean, then

$$\mathbf{R}_{\bar{\mathbf{y}}\psi}(n) = \mathbf{R}^{\mathrm{T}}_{\psi\bar{\mathbf{y}}}(-n) = E[\bar{\mathbf{y}}(k)\psi^{\mathrm{T}}(k-n)], \quad n \geq 0 \tag{5-78}$$

But, by substituting Eq. (5-77) in Eq. (5-78) and, since the expectation is a linear operator, then

$$\mathbf{R}_{\bar{\mathbf{y}}\psi}(n) = -\sum_{i=1}^{4} \alpha_i E[\bar{\mathbf{y}}(k-i)\psi^{\mathrm{T}}(k-n)] + \sum_{j=0}^{2} \varsigma_j E[\psi(k-j)\psi^{\mathrm{T}}(k-n)] \tag{5-79}$$

which can be modified to be

$$\mathbf{R}_{\bar{\mathbf{y}}\psi}(n) = -\sum_{i=1}^{4} \alpha_i \mathbf{R}_{\bar{\mathbf{y}}\psi}(n-i) + \sum_{j=0}^{2} \varsigma_j \mathbf{R}_{\psi}(n-j) \tag{5-80}$$

Note, however, that future inputs are independent of past measurements; therefore $E[\bar{\mathbf{y}}(k-i)\psi^{\mathrm{T}}(k-n)]$ is a zero matrix for $n-i<0$. Further, the input $\psi(k)$ is independent at every time step. Thus Eq. (5-80) can be rewritten as

$$\mathbf{R}_{\bar{y}\psi}(n) = -\sum_{i=1}^{\min(4,n)} \alpha_i \mathbf{R}_{\bar{y}\psi}(n-i) + \sum_{j=0}^{2} \varsigma_j \mathbf{R}_{\psi}(n-j)\delta_{nj} \tag{5-81}$$

where δ_{nj} is the Kronecker delta. Thus,

$$\begin{aligned}
&\mathbf{R}_{\bar{y}\psi}(0) = \varsigma_0 \mathbf{C}_{\psi} \\
&\mathbf{R}_{\bar{y}\psi}(1) = (-\alpha_1\varsigma_0 + \varsigma_1)\mathbf{C}_{\psi} \\
&\mathbf{R}_{\bar{y}\psi}(2) = [(\alpha_1\alpha_1 - \alpha_2)\varsigma_0 - \alpha_1\varsigma_1 + \varsigma_2]\mathbf{C}_{\psi} \\
&\mathbf{R}_{\bar{y}\psi}(3) = [(-\alpha_1\alpha_1\alpha_1 + \alpha_1\alpha_2 + \alpha_2\alpha_1 - \alpha_3)\varsigma_0 + (\alpha_1\alpha_1 - \alpha_2)\varsigma_1 - \alpha_1\varsigma_2]\mathbf{C}_{\psi} \\
&\mathbf{R}_{\bar{y}\psi}(n) = -\alpha_1 R_{\bar{y}\psi}(n-1) - \alpha_2 R_{\bar{y}\psi}(n-2) - \alpha_3 R_{\bar{y}\psi}(n-3) - \alpha_4 R_{\bar{y}\psi}(n-4),\ n > 3 \\
&\mathbf{R}_{\bar{y}\psi}(n) = \mathbf{0},\ n < 0
\end{aligned} \tag{5-82}$$

where $\mathbf{C}_{\psi}$ is the covariance matrix of the stochastic input.

5.2.4.2 Evaluation of the Autocorrelation of the Measured Response

Using the cross correlation between the stochastic input and the measured response, the autocorrelation of the measured response can be obtained. Postmultiplying both sides of Eq. (5-77) by $\bar{\mathbf{y}}^{\mathrm{T}}(k-n)$ gives

$$\bar{\mathbf{y}}(k)\bar{\mathbf{y}}^{\mathrm{T}}(k-n) = -\sum_{i=1}^{4} \alpha_i \bar{\mathbf{y}}(k-i)\bar{\mathbf{y}}^{\mathrm{T}}(k-n) + \sum_{j=0}^{2} \varsigma_j \psi(k-j)\bar{\mathbf{y}}^{\mathrm{T}}(k-n) \tag{5-83}$$

Then, by taking the expectation,

$$\mathbf{R}_{\bar{y}}(n) = -\sum_{i=1}^{4} \alpha_i \mathbf{R}_{\bar{y}}(n-i) + \sum_{j=0}^{2} \varsigma_j \mathbf{R}_{\psi\bar{y}}(n-j) \tag{5-84}$$

which indicates that the autocorrelation function of the output response $\bar{\mathbf{y}}$ satisfies the finite linear difference equation. Then, by expanding for n=0,1,2,3 and 4, a system of equations is formed

$$\begin{aligned}
\mathbf{R}_{\bar{y}}(0) &= -\alpha_1 \mathbf{R}_{\bar{y}}^{T}(1) - \alpha_2 \mathbf{R}_{\bar{y}}^{T}(2) - \alpha_3 \mathbf{R}_{\bar{y}}^{T}(3) - \alpha_4 \mathbf{R}_{\bar{y}}^{T}(4) + \varsigma_0 \mathbf{R}_{\bar{y}\psi}^{T}(0) + \varsigma_1 \mathbf{R}_{\bar{y}\psi}^{T}(1) + \varsigma_2 \mathbf{R}_{\bar{y}\psi}^{T}(2) \\
\mathbf{R}_{\bar{y}}(1) &= -\alpha_1 \mathbf{R}_{\bar{y}}(0) - \alpha_2 \mathbf{R}_{\bar{y}}^{T}(1) - \alpha_3 \mathbf{R}_{\bar{y}}^{T}(2) - \alpha_4 \mathbf{R}_{\bar{y}}^{T}(3) + \varsigma_1 \mathbf{R}_{\bar{y}\psi}^{T}(0) + \varsigma_2 \mathbf{R}_{\bar{y}\psi}^{T}(1) \\
\mathbf{R}_{\bar{y}}(2) &= -\alpha_1 \mathbf{R}_{\bar{y}}(1) - \alpha_2 \mathbf{R}_{\bar{y}}(0) - \alpha_3 \mathbf{R}_{\bar{y}}^{T}(1) - \alpha_4 \mathbf{R}_{\bar{y}}^{T}(2) + \varsigma_2 \mathbf{R}_{\bar{y}\psi}^{T}(0) \\
\mathbf{R}_{\bar{y}}(3) &= -\alpha_1 \mathbf{R}_{\bar{y}}(2) - \alpha_2 \mathbf{R}_{\bar{y}}(1) - \alpha_3 \mathbf{R}_{\bar{y}}(0) - \alpha_4 \mathbf{R}_{\bar{y}}^{T}(1) \\
\mathbf{R}_{\bar{y}}(4) &= -\alpha_1 \mathbf{R}_{\bar{y}}(3) - \alpha_2 \mathbf{R}_{\bar{y}}(2) - \alpha_3 \mathbf{R}_{\bar{y}}(1) - \alpha_4 \mathbf{R}_{\bar{y}}(0)
\end{aligned} \tag{5-85}$$

where the property that $\mathbf{R}_x(n) = \mathbf{R}_x^T(-n)$ has been applied.

The autocorrelation functions of the output response $\bar{\mathbf{y}}$ for n=0,1,2,3 and 4 can then be obtained from

$$\begin{bmatrix} \tilde{\mathbf{R}}_{\bar{y}}(0) \\ \tilde{\mathbf{R}}_{\bar{y}}(1) \\ \tilde{\mathbf{R}}_{\bar{y}}(2) \\ \tilde{\mathbf{R}}_{\bar{y}}(3) \\ \tilde{\mathbf{R}}_{\bar{y}}(4) \end{bmatrix} = \begin{bmatrix} \overline{\mathbf{A}}_1 & \overline{\mathbf{A}}_2 \\ \overline{\mathbf{A}}_3 & \overline{\mathbf{A}}_4 \end{bmatrix}^{-1} \begin{bmatrix} \tilde{\mathbf{P}}_1 \\ \tilde{\mathbf{P}}_2 \\ \tilde{\mathbf{P}}_3 \\ \mathbf{0} \\ \mathbf{0} \end{bmatrix} \tag{5-86}$$

where

$$\overline{\mathbf{A}}_1 = \begin{bmatrix} 1 & 0 & 0 & 0 & \alpha_{11}^{(1)} & \alpha_{12}^{(1)} & 0 & 0 & \alpha_{11}^{(2)} & \alpha_{12}^{(2)} \\ 0 & 1 & 0 & 0 & 0 & 0 & \alpha_{11}^{(1)} & \alpha_{12}^{(1)} & 0 & 0 \\ 0 & 0 & 1 & 0 & \alpha_{21}^{(1)} & \alpha_{22}^{(1)} & 0 & 0 & \alpha_{21}^{(2)} & \alpha_{22}^{(2)} \\ 0 & 0 & 0 & 1 & 0 & 0 & \alpha_{21}^{(1)} & \alpha_{22}^{(1)} & 0 & 0 \\ \alpha_{11}^{(1)} & 0 & \alpha_{12}^{(1)} & 0 & 1+\alpha_{11}^{(2)} & \alpha_{12}^{(2)} & 0 & 0 & \alpha_{11}^{(3)} & \alpha_{12}^{(3)} \\ 0 & \alpha_{11}^{(1)} & 0 & \alpha_{12}^{(1)} & 0 & 1 & \alpha_{11}^{(2)} & \alpha_{12}^{(2)} & 0 & 0 \\ \alpha_{21}^{(1)} & 0 & \alpha_{22}^{(1)} & 0 & \alpha_{21}^{(2)} & \alpha_{22}^{(2)} & 1 & 0 & \alpha_{21}^{(3)} & \alpha_{22}^{(3)} \\ 0 & \alpha_{21}^{(1)} & 0 & \alpha_{22}^{(1)} & 0 & 0 & \alpha_{21}^{(2)} & 1+\alpha_{22}^{(2)} & 0 & 0 \\ \alpha_{11}^{(2)} & 0 & \alpha_{12}^{(2)} & 0 & \alpha_{11}^{(1)}+\alpha_{11}^{(3)} & \alpha_{12}^{(3)} & \alpha_{12}^{(1)} & 0 & 1+\alpha_{11}^{(4)} & \alpha_{12}^{(4)} \\ 0 & \alpha_{11}^{(2)} & 0 & \alpha_{12}^{(2)} & 0 & \alpha_{11}^{(1)} & \alpha_{11}^{(3)} & \alpha_{12}^{(3)}+\alpha_{12}^{(1)} & 0 & 1 \end{bmatrix}$$

(5-87)

$$\overline{\mathbf{A}}_2 = \begin{bmatrix} 0 & 0 & \alpha_{11}^{(3)} & \alpha_{12}^{(3)} & 0 & 0 & \alpha_{11}^{(4)} & \alpha_{12}^{(4)} & 0 & 0 \\ \alpha_{11}^{(2)} & \alpha_{12}^{(2)} & 0 & 0 & \alpha_{11}^{(3)} & \alpha_{12}^{(3)} & 0 & 0 & \alpha_{11}^{(4)} & \alpha_{12}^{(4)} \\ 0 & 0 & \alpha_{21}^{(3)} & \alpha_{22}^{(3)} & 0 & 0 & \alpha_{21}^{(4)} & \alpha_{22}^{(4)} & 0 & 0 \\ \alpha_{21}^{(2)} & \alpha_{22}^{(2)} & 0 & 0 & \alpha_{21}^{(3)} & \alpha_{22}^{(3)} & 0 & 0 & \alpha_{21}^{(4)} & \alpha_{22}^{(4)} \\ 0 & 0 & \alpha_{11}^{(4)} & \alpha_{12}^{(4)} & 0 & 0 & 0 & 0 & 0 & 0 \\ \alpha_{11}^{(3)} & \alpha_{12}^{(3)} & 0 & 0 & \alpha_{11}^{(4)} & \alpha_{12}^{(4)} & 0 & 0 & 0 & 0 \\ 0 & 0 & \alpha_{21}^{(4)} & \alpha_{22}^{(4)} & 0 & 0 & 0 & 0 & 0 & 0 \\ \alpha_{21}^{(3)} & \alpha_{22}^{(3)} & 0 & 0 & \alpha_{21}^{(4)} & \alpha_{22}^{(4)} & 0 & 0 & 0 & 0 \\ 0 & 0 & 0 & 0 & 0 & 0 & 0 & 0 & 0 & 0 \\ \alpha_{11}^{(4)} & \alpha_{12}^{(4)} & 0 & 0 & 0 & 0 & 0 & 0 & 0 & 0 \end{bmatrix}$$

(5-88)

$$\overline{\mathbf{A}}_3 = \begin{bmatrix}
\alpha_{21}^{(2)} & 0 & \alpha_{22}^{(2)} & 0 & \alpha_{21}^{(1)}+\alpha_{21}^{(3)} & \alpha_{22}^{(3)} & \alpha_{22}^{(1)} & 0 & \alpha_{21}^{(4)} & \alpha_{22}^{(4)} \\
0 & \alpha_{21}^{(2)} & 0 & \alpha_{22}^{(2)} & 0 & \alpha_{21}^{(1)} & \alpha_{21}^{(3)} & \alpha_{22}^{(1)}+\alpha_{22}^{(3)} & 0 & 0 \\
\alpha_{11}^{(3)} & 0 & \alpha_{12}^{(3)} & 0 & \alpha_{11}^{(2)}+\alpha_{11}^{(4)} & \alpha_{12}^{(4)} & \alpha_{12}^{(2)} & 0 & \alpha_{11}^{(1)} & 0 \\
0 & \alpha_{11}^{(3)} & 0 & \alpha_{12}^{(3)} & 0 & \alpha_{11}^{(2)} & \alpha_{11}^{(4)} & \alpha_{12}^{(2)}+\alpha_{12}^{(4)} & 0 & \alpha_{11}^{1} \\
\alpha_{21}^{(3)} & 0 & \alpha_{22}^{(3)} & 0 & \alpha_{21}^{(2)}+\alpha_{21}^{(4)} & \alpha_{22}^{(4)} & \alpha_{22}^{(2)} & 0 & \alpha_{21}^{(1)} & 0 \\
0 & \alpha_{21}^{(3)} & 0 & \alpha_{22}^{(3)} & 0 & \alpha_{21}^{(2)} & \alpha_{21}^{(4)} & \alpha_{22}^{(2)}+\alpha_{22}^{(4)} & 0 & \alpha_{21}^{(1)} \\
\alpha_{11}^{(4)} & 0 & \alpha_{12}^{(4)} & 0 & \alpha_{11}^{(3)} & 0 & \alpha_{12}^{(3)} & 0 & \alpha_{11}^{(2)} & 0 \\
0 & \alpha_{11}^{(4)} & 0 & \alpha_{12}^{(4)} & 0 & \alpha_{11}^{(3)} & 0 & \alpha_{12}^{(3)} & 0 & \alpha_{11}^{(2)} \\
\alpha_{21}^{(4)} & 0 & \alpha_{22}^{(4)} & 0 & \alpha_{21}^{(3)} & 0 & \alpha_{22}^{(3)} & 0 & \alpha_{21}^{(2)} & 0 \\
0 & \alpha_{21}^{(4)} & 0 & \alpha_{22}^{(4)} & 0 & \alpha_{21}^{(3)} & 0 & \alpha_{22}^{(3)} & 0 & \alpha_{21}^{(2)}
\end{bmatrix} \tag{5-89}$$

$$\overline{\mathbf{A}}_4 = \begin{bmatrix}
1 & 0 & 0 & 0 & 0 & 0 & 0 & 0 & 0 & 0 \\
\alpha_{21}^{(4)} & 1+\alpha_{22}^{(4)} & 0 & 0 & 0 & 0 & 0 & 0 & 0 & 0 \\
\alpha_{12}^{(1)} & 0 & 1 & 0 & 0 & 0 & 0 & 0 & 0 & 0 \\
0 & \alpha_{12}^{(1)} & 0 & 1 & 0 & 0 & 0 & 0 & 0 & 0 \\
\alpha_{22}^{(1)} & 0 & 0 & 0 & 1 & 0 & 0 & 0 & 0 & 0 \\
0 & \alpha_{22}^{(1)} & 0 & 0 & 0 & 1 & 0 & 0 & 0 & 0 \\
\alpha_{12}^{(2)} & 0 & \alpha_{11}^{(1)} & 0 & \alpha_{12}^{(1)} & 0 & 1 & 0 & 0 & 0 \\
0 & \alpha_{12}^{(2)} & 0 & \alpha_{11}^{(1)} & 0 & \alpha_{12}^{(1)} & 0 & 1 & 0 & 0 \\
\alpha_{22}^{(2)} & 0 & \alpha_{21}^{(1)} & 0 & \alpha_{22}^{(1)} & 0 & 0 & 0 & 1 & 0 \\
0 & \alpha_{22}^{(2)} & 0 & \alpha_{21}^{(1)} & 0 & \alpha_{22}^{(1)} & 0 & 0 & 0 & 1
\end{bmatrix} \tag{5-90}$$

and the vectors

$$\widetilde{\mathbf{R}}_{\bar{\mathbf{y}}}(i) = \left[R_{\bar{y}_1\bar{y}_1}(i) \quad R_{\bar{y}_1\bar{y}_2}(i) \quad R_{\bar{y}_2\bar{y}_1}(i) \quad R_{\bar{y}_2\bar{y}_2}(i)\right]^{\mathrm{T}} \tag{5-91}$$

and the vectors

$$\tilde{\mathbf{P}}_1 = \begin{bmatrix} \varsigma_{11}^{(0)} R_{\bar{y}_1\psi_1}(0) + \varsigma_{12}^{(0)} R_{\bar{y}_1\psi_2}(0) + \varsigma_{13}^{(0)} R_{\bar{y}_1\psi_3}(0) + \varsigma_{14}^{(0)} R_{\bar{y}_1\psi_4}(0) \\ + \varsigma_{11}^{(1)} R_{\bar{y}_1\psi_1}(1) + \varsigma_{12}^{(1)} R_{\bar{y}_1\psi_2}(1) + \varsigma_{13}^{(1)} R_{\bar{y}_1\psi_3}(1) + \varsigma_{14}^{(1)} R_{\bar{y}_1\psi_4}(1) \\ + \varsigma_{11}^{(2)} R_{\bar{y}_1\psi_1}(2) + \varsigma_{12}^{(2)} R_{\bar{y}_1\psi_2}(2) + \varsigma_{13}^{(2)} R_{\bar{y}_1\psi_3}(2) + \varsigma_{14}^{(2)} R_{\bar{y}_1\psi_4}(2) \\ \hline \varsigma_{11}^{(0)} R_{\bar{y}_2\psi_1}(0) + \varsigma_{12}^{(0)} R_{\bar{y}_2\psi_2}(0) + \varsigma_{13}^{(0)} R_{\bar{y}_2\psi_3}(0) + \varsigma_{14}^{(0)} R_{\bar{y}_2\psi_4}(0) \\ + \varsigma_{11}^{(1)} R_{\bar{y}_2\psi_1}(1) + \varsigma_{12}^{(1)} R_{\bar{y}_2\psi_2}(1) + \varsigma_{13}^{(1)} R_{\bar{y}_2\psi_3}(1) + \varsigma_{14}^{(1)} R_{\bar{y}_2\psi_4}(1) \\ + \varsigma_{11}^{(2)} R_{\bar{y}_2\psi_1}(2) + \varsigma_{12}^{(2)} R_{\bar{y}_2\psi_2}(2) + \varsigma_{13}^{(2)} R_{\bar{y}_2\psi_3}(2) + \varsigma_{14}^{(2)} R_{\bar{y}_2\psi_4}(2) \\ \hline \varsigma_{21}^{(0)} R_{\bar{y}_1\psi_1}(0) + \varsigma_{22}^{(0)} R_{\bar{y}_1\psi_2}(0) + \varsigma_{23}^{(0)} R_{\bar{y}_1\psi_3}(0) + \varsigma_{24}^{(0)} R_{\bar{y}_1\psi_4}(0) \\ + \varsigma_{21}^{(1)} R_{\bar{y}_1\psi_1}(1) + \varsigma_{22}^{(1)} R_{\bar{y}_1\psi_2}(1) + \varsigma_{23}^{(1)} R_{\bar{y}_1\psi_3}(1) + \varsigma_{24}^{(1)} R_{\bar{y}_1\psi_4}(1) \\ + \varsigma_{21}^{(2)} R_{\bar{y}_1\psi_1}(2) + \varsigma_{22}^{(2)} R_{\bar{y}_1\psi_2}(2) + \varsigma_{23}^{(2)} R_{\bar{y}_1\psi_3}(2) + \varsigma_{24}^{(2)} R_{\bar{y}_1\psi_4}(2) \\ \hline \varsigma_{21}^{(0)} R_{\bar{y}_2\psi_1}(0) + \varsigma_{22}^{(0)} R_{\bar{y}_2\psi_2}(0) + \varsigma_{23}^{(0)} R_{\bar{y}_2\psi_3}(0) + \varsigma_{24}^{(0)} R_{\bar{y}_2\psi_4}(0) \\ + \varsigma_{21}^{(1)} R_{\bar{y}_2\psi_1}(1) + \varsigma_{22}^{(1)} R_{\bar{y}_2\psi_2}(1) + \varsigma_{23}^{(1)} R_{\bar{y}_2\psi_3}(1) + \varsigma_{24}^{(1)} R_{\bar{y}_2\psi_4}(1) \\ + \varsigma_{21}^{(2)} R_{\bar{y}_2\psi_1}(2) + \varsigma_{22}^{(2)} R_{\bar{y}_2\psi_2}(2) + \varsigma_{23}^{(2)} R_{\bar{y}_2\psi_3}(2) + \varsigma_{24}^{(2)} R_{\bar{y}_2\psi_4}(2) \end{bmatrix}$$

$$\tilde{\mathbf{P}}_2 = \begin{bmatrix} \varsigma_{11}^{(1)} R_{\bar{y}_1\psi_1}(0) + \varsigma_{12}^{(1)} R_{\bar{y}_1\psi_2}(0) + \varsigma_{13}^{(1)} R_{\bar{y}_1\psi_3}(0) + \varsigma_{14}^{(1)} R_{\bar{y}_1\psi_4}(0) \\ + \varsigma_{11}^{(2)} R_{\bar{y}_1\psi_1}(1) + \varsigma_{12}^{(2)} R_{\bar{y}_1\psi_2}(1) + \varsigma_{13}^{(2)} R_{\bar{y}_1\psi_3}(1) + \varsigma_{14}^{(2)} R_{\bar{y}_1\psi_4}(1) \\ \hline \varsigma_{11}^{(1)} R_{\bar{y}_2\psi_1}(0) + \varsigma_{12}^{(1)} R_{\bar{y}_2\psi_2}(0) + \varsigma_{13}^{(1)} R_{\bar{y}_2\psi_3}(0) + \varsigma_{14}^{(1)} R_{\bar{y}_2\psi_4}(0) \\ + \varsigma_{11}^{(2)} R_{\bar{y}_2\psi_1}(1) + \varsigma_{12}^{(2)} R_{\bar{y}_2\psi_2}(1) + \varsigma_{13}^{(2)} R_{\bar{y}_2\psi_3}(1) + \varsigma_{14}^{(2)} R_{\bar{y}_2\psi_4}(1) \\ \hline \varsigma_{21}^{(1)} R_{\bar{y}_1\psi_1}(0) + \varsigma_{22}^{(1)} R_{\bar{y}_1\psi_2}(0) + \varsigma_{23}^{(1)} R_{\bar{y}_1\psi_3}(0) + \varsigma_{24}^{(1)} R_{\bar{y}_1\psi_4}(0) \\ + \varsigma_{21}^{(2)} R_{\bar{y}_1\psi_1}(1) + \varsigma_{22}^{(2)} R_{\bar{y}_1\psi_2}(1) + \varsigma_{23}^{(2)} R_{\bar{y}_1\psi_3}(1) + \varsigma_{24}^{(2)} R_{\bar{y}_1\psi_4}(1) \\ \hline \varsigma_{21}^{(1)} R_{\bar{y}_2\psi_1}(0) + \varsigma_{22}^{(1)} R_{\bar{y}_2\psi_2}(0) + \varsigma_{23}^{(1)} R_{\bar{y}_2\psi_3}(0) + \varsigma_{24}^{(1)} R_{\bar{y}_2\psi_4}(0) \\ + \varsigma_{21}^{(2)} R_{\bar{y}_2\psi_1}(1) + \varsigma_{22}^{(2)} R_{\bar{y}_2\psi_2}(1) + \varsigma_{23}^{(2)} R_{\bar{y}_2\psi_3}(1) + \varsigma_{24}^{(2)} R_{\bar{y}_2\psi_4}(1) \end{bmatrix} \tag{5-92}$$

$$\tilde{\mathbf{P}}_2 = \begin{bmatrix} \varsigma_{11}^{(2)} R_{\bar{y}_1\psi_1}(0) + \varsigma_{12}^{(2)} R_{\bar{y}_1\psi_2}(0) + \varsigma_{13}^{(2)} R_{\bar{y}_1\psi_3}(0) + \varsigma_{14}^{(2)} R_{\bar{y}_1\psi_4}(0) \\ \hline \varsigma_{11}^{(2)} R_{\bar{y}_2\psi_1}(0) + \varsigma_{12}^{(2)} R_{\bar{y}_2\psi_2}(0) + \varsigma_{13}^{(2)} R_{\bar{y}_2\psi_3}(0) + \varsigma_{14}^{(2)} R_{\bar{y}_2\psi_4}(0) \\ \hline \varsigma_{21}^{(2)} R_{\bar{y}_1\psi_1}(0) + \varsigma_{22}^{(2)} R_{\bar{y}_1\psi_2}(0) + \varsigma_{23}^{(2)} R_{\bar{y}_1\psi_3}(0) + \varsigma_{24}^{(2)} R_{\bar{y}_1\psi_4}(0) \\ \hline \varsigma_{21}^{(2)} R_{\bar{y}_2\psi_1}(0) + \varsigma_{22}^{(2)} R_{\bar{y}_2\psi_2}(0) + \varsigma_{23}^{(2)} R_{\bar{y}_2\psi_3}(0) + \varsigma_{24}^{(2)} R_{\bar{y}_2\psi_4}(0) \end{bmatrix}$$

Knowing $\mathbf{R}_{\bar{y}}(0)$, $\mathbf{R}_{\bar{y}}(1)$, $\mathbf{R}_{\bar{y}}(2)$, $\mathbf{R}_{\bar{y}}(3)$ and $\mathbf{R}_{\bar{y}}(4)$, then

$$\mathbf{R}_{\bar{y}}(n) = -\boldsymbol{\alpha}_1\mathbf{R}_{\bar{y}}(n-1) - \boldsymbol{\alpha}_2\mathbf{R}_{\bar{y}}(n-2) - \boldsymbol{\alpha}_3\mathbf{R}_{\bar{y}}(n-3) - \boldsymbol{\alpha}_4\mathbf{R}_{\bar{y}}(n-4),\ n > 4 \qquad (5\text{-}93)$$

5.2.4.3 Evaluation of the Cross Correlation between the Prediction Error and the Measured Response

The cross correlation between the prediction error and the output response can be also evaluated in a similar procedure. Postmultiplying both sides of Eq. (5-42) by $\bar{\mathbf{y}}^{\mathrm{T}}(k-n)$ gives

$$\boldsymbol{\varepsilon}(k)\bar{\mathbf{y}}^{\mathrm{T}}(k-n) = \bar{\mathbf{y}}(k)\bar{\mathbf{y}}^{\mathrm{T}}(k-n) - \hat{\mathbf{y}}(k \mid k-1)\bar{\mathbf{y}}^{\mathrm{T}}(k-n) \qquad (5\text{-}94)$$

Taking the expectation of both sides of Eq. (5-94) and assuming stationary behavior gives

$$\mathbf{R}_{\varepsilon\bar{y}}(n) = \mathbf{R}_{\bar{y}}(n) - E[\hat{\mathbf{y}}(k \mid k-1)\bar{\mathbf{y}}^{\mathrm{T}}(k-n)] \qquad (5\text{-}95)$$

Expanding the predicted response $\hat{\mathbf{y}}(k \mid k-1)$ using Eq. (5-45) gives

$$\begin{aligned}\mathbf{R}_{\varepsilon\bar{y}}(n) = {} & \mathbf{R}_{\bar{y}}(n) + \boldsymbol{\alpha}_1\mathbf{R}_{\bar{y}}(n-1) + \boldsymbol{\alpha}_2\mathbf{R}_{\bar{y}}(n-2) + \boldsymbol{\alpha}_3\mathbf{R}_{\bar{y}}(n-3) + \boldsymbol{\alpha}_4\mathbf{R}_{\bar{y}}(n-4) \\ & - \mathbf{C}_2\mathbf{C}_1^{-1}\mathbf{R}_{\varepsilon\bar{y}}(n-1)\end{aligned} \qquad (5\text{-}96)$$

where $\mathbf{C}_1$ and $\mathbf{C}_2$ are coefficient matrices of the disturbance $\mathbf{e}$ in the finite linear difference equation of the ARMAX model. Note that using Eq. (5-45) implicitly assumes $\mathbf{h}(0)=\mathbf{C}_0=\mathbf{0}$ (*i.e.*, the ambient ground excitation case).

The equation for $\mathbf{R}_{\varepsilon\bar{y}}(n)$ can be written as

$$\mathbf{R}_{\varepsilon\bar{y}}(n) = \overline{\overline{\mathbf{R}}}_{\bar{y}}(n) + \Omega\mathbf{R}_{\varepsilon\bar{y}}(n-1) \tag{5-97}$$

where

$$\overline{\overline{\mathbf{R}}}_{\bar{y}}(n) = \mathbf{R}_{\bar{y}}(n) + \alpha_1\mathbf{R}_{\bar{y}}(n-1) + \alpha_2\mathbf{R}_{\bar{y}}(n-2) + \alpha_3\mathbf{R}_{\bar{y}}(n-3) + \alpha_4\mathbf{R}_{\bar{y}}(n-4) \tag{5-98}$$

and

$$\Omega = -\mathbf{C}_2\mathbf{C}_1^{-1} \tag{5-99}$$

Based on Eqs. (5-97) to (5-99) and by expanding the $\mathbf{R}_{\varepsilon\bar{y}}(n)$ for $n = 1,2,\ldots$

$$\begin{aligned}
\mathbf{R}_{\varepsilon\bar{y}}(1) &= \overline{\overline{\mathbf{R}}}_{\bar{y}}(1) + \Omega\mathbf{R}_{\varepsilon\bar{y}}(0) \\
\mathbf{R}_{\varepsilon\bar{y}}(2) &= \overline{\overline{\mathbf{R}}}_{\bar{y}}(2) + \Omega[\overline{\overline{\mathbf{R}}}_{\bar{y}}(1) + \Omega\mathbf{R}_{\varepsilon\bar{y}}(0))] \\
&\vdots \\
\mathbf{R}_{\varepsilon\bar{y}}(n) &= \overline{\overline{\mathbf{R}}}_{\bar{y}}(n) + \Omega^n\overline{\mathbf{R}}_{\varepsilon\bar{y}}(0) + \sum_{k=0}^{n-1}\Omega^k\overline{\overline{\mathbf{R}}}_{\bar{y}}(n-k)
\end{aligned} \tag{5-100}$$

But, for n sufficiently large, then the following applies

$$\lim_{n\to-\infty}\overline{\overline{\mathbf{R}}}_{\bar{y}}(n) = \mathbf{0} \quad \text{and} \quad \lim_{n\to-\infty}\mathbf{R}_{\varepsilon\bar{y}}(n) = \mathbf{0} \tag{5-101}$$

Accordingly, an expression of $\mathbf{R}_{\varepsilon\bar{y}}(0)$ is

$$\mathbf{R}_{\varepsilon\bar{y}}(0) = \lim_{n\to\infty}\left[\Omega^n\overline{\mathbf{R}}_{\varepsilon\bar{y}}(-n) + \sum_{k=0}^{n}\Omega^k\overline{\overline{\mathbf{R}}}_{\bar{y}}(-k)\right] = \sum_{k=0}^{\infty}\Omega^k\overline{\mathbf{R}}_{\bar{y}}(-k) \tag{5-102}$$

Given $\mathbf{R}_{\varepsilon\bar{y}}(0)$, $\mathbf{R}_{\varepsilon\bar{y}}(n)$, n>0, can be obtained from Eq. (5-100).

It should be noted that, for a scalar system, solving the linear equations for $R_{\varepsilon\bar{y}}(0)$ and $R_{\varepsilon\bar{y}}(1)$

$$\begin{bmatrix} R_{\varepsilon\bar{y}}(0) \\ R_{\varepsilon\bar{y}}(1) \end{bmatrix} = \begin{bmatrix} \mathbf{I} & \mathbf{C}_2\mathbf{C}_1^{-1} \\ \mathbf{C}_2\mathbf{C}_1^{-1} & \mathbf{I} \end{bmatrix}^{-1} \begin{bmatrix} R_{\bar{y}}(0) + \alpha_1 R_{\bar{y}}(1) + \alpha_2 R_{\bar{y}}(2) + \alpha_3 R_{\bar{y}}(3) + \alpha_4 R_{\bar{y}}(4) \\ R_{\bar{y}}(1) + \alpha_1 R_{\bar{y}}(0) + \alpha_2 R_{\bar{y}}(1) + \alpha_3 R_{\bar{y}}(2) + \alpha_4 R_{\bar{y}}(3) \end{bmatrix} \tag{5-103}$$

5.2.4.4 Evaluation of the Autocorrelation of the Prediction Error

Postmultiplying each side of Eq. (5-42) by $\boldsymbol{\varepsilon}^{\mathrm{T}}(k-n)$ yields

$$\boldsymbol{\varepsilon}(k)\boldsymbol{\varepsilon}^{\mathrm{T}}(k-n) = \bar{\mathbf{y}}(k)\boldsymbol{\varepsilon}^{\mathrm{T}}(k-n) - \hat{\mathbf{y}}(k|k-1)\boldsymbol{\varepsilon}^{\mathrm{T}}(k-n) \tag{5-104}$$

Taking the expectation of both sides and expanding the predicted response $\hat{\mathbf{y}}(k \mid k-1)$ using Eq. (5-45) gives

$$\begin{aligned} \mathbf{R}_{\varepsilon}(n) = {} & \mathbf{R}_{\bar{y}\varepsilon}(n) + \boldsymbol{\alpha}_1\mathbf{R}_{\bar{y}\varepsilon}(n-1) + \boldsymbol{\alpha}_2\mathbf{R}_{\bar{y}\varepsilon}(n-2) + \boldsymbol{\alpha}_3\mathbf{R}_{\bar{y}\varepsilon}(n-3) + \boldsymbol{\alpha}_4\mathbf{R}_{\bar{y}\varepsilon}(n-4) \\ & - \mathbf{C}_2\mathbf{C}_1^{-1}\mathbf{R}_{\varepsilon}(n-1) \end{aligned} \tag{5-105}$$

A procedure similar to the evaluation of $\mathbf{R}_{\varepsilon\bar{y}}(n)$ in Eqs. (5-97) to (5-102) can be applied to evaluate $\mathbf{R}_{\varepsilon}(0)$, from which the series $\mathbf{R}_{\varepsilon}(n)$, n>0, can be obtained.

Similarly, for a scalar system, a system of equations can be obtained from for n=0 and n=1 to solve for $R_{\varepsilon}(0)$ and $R_{\varepsilon}(1)$

$$\begin{bmatrix} R_{\varepsilon}(0) \\ R_{\varepsilon}(1) \end{bmatrix} = \begin{bmatrix} \mathbf{I} & \mathbf{C}_2\mathbf{C}_1^{-1} \\ \mathbf{C}_2\mathbf{C}_1^{-1} & \mathbf{I} \end{bmatrix}^{-1} \begin{bmatrix} R_{\bar{y}\varepsilon}(0) + \alpha_1 R_{\bar{y}\varepsilon}(1) + \alpha_2 R_{\bar{y}\varepsilon}(2) + \alpha_3 R_{\bar{y}\varepsilon}(3) + \alpha_4 R_{\bar{y}\varepsilon}(4) \\ R_{\bar{y}\varepsilon}(1) + \alpha_1 R_{\bar{y}\varepsilon}(0) + \alpha_2 R_{\bar{y}\varepsilon}(1) + \alpha_3 R_{\bar{y}\varepsilon}(2) + \alpha_4 R_{\bar{y}\varepsilon}(3) \end{bmatrix} \tag{5-106}$$

5.2.4.5 Evaluation of the Autocorrelation of the Control Force

Herein, the control force is assumed to be a function of the control gain and measured responses. The autocorrelation of the control force for the 2DOF bridge problem (p=2), can be formed by multiplying Eq. (5-57) by its transpose at time (k–n) and taking the expectation such that

$$E[\mathbf{u}(k)\mathbf{u}^{\mathrm{T}}(k-n)] = \widetilde{\mathbf{K}}_1 E[\mathbf{y}(k-1)\mathbf{y}^{\mathrm{T}}(k-n-1)]\widetilde{\mathbf{K}}_1^{\mathrm{T}} + \widetilde{\mathbf{K}}_2 E[\mathbf{y}(k-2)\mathbf{y}^{\mathrm{T}}(k-n-2)]\widetilde{\mathbf{K}}_2^{\mathrm{T}} + \widetilde{\mathbf{K}}_1 E[\mathbf{y}(k-1)\mathbf{y}^{\mathrm{T}}(k-n-2)]\widetilde{\mathbf{K}}_2^{\mathrm{T}} + \widetilde{\mathbf{K}}_2 E[\mathbf{y}(k-2)\mathbf{y}^{\mathrm{T}}(k-n-1)]\widetilde{\mathbf{K}}_1^{\mathrm{T}} \tag{5-107}$$

which, by further simplification, yields the general equation of the autocorrelation of the input control force for a 2DOF system.

$$\mathbf{R}_u(n) = \widetilde{\mathbf{K}}_1 \mathbf{R}_{\bar{\mathbf{y}}}(n)\widetilde{\mathbf{K}}_1^{\mathrm{T}} + \widetilde{\mathbf{K}}_2 \mathbf{R}_{\bar{\mathbf{y}}}(n)\widetilde{\mathbf{K}}_2^{\mathrm{T}} + \widetilde{\mathbf{K}}_1 \mathbf{R}_{\bar{\mathbf{y}}}(n+1)\widetilde{\mathbf{K}}_2^{\mathrm{T}} + \widetilde{\mathbf{K}}_2 \mathbf{R}_{\bar{\mathbf{y}}}(n-1)\widetilde{\mathbf{K}}_1^{\mathrm{T}} \tag{5-108}$$

A similar derivation can be found for more complex systems with p>2.

5.2.4.6 Evaluation of the Cross Correlation between the Control Force and the Measured Response

Postmultiplying both sides of Eq. (5-57) with p=2 by $\bar{\mathbf{y}}^{\mathrm{T}}(k-n)$ and taking expectation gives

$$E[\mathbf{u}(k)\bar{\mathbf{y}}^{\mathrm{T}}(k-n)] = -\widetilde{\mathbf{K}}_1 E[\bar{\mathbf{y}}(k-1)\bar{\mathbf{y}}^{\mathrm{T}}(k-n)] - \widetilde{\mathbf{K}}_2 E[\bar{\mathbf{y}}(k-2)\bar{\mathbf{y}}^{\mathrm{T}}(k-n)] \tag{5-109}$$

which, by further simplification, yields the general equation of the autocorrelation of the input control force for the 2DOF system

$$\mathbf{R}_{u\bar{y}}(n) = -\widetilde{\mathbf{K}}_1 \mathbf{R}_{\bar{y}}(n-1) - \widetilde{\mathbf{K}}_2 \mathbf{R}_{\bar{y}}(n-2) \tag{5-110}$$

5.2.4.7 Evaluation of the Cross Correlation between the Control Force and the Prediction Error

In a similar way, by postmultiplying the control force equation for the 2DOF model by $\boldsymbol{\varepsilon}^{\mathrm{T}}(k-n)$ and taking expectation, a general form for the cross correlation between the control force and the prediction error is obtained as

$$\mathbf{R}_{u\varepsilon}(n) = -\widetilde{\mathbf{K}}_1 \mathbf{R}_{\bar{y}\varepsilon}(n-1) - \widetilde{\mathbf{K}}_2 \mathbf{R}_{\bar{y}\varepsilon}(n-2) \tag{5-111}$$

5.3 Illustrative Example: 2DOF Bridge Model

The test bed for the control approach introduced here is the 2DOF bridge model, introduced in Chapter 3 in Section 3.4.2. The stiffnesses and the damping coefficients of the 2DOF bridge model are given in Section 3.5.2. The structure is assumed subjected to ambient ground excitation at the base and to ambient traffic loading at the deck level. The system is assumed linear and time-invariant since the magnitude of the excitations is small enough that the structure is expected to behave in a linear manner. Two outputs, $y_1(k)$ and $y_2(k)$, the absolute accelerations of the pier and the deck, respectively, are to be measured.

A control force, $u(k)$, given by the control gains and previous observations as described in Eq. (5-6) is exerted in the bearing level between the pier and the deck. The control force, in this case, is expressed by the following equation

$$u(k) = -\tilde{\mathbf{K}}_1 \mathbf{y}(k-1) - \tilde{\mathbf{K}}_2 \mathbf{y}(k-2) \tag{5-112}$$

where the control gains, $\tilde{\mathbf{K}}_1$ and $\tilde{\mathbf{K}}_2$, are two row vectors of dimension 1×2 such that

$$\tilde{\mathbf{K}}_1 = [\tilde{k}_1^{(1)} \quad \tilde{k}_2^{(1)}] \quad \text{and} \quad \tilde{\mathbf{K}}_2 = [\tilde{k}_1^{(2)} \quad \tilde{k}_2^{(2)}] \tag{5-113}$$

and the output response observation vectors $\mathbf{y}(k-1)$ and $\mathbf{y}(k-2)$ are column vectors of dimension 2×1 such that

$$\mathbf{y}(k-1) = \begin{bmatrix} y_1(k-1) \\ y_2(k-1) \end{bmatrix} \quad \text{and} \quad \mathbf{y}(k-2) = \begin{bmatrix} y_1(k-2) \\ y_2(k-2) \end{bmatrix} \tag{5-114}$$

As explained earlier in this chapter, an ARMAX model is chosen to represent the system. The exact ARMAX model coefficients can be obtained from the exact physical properties (masses, stiffnesses and damping coefficients) of the structure model; this procedure is thoroughly explained in Appendix C. The finite linear difference equation of the 2DOF bridge model takes the following form for the ARMAX model

$$\begin{aligned} \bar{\mathbf{y}}(k) = &-\mathbf{A}_1 \bar{\mathbf{y}}(k-1) - \mathbf{A}_2 \bar{\mathbf{y}}(k-2) + \mathbf{B}_1 u(k-1) + \mathbf{B}_2 u(k-2)) + [\mathbf{C}_0 \quad \mathbf{I}][\mathbf{e}^{\mathrm{T}}(k) \quad \mathbf{v}^{\mathrm{T}}(k)]^{\mathrm{T}} \\ &+ [\mathbf{C}_1 \quad \mathbf{A}_1][\mathbf{e}^{\mathrm{T}}(k-1) \quad \mathbf{v}^{\mathrm{T}}(k-1)]^{\mathrm{T}} + [\mathbf{C}_2 \quad \mathbf{A}_2][\mathbf{e}^{\mathrm{T}}(k-2) \quad \mathbf{v}^{\mathrm{T}}(k-2)]^{\mathrm{T}} \end{aligned} \tag{5-115}$$

where the coefficient matrices are

$$\mathbf{A}_1=\begin{bmatrix} a_{11}^{(1)} & a_{12}^{(1)} \\ a_{21}^{(1)} & a_{22}^{(1)} \end{bmatrix},\ \mathbf{A}_2=\begin{bmatrix} a_{11}^{(2)} & a_{12}^{(2)} \\ a_{21}^{(2)} & a_{22}^{(2)} \end{bmatrix},\ \mathbf{B}_1=\begin{bmatrix} b_{11}^{(1)} \\ b_{12}^{(1)} \end{bmatrix},\ \mathbf{B}_2=\begin{bmatrix} b_{11}^{(2)} \\ b_{12}^{(2)} \end{bmatrix},$$

$$\mathbf{C}_0=\begin{bmatrix} c_{11}^{(0)} & c_{12}^{(0)} \\ c_{21}^{(0)} & c_{22}^{(0)} \end{bmatrix},\ \mathbf{C}_1=\begin{bmatrix} c_{11}^{(1)} & c_{12}^{(1)} \\ c_{21}^{(1)} & c_{22}^{(1)} \end{bmatrix},\ \mathbf{C}_2=\begin{bmatrix} c_{11}^{(2)} & c_{12}^{(2)} \\ c_{21}^{(2)} & c_{22}^{(2)} \end{bmatrix} \tag{5-116}$$

Thus, by using Eq. (5-112) in Eq. (5-115), a stochastic ARMA model is obtained as

$$\begin{aligned}\overline{\mathbf{y}}(k) &= -(\mathbf{A}_1)\overline{\mathbf{y}}(k-1)-(\mathbf{A}_2+\mathbf{B}_1\widetilde{\mathbf{K}}_1)\overline{\mathbf{y}}(k-2)-(\mathbf{B}_1\widetilde{\mathbf{K}}_2+\mathbf{B}_2\widetilde{\mathbf{K}}_1)\overline{\mathbf{y}}(k-3)\\ &\quad -(\mathbf{B}_2\widetilde{\mathbf{K}}_2)\overline{\mathbf{y}}(k-4)+\begin{bmatrix}\mathbf{C}_0 & \mathbf{I}\end{bmatrix}\begin{bmatrix}\mathbf{e}^{\mathrm{T}}(k) & \mathbf{v}^{\mathrm{T}}(k)\end{bmatrix}^{\mathrm{T}}+\begin{bmatrix}\mathbf{C}_1 & \mathbf{A}_1\end{bmatrix}\begin{bmatrix}\mathbf{e}^{\mathrm{T}}(k-1) & \mathbf{v}^{\mathrm{T}}(k-1)\end{bmatrix}^{\mathrm{T}}\\ &\quad +\begin{bmatrix}\mathbf{C}_2 & \mathbf{A}_2\end{bmatrix}\begin{bmatrix}\mathbf{e}^{\mathrm{T}}(k-2) & \mathbf{v}^{\mathrm{T}}(k-2)\end{bmatrix}^{\mathrm{T}}\end{aligned} \tag{5-117}$$

The ground and traffic ambient excitations, to which the system is subjected, are assumed to be Gaussian pulse processes such that $\mathrm{E}[\mathbf{e}(l)\mathbf{e}^{\mathrm{T}}(m)]=\mathbf{Q}\delta_{lm}$, where $\mathbf{e}(k)=[e_{\mathrm{gr}}(k) \quad e_{\mathrm{tr}}(k)]^{\mathrm{T}}$ and $\mathbf{Q}$ is the diagonal covariance matrix of the disturbance vector. $e_{\mathrm{gr}}(k)$ is the disturbance due to the ground ambient excitation, and $e_{\mathrm{tr}}(k)$ stands for the disturbance in the stochastic model due to ambient traffic excitation at the deck level. In the numerical example, the RMS (Root Mean Square) of both the ground and traffic ambient excitations is suggested to be 0.02 m/s^2. Also, the sensor noise, $\mathbf{v}(k)$, is added to the exact structural response (absolute accelerations observations in both the pier and the deck), with suggested RMS of 10^{-6} m/s^2 such that $E[\mathbf{v}(l)\mathbf{v}^{\mathrm{T}}(m)]=\mathbf{\Gamma}\delta_{lm}$ where $\mathbf{v}(k)=[v_1(k) \quad v_2(k)]^{\mathrm{T}}$ and $\mathbf{\Gamma}$ is the diagonal

covariance matrix ($\mathbf{I}(10^{-6}\text{m/s}^2)^2$ in this example). With these disturbance and noise RMS values, the resulting RMS of the prediction error, $\varepsilon(k)$, should be two orders of magnitude less than that of the absolute accelerations of the pier and deck of the structure.

To maintain a vector form for the unknown system parameters $\boldsymbol{\theta}$, it is expressed as

$$\boldsymbol{\theta}=[a_{11}^{(1)}\ a_{12}^{(1)}\ a_{21}^{(1)}\ a_{22}^{(1)}\ a_{11}^{(2)}\ a_{12}^{(2)}\ a_{21}^{(2)}\ a_{22}^{(2)}\ b_{11}^{(1)}\ b_{21}^{(1)}\ b_{11}^{(2)}\ b_{21}^{(2)}\ \bar{c}_{11}^{(1)}\ \bar{c}_{12}^{(1)}\ \bar{c}_{21}^{(1)}\ \bar{c}_{22}^{(1)}]^{\mathrm{T}} \quad (5\text{-}118)$$

where

$$\overline{\mathbf{C}}_1=\mathbf{C}_2\mathbf{C}_1^{-1}=\begin{bmatrix}\bar{c}_{11}^{(1)} & \bar{c}_{12}^{(1)}\\ \bar{c}_{21}^{(1)} & \bar{c}_{22}^{(1)}\end{bmatrix} \quad (5\text{-}119)$$

It is assumed that the coefficient matrix $\mathbf{C}_0$ is a zero matrix. Also, the coefficient matrix $\mathbf{C}_1$ is assumed known *a priori*; justification for this assumption is discussed in Appendix C. However, knowing $\mathbf{C}_1$ *a priori* requires previous knowledge of the masses, m_1 and m_2, of the pier and the deck of the bridge model and requires the sampling time for the measured data to be small. The data sampling time is, thus, chosen to be 0.01 s.

The information matrix including older data, $\boldsymbol{\varphi}$, as per Eqs. (5-50) to (5-52) except $\boldsymbol{\varphi}_\varepsilon$ only goes back to time (k-n_c+1) instead of (k-n_c), is organized, for the bridge model example, to suit the form of the vector of unknown structural parameters $\boldsymbol{\theta}$. Thus, $\boldsymbol{\varphi}$ takes the form

$$\boldsymbol{\varphi} = \begin{bmatrix} -y_1(k-1) & -y_2(k-1) & 0 & 0 & -y_1(k-2) & -y_2(k-2) \\ 0 & 0 & -y_1(k-1) & -y_2(k-1) & 0 & 0 \end{bmatrix}$$

$$\begin{matrix} 0 & 0 & u(k-1) & 0 & u(k-2) & 0 \\ -y_1(k-2) & -y_2(k-2) & 0 & u(k-1) & 0 & u(k-2) \end{matrix}$$

$$\begin{bmatrix} \varepsilon_1(k-1) & \varepsilon_2(k-1) & 0 & 0 \\ 0 & 0 & \varepsilon_1(k-1) & \varepsilon_2(k-1) \end{bmatrix}^{\mathrm{T}} \tag{5-120}$$

such that

$$\hat{\mathbf{y}}(k \mid k-1) = \boldsymbol{\varphi}^{\mathrm{T}}(k)\boldsymbol{\theta} \tag{5-121}$$

5.3.1 Modified Cost Function and Minimization with Respect to the Control Gains

In order to obtain the control gains necessary to improve the estimation of the structural parameters, the cost function in Eq. (5-6) is minimized with respect to the control gains and a system of equations is obtained then solved for them. Generally, the cost function in Eq. (5-6) is designed to minimize the error between the estimated system parameters, $\hat{\boldsymbol{\theta}}$, and the actual system parameters, $\boldsymbol{\theta}$. However, as observed from Eq. (5-60), the evaluation of the estimated system parameters vector, at the end of control horizon $[k_0, k_f]$ is complicated by the fact that future unknown measurements exist in the equation. In addition, finding the inverse of the summation of the product of vectors $\boldsymbol{\varphi}(k)\boldsymbol{\varphi}^{\mathrm{T}}(k)$ over the duration of the control horizon is quite expensive and may be infeasible in terms of computer memory and processor time.

Accordingly, an alternative cost function is used that replaces the first term of the cost function in Eq. (5-6), the error in the parameter estimation, with its numerator. Thus, the modified cost function is expressed as

$$J(k_0) = E[\mathbf{V}^{\mathrm{T}}\boldsymbol{\Sigma}\mathbf{V}] + \frac{1}{2}\sum_{k=k_0}^{k_f} \mathrm{E}\left[\mathbf{u}^{\mathrm{T}}(k)\mathbf{R}\mathbf{u}(k)\right] \tag{5-122}$$

The information matrix, $\boldsymbol{\varphi}$, is evaluated using the autocorrelation and cross correlation functions as shown in Sections 5.2.4.1 to 5.2.4.7.

By differentiating the modified cost function with respect to the control gains ($k_1^{(1)}$, $k_2^{(1)}$, $k_1^{(2)}$ and $k_2^{(2)}$), a system of four nonlinear equations is obtained. Solving the resulting equations gives the control gains that minimize the cost function. The MATLAB® function `fsolve` is used to solve the nonlinear equations for the control gains. However, this may require obtaining the gradients and the Jacobians for the system of equations with respect to the control gains. Therefore, consider the vector

$$\mathbf{V} = \frac{1}{N-1}\sum_{k_0}^{k_f} \boldsymbol{\varphi}(k)\mathbf{y}(k) - \left[\frac{1}{N-1}\sum_{k_0}^{k_f} \boldsymbol{\varphi}(k)\boldsymbol{\varphi}^{\mathrm{T}}(k)\right]\boldsymbol{\theta} \tag{5-123}$$

Then, the gradient of the modified cost function for any scalar control gain $\tilde{k}$ is obtained from

$$\frac{\partial J(k_0)}{\partial \tilde{k}} = \left[\mathbf{V}^{\mathrm{T}}\boldsymbol{\Sigma}\frac{\partial \mathbf{V}}{\partial \tilde{k}}\right]^{\mathrm{T}} + \left[\left(\frac{\partial \mathbf{V}}{\partial \tilde{k}}\right)^{\mathrm{T}}\boldsymbol{\Sigma}\mathbf{V}\right] + \frac{1}{2}\mathbf{R}\frac{\partial R_u(0)}{\partial \tilde{k}} \tag{5-124}$$

which, by simplification, leads to

$$\frac{\partial J(k_0)}{\partial \tilde{k}} = 2\left[\left(\frac{\partial \mathbf{V}}{\partial \tilde{k}}\right)^{\mathrm{T}} \boldsymbol{\Sigma}\mathbf{V}\right] + \frac{1}{2}\mathbf{R}\frac{\partial R_u(0)}{\partial \tilde{k}} \tag{5-125}$$

Moreover, by considering the matrix $\mathbf{P}$ being defined as

$$\mathbf{P} = \frac{\partial \mathbf{V}}{\partial \tilde{k}} \tag{5-126}$$

the Jacobian of the resulting system of equations, considering any scalar control gain $\tilde{\tilde{k}}$, is

$$\frac{\partial^2 J(k_0)}{\partial \tilde{k}\partial \tilde{\tilde{k}}} = 2\left[\left[\mathbf{P}^{\mathrm{T}}\boldsymbol{\Sigma}\frac{\partial \mathbf{V}}{\partial \tilde{\tilde{k}}}\right]^{\mathrm{T}} + \left[\frac{\partial \mathbf{P}}{\partial \tilde{\tilde{k}}}\right]^{\mathrm{T}} \boldsymbol{\Sigma}\mathbf{V}\right] + \frac{1}{2}\mathbf{R}\frac{\partial^2 R_u(0)}{\partial \tilde{k}\partial \tilde{\tilde{k}}} \tag{5-127}$$

Finally, since both the gradients Eq. (5-125) and the Jacobian Eq. (5-127) include the unknown estimated parameters implicitly, then the most updated estimate of the unknown system parameters, $\hat{\boldsymbol{\theta}}$, is required for their evaluation. The estimate of the system parameters, $\hat{\boldsymbol{\theta}}$, is based on Eq. (5-60). Moreover, for better performance of the control approach and better usage of the collected data, the estimate of the system parameters is obtained by using a code running in parallel to the control code. This is done such that at the end of each control horizon $[k_0, k_f]$, there is an updated estimate of the system parameters based on the control gains obtained at time k_0. This iterative process between the estimation of the control gains and the estimation of the system parameters continues for n_k consecutive

times, each for 20 seconds. The results can be compared to the case of having no actuators with an equivalent amount of data.

The weighting matrix, Σ, is assumed a diagonal matrix with diagonal elements equivalent to the square of the reciprocal of each of the elements of the exact values of $\boldsymbol{\theta}$; consequently, the first term in the cost function in Eq. (5-6) is the relative square error of the elements of $\boldsymbol{\theta}$. The weighting matrix, **R**, is a scalar value, suggested to be taken equivalent to 10^{-20} N^{-2}. Also, in the application of the control approach introduced in the 2DOF example, an initial guess of the control gains is required for the solution of the nonlinear equations.

The controlled SHM approach is applied for n_s different sequences of disturbances and noises. For each sequence, the online controlled monitoring approach introduced herein is applied for n_k consecutive control horizons. Each time the approach is applied, an estimate of structural parameters is obtained. Subsequently, the norm of the total relative identification error, $\tilde{e}$, in the identified parameters, $\hat{\boldsymbol{\theta}}$, compared to the exact values, $\boldsymbol{\theta}$, is evaluated. The identification error, $\tilde{e}$, is defined as

$$\tilde{e} = \sqrt{e_{\theta_1}^2 + e_{\theta_2}^2 + \ldots + e_{\theta_n}^2} \tag{5-128}$$

where the error, for each of the identified parameters, is defined as the ratio between the difference between the identified and exact parameter, and the exact value of this parameter

$$e_{\theta_i} = (\hat{\theta}_i - \theta_i)/\theta_i \tag{5-129}$$

The resulting total relative identification error, $\tilde{e}$, in each consecutive application of the approach, can be compared to that for the conventional structure approach. This should be done for every noise sequence. Finally, the RMS of the total relative identification error, $\tilde{e}$, of the system parameters estimate, $\hat{\boldsymbol{\theta}}$, in each of the consecutive control cycles, for the n_s different data time histories, should be obtained for both the controlled and the conventional structure approaches. The vector, $\hat{\boldsymbol{\theta}}$, used in the comparison, include only the elements of the $\mathbf{A}_i$ and $\mathbf{C}_i$ coefficient matrices since the $\mathbf{B}_i$ coefficients only concern the controlled approach.

Moreover, the RMS of the relative identification error, $\tilde{\tilde{e}}$, in the elements of the matrix coefficients $\mathbf{A}_1$ and $\mathbf{A}_2$ only, should be studied. This is because the system matrix, $\mathbf{A}$, of the equivalent discrete-time observable canonical form state space model, is formed out of these matrix coefficients, as shown in Appendix C, Eq. (C-13).

Future research should consider follow running this illustrative example in a numerical solution. Also, other predictive control methods should be considered (though they may require much faster computers and larger available computer memories, with more powerful programs) in order to deal with the complex nature of such parametric approaches as the one introduced in this chapter. Ambient vibration measurement data from actual structures should be considered to deal with other problems that may not evolve in theoretical studies. In addition, structures with

higher degrees of freedom should be a main focus in future as well, such as high-rise buildings and complex structures.

6 CONCLUSIONS

The research introduced in this thesis studies the improvements in the health monitoring of structures that are available by using semiactive variable stiffness and damping devices (VSDDs). The work here demonstrates the effectiveness of using VSDDs to improve the estimates of structural parameters for SHM and damage detection.

In general, the research in this dissertation is divided into three major parts. The first part focuses on the improvements in the identification of the structural parameters when using frequency domain identification techniques. A traditional technique, that is introduced in the literature review by Levy (1959), is modified to obtain an iterative method, the Iterative Least Squares Numerator (ILSN) method, that approximates the more complicated conventional error in the transfer function and, finally, minimizes this error to give fairly accurate estimates through least squares optimization. It is shown that, using the ILSN technique in identification of parameters, the variable stiffness and damping induced by the semiactive device in the structure helps reduce the variation of the estimates of the structural parameters. This is the case when using relatively small additional stiffnesses (a fraction of the corresponding stories stiffnesses) induced by the semiactive devices. The means of the structural parameter estimates are improved and their variations are found to be substantially reduced when using larger induced stiffnesses and damping coefficients

than those of the corresponding stories. The test beds in the research herein are a 2DOF bridge model and two-story and six-story shear building models.

Moreover, the first part introduces another newly modified technique, INVFLS, that identifies the coefficients of the numerator and denominator polynomials of the transfer function and uses the resulting values in identifying the stiffnesses and the damping coefficients of the structure. The resulting identified parameters from applying this technique consistently confirm the improvements obtained in the identification process of the structural parameters in terms of reduced variations when using VSDDs. However, the results are not as impressive as those obtained from the ILSN technique. In addition, the improvements in the identification of the structural parameters are studied in the context of the Eigensystem Realization Algorithm (ERA). The ERA is applied with and without the semiactive devices. The results indicate that the root mean square error in the identified parameters is clearly reduced by using semiactive devices in the structure.

The second part of this dissertation studies the effect of using variable stiffnesses in an experimental structure for improving identified structural parameters. A 2DOF shear building structure, composed of horizontal plexi-glass plates, vertical aluminum plates and two pairs of soft springs as bracings, is used in the lab experiment. Stiff springs are used in pairs to replicate the effect of VSDDs in the structure. The structure is excited through a small-scale shaking table in the SHM and Control Lab at the University of Southern California. The excitation takes two forms: a band limited white noise and a filtered band limited white noise. The

absolute accelerations of the shake table and the first and second stories of the experimental structure are measured using one accelerometer fixed to each of the three levels. It is assumed that the masses and the damping coefficients are known *a priori*. Damage is incurred in the structure by removing a pair of the weak springs. The resulting estimates of the reduction in the story stiffness due to damage in the structure indicate more accuracy in the mean estimates when using four different configurations of additional stiffnesses (replicating the effect of VSDDs) compared to the case of the conventional structure. In addition, using the conventional structure approach shows more sensitivity to noise such that the variation in the identified parameters is sometimes much larger than using the VSDD approach. In general, the results of the experimental work are consistent with the results from the analytical work since they indicate better mean estimates and sometimes considerably less variations when VSDDs are used in the structure.

The third part of the dissertation studies realtime controlled health monitoring of structures in the context of time domain identification techniques. An ARMA/ARMAX black box model of the 2DOF bridge model is used as a test bed of the approach. A quadratic cost function, that includes the error in the estimated system parameters and the force exerted by the actuator, is defined. Some techniques for evaluating the autocorrelation functions of the measurements and the inputs in terms of the control gains minimizing the cost function are introduced. The resulting autocorrelations functions are used to evaluate the cost function. The equivalent ARMA/ARMAX coefficients are evaluated based on the physical properties of the

bridge model (stiffnesses and damping coefficients). The resulting model is assumed to be excited by ambient traffic excitation acting on the deck and ambient ground excitation at the support of the pier. The ambient excitations and the associated measurements noises are all assumed Gaussian pulse processes. An illustrative example for testing the introduced controlled approach is introduced for future studies.

Future research studying the improvements in identification of structural parameters should include data from real structures. The dynamics of the VSDD should be incorporated, for more accurate behavior rather than assuming ideal behavior for VSDDs. Also, more complicated structures should be examined, in order to generalize the VSDD approach.

7 REFERENCES

Ang, A.H-S., and W.H. Tang (1975). *Probability Concepts in Engineering Planning and Design, Basic Principles*, Vol. I. Wiley, NY.

Arizona Dept. of Transportation (ADOT) (2001). "Superstition Freeway," web page http://www.superstitionfreeway.com/

Au, S.K., K.V. Yuen and J.L. Beck (2000). "Two-Stage System Identification Results for Benchmark Structure." Proceedings of the 14th ASCE Engineering Mechanics Conference, Austin, Texas, 21–24 May 2000.

Battaini, G. Y., G. Yang and B.F. Spencer, Jr., (2000). "Bench-Scale Experiment for Structural Control." *Journal of Engineering Mechanics*, **126**(2), 140-148.

Beck, J.L. (1978). Determining Models of Structures from Earthquake Records. Report EERL78-01, California Institute of Technology.

Beck, J.L. (1990). "Statistical System Identification of Structures." In A.H-S. Ang, M. Shinozuka and G.I. Schuëller (eds.), *Structural Safety and Reliability* (ASCE, New York), 1395–1402.

Beck, J.L., B.S. May and D.C. Polidori (1994a). "Determination of Modal Parameters from Ambient Vibration Data for Structural Health Monitoring." *First World Conference on Structural Control*, Los Angeles, California, 3–5 August 1994.

Beck, J.L., M.W. Vanik and L.S. Katafygiotis (1994b). "Determination of Stiffness Changes from Modal Parameter Changes for Structural Health Monitoring." *First World Conference on Structural Control*, Los Angeles, California, 3–5 August 1994.

Beck, J.L., S. Au and M.W. Vanik (2001). "Monitoring Structural Health using a Probabilistic Measure." *Computer-Aided Civil and Infrastructure Engineering*, **16**, 1–11.

Béliveau, J.G., and S. Chater (1984). "System Identification of Structures from Ambient Wind Measurements." *Proceedings of the Eighth World Conference on Earthquake Engineering*, Prentice-Hall, Inc., Englewood Cliffs, New Jersey, 1984, **IV**, 307–314.

Bendat, J.S., and A.G. Piersol (2000). *Random Data: Analysis and Measurement Procedures*. Wiley, NY.

Bernal, D., and B. Gunes (2000). "Observer/Kalman and Subspace Identification of the UBC Benchmark Structural Model." *Proceedings of the 14th ASCE Engineering Mechanics Conference*, Austin, Texas, 21–24 May 2000.

Bernal, D., and B. Gunes (2004). "Flexibility Based Approach for Damage Characterization: Benchmark Application." *Journal of Engineering Mechanics*, ASCE, **130**(1), 61-70.

Bodeux, J.B., and J.C. Golinval (2001). "Application of ARMAV Models to the Identification and Damage Detection of Mechanical and Civil Engineering Structures." *Smart Materials and Structures*, **10**, 479-489.

Brincker, R., L. Zhang and P. Anderson (2001). "Modal Identification of Output-Only Systems using Frequency Domain Decomposition." *Smart Materials and Structures*, **10**, 441-445.

Brownjohn, J.M.W. (2003). "Ambient Vibration Studies for System Identification of Tall Buildings." *Earthquake Engineering and Structural Dynamics*, **32,** 71-95.

Caicedo, J.M., S.J. Dyke and E.A. Johnson (2004). "Natural Excitation Technique and Eigensystem Realization Algorithm for Phase I of the IASC-ASCE Benchmark Problem: Simulated Data." *Journal of Engineering Mechanics*, ASCE, **130**(1), 49-60.

Capecchi, D., and F. Vestroni (1999). "Monitoring of Structural Systems by Using Frequency Data." *Earthquake Engineering and Structural Dynamics*, **28**, 447–461.

Chang, F.-K. (1999). *Structural Health Monitoring 2000. Proceedings of the 2nd International Workshop on Structural Health Monitoring*, Stanford University, 8–10 September 1999, Technomic Publishing Co., Lancaster, PA.

Chen, C.-T. (1999). *Linear System Theory and Design, 3rd Edition.* Oxford University Press, New York.

Chopra, A.K. (1995). *Dynamics of Structures, Theory and Applications to Earthquake Engineering.* Prentice Hall, Englewood Cliffs, New Jersey.

Christenson, R.E., B.F. Spencer, Jr., N. Hori and K. Seto (2001). "Coupled Building Control Using Acceleration Feedback." *Computer-Aided Civil and Infrastructure Engineering*, accepted, **18**, 3–17, 2003.

Corbin, M., A. Hera and Z. Hou (2000). "Locating Damage Regions Using Wavelet Approach." *Proceedings of the 14th ASCE Engineering Mechanics Conference*, Austin, Texas, 21–24 May 2000.

Doebling, S.W., C.R. Farrar and M.B. Prime (1998). "A Summary Review of Vibration-Based Damage Identification Methods." *The Shock and Vibration Digest*, **30**(2), 91–105.

Doebling, S.W., C.R. Farrar, M.B. Prime and D.W. Shevitz (1996). "Damage Identification and Health of Structural and Mechanical Systems from Changes in their Vibration Characteristics: A Literature Monitoring Review." Los Alamos National Laboratory Report, LA-13070-MS, Los Alamos, New Mexico.

Dyke, S.J., B.F. Spencer, Jr., M.K. Sain and J.D. Carlson (1996a). "Modeling and Control of Magnetorheological Dampers for Seismic Response Reduction." *Smart Materials and Structures*, **5**, 567–575.

Dyke, S.J., B.F. Spencer, Jr., P. Quast, D.C. Kaspari, Jr., and M.K. Sain (1996b). "Implementation of an Active Mass Driver using Acceleration Feedback Control." *Microcomputers in Civil Engineering: special issue on active and hybrid structural control*, **11**, 304-323.

East Bay Business Times (EBBT) (2002). State Budget Deficit Could Hit $20 billion." http://eastbay.bizjournals.com/eastbay/stories/2002/04/01/daily48.html, Web page, 3 April 2002.

Ehrgott, R.C., and S.F. Masri (1992). "Modeling the Oscillatory Dynamic Behavior of Electrorheological Materials in Shear." *Smart Materials and Structures*, **1**(4), 275–285.

Elmasry, M.I.S., and E.A. Johnson (2002). "Parametric Frequency Domain Identification in Multiconfiguration Structures." *15th ASCE Engineering Mechanics Conference (EM2002)*, Columbia University, New York, 2-5 June 2002.

Elmasry, M.I.S., and E.A. Johnson (2004a). "Health Monitoring of Structures Under Ambient Vibrations Using Semiactive Devices." *American Control Conference 2004 (ACC2004)*, Boston Sheraton Hotel, Boston, 30 June - 2 July 2004.

Elmasry, M.I., and E.A. Johnson (2004b). "Improvements in Structural Parameter for SHM using VSDDs." *9th ASCE Specialty Conference on Probabilistic Mechanics and Structural Reliability (PMC2004)*, Albuquerque, NM, 26-28 July 2004.

Erkus, B., A. Masato and Y. Fujino (2002). "Investigation of Semiactive Control for Seisimic Protection of Elevated Highway Bridges." *Engineering Structures*, **24**, 281–293.

Federal Highway Administration (FHWA) (2002). "National Bridge Inventory." Web pages, http://www.fhwa.dot.gov/bridge/britab.html

Gavin, G.P., R.D. Hanson and F.E. Filisko (1996a). "Electrorheological Dampers. Part I: Analysis and Design." *Journal of Applied Mechanics*, **63**, 669–675.

Gavin, G.P., R.D. Hanson and F.E. Filisko (1996b). "Electrorheological dampers. Part I: Testing and Modeling." *Journal of Applied Mechanics*, **63**, 676–682.

Hall, J.F., ed. (1995). "Northridge Earthquake of January 17, 1994, Reconnaissance Report." *Earthquake Spectra*, **11** supplement C.

Hera, A., and Z. Hou (2004). "Application of Wavelet Approach for ASCE Structural Health Monitoring Benchmark Studies." *Journal of Engineering Mechanics*, ASCE, **130**(1), 96-104.

Ho, B.L., and R.E. Kalman (1965). "Effective Construction of the Linear State-variable Models from Input/Output Data." *3rd Annual Allerton Conference on Circuit and System Theory*, 449–459; also *Regelungstechnik*, **14**, 545–548.

Housner, G.W., L.A. Bergman, T.K. Caughey, A.G. Chassiakos, R.O. Claus, S.F. Masri, R.E. Skelton, T.T. Soong, B.F. Spencer, Jr. and J.T.P. Yao (1997). "Structural Control: Past Present, and Future." *Journal of Engineering Mechanics*, ASCE, **123**, 897–971.

Housner, G.W., T.T. Soong and S.F. Masri (1994). "Second Generation of Active Structural Control in Civil Engineering." *Proceedings of the 1st World Conf on Structural Control*, Pasadena, Panel: 3-18.

Housner, G.W., T.T. Soong and S.F. Masri (1994b). "Second Generation of Active Structural Control in Civil Engineering." *Microcomp. in Civil Eng.*, **11**(5), 289-296.

Ikonen, E., and K. Najim (2002). *Advanced Process Identification and Control.* Marcel Dekker, New York.

Inman, D.J. (1989). *Vibration: with Control, Measurement, and Stability.* Prentice Hall, Englewood Cliffs, New Jersey.

Johnson, E.A. (1997b). O*nline Monitoring, Control, and Reliability of Structural Dynamical Systems*, Ph.D. thesis, University of Illinois at Urbana-Champaign.

Johnson, E.A., and M.I.S. Elmasry (2003). *Parametric Frequency Domain Identification Using Variable Stiffness and Damping Devices*, METRANS Report, Research Project 01-10.

Johnson, E.A., and M.I.S. Elmasry (2005a). *Analytical and Experimental Structural System Identification Using Variable Stiffness and Damping Devices*, METRANS Report, Research Project 03-17.

Johnson, E.A., and M.I.S. Elmasry (2005b). "Structural Health Monitoring Using Variable Stiffness and Damping Devices," *Journal of Engineering Mechanics*, ASCE, in review.

Johnson, E.A., H.F. Lam, L.S. Katafygiotis and J.L. Beck. (2004). "Phase I IASC-ASCE Structural Health Monitoring Benchmark Study Using Simulated Data." *Journal of Engineering Mechanics*, ASCE, **130**(1), 3-15.

Johnson, E.A., L.A. Bergman and P.G. Voulgaris (1997). *Online Modal State Monitoring of Slowly Time-Varying Structures*, NASA Contractor Report 198057.

Johnson, E.A., R.E. Christenson and B.F. Spencer, Jr. (2003). "Semiactive Damping of Cables with Sag." *Computer Aided Civil and Infrastructure Engineering*, **18**(2), 132–146.

Juang, J. (1994). *Applied System Identification*. Prentice Hall, Englewood Cliffs, New Jersey.

Juang, J., and M.Q. Phan (2001). *Identification and Control of Mechanical Systems*. Cambridge University Press, New York.

Juang, J., and R.S. Pappa (1985). "An Eigen System Realization Algorithm for Modal Parameters Identification and Model Reduction." *Journal of Guidance*, **8**(5), 620–627.

Juang, J., J.E. Cooper and J.R. Wright (1988). "An Eigen System Realization Algorithm using Data Correlations (ERA/DC) for Modal Parameter Identification." *Control-Theory and Advanced Technology*, **4**(1), 5–14.

Kanai, K. (1957). "Semi-emperical Formula for the Seismic Characteristics of the ground." *Bulletin of Earthquake Research Inst.*, University of Tokyo, **35**, 309-325.

Katafygiotis, L.S., and K. Yuen (2001). "Bayesian Spectral Density Approach for Modal Updating using Ambient Data." *Earthquake Engineering and Structural Dynamics*, **30**(8) 1103–1123.

Katafygiotis, L.S., H.F. Lam and N. Mickleborough (2000). "Application of a Statistical Approach on a Benchmark Damage Detection Problem." *Proceedings of the 14th ASCE Engineering Mechanics Conference*, Austin, Texas, 21–24 May 2000.

Kiremedjian, A.S. (1999). "Vulnerability and Damage of Structures from Earthquakes." Presentation, *Uncertaininty of Damageability Conference*, Risk Prediction Initiative, web page: http//:www.bbsr.edu/rpi/meetpart/Nov99

Kobori, T., and M. Takahashi (1993). "Seismic Response Controlled Structure with Active Variable Stiffness System." *Earthquake Engineering and Structural Dynamics*, **22**(12), 925–941.

Kurata, N., T. Kobori, S.M. Takahashi, T. Ishibashi, N. Niwal, J. Tagami and H. Midorikawa (2000). "Forced Vibration Test of a Building with Semiactive Damper System." *Earthquake Engineering and Structural Dynamics*, **29**, 629–645.

Lam, H.F., L.S. Katafygiotis and N.C. Mickleborough (2004). "Application of a Statistical Model Updating Approach on Phase I of the IASC-ASCE Structural Health Monitoring Benchmark Study." *Journal of Engineering Mechanics*, ASCE, **130**(1), 34-48.

Levy, E. (1959). "Complex Curve Fitting." *IRE Transactions on Automatic Control*, **AC-4**(1), 37–44.

Ljung, L. (1999). *System Identification: Theory for the User* (2nd ed.), Prentice Hall, Englewood Cliffs, New Jersey.

Luş, H., and R. Betti (2000). "Damage Identification in Linear Structural Systems." *Proceedings of the 14th ASCE Engineering Mechanics Conference*, Austin, Texas, 21–24 May 2000.

Luş, H., R. Betti and R. W. Longman (1999). "Identification of Linear Structural Systems Using Earthquake-Induced Vibration Data." *Earthquake Engineering and Structural Dynamics*, **28**, 1449–1467.

Luş, H., R. Betti, J. Yu and M. De Angelis (2004). "Investigation of a System Identification Methodology in the Context of the ASCE Benchmark Problem." *Journal of Engineering Mechanics*, ASCE, **130**(1), 71-84.

Lutes, L.D., and S. Sarkani (2004). *Random Vibrations, Analysis of Structural and Mechanical Systems*. Elsevier, Burlington, Massachusetts.

Makris, N., S.A. Burton, D. Hill and M. Jordon (1996). "Analysis and Design of ER Damper for Seismic Protection of Structure." *Journal of Engineering Mechanics*, ASCE, **122**(10), 1003–1011.

MATLAB® (1999). The Math Works Inc., Natick, Massachusetts.

Mita, A. (1999). "Emerging Needs in Japan for Health Monitoring Technologies in Civil and Building Structures." In F.-K. Chang (ed.), *Structural Health Monitoring 2000: Proceedings of the 2nd International Workshop on Structural Health Monitoring*, Stanford University, 8–10 September 1999 (Technomic Publishing Co., Lancaster, PA), 56–67.

Moses, F., C.G. Schilling and K.S. Raju (1987). "Fatigue Evaluation Procedures for Steel Bridges." National Cooperative Highway Research Program, Report (**299**), Transportation Research Board, National Research Council, Washington, DC, ISSN 0077-5614.

Nagarajaiah, S., and X. Ma (1996). "System Identification Study of a 1:10 Scale Steel Model Using Earthquake Simulator," *Proc. of Eng. Mech. Conf.*, ASCE, **2**, 764–767.

Nagarajaiah, S., and X. Sun (2001). "Base-Isolated FCC Building: Impact Response in Northridge Earthquake." *Journal of Structural Engineering*, ASCE, **127**(9), 1063-1075.

Patten, W.N., S. Jinghui, L. Guangjun, J. Kuehn and G. Song (1999). "Field Test of an Intelligent Stiffener for Bridges at The I-35 Walnut Creek Bridge." *Earthquake Engineering and Structural Dynamics,* **28**, 109–126.

Quanser Consulting Inc. (1995). *User Manuals*. Ontario, Canada.

Quek, S.T., W. Wang and C.G. Koh (1999). "System Identification of Linear MDOF Structures Under Ambient Excitation." *Earthquake Engineering and Structural Dynamics*, **28**, 61–77.

Rabinow, J. (1948). "The Magnetic Fluid Clutch." *AIEE Trans.*, **67**, 1308–1315.

Ramallo, J.C., E.A. Johnson and B.F. Spencer, Jr. (2002). "'Smart' Base Isolation Systems." *Journal of Engineering Mechanics*, ASCE, **128**, 1088–1099.

Ray, L.R., and L. Tian (1999). "Damage Detection in Smart Structures through Sensitivity Enhancing Feed-back Control." *Journal of Sound and Vibration*, **227**(5), 987–1002.

Ribakov, Y., and J. Gluck (1999). "Active Control of MDOF Structures with Supplemental Electrorheological Fluid Dampers." *Earthquake Engineering and Structural Dynamics*, **28**, 143–156.

Sanayei, M.S., W. Doebling, C.R. Farrar, S. Wadia-Fascetti and B. Arya (1998). "Challenges in Parameter Estimation for Condition Assessment of Structures." *Structural Engineering World Wide, Proc. Structural Engineers World Congress*, San Francisco, CA, July 1998, Elsevier, New York, paper ref. T216-5.

Simiu, E., and R.H. Scanlan (1996). *Wind Effects on Structures* (3rd Ed.), Wiley & Sons, New York, England.

SIMULINK® (1999). The Math Works Inc., Natick, Massachusetts.

Smith, J.W. (1988) *Vibration of Structures: Applications in Civil Engineering Design,* Chapman & Hall, London, England.

Sohn, H., and C. R. Farrar (2001). "Damage Diagnosis using Time Series Analysis of Vibration Signals." *Smart Materials and Structures*, **10**, 446-451.

Sohn, H., and K.H. Law (2000). "Bayesian Probabilistic Damage Detection of a Reinforced Concrete Bridge Column." *Earthquake Engineering and Structural Dynamics*, **29**, 1131–1152.

Soong, T.T., and B.F. Spencer, Jr. (2002). "Supplemental Energy Dissipation: State-of-the-Art and State-of-the-Practice." *Engineering Structures*, **24**, 243–259.

Soong, T.T., and G.F. Dargush (1997). *Passive Energy Dissipation Systems in Structural Engineering*, Wiley & Sons, Chichester, England.

Soong, T.T., and M. Grigoriu (1993). *Random Vibration of Mechanical and Structural Systems*. Prentice Hall, Englewood Cliffs, New Jersey.

Spencer, B.F., Jr., and M.K. Sain (1997). "Controlling Buildings: A New Frontier in Feedback." *IEEE Control Systems Magazine*, **17**(6), 19–35.

Spencer, B.F., Jr., G.Q. Yang, J.D. Carlson and M.K. Sain (1998). "Smart Dampers for Seismic Protection of Structures: a Full-Scale Study." *Proceedings of the 2nd World Conference on Structural Control*, Kyoto, Japan, 417–426.

Spencer, B.F., Jr., S.J. Dyke, M.K. Sain and J.D. Carlson (1997). "Phenomenological Model for Magnetorheological Dampers." *Journal of Engineering Mechanics*, ASCE, **123**(3), 230-238.

Symans, M.D., and M.C. Constantinou (1997). "Seismic Testing of a Building Structure with a Semiactive Fluid Damper Control System." *Earthquake Engineering and Structural Dynamics*, **26**, 759–777.

Symans, M.D., and M.C. Constantinou (1999). "Semiactive Control Systems for Seismic Protection of Structures: a state-of the-art review." *Engineering Structures*, **21**, 469-487.

Tajimi, H. (1960). "A Statistical Method of Determining the Maximum Response of a Building Structure during an Earthquake." *Proceedings of 2nd World Conference on Earthquake Eng.*, Japan, 781-797.

Takewaki, I., and M. Nakamura (2000). "Stiffness-Damping Simultaneous Identification using Limited Earthquake Records." *Earthquake Engineering and Structural Dynamics*, **29**, 1219–1238.

Vanik, M.W., J.L. Beck and S.K. Au (2000). "Bayesian Probabilistic Approach to Structural Health Monitoring." *Journal of Engineering Mechanics*, ASCE, **126**(7), 738–745.

Varadarajan, N., and S. Nagarajaiah (2000). "Semi-Active Variable Stiffness Tuned Mass Damper for Response Control of Wind Excited Tall Buildings: Benchmark Problem." *Proceedings of the 14th ASCE Engineering Mechanics Conference*, Austin, Texas, 21–24 May 2000.

Wang, C.S., and F.-K. Chang (1999). "Built-In Diagnostics for Impact Damage Identification of Composite Structures." in F.-K. Chang (ed.), Structural Health Monitoring 2000: Proceedings of the 2nd International Workshop on Structural Health Monitoring, Stanford University, 8–10 September 1999 (Technomic Publishing Co., Lancaster, PA), 612–621.

Winslow, W.M. (1949). "Induced Vibration of Suspensions." *J. Applied Physics*, **20,** 1137–1140.

Xu, Y.L.,W.L. Ku and J.M. Ko (2000). "Seismic Response Control of Frame Structures using Magnetorheological/Electrorheological Dampers." *Earthquake Engineering and Structural Dynamics*, **29**, 557–575.

Yang, G., B.F. Spencer, Jr., J.D. Carlson and M.K. Sain (2002). "Large-Scale MR Fluid Dampers: Modeling and Dynamic Performance Considerations." Engineering Structures, 24, 309-323.

Yang, J.N., J.C. Wu and Z. Li (1996). "Control of Seismic-Excited Buildings Using Active variable Stiffness Systems." *Engineering Structures*, **18**(8), 589–596.

Yang, J.N., Y. Lei, S. Lin and N. Huang (2004). "Hilbert-Huang Based Approach for Structural Damage Detection." *Journal of Engineering Mechanics*, ASCE, **130**(1), 85-95.

Yuen K.-V., S.K. Au and J.L. Beck (2004). "Two-Stage Structural Health Monitoring Approach for Phase I Benchmark Studies." *Journal of Engineering Mechanics*, ASCE, **130**(1), 16-33.

Appendix A

A.1 Computational Procedure for 6DOF Shear Building Model

While using the symbolic math capabilities of MATLAB® to formulate the iterative least-squares frequency-domain identification is convenient, it is not very efficient for larger problems, requiring the development of a semi-numerical solution procedure. The core of this alternate solution procedure lies in recognizing that the residual error $\hat{\mathbf{e}}_l$ in Eq. (3-12) can be separated into a set of numerical coefficients and a numeric representation of the symbolic unknowns. The r^{th} element of the $m \times 1$ error $\hat{\mathbf{e}}_l$ in Eq. (3-12) can be modified as

$$\hat{e}_{rl}(j\omega_i, \boldsymbol{\theta}, \boldsymbol{\kappa}_k) = \frac{B_r(j\omega_i, \boldsymbol{\theta}, \boldsymbol{\kappa}_k) - A(j\omega_i, \boldsymbol{\theta}, \boldsymbol{\kappa}_k)\hat{H}_r(j\omega_i, \boldsymbol{\kappa}_k)}{\hat{A}_l(j\omega_i, \boldsymbol{\kappa}_k)} = \mathbf{c}_{rl}^{\mathrm{T}}(j\omega_i, \boldsymbol{\kappa}_k)\mathbf{v}_r(\boldsymbol{\theta}) \quad \text{(A-1)}$$

where $\mathbf{c}_{rl}(j\omega_i, \boldsymbol{\kappa}_k)$ is an $n_{\mathbf{v}_r} \times 1$ vector of numeric coefficients of the corresponding elements of $\mathbf{v}_r(\boldsymbol{\theta})$, which themselves are each of the form

$$v_{sr}(\boldsymbol{\theta}) = \prod_{i=1}^{n} \theta_i^{p_i^{rs}}, \; s = 1, \ldots, n_{\mathbf{v}_r}, \; r = 1, \ldots, m \quad \text{(A-2)}$$

where the p_i^{rs} are non-negative integer exponents that can be arranged in $n \times 1$ vectors $\mathbf{p}^{rs}$ which can be collected into set $P_r = \{\mathbf{p}^{r1}, \ldots, \mathbf{p}^{rn_{\mathbf{v}_r}}\}$. The symbolic $\mathbf{v}_r(\boldsymbol{\theta})$ is a polynomial function only of the unknown parameters and is different for each element of the transfer function error. The coefficient vector $\mathbf{c}_{rl}(j\omega_i, \boldsymbol{\kappa}_k)$ depends on

the frequencies and the known parameters, and is different in each iteration and for each element of the transfer function matrix. Since the $\mathbf{v}_r(\boldsymbol{\theta})$ can be defined by the numeric exponents of the elements of the unknown $\boldsymbol{\theta}$, they can be stored and manipulated just through a numeric tensor p_i^{rs}.

Substituting Eq. (A-1) into the square error Eq. (3-13), results in

$$\Delta_l^2(\boldsymbol{\theta}) = \sum_r \sum_i \sum_k \mathbf{v}_r^{\mathrm{T}}(\boldsymbol{\theta}) \mathbf{c}_{rl}^{\dagger}(j\omega_i, \boldsymbol{\kappa}_k) \mathbf{c}_{rl}^{\mathrm{T}}(j\omega_i, \boldsymbol{\kappa}_k) \mathbf{v}_r(\boldsymbol{\theta}) \tag{A-3}$$

where $(\cdot)^{\dagger}$ denotes complex conjugation. The order of summation and multiplication can be rearranged since $\mathbf{v}_r(\boldsymbol{\theta})$ is independent of i and k, giving

$$\Delta_l^2(\boldsymbol{\theta}) = \sum_r \mathbf{v}_r^{\mathrm{T}}(\boldsymbol{\theta}) \left[\sum_i \sum_k \mathbf{c}_{rl}^{\dagger}(j\omega_i, \boldsymbol{\kappa}_k) \mathbf{c}_{rl}^{\mathrm{T}}(j\omega_i, \boldsymbol{\kappa}_k) \right] \mathbf{v}_r(\boldsymbol{\theta}) \tag{A-4}$$

The quantity in brackets is purely numerical and can be computed quite easily; let it be defined

$$\mathbf{C}_{rl} = \sum_i \sum_k \mathbf{c}_{rl}^{\dagger}(j\omega_i, \boldsymbol{\kappa}_k) \mathbf{c}_{rl}^{\mathrm{T}}(j\omega_i, \boldsymbol{\kappa}_k), \; r = 1, \ldots, m \tag{A-5}$$

which incorporates all of the information for the data frequency points $j\omega_i$ and the different sets of known parameters $\boldsymbol{\kappa}_k$.

The vectors $\mathbf{v}_r(\boldsymbol{\theta})$ are not all the same. It is convenient to define a single similar vector $\mathbf{v}(\boldsymbol{\theta})$ that contains all of the symbolic products of powers of all unknown $\boldsymbol{\theta}$ contained in the individual $\mathbf{v}_r(\boldsymbol{\theta})$.

$$v_s(\boldsymbol{\theta}) = \prod_{i=1}^{n} \theta_i^{p_i^s}\ ,\ s = 1,\ldots,n_{\mathrm{v}} \tag{A-6}$$

where the p_i^s are non-negative integer exponents that can be arranged in n_{v} $n \times 1$ vectors $\mathbf{p}^s$ that can be collected as set $P = \{\mathbf{p}^1,\ldots,\mathbf{p}^{n_{\mathrm{v}}}\}$, which is the union of the individual sets for each element of the transfer function,

$$P = \bigcup_{r=1}^{m} P_r \tag{A-7}$$

The individual symbolic vectors $\mathbf{v}_r(\boldsymbol{\theta})$ can be related to the global symbolic vector by

$$\mathbf{v}_r(\boldsymbol{\theta}) = \mathbf{T}_r \mathbf{v}(\boldsymbol{\theta}),\ r = 1,\ldots,m \tag{A-8}$$

where $\mathbf{T}_r$ is a transformation matrix containing ones and zeros

$$[\mathbf{T}_r]_{is} = I(\mathbf{p}^{ri},\mathbf{p}^s)\ ,\ r = 1,\ldots,m,\ i = 1,\ldots,n_{\mathrm{v}_r},\ s = 1,\ldots,n_{\mathrm{v}} \tag{A-9}$$

where $I(\mathbf{x},\mathbf{y})$ is an indicator function that has value 1 when every element of $\mathbf{x}$ matches the corresponding element of $\mathbf{y}$.

Substituting Eqs. (A-5) and (A-8) into the square error Eq. (A-4) gives

$$\Delta_l^2(\boldsymbol{\theta}) = \sum_r \mathbf{v}^{\mathrm{T}}(\boldsymbol{\theta}) \mathbf{T}_r^{\mathrm{T}} \mathbf{C}_{rl} \mathbf{T}_r \mathbf{v}(\boldsymbol{\theta}) \tag{A-10}$$

which can be simplified since $\mathbf{v}(\boldsymbol{\theta})$ is independent of transfer function index r

$$\Delta_l^2(\boldsymbol{\theta}) = \mathbf{v}^{\mathrm{T}}(\boldsymbol{\theta}) \left[\sum_r \mathbf{T}_r^{\mathrm{T}} \mathbf{C}_{rl} \mathbf{T}_r \right] \mathbf{v}(\boldsymbol{\theta}) = \mathbf{v}^{\mathrm{T}}(\boldsymbol{\theta}) \mathbf{C}_l \mathbf{v}(\boldsymbol{\theta}) \tag{A-11}$$

where $\mathbf{C}_l$ is a $n_v \times n_v$ symmetric numeric matrix with elements c_{rs}^l. Computing these elements can be done quite efficiently; the slowest part is the process of forming the union of the exponent sets and building the resulting transformation matrices $\mathbf{T}_r$.

Determining the least-square estimates of the unknowns, then, requires the gradient of $\Delta_l^2(\boldsymbol{\theta})$

$$\frac{\partial}{\partial \boldsymbol{\theta}}\left[\Delta_l^2(\boldsymbol{\theta})\right] = 2\sum_{r=1}^{n_v}\sum_{s=1}^{n_v} c_{rs}^l v_r(\boldsymbol{\theta})\frac{\partial v_s(\boldsymbol{\theta})}{\partial \boldsymbol{\theta}} \tag{A-12}$$

and the elements of its corresponding Jacobian

$$\frac{\partial^2}{\partial\theta_i\partial\theta_j}\left[\Delta_l^2(\boldsymbol{\theta})\right] = 2\sum_{r=1}^{n_v}\sum_{s=1}^{n_v} c_{rs}^l\left[v_r\frac{\partial^2 v_s}{\partial\theta_i\partial\theta_j} + \frac{\partial v_r}{\partial\theta_i}\frac{\partial v_s}{\partial\theta_j} + \frac{\partial v_r}{\partial\theta_j}\frac{\partial v_s}{\partial\theta_i} + \frac{\partial^2 v_r}{\partial\theta_i\partial\theta_j}v_s\right] \tag{A-13}$$

The j^{th} element of the gradient can be simplified to a set of products of powers of unknowns and the corresponding coefficients

$$\frac{\partial}{\partial\theta_j}\left[\Delta_l^2(\boldsymbol{\theta})\right] = 2\sum_{r=1}^{n_v}\sum_{s=1}^{n_v}\tilde{c}_{rs,j}^l\tilde{v}_{rs,j}(\boldsymbol{\theta}) \tag{A-14}$$

where

$$\tilde{c}_{rs,j}^l = c_{rs}^l p_j^s \quad \text{and} \quad \tilde{v}_{rs,j}(\boldsymbol{\theta}) = \prod_{i=1}^{n}\theta_i^{p_i^r + p_i^s - \delta_{ij}} = \prod_{i=1}^{n}\theta_i^{\tilde{p}_{i,j}^{rs}} \tag{A-15}$$

The elements of the Jacobian can be formed in a similar manner, resulting in a set of coefficients and exponents.

Equation (A-14), then, is a nonlinear equation that is the linear combination of products of powers of the unknowns and the zeros can be found through standard numerical root solving algorithms — this study used the function `fsolve( )` in MATLAB's Optimization Toolbox. The coefficients $\tilde{c}_{rs,j}^{I}$ and the exponents $\tilde{p}_{i,j}^{rs}$ can be computed in a purely numeric procedure from the assumed structural model, and the root solver is numerical. Thus, this alternate numerical solution avoids symbolic computation entirely. The result is that the 2DOF identification problems can be solved in a few seconds on a 2.4GHz Pentium 4, whereas a mostly symbolic computation takes on the order of several minutes on the same computer.

Appendix B

B.1 Testing Reports of Springs Used in the Lab Experiment as Issued from Supplier

B.1.a Weak Steel Springs Report (spring #80039)

Century Spring
212 E. 16 USA

Larson Systems Inc. Tester

Model : Super DHT
Version Number : 2.54
Load Cell : 110.000 lb
Date : 06/11/04
Time : 02:25:09 pm
Operator :_____

Two Point with Rate Mode

Test Number	Tp 1 Length (in)	Tp 1 Force (lb)	Tp 2 Length (in)	Tp 2 Force (lb)	Rate (lb/in)
1	3.0000	-0.152	3.9995	-0.620	0.468
2	3.0000	-0.156	3.9995	-0.632	0.476
3	3.0000	-0.190	3.9995	-0.672	0.482
4	3.0000	-0.190	3.9995	-0.660	0.470

END OF DATA

SUMMARY DATA

Test Number	Tp 1 Length (in)	Tp 1 Force (lb)	Tp 2 Length (in)	Tp 2 Force (lb)	Rate (lb/in)
Mean	3.00000	-0.1720	3.99950	-0.6460	0.4740
Std Dev	0.00000	0.0208	0.00000	0.0241	0.0063
Maximum	3.0000	-0.152	3.9995	-0.620	0.482
Minimum	3.0000	-0.190	3.9995	-0.672	0.468
Range	0.0000	0.038	0.0000	0.052	0.014

END OF SUMMARY

B.1.b Stiff Steel Springs Report (spring #80222)

Century Spring
212 E. 16 USA

Larson Systems Inc. Tester

Model : Super DHT
Version Number : 2.54
Load Cell : 110.000 lb
Date : 06/02/04
Time : 08:43:23 am
Operator :_____

Two Point with Rate Mode

Test Number	Tp 1 Length (in)	Tp 1 Force (lb)	Tp 2 Length (in)	Tp 2 Force (lb)	Rate (lb/in)
1	3.5000	-5.224	3.9995	-8.042	5.642
2	3.5000	-4.980	3.9995	-7.756	5.558
3	3.5000	0.002	3.5000	0.002	0.000
4	3.5000	0.002	3.5000	0.002	0.000
5	3.5000	0.000	3.5000	0.000	0.000
6	3.5000	-4.670	3.9995	-7.412	5.489
7	3.5000	-5.012	3.9995	-7.798	5.578
8	3.5000	-4.972	3.9995	-7.796	5.654
9	3.5000	-4.982	3.9995	-7.744	5.530
10	3.5000	0.004	3.5000	0.004	0.000
11	3.5000	-5.036	3.9995	-7.866	5.666
12	3.5000	-5.066	3.9995	-7.860	5.594
13	3.5000	-5.006	3.9995	-7.800	5.594
14	3.5000	-5.016	3.9995	-7.768	5.510
15	3.5000	-5.112	3.9995	-7.856	5.493
16	3.5000	-5.130	3.9995	-7.886	5.518

END OF DATA

SUMMARY DATA

Test Number	Tp 1 Length (in)	Tp 1 Force (lb)	Tp 2 Length (in)	Tp 2 Force (lb)	Rate (lb/in)
Mean	3.50000	-3.7623	3.87463	-5.8485	4.1766
Std Dev	0.00000	2.2475	0.22338	3.4908	2.4910
Maximum	3.5000	0.004	3.9995	0.004	5.666
Minimum	3.5000	-5.224	3.5000	-8.042	0.000
Range	0.0000	5.228	0.4995	8.046	5.666

END OF SUMMARY

Tests 1-2,6-9,and 11-16 correspond to spring samples 1-2,3-6, and 7-12 in Table 4-8.

Appendix C

C.1 Getting the Equivalent ARMA/ARMAX Model of 2DOF Bridge Model from Available Physical Structural Properties

In order to apply the controlled realtime health monitoring technique applied in Chapter 5, an equivalent discrete time ARMAX model, corresponding to the bridge model in Chapter 3, is used. However, the original bridge model parameters are the physical quantities of the bridge including the stiffnesses, damping coefficients, and masses. Thus, a technique is needed to transform these parameters into the equivalent matrix coefficients of the finite linear difference equation.

The procedure starts with evaluating the mass matrix, **M**, the stiffness matrix, **K**, and the damping matrix, **C**, based on the available model data such that

$$\mathbf{M}=\begin{bmatrix} m_1 & 0 \\ 0 & m_2 \end{bmatrix},\quad \mathbf{K}=\begin{bmatrix} k_1+k_2 & -k_2 \\ -k_2 & k_2 \end{bmatrix} \quad \text{and} \quad \mathbf{C}=\begin{bmatrix} c_1+c_2 & -c_2 \\ -c_2 & c_2 \end{bmatrix} \qquad \text{(C-1)}$$

where m_1 and m_2 are the masses of the pier and the deck, respectively, k_1 and k_2 are the stiffnesses of the pier and the isolator, respectively, and c_1 and c_2 are the damping coefficients of the pier and the isolator, respectively. Consequently, a continuous time state space model, with absolute accelerations at the pier and the deck as observations and the ground acceleration and the deck acceleration due to traffic plus the control force as inputs, can be obtained. Thus, the resulting continuous time state space model is

$$\dot{\mathbf{x}} = \mathbf{A}_c\mathbf{x} + \mathbf{B}_c[u \quad e_{gr} \quad e_{tr}]^T, \qquad \mathbf{y} = \mathbf{C}_y\mathbf{x} + \mathbf{D}_y[u_{act} \quad e_{gr} \quad e_{tr}]^T \tag{C-2}$$

where u is the actuator force, e_{gr} is the ambient excitation at the base, e_{tr} is the traffic ambient excitation at the deck level, and the matrices are

$$\mathbf{A}_c = \begin{bmatrix} \mathbf{0}_{2\times2} & \mathbf{I}_{2\times2} \\ -\mathbf{M}^{-1}\mathbf{K} & -\mathbf{M}^{-1}\mathbf{C} \end{bmatrix}, \ \mathbf{B}_c = \begin{bmatrix} 0 & 0 & 0 \\ 0 & 0 & 0 \\ -1/m_1 & -1 & 0 \\ 1/m_2 & -1 & -1 \end{bmatrix} \tag{C-3}$$

$$\mathbf{C}_y = [-\mathbf{M}^{-1}\mathbf{K} \quad -\mathbf{M}^{-1}\mathbf{C}] \quad \text{and} \quad \mathbf{D}_y = \begin{bmatrix} 0 & 0 & 0 \\ 0 & 0 & 0 \end{bmatrix} \tag{C-4}$$

where the matrix $\mathbf{D}_y$ is taken as a zero matrix because of the expected delay encountered between the action of external forces or vibrations, such as traffic vibrations or ground vibrations, and the response of the system to these excitations.

By changing the continuous time state space model to a discrete time state space model, the state space matrix and the input influence matrices become

$$\mathbf{A} = e^{\mathbf{A}_c\Delta t} \qquad \text{and} \qquad \mathbf{B} = \int_0^{\Delta t} e^{\mathbf{A}_c\tau} d\tau \mathbf{B}_c \tag{C-5}$$

where Δt is the sampling time. This is done such that the sampling frequency is 40 times that of the highest natural frequency of the 2DOF bridge model, resulting in a sampling time of 0.01 second. Then, the resulting discrete time state space model is changed to an observable canonical form using the observability matrix as the transformation matrix

$$\mathbf{A}_{obs} = \mathbf{TAT}^{-1}, \quad \mathbf{B}_{obs} = \mathbf{TB} \quad \text{and} \quad \mathbf{C}_{obs} = \mathbf{CT}^{-1} \tag{C-6}$$

where the observability matrix is obtained from the first row of the observation matrix, $\mathbf{C}_y$, and the state matrix, **A**. This is based on the fact that a system must be observable starting from the first observation.

$$\mathbf{T} = [\overline{\mathbf{C}}, \overline{\mathbf{C}}\mathbf{A}, \overline{\mathbf{C}}\mathbf{A}^2, \overline{\mathbf{C}}\mathbf{A}^3]^{\mathrm{T}} \text{ and } \overline{\mathbf{C}} = [\mathbf{C}_y(1,1) \quad \mathbf{C}_y(1,2) \quad \mathbf{C}_y(1,3) \quad \mathbf{C}_y(1,4)] \tag{C-7}$$

In the meantime, the finite linear difference equation of the ARMAX model can be expressed as

$$\mathbf{y}(k) + \mathbf{A}_1\mathbf{y}(k-1) + \mathbf{A}_2\mathbf{y}(k-2) = \mathbf{B}_1 u(k-1) + \mathbf{B}_2 u(k-2) + \mathbf{C}_1\mathbf{e}(k-1) + \mathbf{C}_2\mathbf{e}(k-2) \tag{C-8}$$

where $u(k)$ is the control force at time k, the term **e** represents the ground ambient excitation, e_{gr}, and the deck traffic ambient excitation, e_{tr}

$$\mathbf{e}(k) = [e_{gr}(k) \quad e_{tr}(k)]^{\mathrm{T}} \tag{C-9}$$

For i=1,2, the matrix coefficients of the observations, $\mathbf{A}_i$, and the matrix coefficients of the ambient excitations from the ground and traffic loads on the deck, $\mathbf{C}_i$, are 2×2 dimensional matrices, whereas the coefficients $\mathbf{B}_i$ are vectors of dimension 2×1. As shown in Eq. (C-6), $\mathbf{B}_0$=0 due to the time delay in the control force and $\mathbf{C}_0$=0 due to time delay in the effect from both the ground ambient loading and the deck traffic loading.

By changing the ARMAX model to an equivalent ARMA model where,

$$\mathbf{y}(k)+\mathbf{A}_1\mathbf{y}(k-1)+\mathbf{A}_2\mathbf{y}(k-2)=\overline{\mathbf{B}}_1\mathbf{U}(k-1)+\overline{\mathbf{B}}_2\mathbf{U}(k-2) \qquad \text{(C-10)}$$

where

$$\mathbf{y}(k)=\begin{bmatrix} y_1(k) \\ y_2(k) \end{bmatrix}, \qquad \mathbf{U}(k)=[u(k) \quad e_{gr}(k) \quad e_{tr}(k)]^T \qquad \text{(C-11)}$$

and

$$\overline{\mathbf{B}}_i(k)=\left[\mathbf{B}_i(k) \quad \mathbf{C}_i(k)\right], \; i=1,2 \qquad \text{(C-12)}$$

and considering an equivalent discrete time state space model to the ARMA model as per Juang (2001) then

$$\mathbf{A}_{ARMA}=\begin{bmatrix} \mathbf{0}_{2\times2} & -\mathbf{A}_2 \\ \mathbf{I}_{2\times2} & -\mathbf{A}_1 \end{bmatrix}, \; \mathbf{B}_{ARMA}=\begin{bmatrix} \overline{\mathbf{B}}_2 \\ \overline{\mathbf{B}}_1 \end{bmatrix}, \; \mathbf{C}_{ARMA}=[\mathbf{0}_{2\times2} \quad \mathbf{I}_{2\times2}]$$

$$\mathbf{D}_{ARMA}=\begin{bmatrix} 0 & 0 & 0 \\ 0 & 0 & 0 \end{bmatrix} \qquad \text{(C-13)}$$

Then, applying the same procedure of transforming the matrices in Eq. (C-13) of the state space corresponding to ARMA model to an observable canonical form using the observability matrix, $\overline{\mathbf{T}}$, where

$$\overline{\mathbf{T}}=[\widetilde{\mathbf{C}},\widetilde{\mathbf{C}}\mathbf{A},\widetilde{\mathbf{C}}\mathbf{A}^2,\widetilde{\mathbf{C}}\mathbf{A}^3]^T \quad \text{and} \quad \widetilde{\mathbf{C}}=[0 \quad 0 \quad 1 \quad 0] \qquad \text{(C-14)}$$

Thus, the resulting matrices in observable canonical form are

$$\mathbf{A}_{ARMA,obs}=\overline{\mathbf{T}}\mathbf{A}_{ARMA}\overline{\mathbf{T}}^{-1}, \; \mathbf{B}_{ARMA,obs}=\overline{\mathbf{T}}\mathbf{B} \text{ and } \mathbf{C}_{ARMA,obs}=\mathbf{C}_{ARMA}\overline{\mathbf{T}}^{-1} \qquad \text{(C-15)}$$

Since the corresponding matrices in Eqs. (C-4) and (C-13) have the same form, then, by equating the corresponding coefficients, a system of equations is obtained that are equal in number to the total number of elements of the matrices, $\mathbf{A}_i$ and $\mathbf{C}_i$, and the vectors, $\mathbf{B}_i$, for i=1,2. Solving the equations yields the elements of the matrix coefficients of the finite linear difference equation of the ARMA model.

C.2 Feasibility of Assuming the $\mathbf{C}_1$ Matrix Coefficient be Known *a Priori* for the 2DOF Bridge Model Online Monitoring

By considering the continuous time state space model as in Eq. (C-2), it can be observed that knowing the masses of the pier and the deck, m_1 and m_2, is sufficient to define the input influence matrix, $\mathbf{B}_c$. Then, by changing the continuous time input influence matrix, $\mathbf{B}_c$, to discrete time matrix, **B,** using

$$\mathbf{B} = \int_0^{\Delta t} e^{\mathbf{A}_c \tau} d\tau \mathbf{B}_c = \left[\mathbf{I}\Delta t + \tfrac{1}{2!}\mathbf{A}_c(\Delta t)^2 + \tfrac{1}{3!}\mathbf{A}_c^2(\Delta t)^3 + \ldots + \text{H.O.T.}\right]\mathbf{B}_c \quad \text{(C-16)}$$

Thus, it can be deduced that, for a considerably low value of the sampling time such as $\Delta t = 0.01\,\text{s}$, which is applied for the solution of the problem in Chapter 5, the higher order terms, starting from the term $\tfrac{1}{2!}\mathbf{A}_c(\Delta t)^2$ within brackets in the right hand side of Eq. (C-14), would tend to zero and have a negligible effect in the evaluation of the influence matrix, **B**, in discrete time. This, consequently, would yield

$$\mathbf{B} = \int_0^{\Delta t} e^{\mathbf{A}_c \tau} d\tau \mathbf{B}_c \cong [\mathbf{I}\Delta t]\mathbf{B}_c \tag{C-17}$$

which indicates that the discrete time influence matrix can be obtained by knowing the masses of the pier and the deck, m_1 and m_2, and the sampling time, Δt. Finally, by applying the transformation in Eq. (C-6) to the influence matrix in Eq. (C-15) and recalling from Eqs. (C-10) and (C-11) that the elements of the coefficient matrix $\mathbf{C}_1$ are parts of the final influence matrix $\mathbf{B}_{\text{ARMA}}$, then it is clear that assuming $\mathbf{C}_1$ is reasonable. The remainder of the input influence matrix, which represents the elements of coefficients matrices, $\mathbf{B}_1$, $\mathbf{B}_2$ and $\mathbf{C}_2$, are considered unknown in the solution procedure.